SPANBETON
PREFAB BOUWOPLOSSINGEN

TU Delft Delft University of Technology

Master Thesis

Torsion in ZIP bridge system

Final version

Name: Evert van Vliet
21-1-2012
Student number: 1304356
E-mail: vvevert@gmail.com

Graduation committee

Chairman

Prof. dr. ir. J.C. Walraven
Department of Structural Engineering, Concrete Structures
Faculty of Civil Engineering and Geosciences
Delft University of Technology

Committee members

Dr.ir. C. van der Veen
Department of Structural Engineering, Concrete Structures
Faculty of Civil Engineering and Geosciences
Delft University of Technology

Dr. ir. P.C.J. Hoogenboom
Department of Structural Engineering, Structural Mechanics
Faculty of Civil Engineering and Geosciences
Delft University of Technology

External committee member

Ir. C. Quartel
Manager infra
Spanbeton B.V. at Koudekerk aan de Rijn

Secretary

Ir. L.J.M. Houben
Department of Structural Engineering, Road and Railway Engineering
Faculty of Civil Engineering and Geosciences
Delft University of Technology

Preface

This master thesis is written to finalize my study Civil Engineering at the department of Concrete Structures at the Delft, University of Technology. The work is done from April 2011 till January 2012 at the office of Spanbeton.

The study is related with the work done by Kassahun Minalu, which was done also at Spanbeton. This study is presented in the thesis 'Finite element modelling of skew slab-girder bridges'. In this study different models with and without end diaphragm beams, with different skew angles and different stiffnesses are studied with a number of finite element models.

The question that was still open after this research was the 'real behaviour' under torsion. Will cracks already appear in Serviceability Limit State or is crack forming delayed till Ultimate Limit State? Can torsion be used for equilibrium? These fundamental questions are studied with the program ATENA of Cervenka Consulting and checked with calculations of the principal stresses.

Without help of others I would not have reached the result presented in this report. First of all I thank Dobromil Pryl, employee of Cervenka Consulting for his help during making a working model in ATENA 3D. The help of Kees Quartel, Sander den Hertog, Dirk Post and Math Pluis at Spanbeton gave a good motivation to do the job, also the other colleagues always were interested and helpful. The advice of Joost Walraven, Cor van der Veen and Pierre Hoogenboom at Delft University was of great importance for the scientific level of the master thesis. Especially the debates with Pierre Hoogenboom about fundamental mechanical issues were very interesting. I will thank them all for their input and help.

For the Dutch reader a translation of the abstract, conclusions and recommendations is included in this report.

Evert van Vliet
Koudekerk aan den Rijn, January 2012

Samenvatting

In scheve bruggen treedt torsie op, wat leidt tot substantiële hoeveelheden wapeningsbeugels. Minalu heeft reeds onderzoek gedaan naar torsie in deze scheve brugdekken met behulp van verschillende typen eindige elementen modellen. De vraag die nog onbeantwoord is en de hoofdvraag van dit onderzoek vormt, is het moment waarop werkelijk torsiescheuren ontstaan en de wapening functioneel wordt.

De focus ligt op een scheef brugdek met een kruisingshoek van 45 graden omdat daarin de grootste torsiemomenten optreden. Zijdelings is ook een recht brugdek geanalyseerd, de torsiemomenten in een recht brugdek zijn namelijk altijd lager dan in een scheef brugdek. De belastingen volgens de Eurocode 1991-2 zijn gebruikt. Twee belangrijke belastingsconfiguraties voor torsie en dwarskracht zijn onderzocht: een configuratie die dagelijks bij Spanbeton wordt gebruikt en een configuratie ontwikkeld door Minalu.

Er is een poging gedaan om het gehele brugdek fysisch niet-lineair te modelleren met ATENA 3D om daarmee torsie-effecten te kunnen analyseren. Dat bleek met de huidige stand van de techniek onmogelijk. Daarom is een vereenvoudigde modellering ontwikkeld waarmee de spanningstoestand en scheurvorming in de eerste ZIP-ligger kunnen worden gesimuleerd. Bij het simuleren van torsiespanningen in een 3D model blijkt het belangrijk te zijn om kwadratische elementen te gebruiken om correcte schuifspanningen te verkrijgen. Uit dat model volgt, ondanks tekortkomingen in het model, duidelijk dat er een groot ongescheurd gebied in de ligger aanwezig is in de uiterste grenstoestand.

Om zekerheid te hebben over de juistheid van het computermodel kunnen de hoofdspanningen in de ligger worden gecontroleerd, dit is gedaan voor de uiterste grenstoestand. De spanningen door voorspanning, het eigen gewicht en het gewicht van het natte dek kunnen met handberekeningen worden bepaald. De spreidingsberekening kan worden uitgevoerd met eindige elementen methoden. Scia Engineer (orthotrope plaat) en ATENA 3D (volume elementen) zijn gebruikt voor deze berekening. Vooral de bepaling van de torsiemomenten uit ATENA door een analyse van de rotaties is interessant. Uit deze berekeningen volgen torsiemomenten, buigende momenten en dwarskrachten.

De hoofdconclusie van dit onderzoek is dat in uiterste grenstoestand geen scheurvorming optreedt in het einde van de beschouwde ligger in het scheve brugdek. Dat betekent dat alleen minimale wapening hoeft worden toegepast en dat de volledige torsiestijfheid in berekeningen kan worden gebruikt. Tot slot is er een praktische methode gepresenteerd om ook hoofdspanningen in andere ZIP brugdekken te controleren.

Conclusies

1. Het is onmogelijk om een gehele brug fysisch niet-lineair met volume-elementen te modelleren. Een grove schatting is dat dit over achttien jaar wel mogelijk is. Het is nu wel mogelijk om de brug lineair elastisch te modelleren met grove lineaire of kwadratische elementen. Door deze modellering is er slechts één element aanwezig over de dikte van het lijf. Torsieschuifspanningen worden in deze grove elementen niet correct berekend. Over de dikte van het lijf zijn minimaal drie kwadratische elementen nodig om accurate torsieschuifspanningen te verkrijgen (Hoofdstuk 4).

2. Het is mogelijk om voor één ligger een nauwkeurig fysisch niet-lineair model te ontwikkelen. In dit model kunnen scheurvorming en scheurwijdtes worden geanalyseerd. Het realistisch aanbrengen van de belasting op deze ligger is moeilijk. In theorie kunnen de elastische

vervormingen, gevonden met het lineair elastische model van de gehele brug, aangebracht worden op de ligger. Het accuraat aanbrengen van deze vervormingen vergt ten eerste veel tijd. Daarnaast ontstaan door het lokaal aanbrengen van de opgelegde vervormingen en onvolkomenheden in de modellering onjuiste spanningen in het model. Het ontwikkelde model geeft ondanks de onvolkomenheden een goede indruk van de aanwezige ongescheurde zone in de ligger (Hoofdstuk 5).

3. Het benaderen van de torsieschuifspanningen in de ligger ter hoogte van het zwaartepunt middels een grove handberekening leidt tot een overschatting in de orde van 40%. Dat komt doordat in de gebruikte doorsnede voor de handberekening de verdeling van de phi-heuvel anders is dan in de echte doorsnede. In de echte doorsnede heeft de phi-heuvel maxima in de verdikking in het lijf en in de onderflens waardoor schuifspanningen naar die zones wordt getrokken. Hierdoor wordt de schuifspanning ter hoogte van het zwaartepunt substantieel verlaagd. Scia Engineer kan gebruikt worden om de schuifspanningen te bepalen waarbij een voldoende fijn net moet worden gebruikt (Hoofdstuk 6).

4. Uit de bepaalde rotaties van de ligger in het lineair elastische volumemodel van de gehele brug kunnen de optredende torsiemomenten worden bepaald. Uit de analyse volgt dat het torsiemoment niet door verhinderde welving (normaalspanningen) maar vooral door zuivere torsie (schuifspanningen) wordt gedragen. Alleen in de zone rond de oplegging heeft verhinderde welving enige invloed, de grootte van de invloed is afhankelijk van de aanwezigheid van een einddwarsdrager (Hoofdstuk 7).

5. Voor de spreidingsberekening kunnen een orthotrope plaat model (Scia Engineer) en een volume model (ATENA 3D) worden gebruikt. Vergelijking van de uitkomsten uit deze modellen laat zien dat de dwarskrachten goed overeen komen, maar dat de torsiemomenten substantiële verschillen vertonen. Dit is opmerkelijk omdat het hier lineair elastische modellen betreft waarvan verwacht zou worden dat ze beter overeen zouden komen (Hoofdstuk 7).

6. In het rapport zijn twee belastingsgevallen parallel uitgewerkt. Het blijkt dat voor het doen van de plastische spanningscontrole beide belastingsgevallen vergelijkbare hoofdspanningen geven. Bij het uitvoeren van een elastische spanningscontrole geeft het belastingsgeval van Minalu de maatgevende hoofdspanningen (Hoofdstuk 7).

7. Uit de berekening van de hoofdtrekspanningen in de eerste ZIP ligger van het beschouwde scheve brugdek volgt dat er in de uiterste grenstoestand een grote ongescheurde zone aanwezig is. Belangrijk is dat hierbij de verstoorde aanhechtzone goed gecontroleerd dient te worden, afhankelijk van de toegestane hoeveelheid plastische herverdeling van de spanningen (Hoofdstuk 7). Impliciet betekent deze conclusie ook dat in de gebruikstoestand geen scheuren zullen optreden. Ook in de rechte brug zal er een soortgelijke ongescheurde zone zichtbaar zijn omdat daarin vergelijkbare dwarskrachten, maar lagere torsiemomenten optreden dan in een scheve brug (Hoofdstuk 5).

Aanbevelingen

A. Dit project is gestart met een tijdrovende fysisch niet-lineaire computermodellering. Het is belangrijk om bij een soortgelijk onderzoek eerst te starten met handberekeningen en lineair elastische computermodellen. Indien nodig kan daarna overgegaan worden naar fysisch niet-lineaire modellen.

B. De hoofdspanningen zijn in dit onderzoek vergeleken met de statische treksterktes van beton. Het aspect vermoeiing van beton is daarbij niet beschouwd. In het geval van een vermoeiingsberekening wordt de toelaatbare treksterkte gereduceerd en moeten ook andere belastingsconfiguraties worden gebruikt. Deze berekening moet nog worden uitgevoerd om te zien of ook daaruit geconcludeerd kan worden dat de ligger een grote ongescheurde zone bevat.

C. Het gepresenteerde onderzoek biedt toekomstperspectieven om de hoeveelheid wapening in de ongescheurde zone te reduceren tot het wettelijke minimum. Uit een onderzoek van één brug met bepaalde geometrische eigenschappen kan geen wetmatigheid worden ontleend. Wel kan een mogelijke procedure worden gepresenteerd om voor elke brug (gebruik makend van ZIP-liggers) te bepalen of het voordeel gebruikt kan worden.

   Mogelijke procedure:
   1) Er dient een spreidingsberekening uitgevoerd te worden waarbij de torsiestijfheid niet wordt gereduceerd. De in het rapport gepresenteerde belastingsgevallen dienen minimaal in beschouwing te worden genomen.
   2) De voorspanning kan berekend worden op de gebruikelijke wijze in de gebruikstoestand. Belangrijk is dat er daarbij in de einden van de ligger geen buigscheuren bovenin de ligger optreden.
   3) De lengte van het ongescheurde gebied in de uiterste grenstoestand kan bepaald worden door te bepalen bij welk buigend moment de treksterkte van beton wordt overschreden. Veilig is om geen trekspanningen toe te laten voor deze berekening. Het is mogelijk dat voor deze berekening het belastingsgeval om het maximale moment in de ligger te bepalen maatgevend is.
   4) De schuifspanningsverdeling door torsie in het profiel kan worden bepaald door met Scia Engineer de doorsnede te analyseren. Het is conservatief om dit met een handberekening te bepalen. De torsieschuifspanningen kunnen plastisch of elastisch verdeeld worden. De schuifspanningen door dwarskracht kunnen op de gebruikelijke manier worden uitgerekend. Deze spanningen kunnen elastisch of plastisch worden gecombineerd.
   5) De optredende normaalspanningsverdeling varieert over de hoogte van de ligger. Belangrijk is de normaalspanning ter hoogte van het zwaartepunt. De hoogte van het zwaartepunt varieert voor de enkele ZIP-ligger en het samengestelde systeem. De maatgevende hoogte ligt ergens tussen deze beide grenzen. Als gekozen wordt om te controle uit te voeren in het zwaartepunt van de ZIP ligger moet rekening gehouden worden met een reductie van de normaalspanning door buigende momenten die optreden in combinatie met het samengestelde zwaartepunt. Dit geldt ook als gekozen wordt om de controle uit te voeren in het samengestelde zwaartepunt Figure 10-17). In dit onderzoek was de reductie maximaal 6%. Daarnaast moet het gunstige effect van de voorspanning in de uiterste grenstoestand moet worden gereduceerd door het te vermenigvuldigen met een factor 0.9.
   6) In het ongescheurde gebied kunnen voor de gevonden schuifspanningen en normaalspanningen de hoofdspanningen worden berekend op de hoogte van het maatgevende zwaartepunt. Als de gevonden spanningen onder de gestelde grenzen liggen kan worden geconcludeerd dat de ligger inderdaad ongescheurd is en de aanname voor volledige torsiestijfheid in het orthotrope plaat model juist was. De minimale wapening voor dwarskracht en torsie dienen te worden toegepast volgens de Eurocode.

Abstract

In skew bridges torsion occurs. This leads to a substantial amount of reinforcement stirrups. Minalu already did research to torsion in bridge decks with different types of finite element models. The question when torsion cracks will really occur is still unanswered. This question is the main subject of this research.

The focus of the research is on a skew bridge with a skew angle of 45 degrees. In that bridge the largest torsional moments will occur. Beside that also a straight bridge is analysed, the torsional moments in a straight bridge are always lower than in a skew one under the same loading. The loads of Eurocode 1991-2 are used. Two important load configurations governing for torsional moments and shear force are used: a configuration which is used in daily practice at Spanbeton and a configuration developed by Minalu.

An attempt is made to model the whole bridge including physically non-linear behaviour with the program ATENA 3D to analyse the torsion effects. With the current state-of-the-art modelling technology that appeared to be impossible. For that reason a simplified model is developed to simulate the stress state and cracking in one ZIP girder. It was concluded that it is important to use more quadratic elements over the thickness of the web to obtain correct torsion shear stresses. From the simplified model it is concluded that, despite some shortcomings, clearly a substantial length at the ends of the girder is uncracked.

To be sure that the computer model is correct a calculation of the principal stresses is carried out at the ultimate limit state. The stresses due to prestressing, own weight and the weight of the fresh poured concrete can be calculated by hand. The calculation of the force distribution of the loads on the deck can be carried out using finite element methods. Scia Engineer (orthotropic plate model) and ATENA 3D (volume elements) are used for this calculation. Especially the determination of the torsional moments from ATENA by using an analysis of the rotations is interesting. This calculation results in the torsional moments, bending moments en shear forces acting on the ends of the girder.

The main conclusion of this research is that in ultimate limit state no cracking will occur in the end of the considered girder in the skew bridge. This means that only the minimal shear reinforcement must be applied and the full torsional stiffness can be used in finite element calculations. A practical method to check this for other bridges using ZIP-girders is proposed.

Contents

1 Introduction

1.1 Background

As mentioned in the preface the cracking behaviour of a ZIP girder is the main topic of this research. The loads in a ZIP bridge system are mainly carried by longitudinal and transverse bending moments but also torsion can also be used to satisfy the equilibrium. Normally in that case a high amount of torsion reinforcement must be applied. In daily practice Spanbeton uses an orthotropic two dimensional plate model to determine the load distribution in a bridge. An interesting question is which torsion stiffnesses are allowed and safe for Serviceability Limit State (SLS) and Ultimate Limit State (ULS).

Logical reasoning results in the following chain of events that occur during loading. In the beginning the beams are uncracked in SLS. In this stage the reinforcement stirrups are not stressed, so unnecessary. After this phase the cracking phase is reached. In this phase the stiffness is reduced and therefore the torsional moments (and related shear stress) will decrease. Depending on the amount of cracks the forces will be carried by longitudinal and transverse moments. It is safe to design the bridge using only bending moments, already stated by Minalu[1]. However, it will be beneficial to use the torsion for equilibrium when that is available.

So, fundamentally the real torsional stiffness is directly related to the amount of cracks present. When no cracks occur the entire stiffness will be available. If cracks do occur a reduction is necessary. ATENA 3D contains tools for physical non-linear modeling which can be used to analyze the reduced stiffness. A finite element model will be developed to analyze this.

Note: In the first stage of the research also investigation of Compressive Membrane Action (CMA) was intended, following a recommendation of Minalu. The work done for that topic is presented in Appendix A.

1.2 Approach

Main points of research are:

1. *Literature.* Some relevant points from the report of Minalu are presented. Also the fundamental theories about torsion in plain and cracked concrete are described.
2. *Finding a working model to simulate torsion effects in the girders.* First an attempt is done to model a whole bridge including physically non-linear behaviour. This appeared to be impossible. A simplification is developed. The occurring stresses and cracking behaviour will be presented and interpreted.
3. *An analytic analysis of the principal stresses in the first ZIP girder.* The stresses in the end of the girder are investigated in detail. Hand calculations are used when possible. When this was not possible calculations with orthotropic plate (Scia Engineer) and volume element (ATENA 3D) models are used.

[1] Minalu, Kassuhun K. (2010), *Finite element modelling of skew slab-girder bridges.* Page 114.

2 Torsion

2.1 Introduction

In bridges torsion occurs. The amount of torsion is dependent on many factors but the most important one for this thesis is the skew angle of the bridge which was investigated by Minalu. In his thesis a comparison was made between different types of FEM but also some conclusions were written about torsion effects.

2.2 Relevant parts from report of Minalu[2]

2.2.1 Considered cases

Minalu investigated the cases presented in Table 2-1 with different modelling techniques.

Number	End diaphragm beams	Girders
a.	Consider stiffness	Full torsional stiffness in SLS
b.	Consider stiffness	Reduced torsional stiffness in ULS
c.	Disregard stiffness	Full torsional stiffness in SLS
d.	Disregard stiffness	Reduced torsional stiffness in ULS
e.	Consider stiffness	Disregard torsional stiffness
f.	Disregarding stiffness	Disregard torsional stiffness

Table 2-1 Performed studies by Minalu

2.2.2 Relevant conclusions

The maximum torsional moment is near the obtuse corner. A governing load case is placing the first design lane load and the axle loads at the first notional lane and leaving the other lanes unloaded.

Ignoring the torsional stiffness of the girders had very little influence on the maximum bending moments. However, detailing rules to avoid excessive cracking should be consulted (Eurocode 1992-1-1).

A linear elastic 3D model gives tension normal force in the transverse direction of the deck. When cracking is included the tensile membrane force becomes a compressive force. Therefore linear elastic analysis is not appropriate to determine the CMA in the deck.

Live load moments in girders of skew bridges are generally smaller than those in straight bridges of the same span and deck width. On the contrary the torsional moments in the obtuse corner of the bridge and the transverse moments in the deck increases with skew angles.

End diaphragm beams decrease the bending and twisting moments in the girders and the deck. However, this reduction was insignificant as compared to the torsional moments occurring in the diaphragm beams.

2.2.3 Relevant recommendations

End diaphragm beams could be excluded from the finite element model. They can be designed with minimum reinforcement.

For small skew angles the presence of end diaphragm beams results only in a small reduction of the longitudinal bending moments and the torsions for vertical loading. The concrete diaphragms could be replaced by simple non-structural elements. Detailed investigation of the consequences is required.

[2] Minalu, Kassuhun K. (2010), *Finite element modelling of skew slab-girder bridges*

2.3 Theory[3,4]

2.3.1 Uncracked beam

In an uncracked beam stresses develop as shown in Figure 2-1. At the middle of the longitudinal edges the maximum stresses occur.

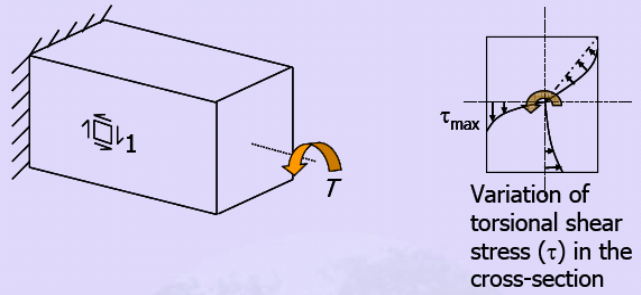

Figure 2-1 Stresses in uncracked beam subjected to torsion

The occurring shear stresses can be expressed in principal stresses using Mohr's circle as shown in Figure 2-2.

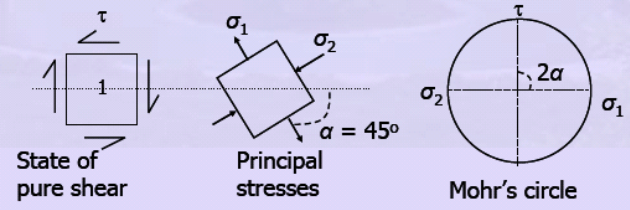

Figure 2-2 State of stresses

These principal stresses explain the crack pattern. Cracks occur perpendicular to the direction of the tensile stresses when the tensile strength is reached. In the uncracked state the stress carried by steel is negligible. After cracking there is redistribution of stresses between concrete and steel.

Saint Venant presented a theory for torsion. In this theory the cross-section rotates and warps (function ψ). There is a differential equation for warping available. A more practical method to calculate shear stresses and torsional stiffness in rectangular cross sections is to use the standardized table, Table 2-2.

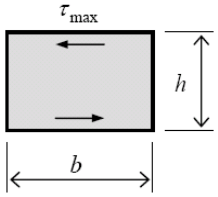

Figure 2-3 Rectangular cross section

[3] Sengupta, dr. Amlan K. et. al. *Prestressed concrete structures*
[4] Hoogenboom, P.C.J. (2010), *Aantekeningen over wringing*

$\frac{b}{h}$	$\frac{I_w}{bh^3}$	$\frac{I_p}{bh^3}$	$\frac{M_w}{\tau_{max}bh^2}$	$1000\frac{C_w}{b^3h^3}$	$\frac{100\ B}{\sigma_{max}b^2h^2}$
1,0	0,141	0,167	0,211	0,134	0,368
1,2	0,166	0,203	0,221	0,352	0,565
1,4	0,187	0,247	0,230	0,838	0,987
1,6	0,204	0,297	0,237	1,418	1,37
1,8	0,218	0,353	0,243	2,000	1,69
2,0	0,229	0,417	0,249	2,540	1,94
2,5	0,250	0,604	0,261	3,640	2,35
3,0	0,264	0,833	0,271	4,416	2,59
4,0	0,281	1,417	0,288	5,354	2,82
5,0	0,292	2,167	0,299	5,865	2,90
10,0	0,314	8,417	0,323	6,642	2,94
50,0	0,331	208,417	0,329	6,931	2,82
∞	0,333	∞	0,333	6,944	2,778

Table 2-2 Properties of rectangular cross-sections (Roark's formulas for stress and strain)

Is it allowed to resist torsion only with plain concrete when that's theoretically possible? In NEN-EN 1992-1-1 the following is stated in 6.3.1.2:
Where, in statically indeterminate structures, torsion arises from consideration of compatibility only, and the structure is not dependent on the torsional resistance for its stability, then it will normally be unnecessary to consider torsion at the ultimate limit state. In such cases a minimum reinforcement, given in Sections 7.3 and 9.2, in the form of stirrups and longitudinal bars should be provided in order to prevent excessive cracking.

2.3.2 Cracked beam

First cracks are visible at the longitudinal edge of the (rectangular) cross-section. Under pure torsion the cracks follow the stresses under 45˚. The formation of cracks is visualised in Figure 2-4. In a real structure always interaction occurs and the crack pattern is more complicated.

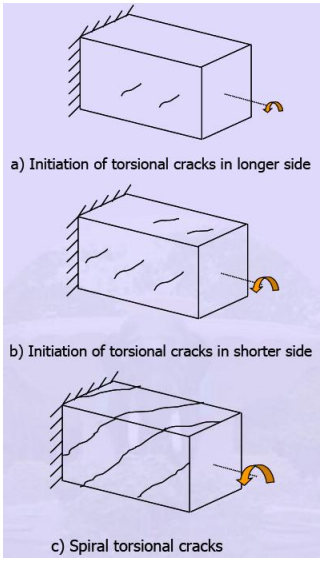

Figure 2-4 Development of cracks under torsion

When the girder is cracked it can be considered as an three-dimensional truss. The steel (longitudinal reinforcement and stirrups) forms the tension elements and the concrete compressive elements the struts (Figure 2-5). The maximum torsion capacity is bounded by the capacity of the concrete struts or the steel tensile elements.

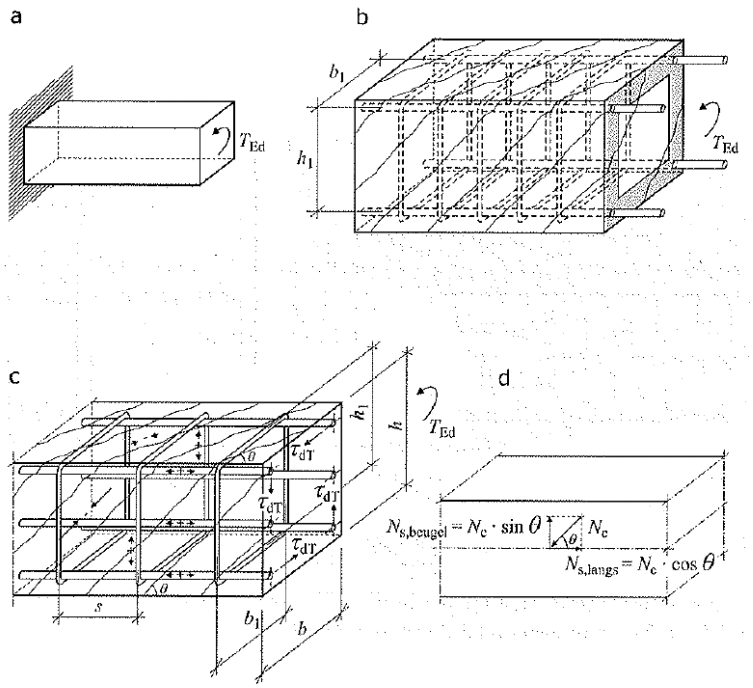

Figure 2-5 Three-dimensional truss model for torsion

2.3.3 Influence prestressing

The level of prestressing has a positive effect on the level that torsion cracks occur (Figure 2-6). The normal stresses can also be incorporated in the calculation of the principal stresses as shown in Figure 2-7. Consequently, the cracking direction will change.

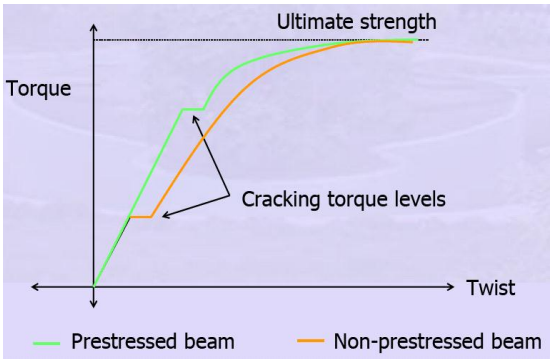

Figure 2-6 Schematized behaviour of concrete beam under torsion load

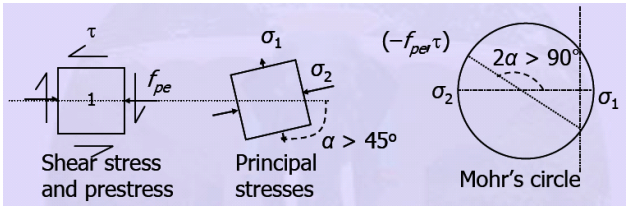

Figure 2-7 State of stresses in a prestressed beam

After cracking the crack width of a spiral crack is low. Thus the aggregate interlock is larger as compared to a non-prestressed beam under the same twisting moment. Zia and McGee showed that the contribution of the concrete to the ultimate torsional strength is much larger for prestressed than for non-prestressed beams.[5] They also present formulas to calculate the beneficial effect of the prestressing.

[5] Zia and McGee (march-april 1974), *Torsion design of prestressed concrete,* , PCI Journal, page 46 – 65

2.3.4 Interaction

2.3.4.1 Torsion and shear

For the interaction between torsion and shear a formula is presented in the NEN-EN 1992-1-1 and NEN-EN 1992-2 to sum up the effects. Both shear and torsion are calculated separately and combined in:

- Only minimum reinforcement:

$$\frac{T_{Ed}}{T_{Rd,c}} + \frac{V_{Ed}}{V_{Rd,c}} \leq 1{,}0$$

- Maximum capacity concrete:

$$\frac{T_{Ed}}{T_{Rd,max}} + \frac{V_{Ed}}{V_{Rd,max}} \leq 1{,}0$$

2.3.4.2 Torsion and bending

In the Eurocodes (mentioned in 2.3.4.1) no demands are set for the interaction between torsion and bending. However, literature is available , named Skew Bending Theory, which shall be briefly presented. [6]

Starting point of the theory is that torsion and bending moments can be combined to one resultant moment. This moment causes compression and tension in a planar surface inclined to the axis of the beam, see Figure 2-8.

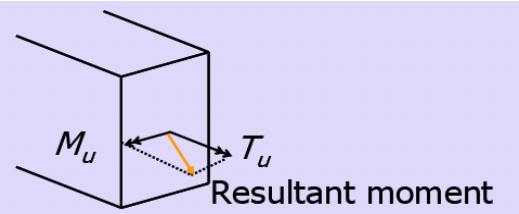

Figure 2-8 Torsional and bending moments combined

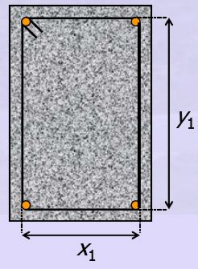

Figure 2-9 Dimensions of closed stirrup

The modes of failure are explained based on the relative magnitudes of the flexural moment (M_u) and torsional moment (T_u) in the ultimate limit state. For each mode an idealised pattern of failure is presented with the resultant compression (C_u) and tension forces (T_u).

[6] Rangan, B. V. and Hall, A. S. (March 1975), *Design of Prestressed Concrete Beams Subjected to Combined Bending, Shear and Torsion*, ACI Journal, American Concrete Institute, Vol. 72, No. 3, page 89 – 93

For design the following steps are important:

1. Calculate equivalent moment M_t from T_u:

$$M_t = T_u \cdot \sqrt{1 + \frac{2D}{b}}$$

2. For design of primary longitudinal reinforcement (bottom) equivalent moment M_{e1} is calculated (mode 1 failure, Figure 2-10):

$$M_{e1} = M_u + M_t$$

3. When $M_t > M_u$ (mode 2 failure, Figure 2-11)

$$M_{e3} = M_t \cdot \left(1 + \frac{x_1}{2e}\right)^2 \left(\frac{1 + \frac{2b}{D}}{1 + \frac{2D}{b}}\right) \; with \; e = \frac{T_u}{V_u}$$

4. When $M_t > M_u$ (mode 3 failure, Figure 2-12):

$$M_{e2} = M_t - M_u$$

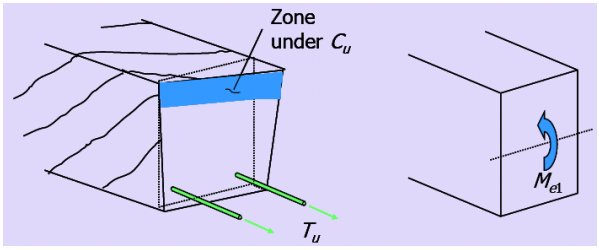

Figure 2-10 Mode 1 failure

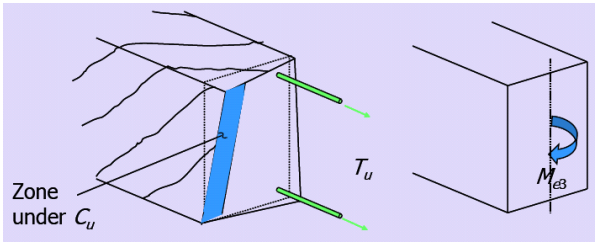

Figure 2-11 Mode 2 failure

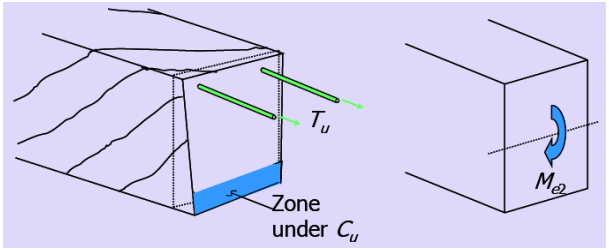

Figure 2-12 Mode 3 failure

3 Description of bridge

3.1 Geometry

The bridges that will be investigated are visualized in Figure 3-1, the axis for the models of the complete bridges are presented in the top view. A cross section is presented in Figure 3-2. The first ZIP is the interesting girder in the research, this girder is shaded grey in the top view.

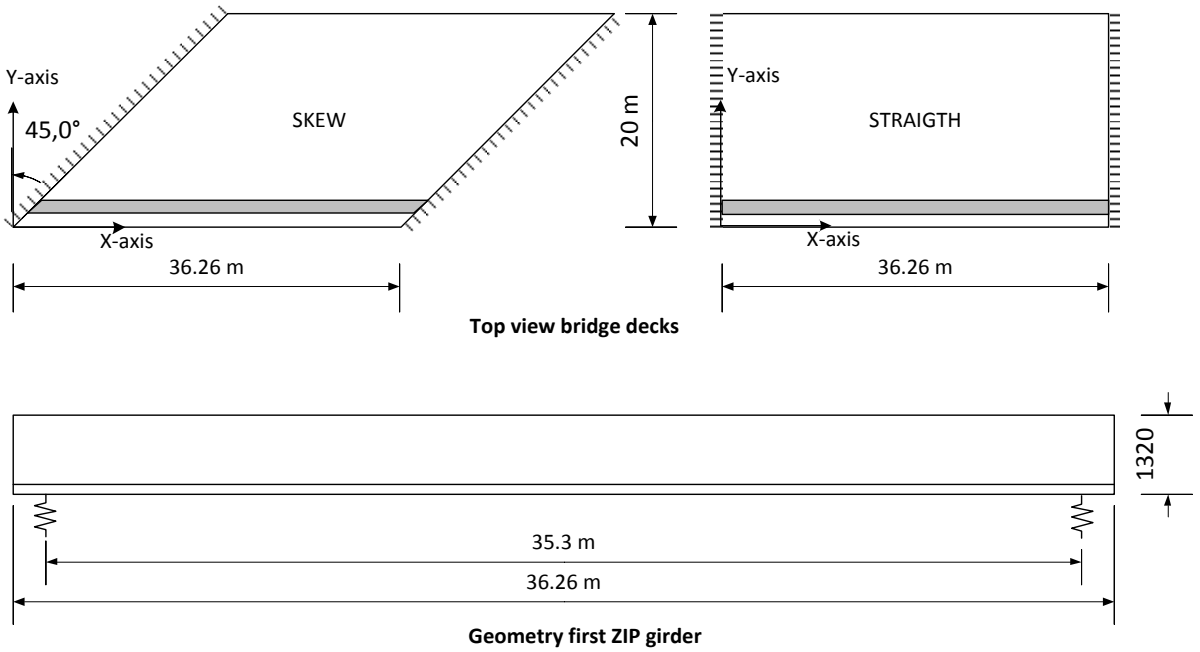

Figure 3-1 Geometry of bridges

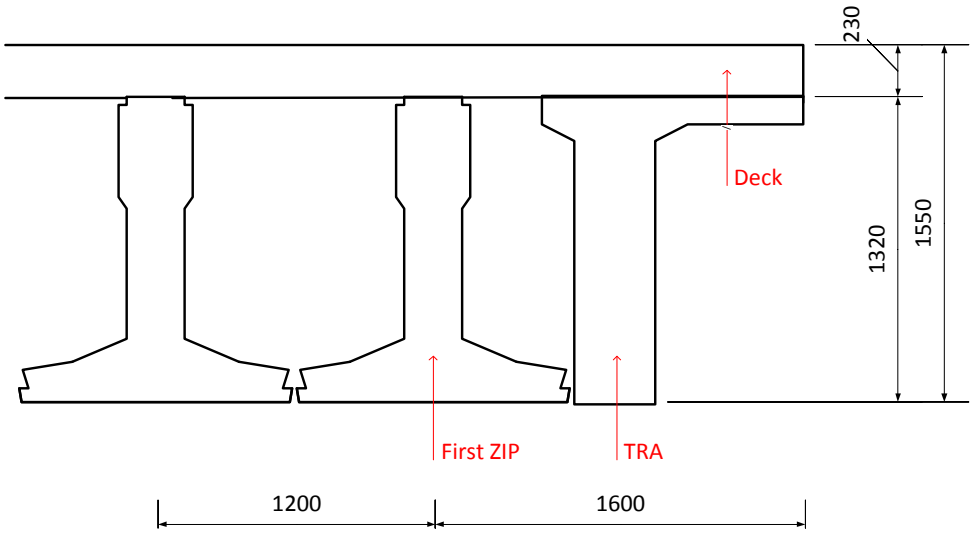

Figure 3-2 Cross-section edge of bridge (simplified height of deck)

3.2 Important properties

Girders:

Concrete quality:	C53/65
E-modulus:	38000 MPa
Poisson's ratio:	0.2

Deck:

Concrete quality:	C28/35
E-modulus:	16000 MPa (half of the stiffness in both directions)
Poisson's ratio:	0.2

Spring stiffness (rubber supports): 1130 MN/m (calculation presented in thesis Minalu[7])

In the calculation full torsional stiffness is used and half of the normal stiffness of the deck (in both directions). This is done because it is impossible to model the bridge else in ATENA. The girder will consequently take larger part of the torsional moment, this is conservative. Later in the project it was noted that for the different longitudinal and transversal bending stiffnesses in the deck a trick can be used using smeared reinforcement in the stiffest direction, this is not applied.

3.3 Construction stages

Important for the analysis is the fact that the bridge will be constructed in several stages:

A. The ZIP-girder is loaded by own weight and prestressing and the fresh poured concrete of the deck.
B. The fresh concrete is hardened and the ZIP-girders forms a system with the deck. This system bears the permanent and variable loads applied on the bridge deck.

3.4 Loads construction stage A

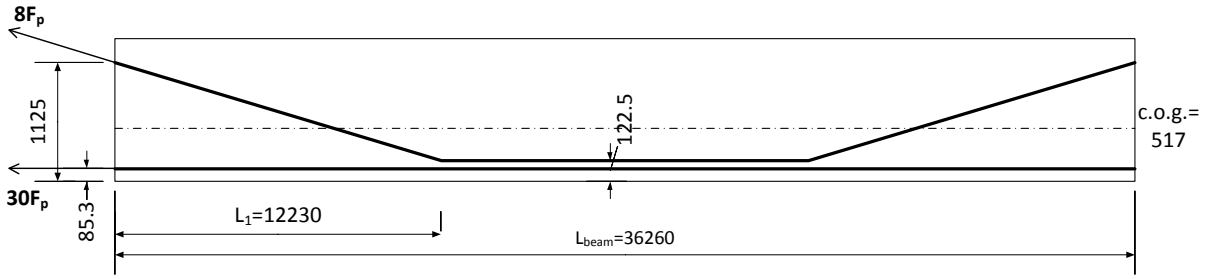

Figure 3-3 Configuration of prestressing strands

Prestressing force:	$161 < F_p < 187$ kN
Dead weight girder:	14.25 kN/m
Fresh poured concrete:	6.1 kN/m

3.5 Loads construction stage B

3.5.1 Permanent loads on deck

Edge load

- Handrail: 2.0 kN/m. Placed 0.17 m from the edge.
- Strip grazing: 0.4x25=10 kN/m^2, uniformly distributed on a width of 380 mm.
- Safety barrier: 1 kN/m. Placed at 0.973 m from edge.
- Footpath: 0.5x(0.215+0.23)x25=5.56 kN/m^2. Placed at 0.38 to 1.145 m from edge.

Asphalt

A layer of 140 mm asphalt is provided for the whole carriage way: 0.14x23=3.22 kN/m^2.
This is applied from 1400 mm to 18600 mm.

[7] Minalu, Kassuhun K. (2010), *Finite element modelling of skew slab-girder bridges*. Page 26.

3.5.2 Variable loads on deck; Load Case Spanbeton

The loads of Eurocode 1991-2 are applied to make a realistic calculation and comparison with the daily practice of calculating ZIP-systems. Spanbeton uses this combination in daily practice to get the governing combination for shear and torsion.

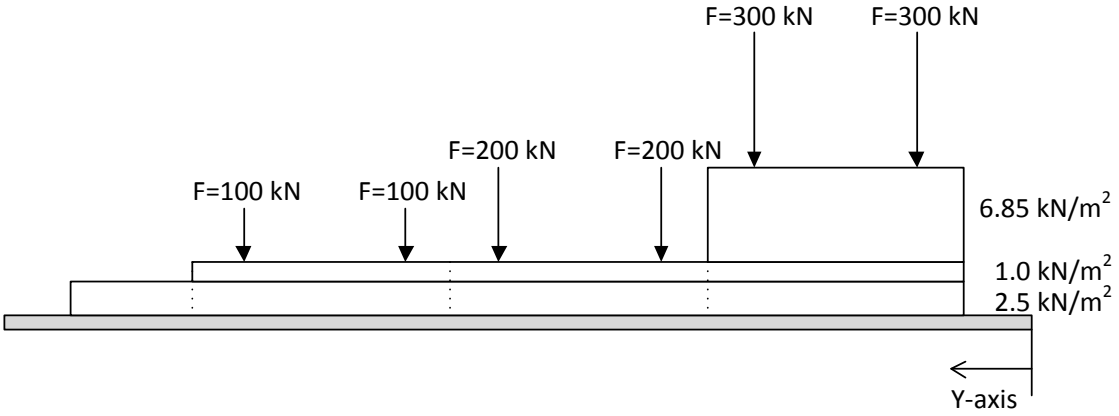

Figure 3-4 Lane loads on deck for the LC of Spanbeton

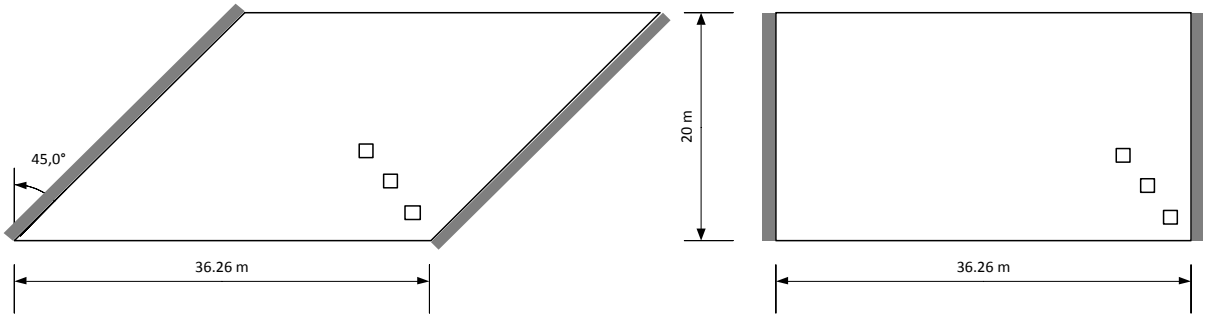

Figure 3-5 Top view of Spanbeton load configuration

UDL whole field with remaining area

UDL: 2.5 kN/m^2. Y = 1400-18600 mm from edge.

UDL whole field without remaining area (extra)

UDL: (1.4x2.5-2.5)=1.0 kN/m^2. Y = 1400-16400 mm from edge.

UDL slow lane (extra)

UDL: (10.35-3.5)=6.85 kN/m^2. Y = 1400-4400 mm from edge.

Axle loads

- Load system: Wheel load 0.5x300/0.4^2=937.5 kN/m^2. Centre of system Y = 2900 mm from edge.
  Longitudinal position 3000 mm from right edge (straight)
  Longitudinal position 6090 mm from right edge (skew)
- Load system: Wheel load 0.5x200/0.4^2=625 kN/m^2. Centre of system Y = 5900 mm from edge.
  Longitudinal position 7000 mm from right edge (straight)
  Longitudinal position 12390 mm from right edge (skew)
- Load system: Wheel load 0.5x100/0.4^2=312.5 kN/m^2. Centre of system Y = 8900 mm from edge.
  Longitudinal position 11000 mm from right edge (straight)
  Longitudinal position 18690 mm from right edge (skew)

3.5.3 Variable loads on deck; Load Case Minalu

Minalu investigated which load configuration, based on loads from Eurocode 1991-2, gives the largest torsional moments. That load is presented here.

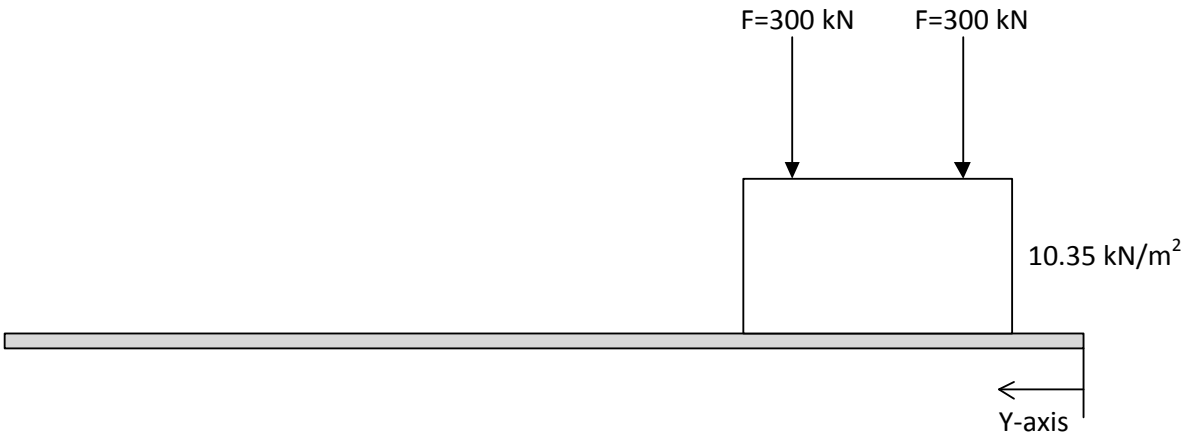

Figure 3-6 Lane loads on deck for the LC of Minalu

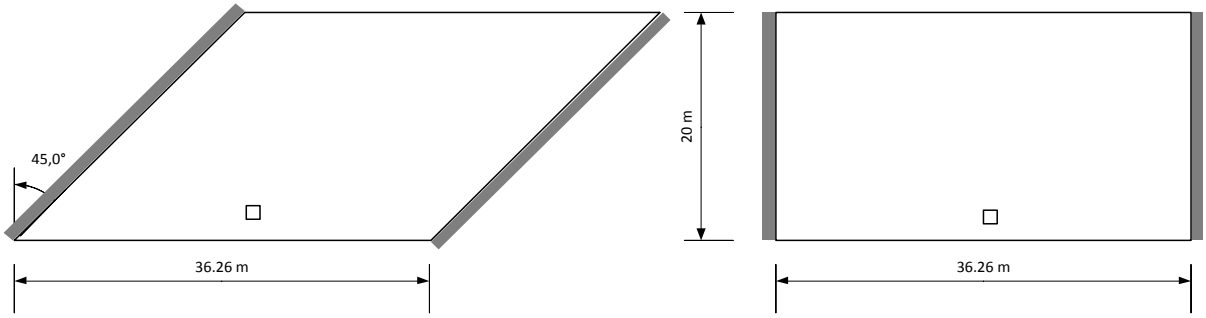

Figure 3-7 Top view of Minalu load configuration

UDL slow lane

UDL: 10.35 kN/m^2. Y = 1400-4400 mm from edge.

Axle loads

Load system: Wheel load 0.5x300/0.4^2=937.5 kN/m^2. Centre of system Y = 2900 mm from edge.
Longitudinal position 18130 mm from right edge (straight)
Longitudinal position 18130 mm from right edge (skew)

3.6 Load combinations

Three load combinations are interesting:

1. Construction stage A: Dead weight and prestressing
2. Construction stage A: Dead weight, prestressing and weight fresh poured concrete
3. Construction stage B: Dead weight, prestressing, weight fresh poured concrete, permanent load on deck.
4. Construction stage B: Dead weight, prestressing, weight fresh poured concrete, permanent and variable load Spanbeton on deck.
5. Construction stage B: Dead weight, prestressing, weight fresh poured concrete, permanent and variable load Minalu on deck.

3.7 Load factors

Serviceability Limit State (SLS)

- All loads: γ=1.0

Ultimate Limit State (ULS)

- All loads (except prestressing): γ=1.35
- Prestressing load: γ=0.9

3.8 Standard Spanbeton calculation

The bridges are calculated using the standard procedure of Spanbeton. Doing this calculation provides insight in the main issues making a calculation of a ZIP bridge system. Because it was intended to do a whole physically non-linear analysis all reinforcement is calculated. The reason to use the Spanbeton procedure is to be able to make a comparison with the reinforcement that would result from their standard procedure.

Minalu investigated a load model which results in the largest torsional moment[8]. To check if this will really give differences a comparison is made between a calculation using the Spanbeton configuration and the configuration of Minalu (Appendix B). Only for the TRA-girder the load configuration of Minalu gives a higher amount of shear reinforcement, but due to the governing fatigue calculation no problems will occur. For the ZIP-girders the Spanbeton load configuration is sufficient. A explanation for this is that the load configuration of Minalu results in higher torsional moments than the load configuration of Spanbeton, but those moments are accompanied by lower shear forces than found with the load configuration of Spanbeton.

[8] Minalu, Kassuhun K. (2010), *Finite element modelling of skew slab-girder bridges.* Page 33.

4 A physical non-linear model of the bridge

4.1 Introduction

The first idea 'a physically non-linear model of the complete bridge' is investigated. Both compressive membrane action (CMA) and torsion can be analysed. Cervenka Consulting believed that it was possible to do this job and gave a lot of help during the process. At the end it appeared to be impossible due to a lot of problems and due to lack of time. The occurring problems are briefly described.

The main reason to make a physical non-linear model is that the effect of cracking on the load distribution in the bridge is visible. When a girder in a skew bridge cracks due to torsion the redistribution over the other beams is be visible.

4.2 Bug in the program

In the first week a bug was discovered in the F.E. program. The program has the possibility to copy macro-elements which saves a lot of time. In one run also the applied loads, supports and springs can be copied. The found bug result in: "when the macro-elements were copied including the springs an error occurred and the total file was unusable". This occurred when the first finite element model was nearly finished.

4.3 Behaviour of individual girders

Dobromil Pryl, employee of Cervenka Consulting advised to model the bridge using as many shell elements as possible to have good accuracy with minimal degrees of freedom. For the end diaphragm beam tetra elements could be used. Using this advice the individual girders where analysed to investigate their behaviour. Furthermore it was found that the CEB-FIB bond model for the prestressing strands as modelled in ATENA will not give correct results, the Bigaj model works better. Applying the prestressing force results in cracks at the end of the girders, as expected.

Unexpected is cracking in in the top of the TRA-girders. Some refinements and other choices of elements types did not help. These cracking is not relevant but increases the calculation time, because the number of iterations increases. This phenomena is not further investigated.

4.4 Construction stages

For linear-elastic calculations the stresses can be simply added to each other. In practice a 'distribution calculation' will be made for the deck loads (using an orthotropic plate model, construction stage B). The results of that calculation are input for a 'detail calculation' in which the effects of the prestressing, dead weight and weight of the fresh poured concrete of deck (construction stage A) also are considered. When a physically non-linear material behaviour is used it is impossible to sum up the stresses because the principle of superposition is only applicable for linear elastic calculations.

The stresses of construction stage A can be applied by loading the girders separately. After that the deck must be present to bear the permanent and variable loads on the deck. It is possible to simulate this in ATENA by using the option 'construction stages'. However, there are limits to this option. First, applying this possibility of the program makes it more difficult to find the sources of errors. Secondly, the optimum is to have large shell-elements for the deck and some finer volume-elements for the girders. The program connects these elements by master-slave relations. Only the larger elements can be the master-element. It would be clear what happens when in the first stage only the girders are active. In that case the master-elements are not available and the program will not run. There is a dummy solution available to avoid this problem: for the deck elements a variable material stiffness can be used. In construction stage A the stiffness of the deck is set very low, in construction stage B the stiffness is adapted to the normal stiffness.

4.5 Eccentricity of TRA

The prestressing of the ZIP-girders will not give horizontal deformations (in theory). For the TRA-girder some horizontal deformation is permitted, limited by L/1000. It is very difficult to design a strand configuration that will give zero horizontal deformation, and indeed some deformation occurred. In the next stage 'pouring fresh concrete of deck' some enlargement of the horizontal deformation was visible which is not happening in practice. Perhaps the connected deck reinforcement will restrain this deformation.

When the deck is modelled with a variable stiffness (low in construction stage A and normal in construction stage B) the deck with low stiffness gives disturbances in the stress distribution of the ZIP-girders close to the edge. This is due to the different height of the centre of gravity of ZIP- and TRA-girders. This will of course occur in the stage when the deck is hardened, but not in the stage that the girders are individually prestressed. For this reason a construction stage for only the edge part of the deck was considered to avoid this problem. That idea appeared to work, but of course makes it more difficult and complex because both solutions (construction stages and variable stiffness of deck) are applied then.

4.6 Convergence and calculation time

One of the largest problems appeared to be the calculation time. Running the model linear-elastic takes already 5-10 hours using the DCG solver on a modern desktop computer. In that model no construction stages and reinforcement bars are included. For linear elastic calculations the convergence is very good, two iterations are normally needed to reach the solution. For a non-linear analysis more iterations and load steps are needed, especially when the post-cracking stage is analysed.

At the moment ATENA do not use the capacity of the modern computers with quad-core processors and 64 bit techniques. Cervenka Consulting is improving that. Due to interaction between modelling and the long time it takes to run a trial calculation no complete calculation is finished. The use of ATENA Console can speed up the calculation significantly for some problems. This is tested for the smaller models and helps indeed.

4.7 Future

The current linear elastic bridge model can be built and analysed conveniently. The non-linear analysis cannot be performed on this model because the computer memory and hard disk capacity are insufficient. Therefore, the single girder model has been built which has far less elements (Chapter 5). Nearly all of the development time has been spend on creating a good mesh and compatible loading. None of this would have been necessary if the linear elastic model of the bridge could have been nonlinearly analysed.

In paragraph 5.6.1 it is shown that the model of the complete bridge would have sufficient accuracy if each linear elastic element is replaced by approximately 18 quadratic elements. The linear elastic elements have 8 nodes each while the quadratic elements have 20 nodes each. Therefore, a nonlinear model of the bridge needs 18 x 20/8 = 54 as many nodes as the current bridge model. The structural stiffness matrix needs 54 x 54 times as much data. However, a smart solver can optimize the matrix band width to perhaps 10 times larger than the current band width. Therefore the structural stiffness matrix needs 54 x 10 = 540 times as much data.

In the future a personal computer will have more capacity. Moore's law states that computer capacity doubles each two years. In 18 years there will be 9 improvements steps of 2 years. Computers will have 2^6 = 512 times as much capacity as nowadays, which is sufficient for the physical non-linear model of the bridge.

4.8 Conclusion

All the mentioned difficulties together made the assignment to make a physical non-linear model of the bridge too complicated. Developing a 3D finite element model requires substantial training and experience, especially when physically non-linear behaviour is included. Due to all occurring side-effects the scope of the research is not clear anymore.

The bottleneck doing this large calculation is the required calculation time and the needed memory. A rough estimation is that within 18 years it is possible to do physical non-linear calculations for complete bridges.

5 Alternative modelling of torsion

5.1 Introduction

To reduce complexity a simplified procedure is developed to simulate the occurring torsion in the first ZIP-girder. This procedure contains the following steps:

1. Make a linear elastic (LE) finite element model of the bridge;
2. Analyse the occurring deformations of the first ZIP-girder;
3. Make a physical non-linear (PNL) model of one ZIP girder;
4. Apply the determined calculations on that model.

Is it valid to simulate the torsion in this way? The relation between stiffness and occurring torsion is neglected now (full torsional stiffness is used in the linear elastic model of the bridge), is that acceptable? For SLS and ULS the answer is different:

- SLS-stage. In this stage no cracking due to bending or shear will occur. For torsion effects this must be investigated, but also these cracks are not expected. In this phase the deformations of the linear elastic model of the bridge will be correct.
- ULS-stage. It is expected that in this stage cracking, sure due to bending, will occur. In that case the linear elastic model of the bridge do not predict the deformations correctly.

In the following paragraphs some important notes about the used models will be made. A detailed description is available in appendix E.

5.2 Make a linear elastic finite element model of the bridge

A linear elastic model of the bridge will be made with end diaphragm beams. Also a model without end diaphragm beams is analysed (in a later stage of research), only to analyse the differences in rotations and to be able to compare with the orthotropic plate model (in which the end diaphragm beam is neglected).

The model must describe the deformations correctly. Accurate deformations are important because they will be applied on the small model of one ZIP-girder. In appendix E a comparison is made between some different meshed girders. The girder meshed as presented in Figure 5-1 has a good balance between calculation time and accuracy. So linear elements are used in the model.

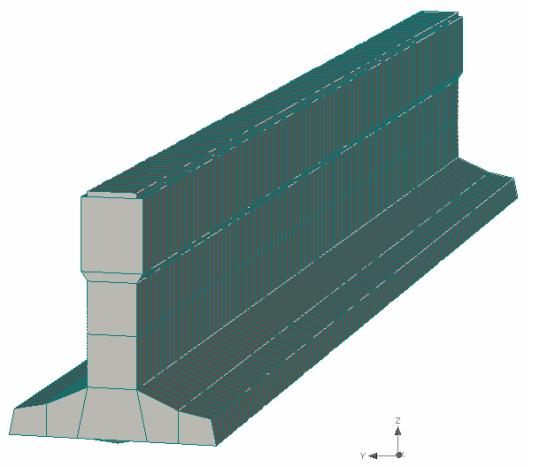

Figure 5-1 Model ZIP-girder for the linear elastic model of the bridge

The model presented in Figure 5-2 and Figure 5-3 is used to determine the deformations in the bridge. The model consists of the following layers:

1. Loading shell, needed to apply the loading on the bridge. Made of ATENA 3D shell elements (4 layers are used).
2. The deck. Made of quadratic brick elements with size 400x400 mm.
3. Girders with end diaphragm beams. The model for the ZIP-girders is already shown in Figure 5-1. The end diaphragm beams consists of tetra-elements.
4. This model is vertically supported by springs. To avoid rigid body movement the model is supported at the top of the first ZIP girder as indicated in Figure 5-3.

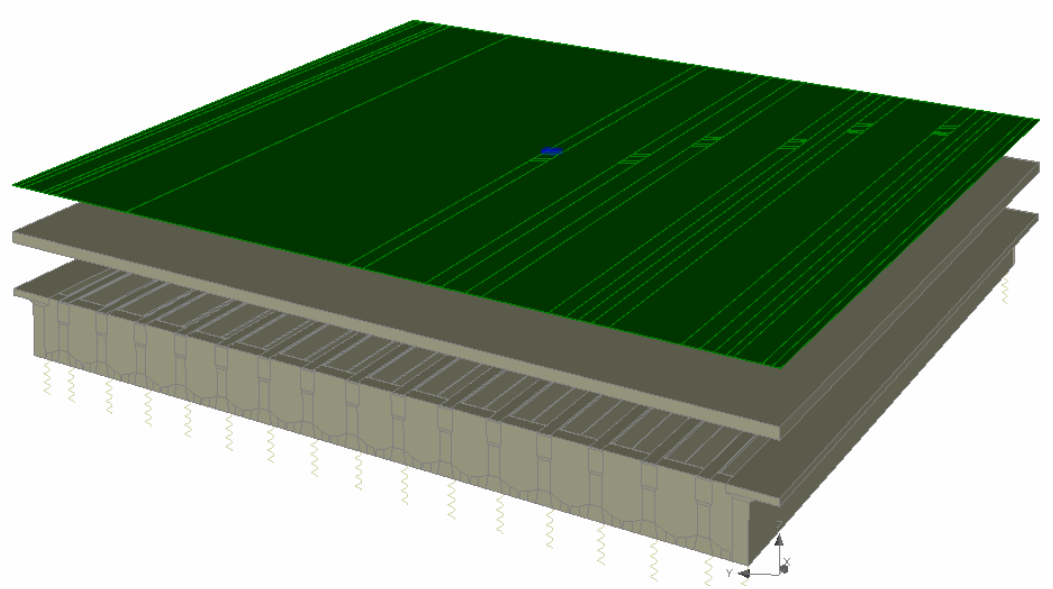

Figure 5-2 Linear elastic model of the bridge

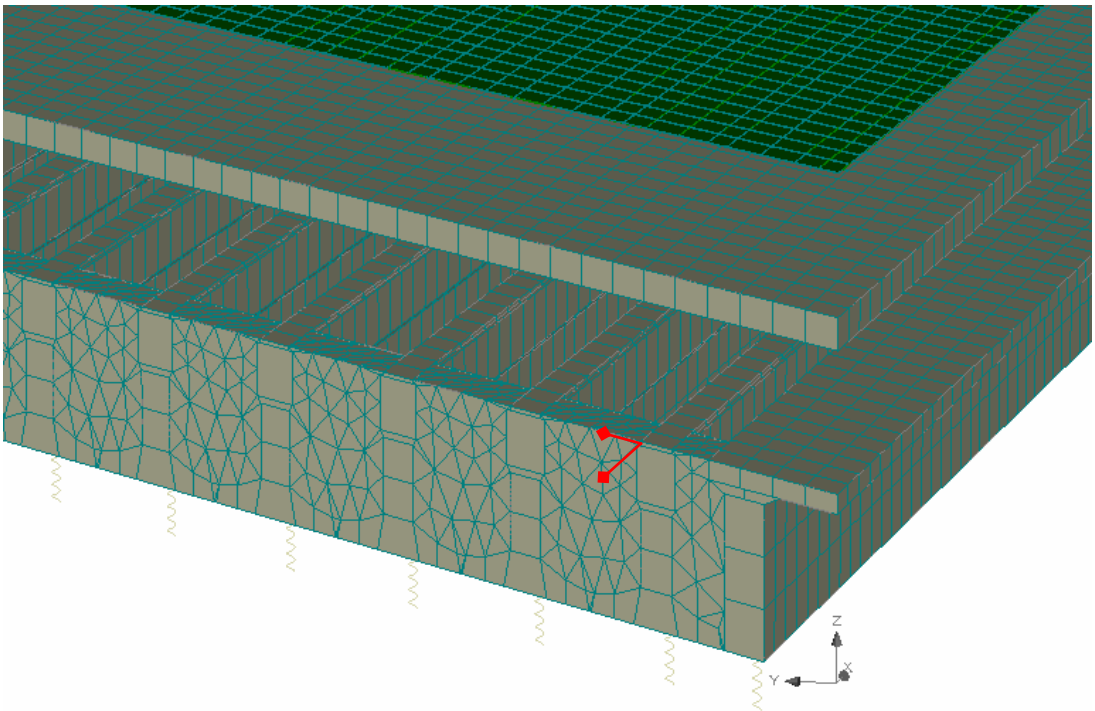

Figure 5-3 Finite element mesh for the LE model of the bridge (horizontal supports indicated in red)

Remarks:

1. During making the model a bug was found (in ATENA). Applying shell-elements for the deck gives strange results, no equilibrium in all directions was found, also the distribution of support reactions seems to be incorrect. Based on some experiments with different models it was found out that applying quadratic volume elements for the deck gives reasonable results. Furthermore an equilibrium calculation is made.
2. The thickness of the deck is not constant at the edge of the bridge between the first ZIP and TRA girders (Figure 3-2). But this gives difficulties in the finite element model. Chosen is to take a constant thickness for the whole deck of 230 mm.

5.3 Analysis of the deformations of first ZIP girder in skew bridge

The deformations of the LE model must be applied on the small PNL model. For that reason first the deformations are investigated. The procedure to get the results from ATENA is presented in appendix F. The orthotropic model, presented in paragraph 9.2, is used to compare the deformations with.

In the linear elastic model of the bridge two load steps are calculated (construction stage B):

1. Permanent loads on deck, with or without end diaphragm beam.
2. Permanent and variable loads on deck, with or without end diaphragm beam. This is done for the load case of Spanbeton and Minalu.

The found data for the first ZIP girder is split up in different components (Figure 5-4) and will be analysed in the next paragraphs:

1. Transverse deflection of top of girder, dY (top)
2. Average vertical deflection of top of girder (representing shear force), dZ average
3. Rotations, ddZ or dY (top) and dY (bottom)

Important is that all deformations are plotted along the length as defined in Figure 5-4.

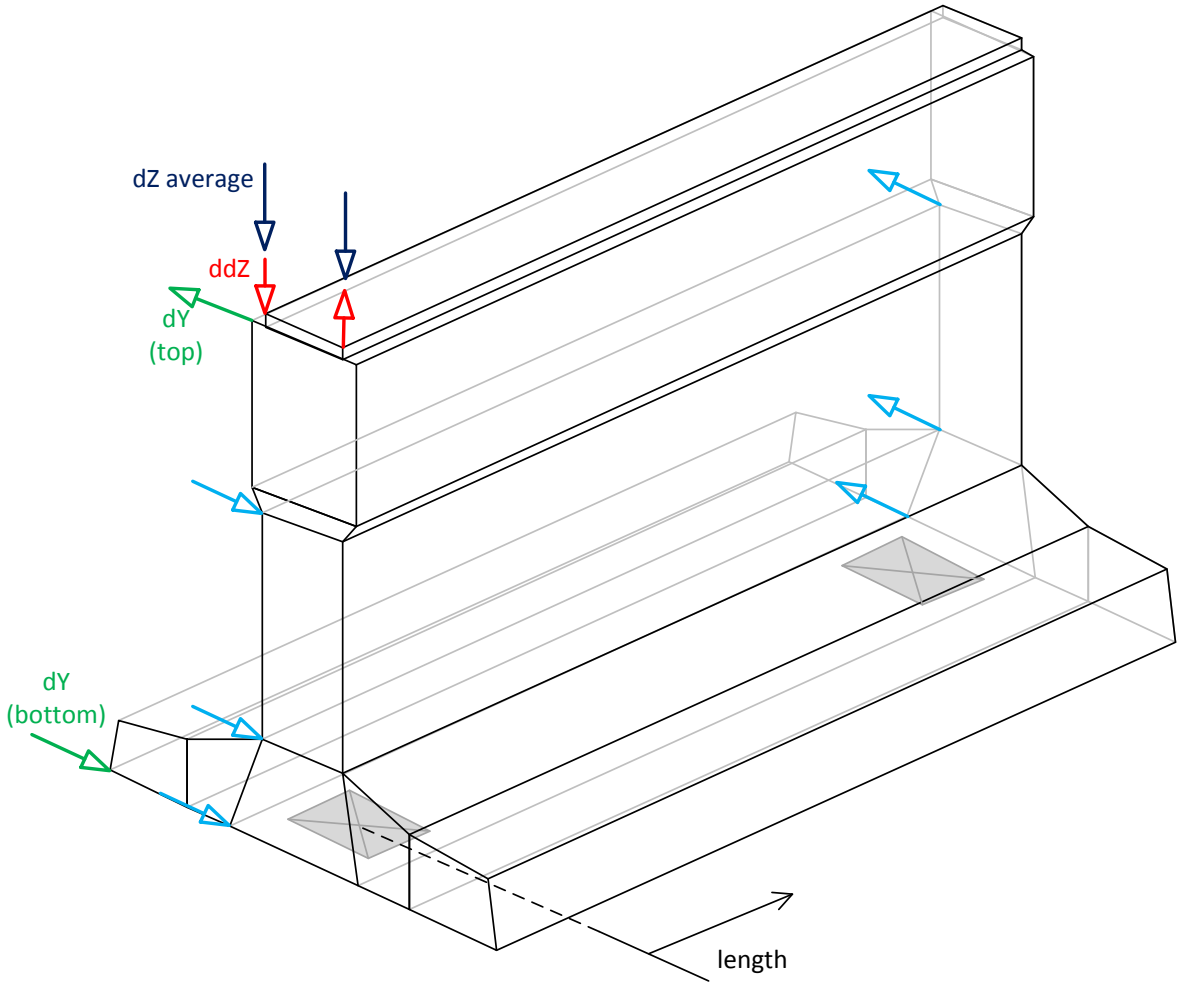

Figure 5-4 Schematized deformations of the girder

5.3.1 Transverse deformation; dY (top)

The distribution of the transverse deformations, dY (top), along the length are presented in Figure 5-5 and Figure 5-6. In both figures the deformations due to load step 1 (permanent load) are identical because only the variable load differs.

In Figure 5-5 and Figure 5-6 some things are remarkable:

- The end diaphragm beam gives a kind of clamping effect causing negative deformations in the zone length = 30 – 36 meter
- The deformations are larger when the end diaphragm beam are neglected
- The shape of the deformations is not changing

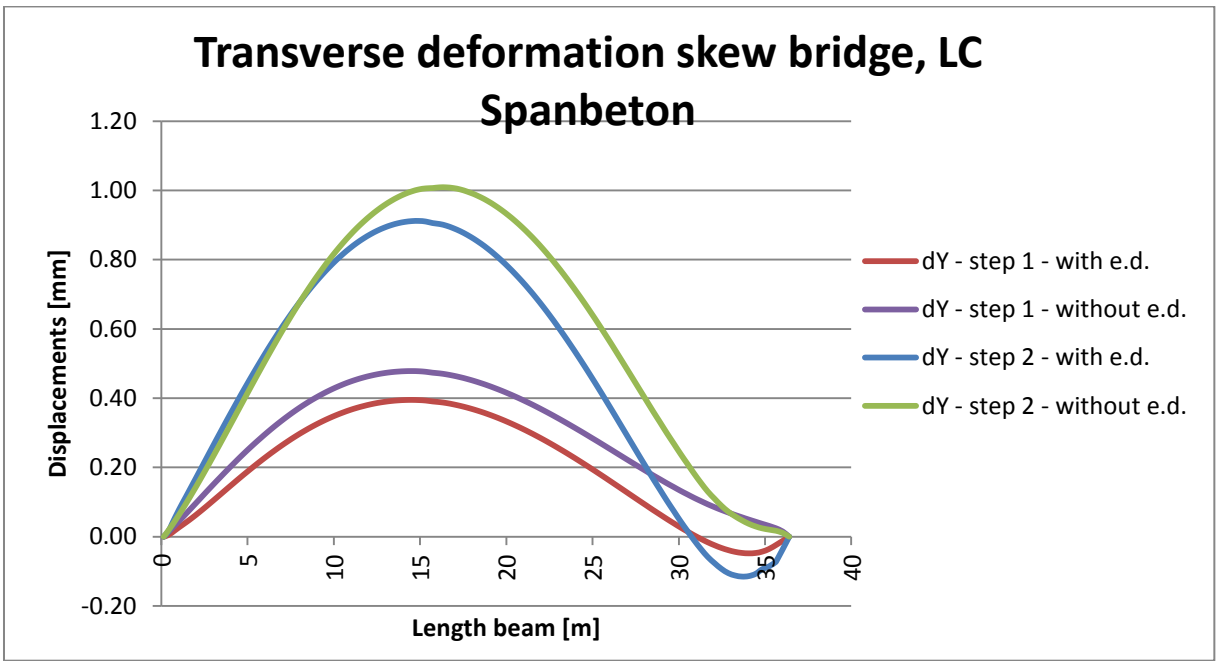

Figure 5-5 Transverse deformation skew bridge, load case Spanbeton

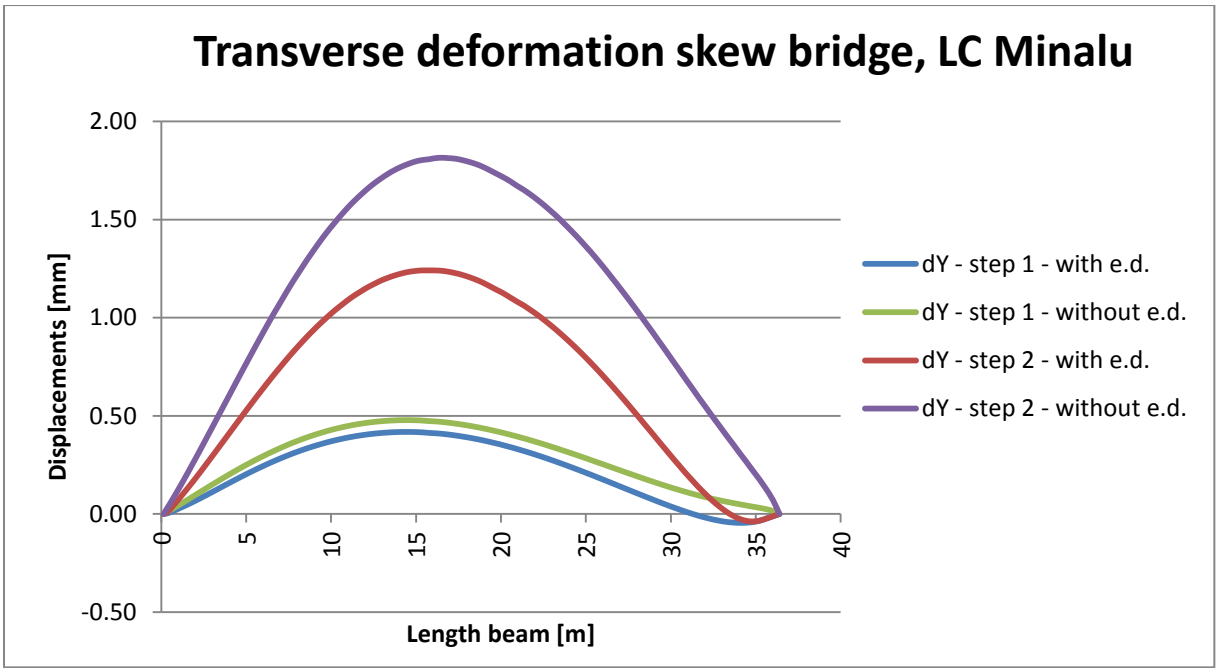

Figure 5-6 Transverse deformation skew bridge, load case Minalu

5.3.2 Average vertical deflection; dZ average

The average vertical deflection represents the bending and shear deformation. The average is taken from the deformations, Figure 5-7.

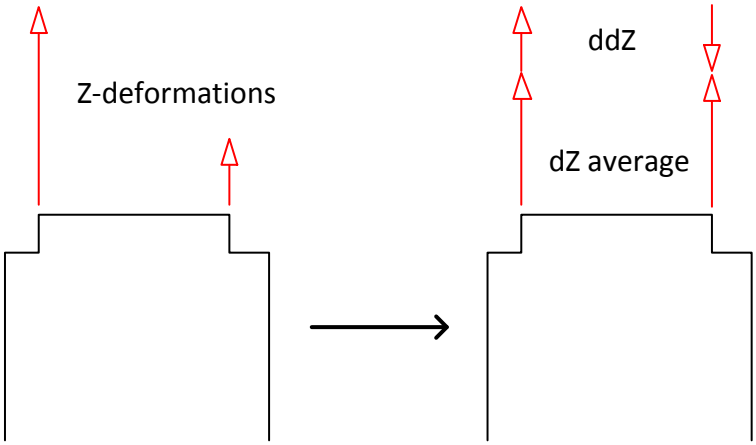

Figure 5-7 Splitting up the Z-deformations

In this paragraph the dZ average deformations are presented, Figure 5-8 and Figure 5-9. Some comments:

- For the first step the deformations are the same
- The end diaphragm beam has a beneficial effect on the deflection.

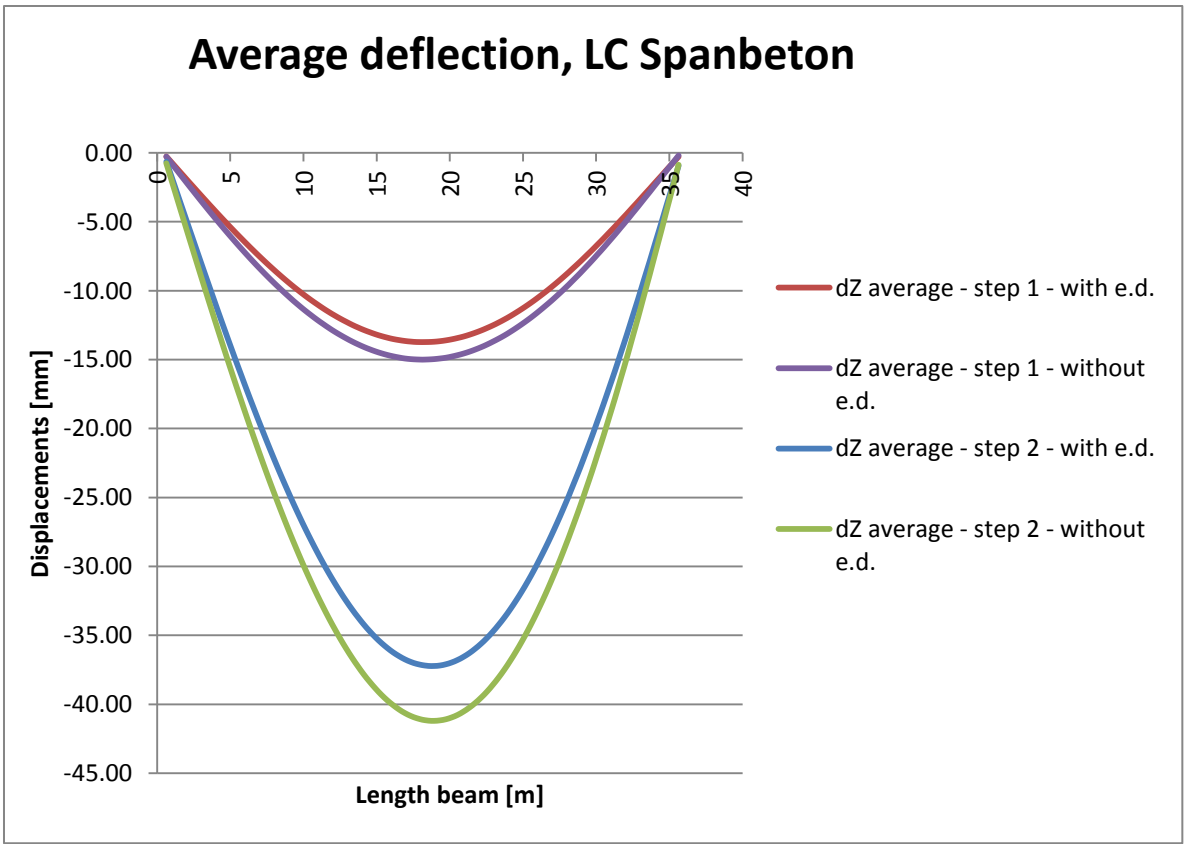

Figure 5-8 Average deflection of beam, load case Spanbeton

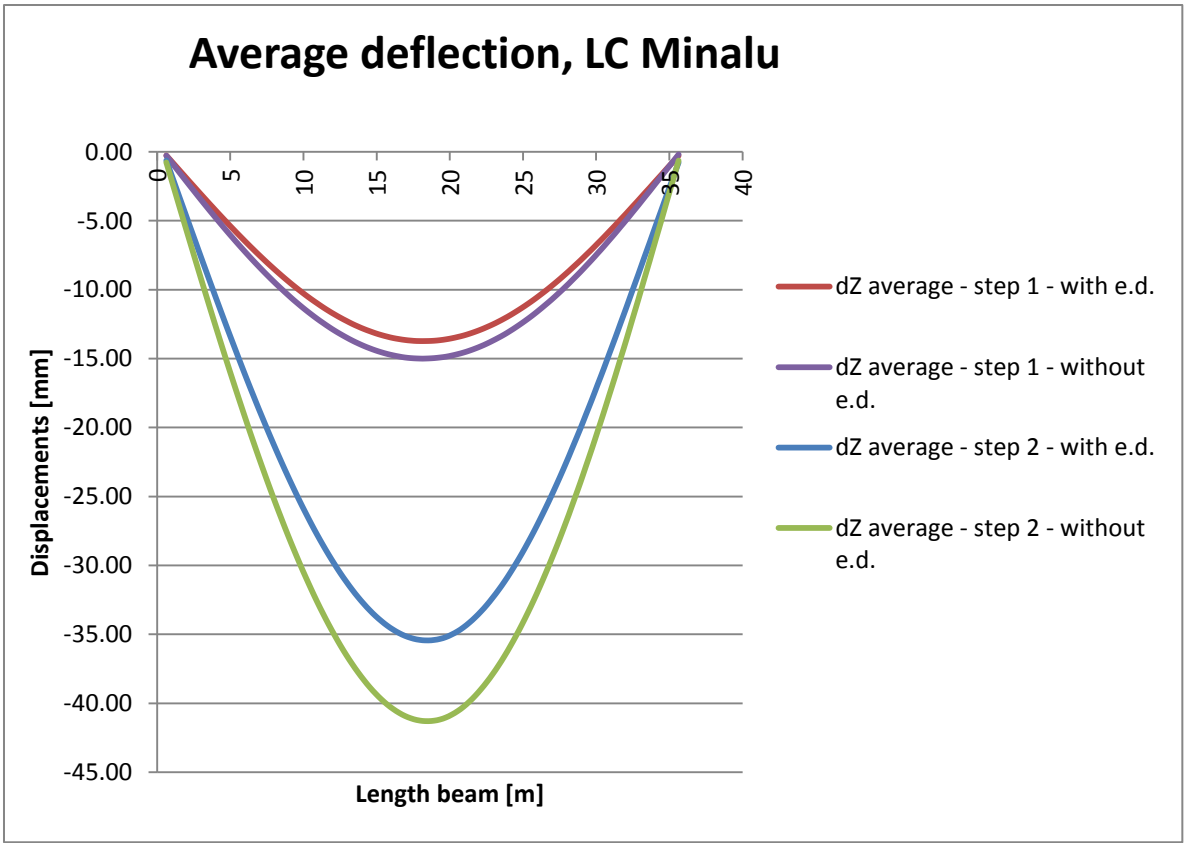

Figure 5-9 Average deflection skew bridge, load case Minalu

The orthotropic plate model gives similar deformations, presented in Figure 5-10, Figure 5-11 and Figure 5-12. It is visible that the deformations for load step 1 and 2 for both load cases are corresponding quite good. From this is concluded that the deformations in the ATENA model are reliable.

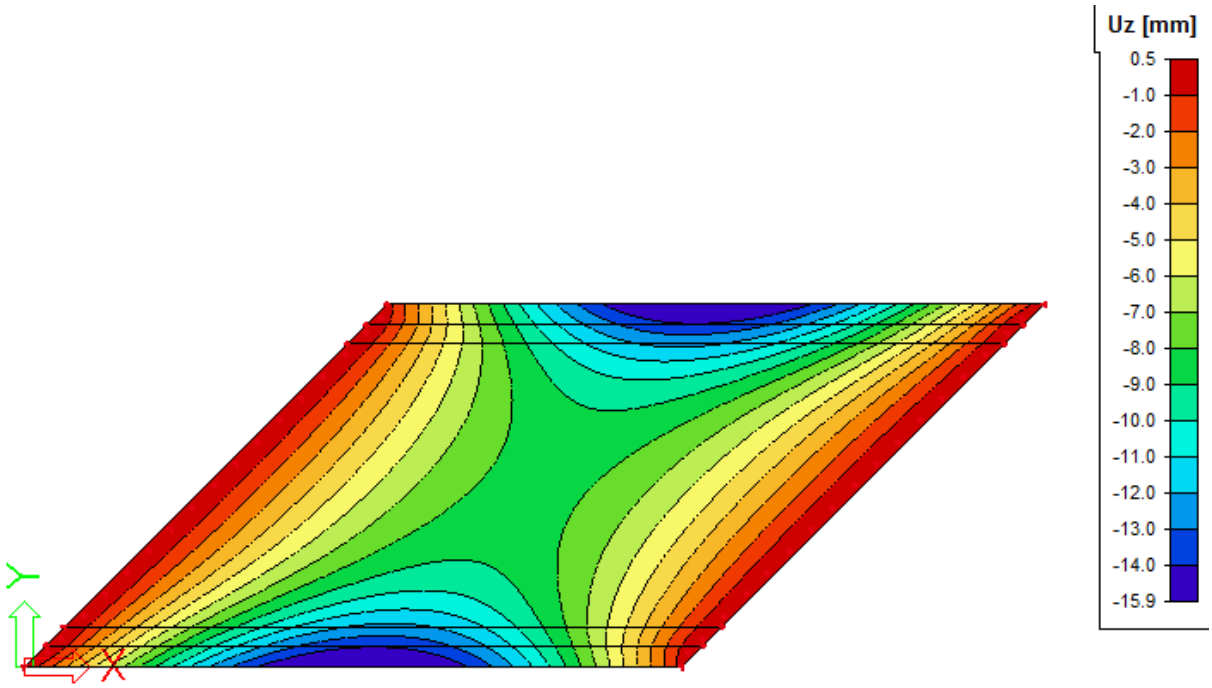

Figure 5-10 Deflection due to permanent load (step 1) calculated with Scia Engineer

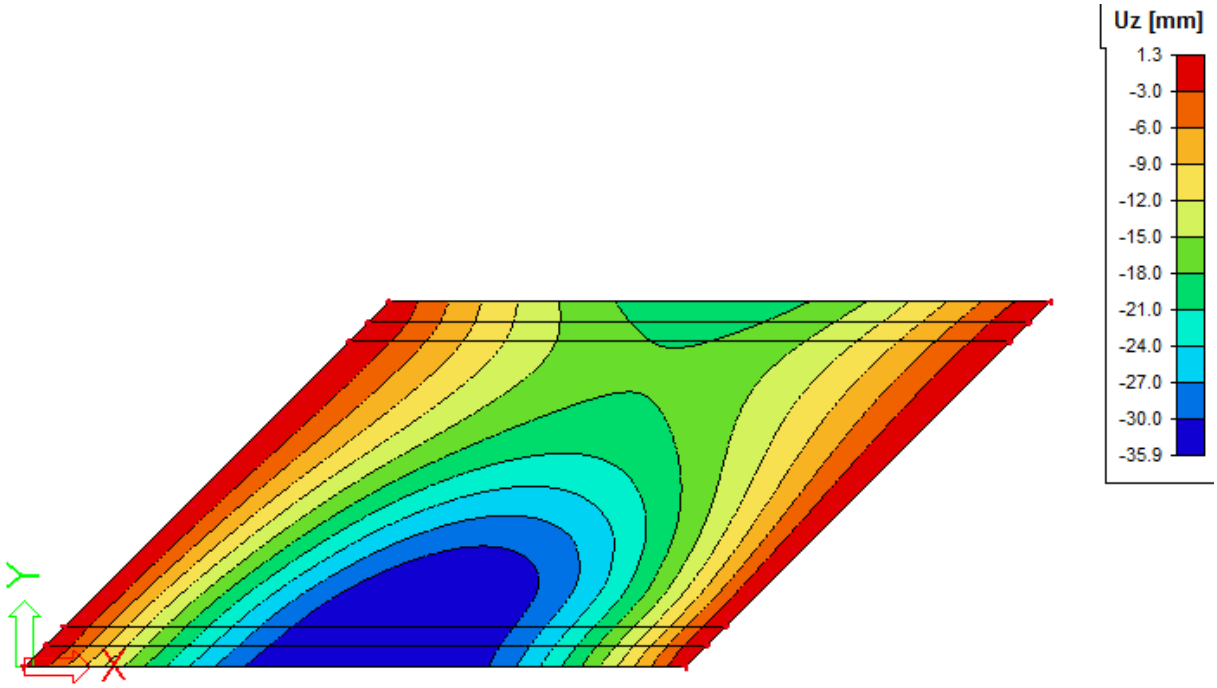

Figure 5-11 Deflection due to permanent load and variable load of Spanbeton (step 2) calculated with Scia Engineer

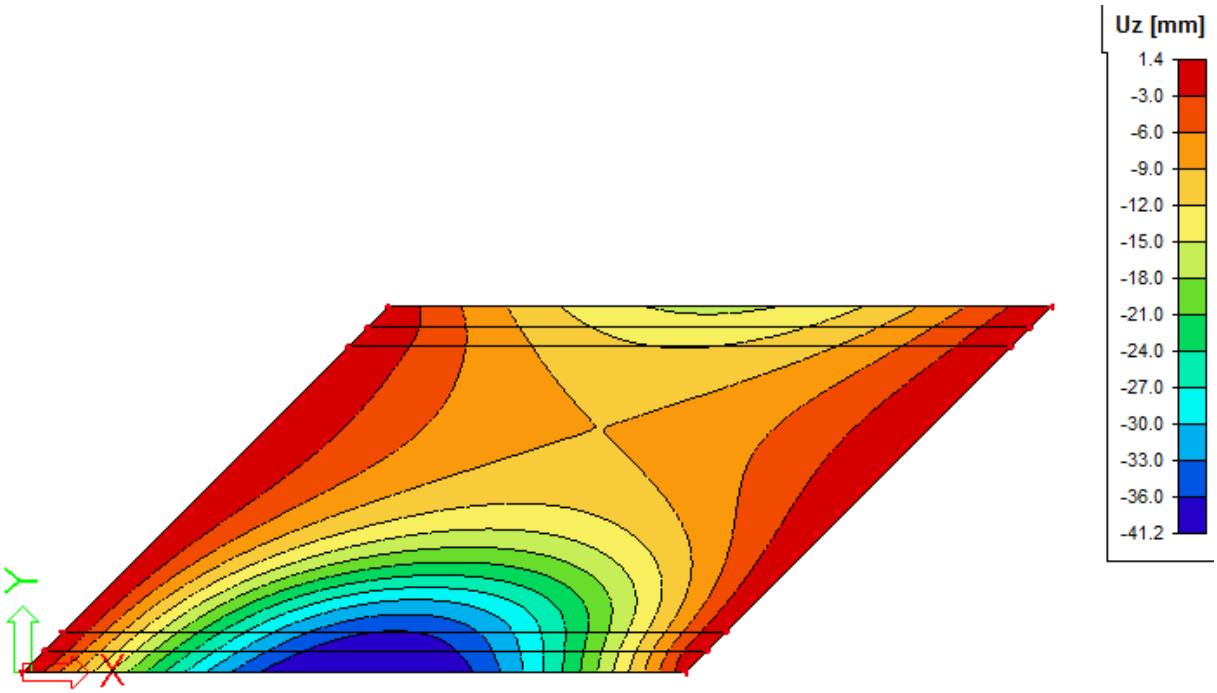

Figure 5-12 Deflection due to permanent load and variable load of Minalu (step 2) calculated with Scia Engineer

5.3.3 Rotations

The rotations of the beam need to be calculated for two directions as illustrated in Figure 5-13.

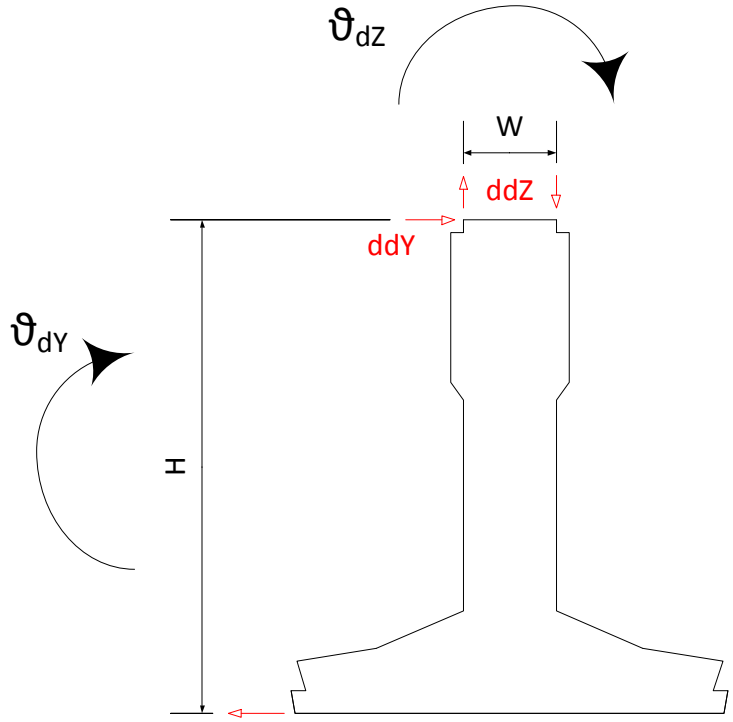

Figure 5-13 Calculation of rotation of beam

The used formulae are:

$$\vartheta_{dY} = \frac{ddY}{H}$$

$$\vartheta_{dZ} = \frac{ddZ}{W}$$

In Figure 5-14 and Figure 5-15 the rotations are plotted and it can be observed that:

- Again the clamping effect of the end diaphragm beam is visible.
- Neglecting the end diaphragm beam gives larger rotations.

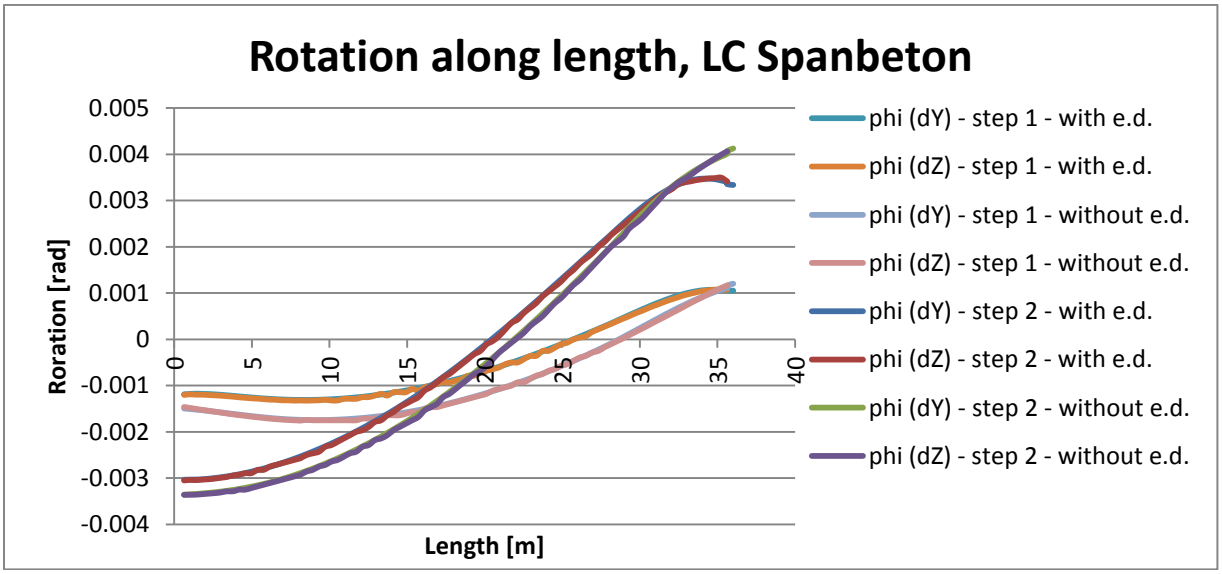

Figure 5-14 Rotation along length for skew bridge, LC Spanbeton

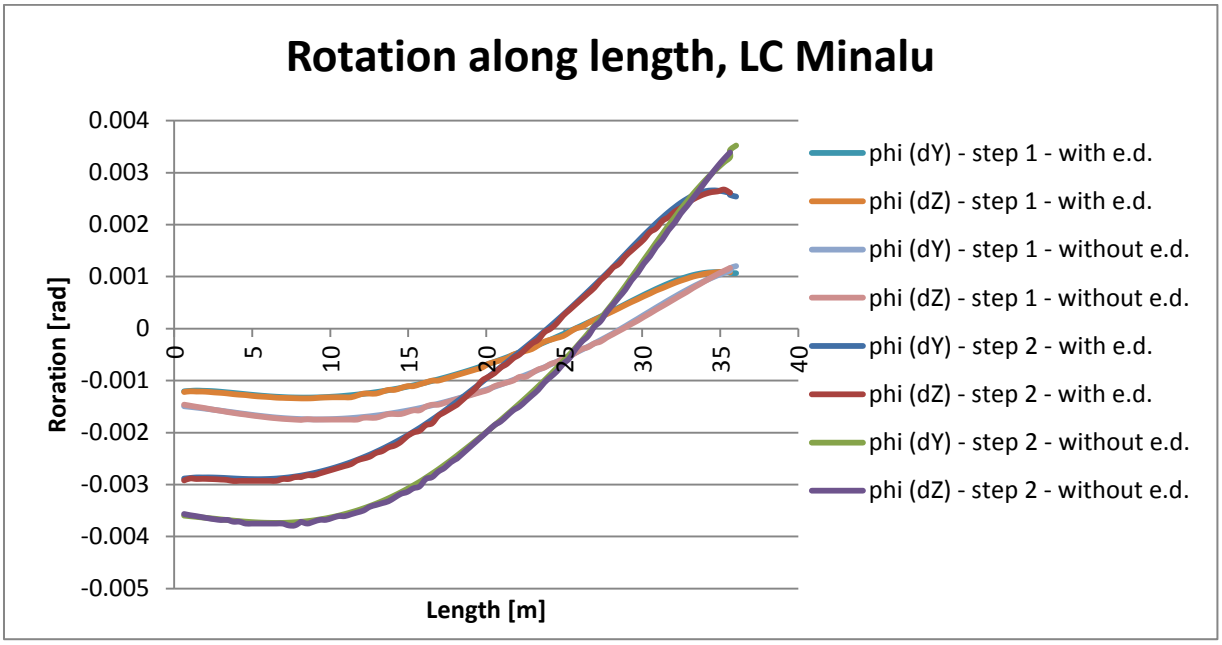

Figure 5-15 Rotation along length for skew bridge, LC Minalu

The Scia 2D-model gives similar rotations, presented in Figure 5-10, Figure 5-11 and Figure 5-12. It is visible that the deformations are corresponding the best for the load case of Minalu. From this is concluded that the rotations are reliable.

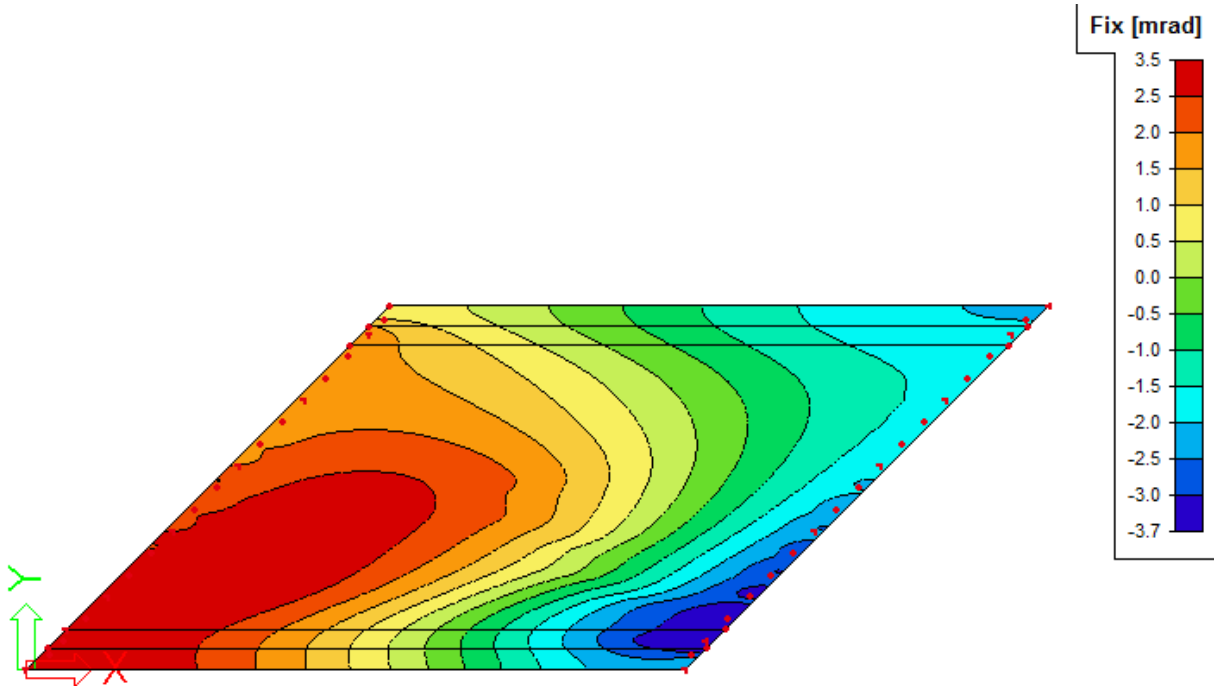

Figure 5-16 Rotations in bridge due to permanent load and variable load of Spanbeton calculated with Scia Engineer

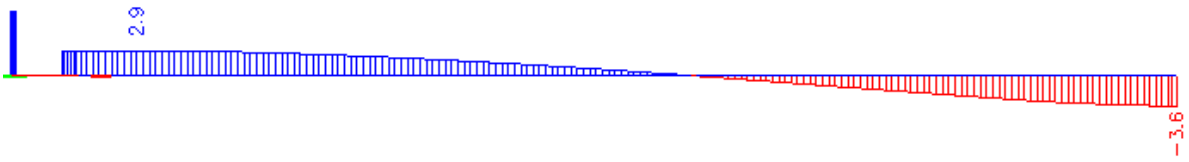

Figure 5-17 Rotations in first ZIP girder due to permanent load and variable load of Spanbeton calculated with Scia Engineer

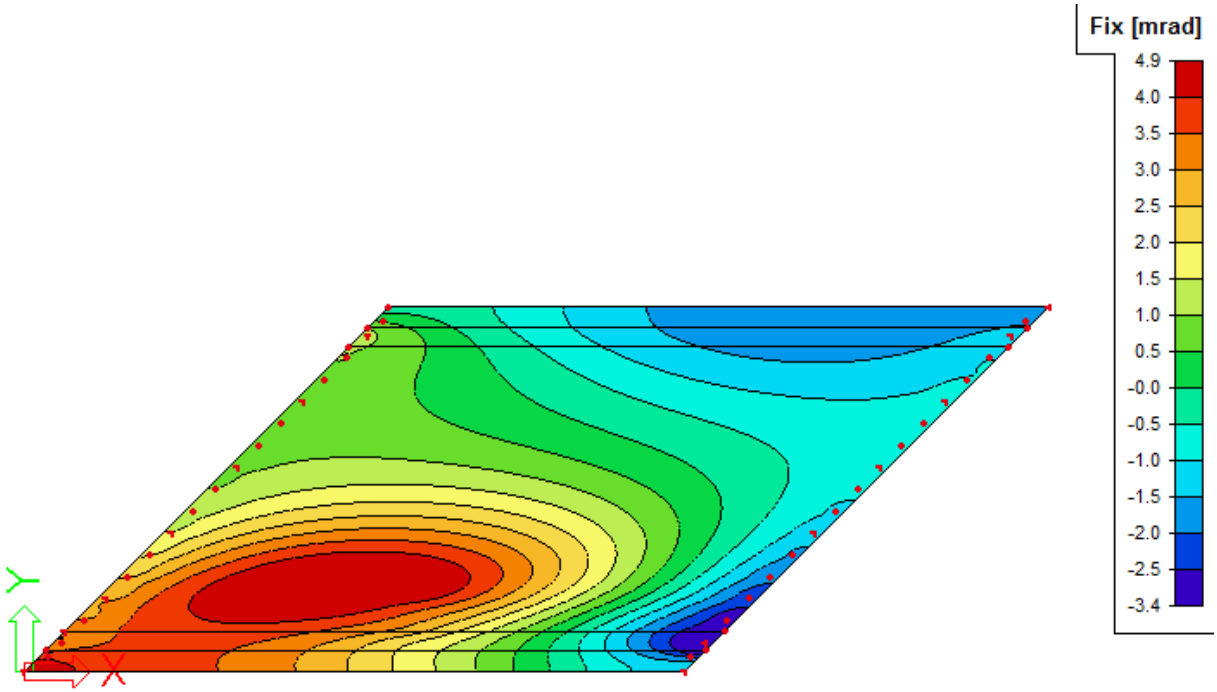

Figure 5-18 Rotations in bridge due to permanent load and variable load of Minalu calculated with Scia Engineer

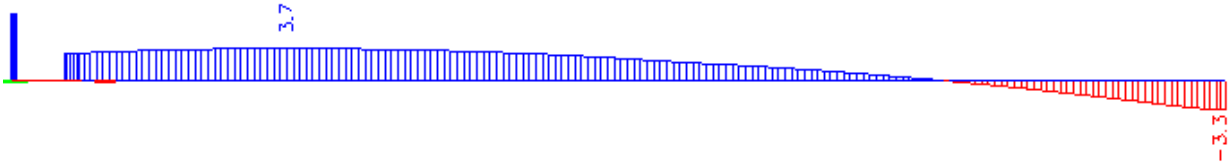

Figure 5-19 Rotations in first ZIP girder due to permanent load and variable load of Minalu calculated with Scia Engineer

5.4 Analysis of the deformations of first ZIP girder in straight bridge

It appeared that the torsion in a straight bridge is much lower than for a skew bridge (paragraph 2.2.2). For that reason only for the load case of Spanbeton the deformations of a straight bridge are investigated and presented briefly.

5.4.1 Transverse deformation; dY (top)

The occurring transverse deformations are very small, five times lower than occurring for the skew bridge, Figure 5-20.

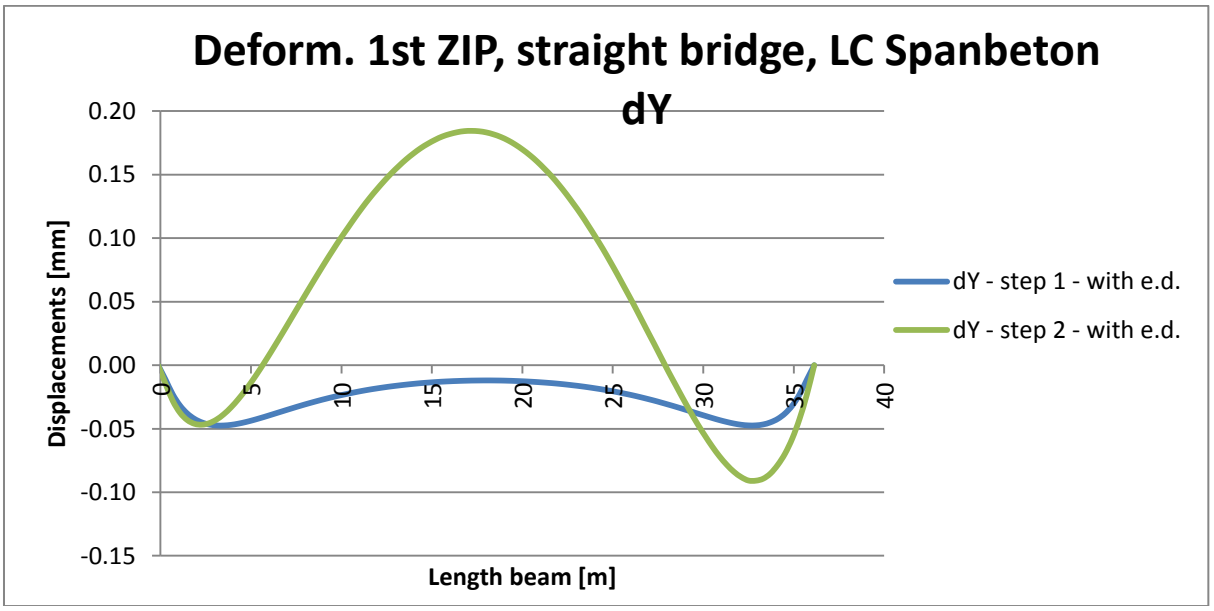

Figure 5-20 Transverse deformation straight bridge, load case Spanbeton

5.4.2 Average vertical deflection; dZ average

The deflection of the beam is larger for the straight bridge than for the skew bridge. This is because more load is carried by bending in a straight bridge, Figure 5-21.

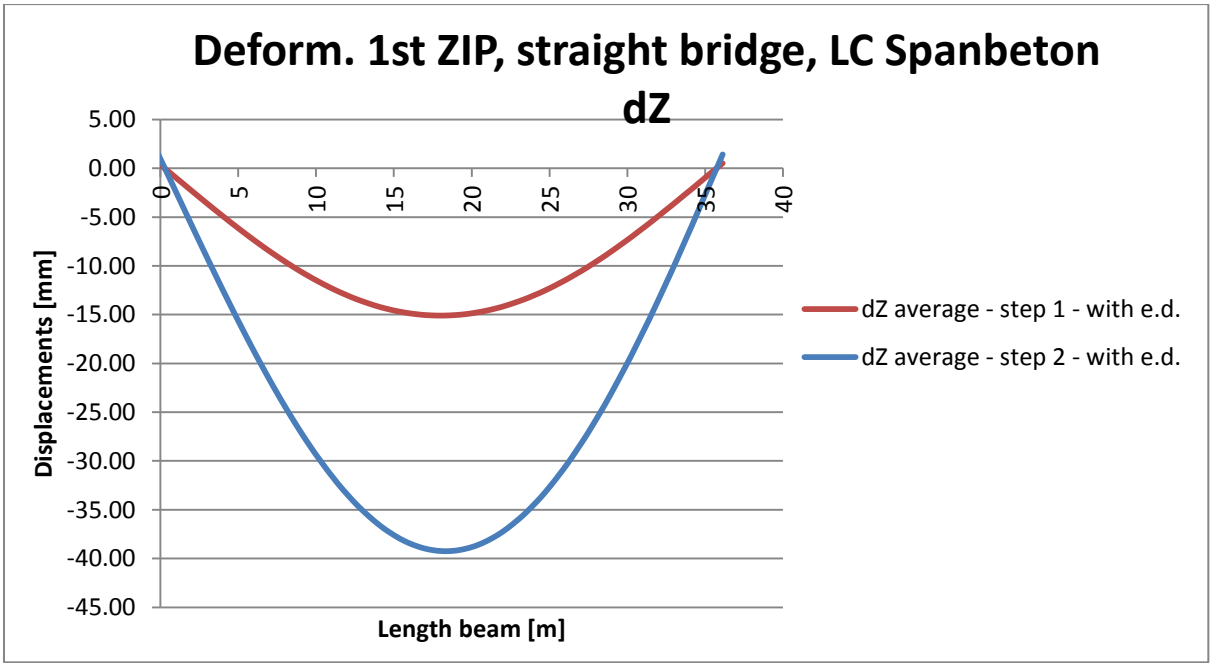

Figure 5-21 Average deflection straight bridge, load case Spanbeton

5.4.3 Rotations

Interesting is that for the observed load case only the permanent load gives the largest rotations, the variable load reduces this, Figure 5-22.

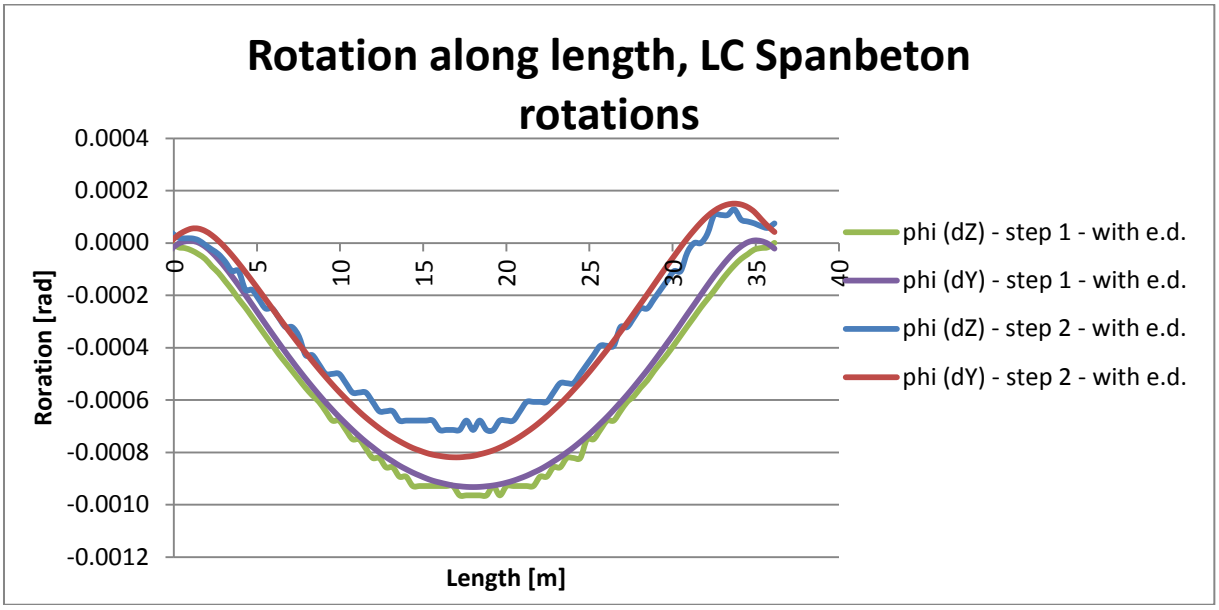

Figure 5-22 Rotation along length for straight bridge, LC Spanbeton

A comparison of the rotations occurring in a skew and straight bridge is illustrative for the behaviour of the bridges, Figure 5-23. When in the first ZIP girder of the skew bridge no torsion cracks appear this will sure not happen in the straight bridge. So first the skew bridge will be investigated. Depending on the results it may be necessary to investigate the straight bridge further.

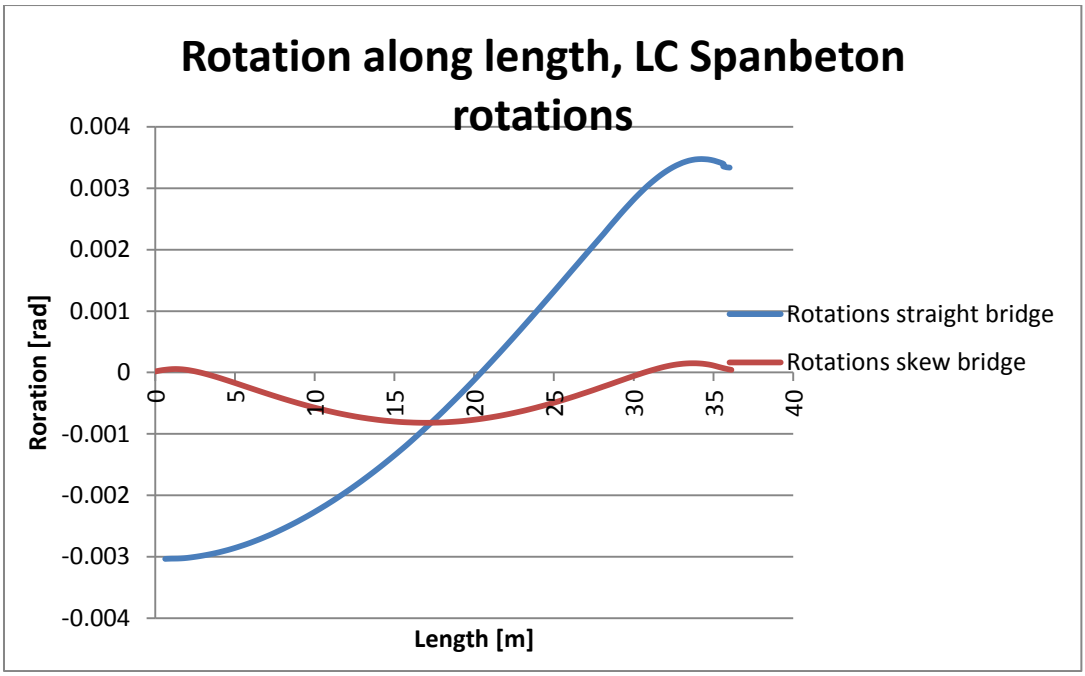

Figure 5-23 Comparison rotations in a fully loaded skew and straight bridge for LC Spanbeton

5.5 Applying loads on the PNL model of one ZIP girder

The deformations from the previous analysis have been investigated. Important is that they should be applied in a correct way on the small model.

The load is applied, using the following steps, the figures are presented below:

1. Dead weight and prestressing. Figure 5-25.
2. Fresh concrete deck. It is assumed that the girder in this phase is supported along the top edge by the reinforcement. Figure 5-25. The eccentricity of this loading is not incorporated.
3. Average deflection. Figure 5-26.
4. Rotations and transverse deflection. Figure 5-27.

The loads 3 and 4 are applied alternately because they are occurring simultaneously.

Loading 4 is the most complicated one. The deformations are correctly applied on the loading plate. But due to the low stiffness of the loading plate the transverse deformations are not applied correctly on the girder, there is some deviation, this is visualized in Figure 5-24. The rotations, the most important deformations, are still correct.

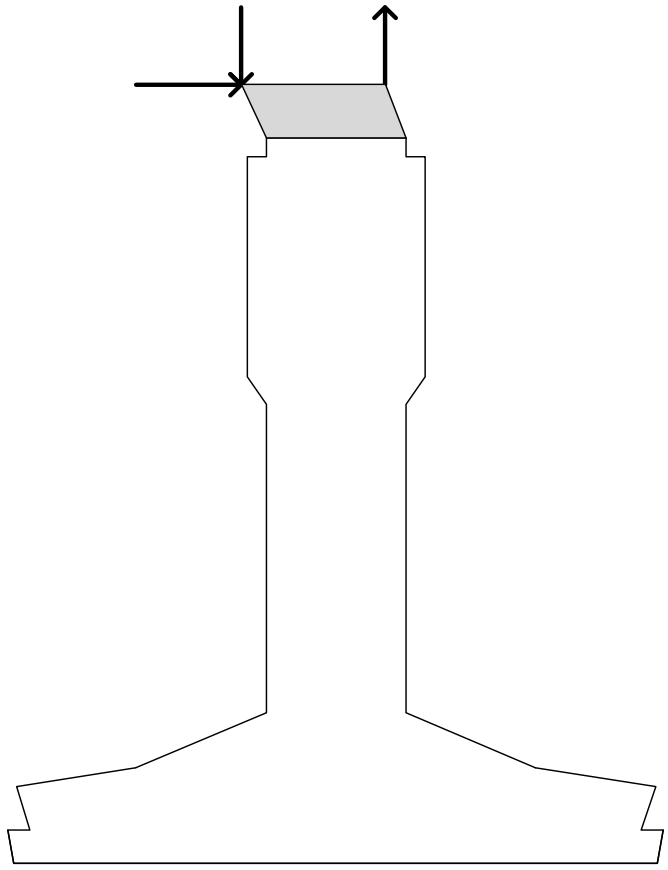

Figure 5-24 Difference in transverse deformation

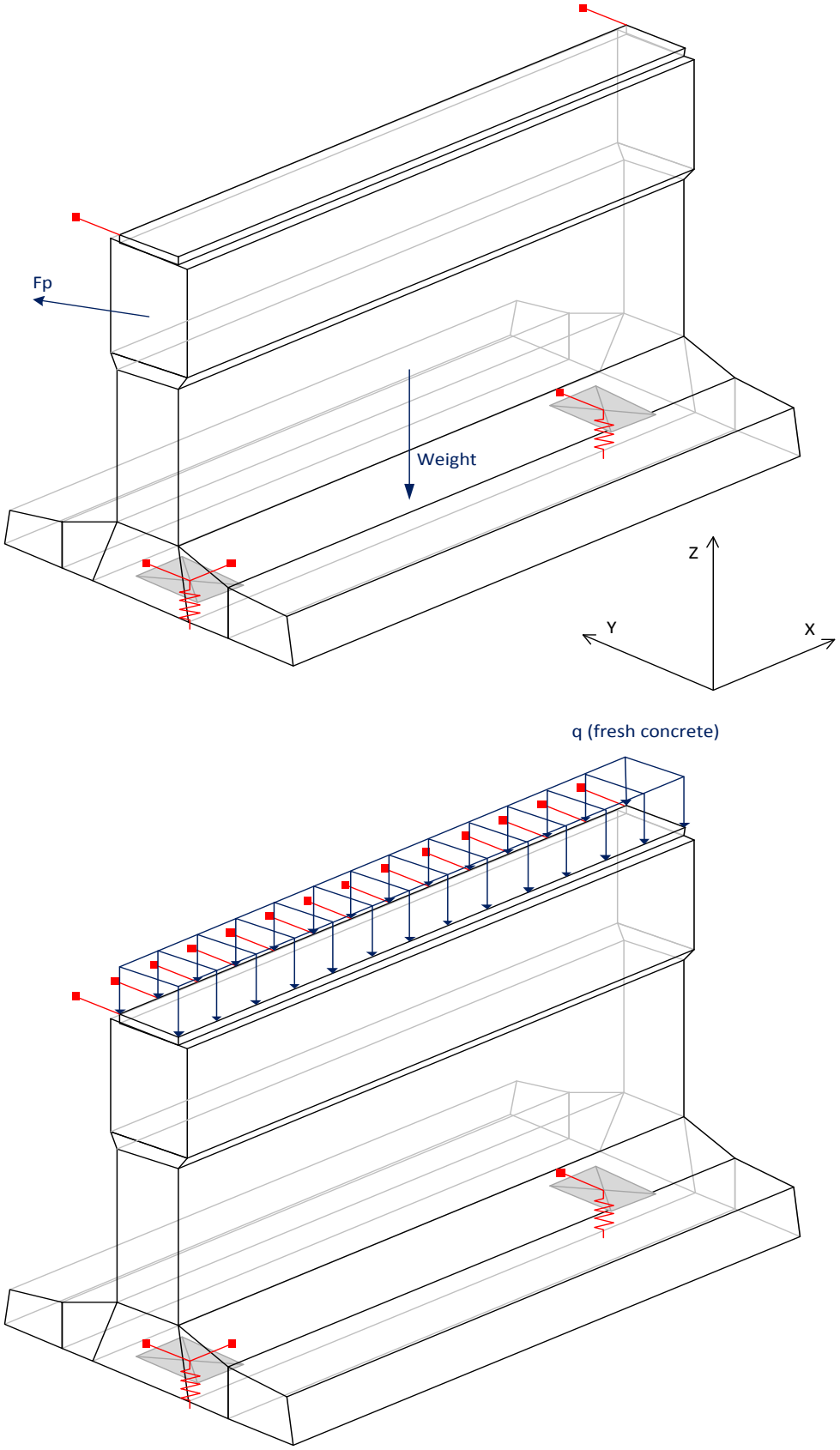

Figure 5-25 Dead weight, prestressing and fresh poured concrete (loads and boundary conditions)

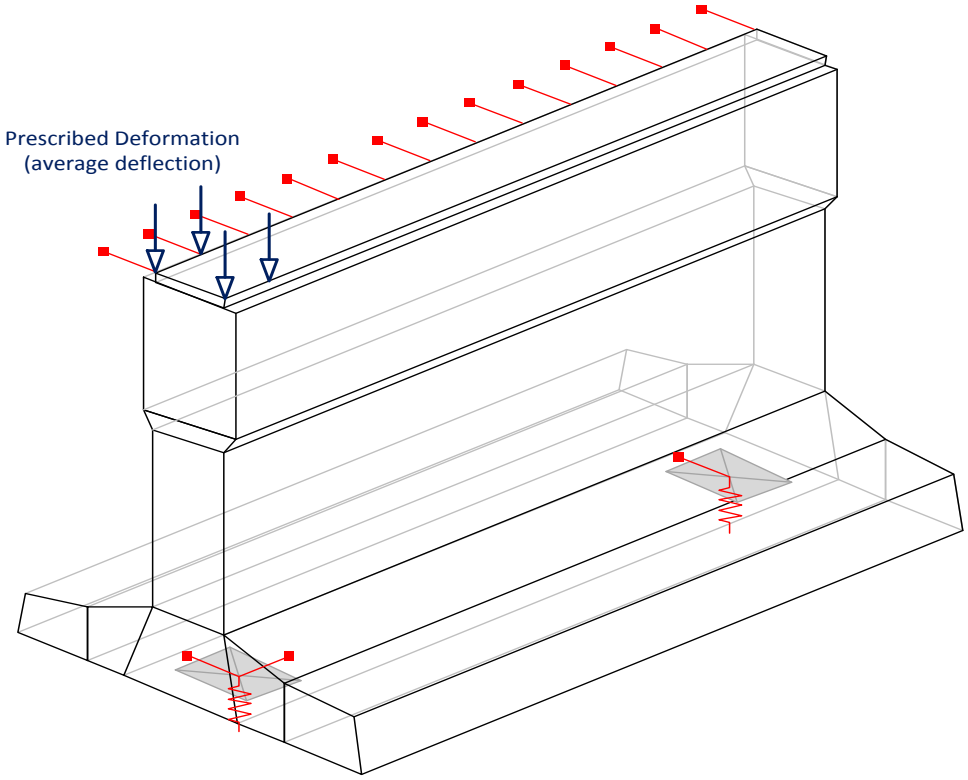

Figure 5-26 Average deflection (prescribed deformations and boundary conditions)

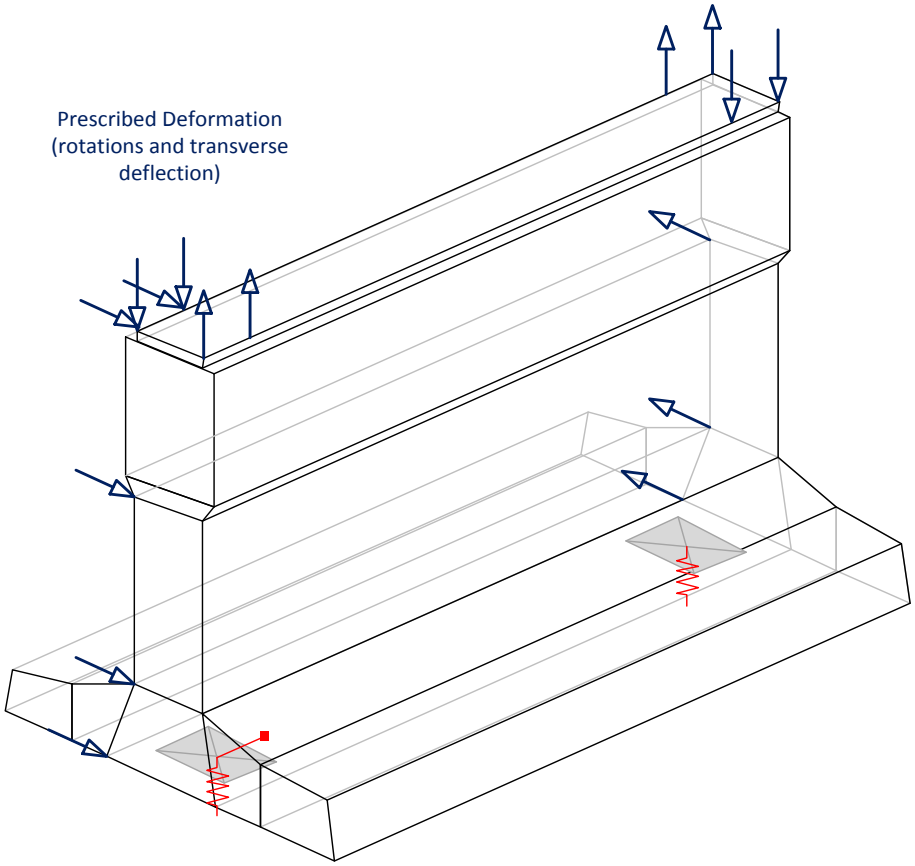

Figure 5-27 Transverse deflection and rotations (prescribed deformations and boundary conditions)

5.6 A physical non-linear model of one ZIP girder

The physical non-linear model of one girder is described in this paragraph. Also the occurring phenomena are presented and explained. In this model the end diaphragm is included.

5.6.1 Torsion stresses in finite elements

It is important that the finite elements can visualize correctly the shear stresses due to torsion. Minalu used coarse elements and integrated stresses to obtain the torsional moments in the girder which gave accurate results.[9] For his research this was sufficient, but for the current model the real occurring torsional stresses in the web are important.

The torsion behaviour is simulated using the rotations of the load case of Spanbeton (paragraph 5.3.3). Linear elastic material properties are used. No prestressing is applied. The maximum torsion is expected at the location 26-27 meter, see Figure 9-9. The occurring torsional moment is 68 kNm. At that location a refinement of the mesh is made (Figure 5-28). The expected shear stress can be calculated using the knowledge from the program ShapeBuilder, paragraph 6.1. The model was carried out in ULS, so a factor of 1.35 must be applied.

$$\tau = 1.35 \cdot \frac{68}{100} \cdot 2 = 1.84 \ {}^{N}/_{mm^2}$$

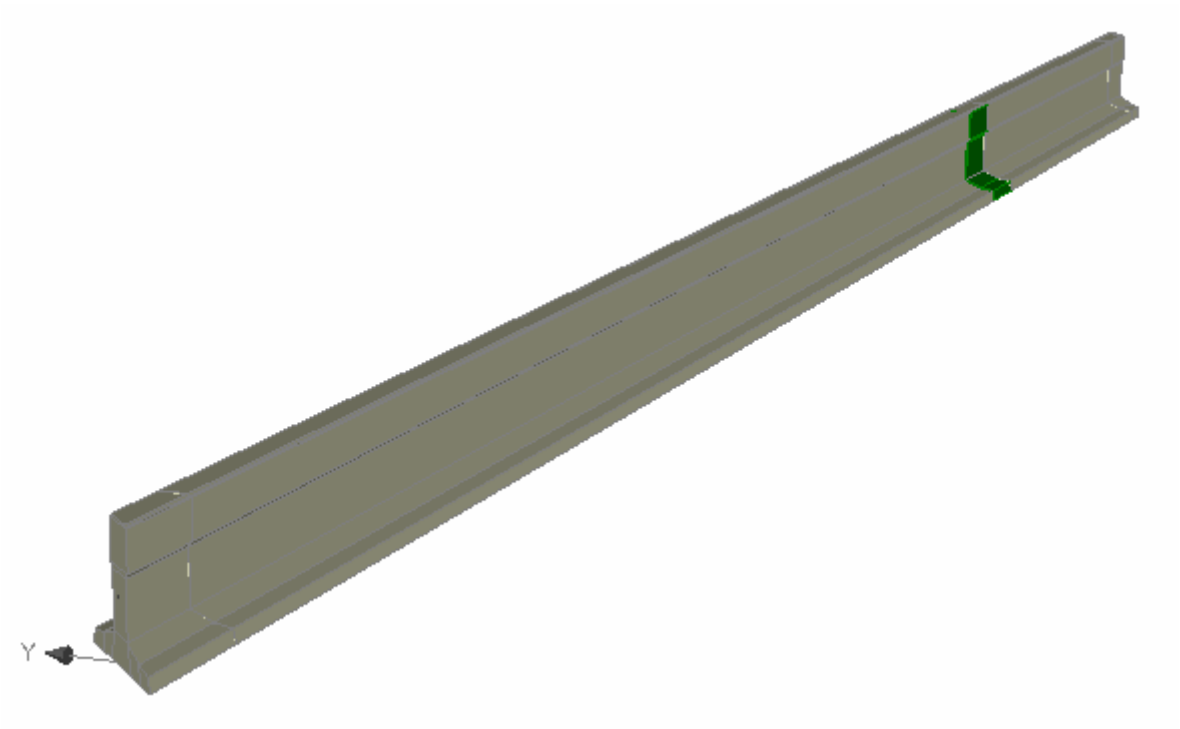

Figure 5-28 Local refinement in ZIP-girder

Five different finite element types or sizes are compared:

1. Coarse linear elements, size 0.2 m
2. Fine linear elements, size 0.04 m
3. Coarse quadratic elements, size 0.2 m
4. Fine quadratic elements, size 0.1 m
5. More refined quadratic elements, size 0.05 m

[9] Minalu, Kassuhun K. (2010), *Finite element modelling of skew slab-girder bridges.* Page 89.

The shear stresses are measured along the surface of the ZIP girders as indicated in Figure 5-29. In the same figure the shear stresses for the five considered cases are presented.

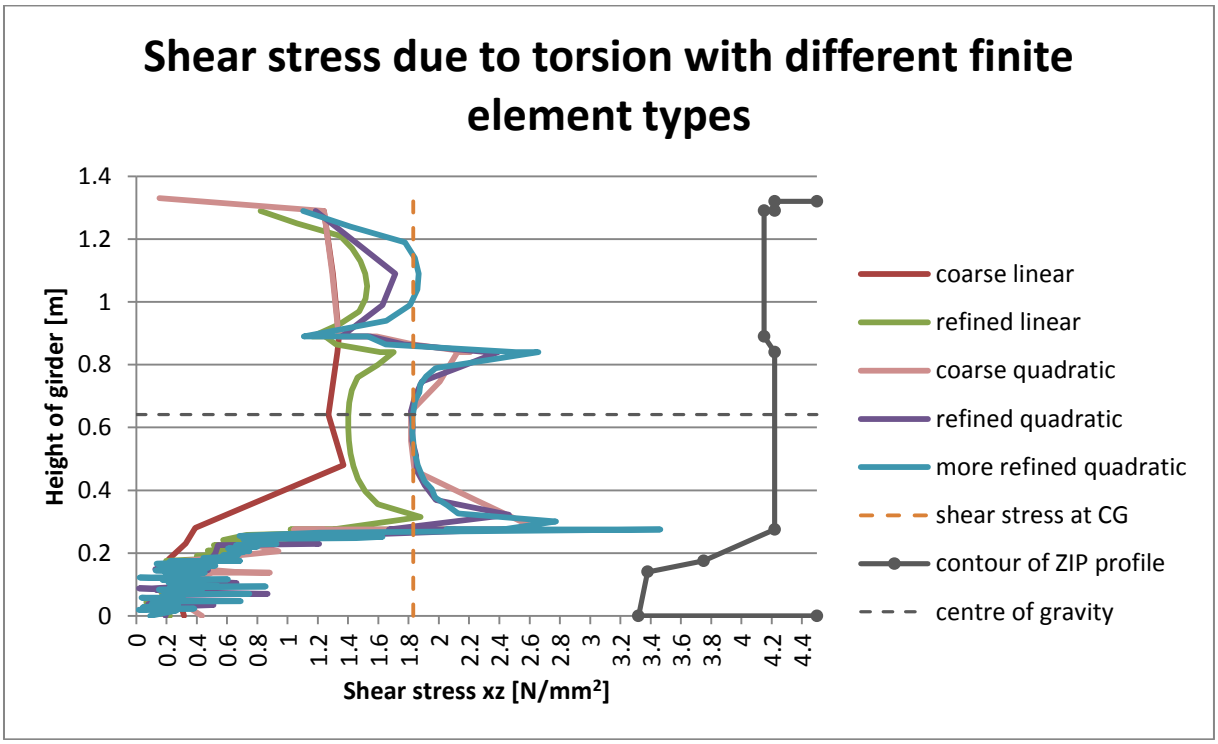

Figure 5-29 Comparison of shear stress due to torsion along perimeter of ZIP girder

The shear stress occurring at the height of the centre of gravity is dependent on the choice of finite element type, see Table 5-1. Especially quadratic elements can visualize shear stresses due to torsion accurately.

Case	Shear stress at centre of gravity
Course linear elements	1.28
Fine linear elements	1.40
Coarse quadratic elements	1.82
Fine quadratic elements	1.83
More refined quadratic elements	1.83

Table 5-1 Comparison shear stresses at centre of gravity

It is visible that quadratic elements calculates the shear stresses due to torsion correctly. The peak stresses are also visible in the analysis of the cross-section made with ShapeBuilder (Figure 6-1). A mesh refinement causes larger peak stresses. These are very local effects and are neglectable.

The coarse and fine quadratic elements shall be used for further analysis. The first chosen mesh is presented in Figure 5-30. Basically this is a mesh using coarse linear elements. Locally the beam can be refined in the important region at the end of the girder. In Figure 5-31 the refinement of the end of the girder is visible using fine quadratic elements, also the coarse quadratic elements can be used to refine this part of the girder. The top part of the girder is roughly meshed to be compatible with the loading plate on top of the girder. This way of modelling causes minimal modelling cracking (not real occurring cracks).

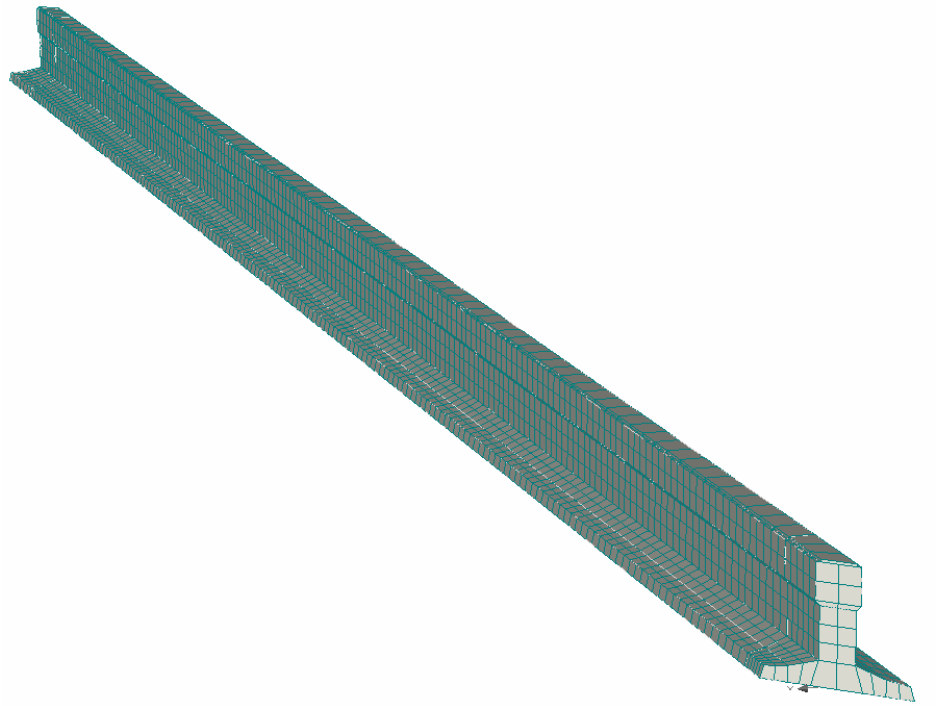

Figure 5-30 Coarse mesh for ZIP-girder in physical non-linear model, size 0.2 m

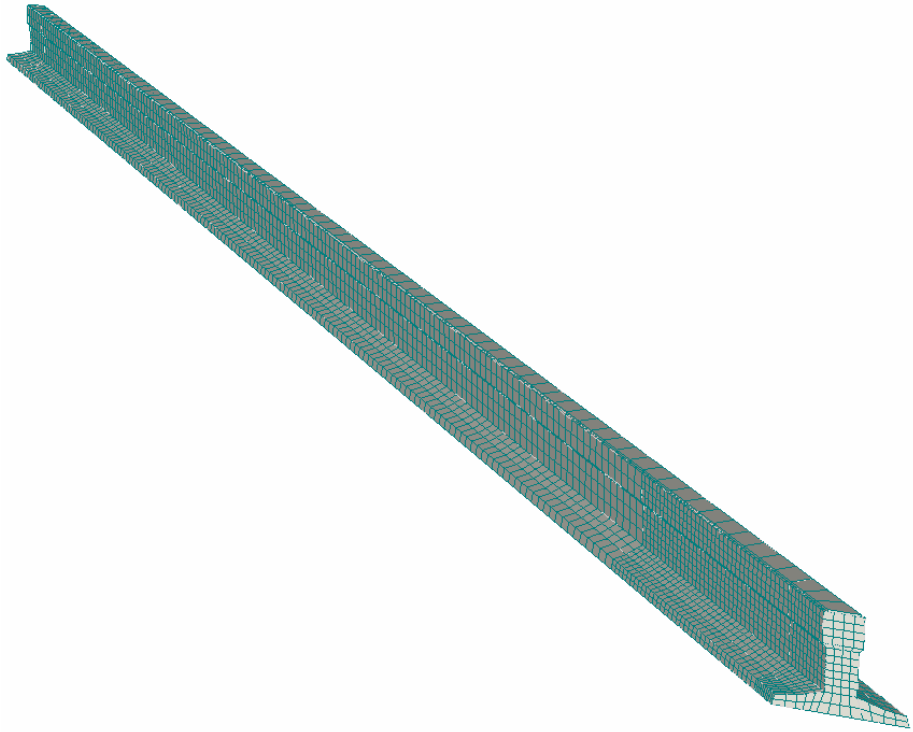

Figure 5-31 Mesh for ZIP-girder in physical non-linear model partially refined with quadratic elements, size 0.1 m

5.6.2 Material properties

The design material properties are used to model the bridge. For detailed information about the used materials, see appendix E.

5.6.3 Prestressing and reinforcement

The strands are positioned using the standard detailing rules of Spanbeton. The Bigaj bond model is used to model the bond between the prestressing cables and the concrete. Only in the ends of the girders the reinforcement stirrups are applied, also the reinforcement bars above the bend in the prestressing cables are modelled. See Figure 5-32 for an impression. For detailed information about the used materials, see appendix E.

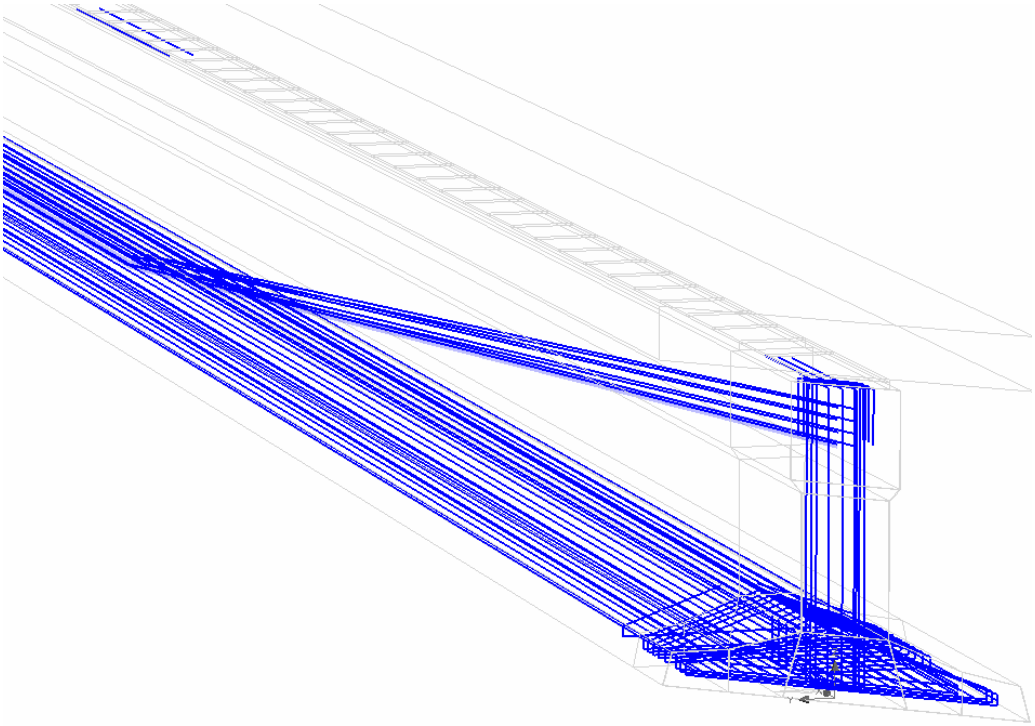

Figure 5-32 Prestressing cables and reinforcement in physical non-linear model of ZIP girder

Note: the Bigaj bond model is used to model the bond between the prestressing cables and the concrete. For that reason not the theoretical normal stresses are found but an approximation.

5.6.4 Connection with deck

The deformations occurring at the connection between the girder and deck are modelled using a loading plate. The loading plate is presented in Figure 5-33. The stiffness used is 10.000 MPa, and the plate thickness is 10 mm. This low values are chosen to avoid a substantial shift of the centre of gravity.

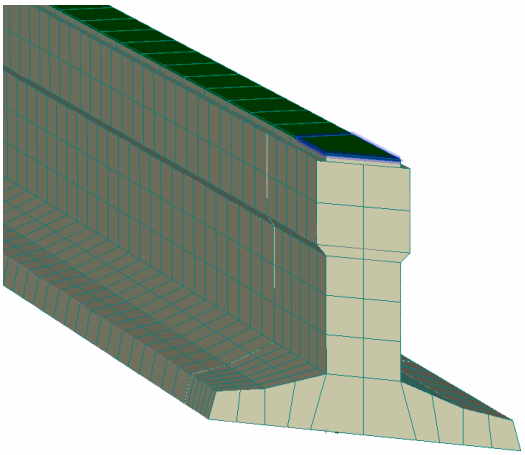

Figure 5-33 Top loading plate

5.6.5 Concrete deck

The first models did not have a deck on top of it. Only the determined Y- and Z-deformations are applied on the top of a ZIP girder, but the corresponding X-deformations are not correct in that case, due to a lower position of the centre of gravity. It can be analysed that, due to a lower level of the centre of gravity, at the top the longitudinal deformations will be too large and at the bottom the longitudinal deformations will be too small. For that reason on top of the loading plate a 'dummy deck' is applied to compensate this, as visualized in Figure 5-34. The stiffness of the deck is used to calibrate the deformations in the PNL-model to the deformations in the LE-model of the complete bridge.

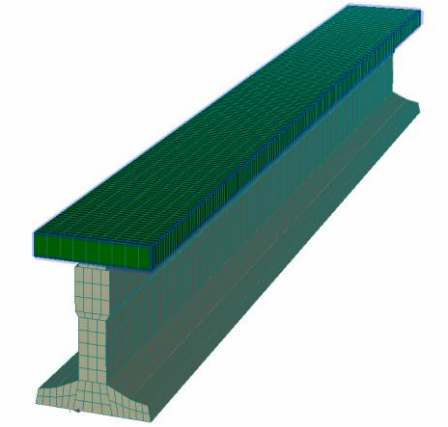

Figure 5-34 Dummy-deck in physical non-linear model

The required stiffness for the 'dummy deck' is determined using a model with coarse linear elements. In Figure 5-35 the reference longitudinal deformation due to load step 2, dX2 reference (following from the LE model of the bridge), is plotted for the bottom of the girder. It would be optimal to reach that deformation. Also the occurring deformation when no dummy deck is applied in the PNL-model, dX2 without dummy deck, is plotted. A large difference is visible.

First the stiffness as used in the LE-model of the bridge (16000 MPa) is applied, but this did not give a correct deformation. Chosen is for a 'trial-and-error' method to determine the stiffness which gives the correct X-deformations. A stiffness of 30000 MPa gives good results. In the figure this process is visible. An explanation for this high stiffness could be that in the total bridge system a larger width carries the normal force.

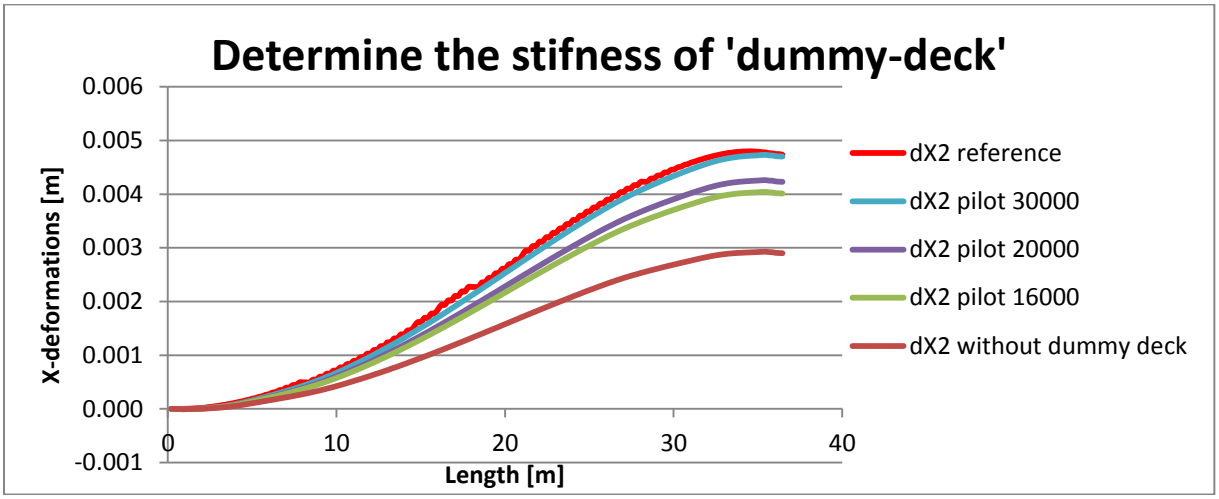

Figure 5-35 Deformations in bottom of girder

5.6.6 End diaphragm beam

5.6.6.1 Description of model

In the detail PNL model the end diaphragm beams must be simulated. It is very complicated to include all the effects of this beam.

Two models are investigated:

1. A loading plate on the ends of the girders, made of steel (Figure 5-36). In the indicated nodes (Figure 5-27) deformations are applied. With this method the 'clamping effect' of the beam is neglected. The loading plate is made of steel, the plate thickness is 10 mm. Only transversal prescribed deformations are applied.
2. A more advanced model which simulates the 'clamping effect' of the end diaphragm beam. This model is presented in Figure 5-37. Steel plates with a minimal thickness of 30 mm are applied. Only transversal prescribed deformations are applied.

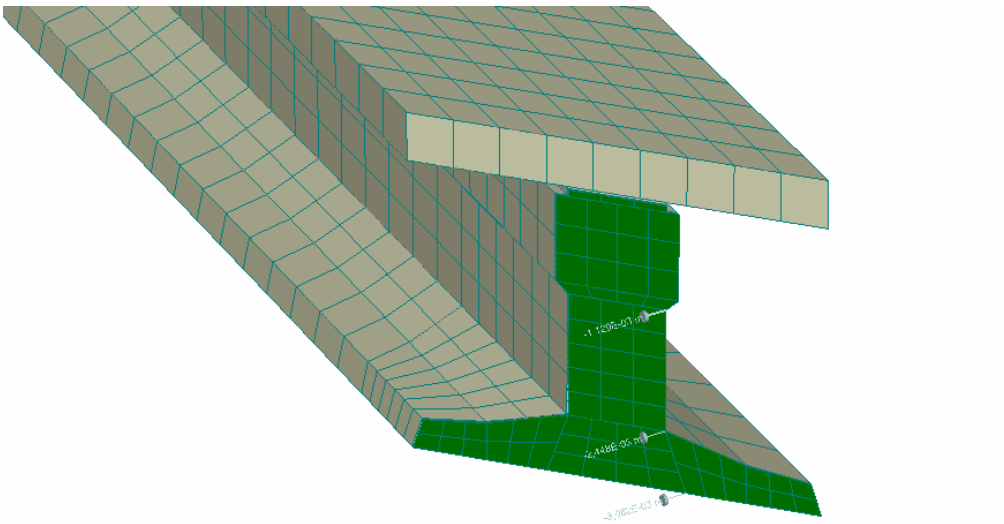

Figure 5-36 End load plate

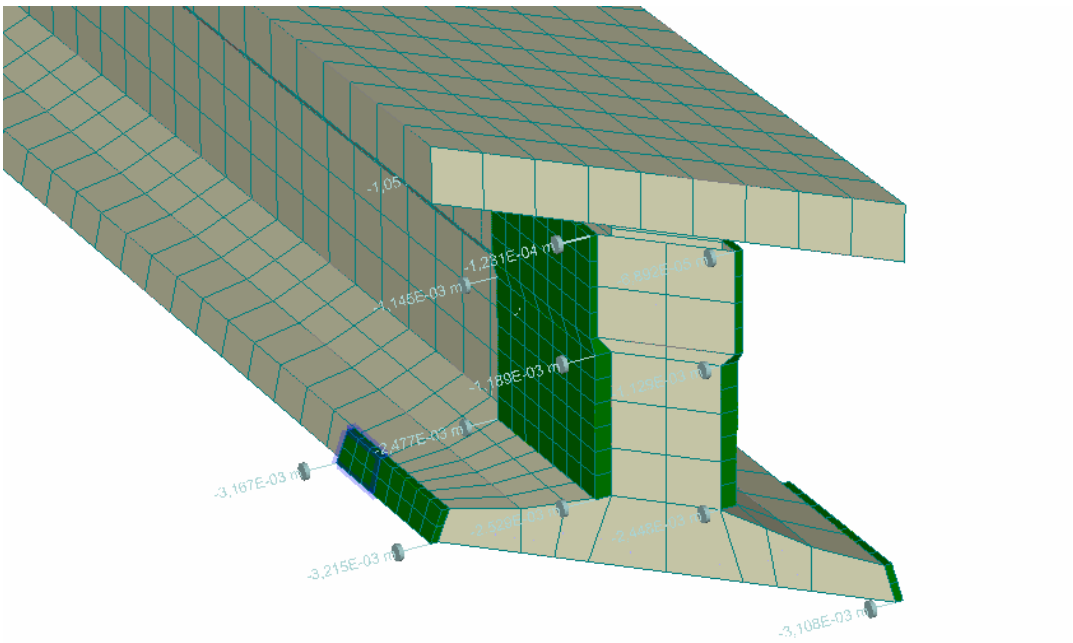

Figure 5-37 More advanced end loading plates

5.6.6.2 Comparison of models

A model of the ZIP-girder refined with coarse quadratic elements is used to analyse the deformations for the different models for the end diaphragm beam. The deformations in X- and Z-direction do not change when a different model for the end diaphragm beam is used, Figure 5-39 and Figure 5-40.

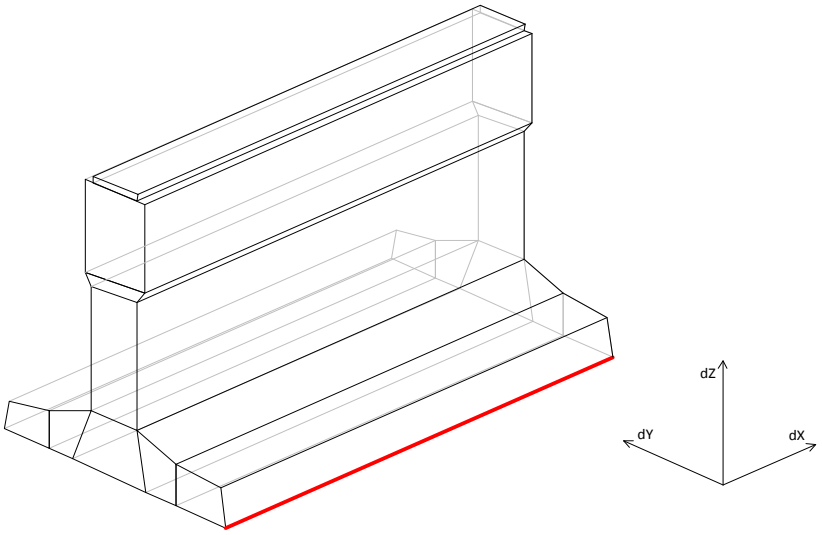

Figure 5-38 Check of deformations in the edge indicated with red

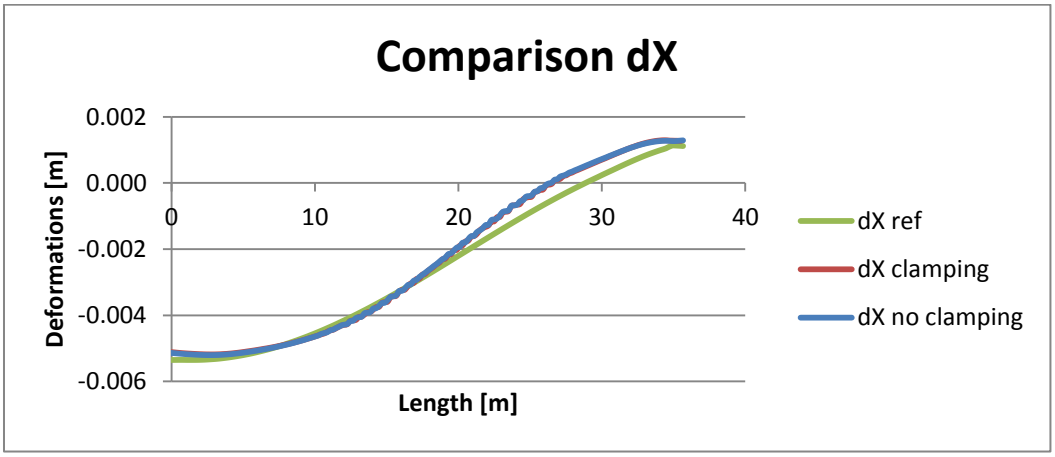

Figure 5-39 Comparison longitudinal deformation, dX

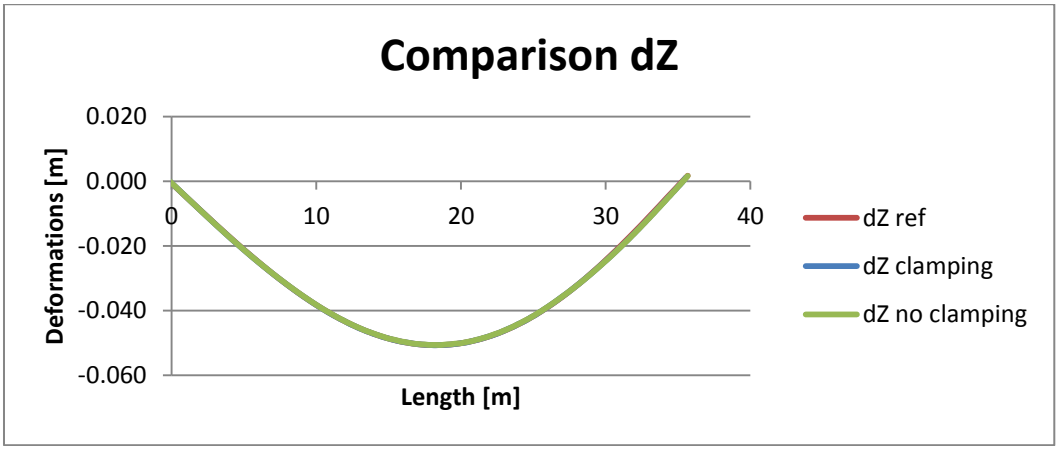

Figure 5-40 Comparison deflection, dZ

The deformation in Y-direction is changing. In Figure 5-41 the deformations are presented. It is visible that in the acute corner the different models do not influence the deformations a lot, at the obtuse corner however a substantial difference is found. The influence of this deviation shall be investigated later.

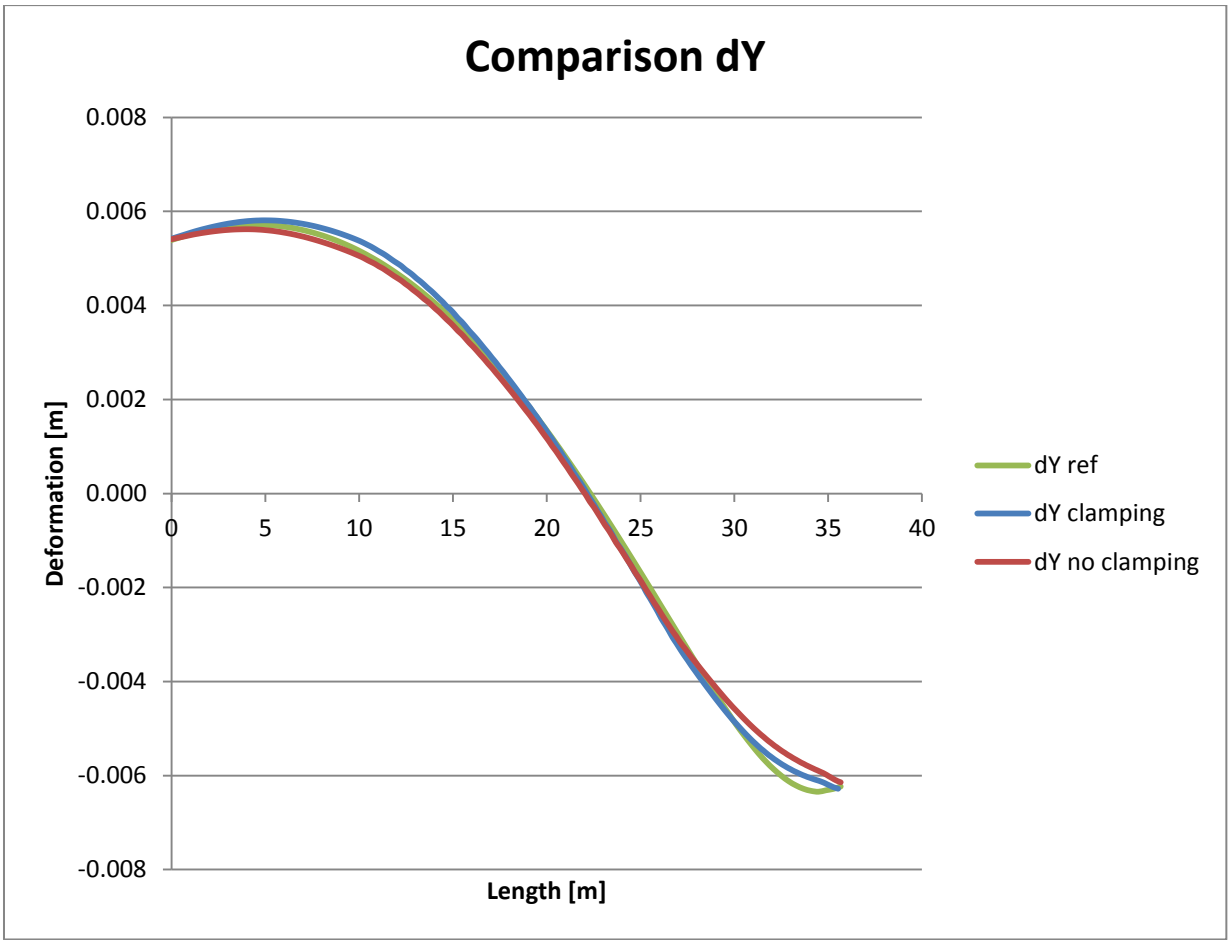

Figure 5-41 Comparison transverse deformation, dY

From the comparison of the two models to simulate the end diaphragm beam follows that including the 'clamping effect' gives better results. That model, Figure 5-37, shall be used in the PNL model for one ZIP girder.

5.7 Results skew bridge for load case Spanbeton

Only the results for the model loaded with the load case of Spanbeton are presented, the load case of Minalu leads to similar results. The models are carried out in ultimate limit state (ULS).

Models carried out:

I. PNL model, locally refined with coarse quadratic elements
II. PNL model, locally refined with fine quadratic elements

5.7.1 PNL model, locally refined with coarse quadratic elements

5.7.1.1 Check deformations

Is already presented in Figure 5-39, Figure 5-40 and Figure 5-41 for the model 'with clamping'. The deformations are reasonable. Note the difference in transverse deformation.

5.7.1.2 Stresses

Sections are made at x=33.08 m to visualize the stresses because at that location maximal stresses occur.

Shear stresses at x=33.08 meter. Shear stress (Figure 5-42):

- Total: 3.30 N/mm^2
- Shear force: 2.73 N/mm^2
- Torsion moment: 0.58 N/mm^2

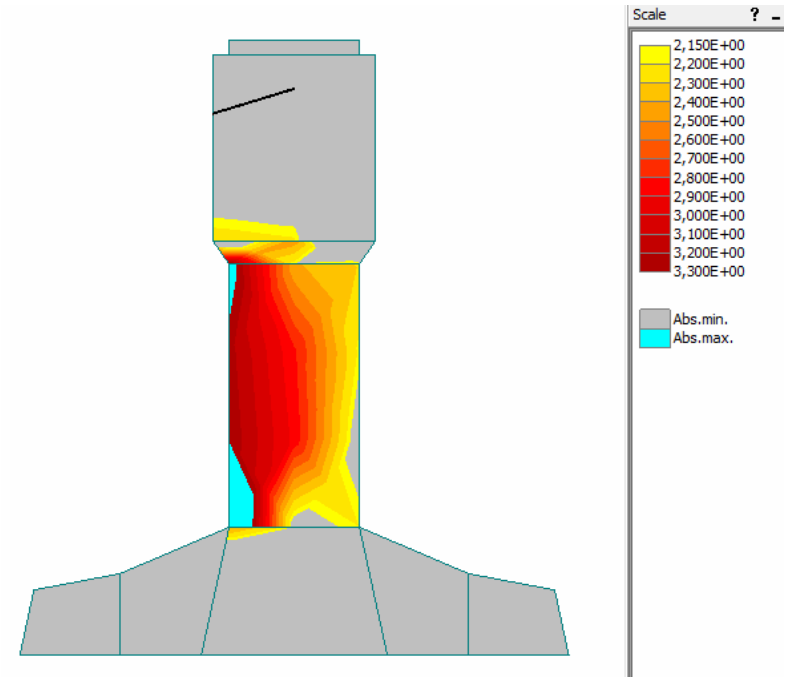

Figure 5-42 Shear stresses in PNL model I

When the principal stresses are studied they are higher than expected. The principal stresses that occur are presented in Figure 5-43. It appeared that vertical stresses occur.

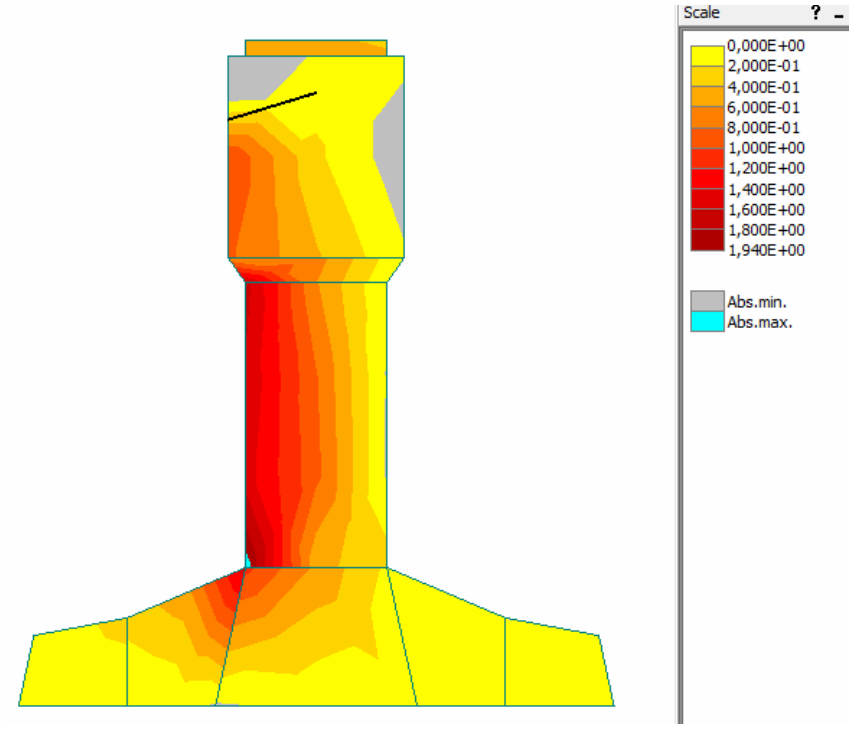

Figure 5-43 Principal stresses in PNL model I

The occurring vertical stresses that occur are presented in Figure 5-44.

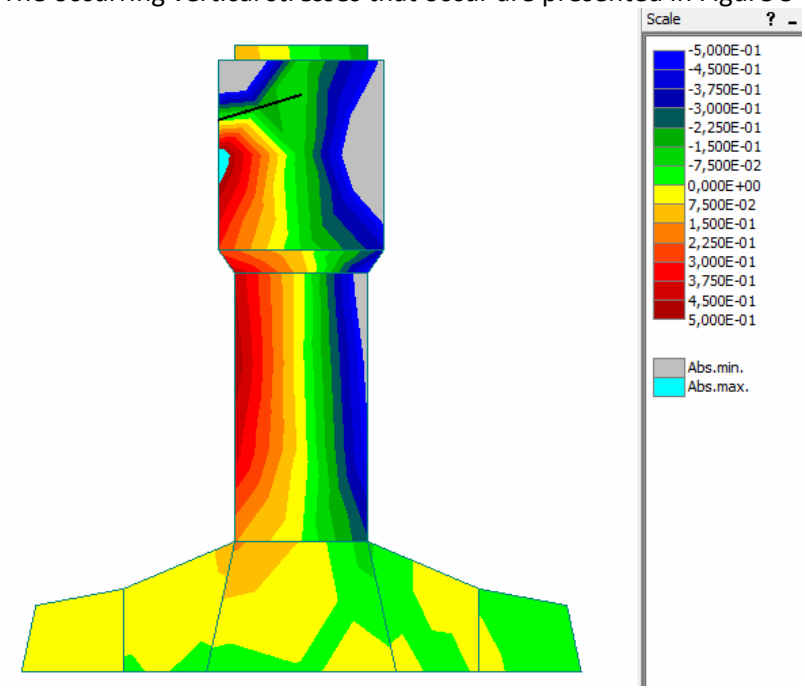

Figure 5-44 Vertical normal stresses in PNL model I

5.7.1.3 Cracking

Due to introduction of the prestressing force in the concrete in the ends of the girders cracks occur. Spanbeton uses standard reinforcement in that area to control the crack widths. In all the following models this cracks are visible but not further investigated.

The skew bridge of 45° is modelled with a sharp end (see presented figures). In practice this corner is not made because it will be simply damaged during handling the girder. Cracking, and all kind of other effects, in the region of this sharp corner are for that reason of no interest.

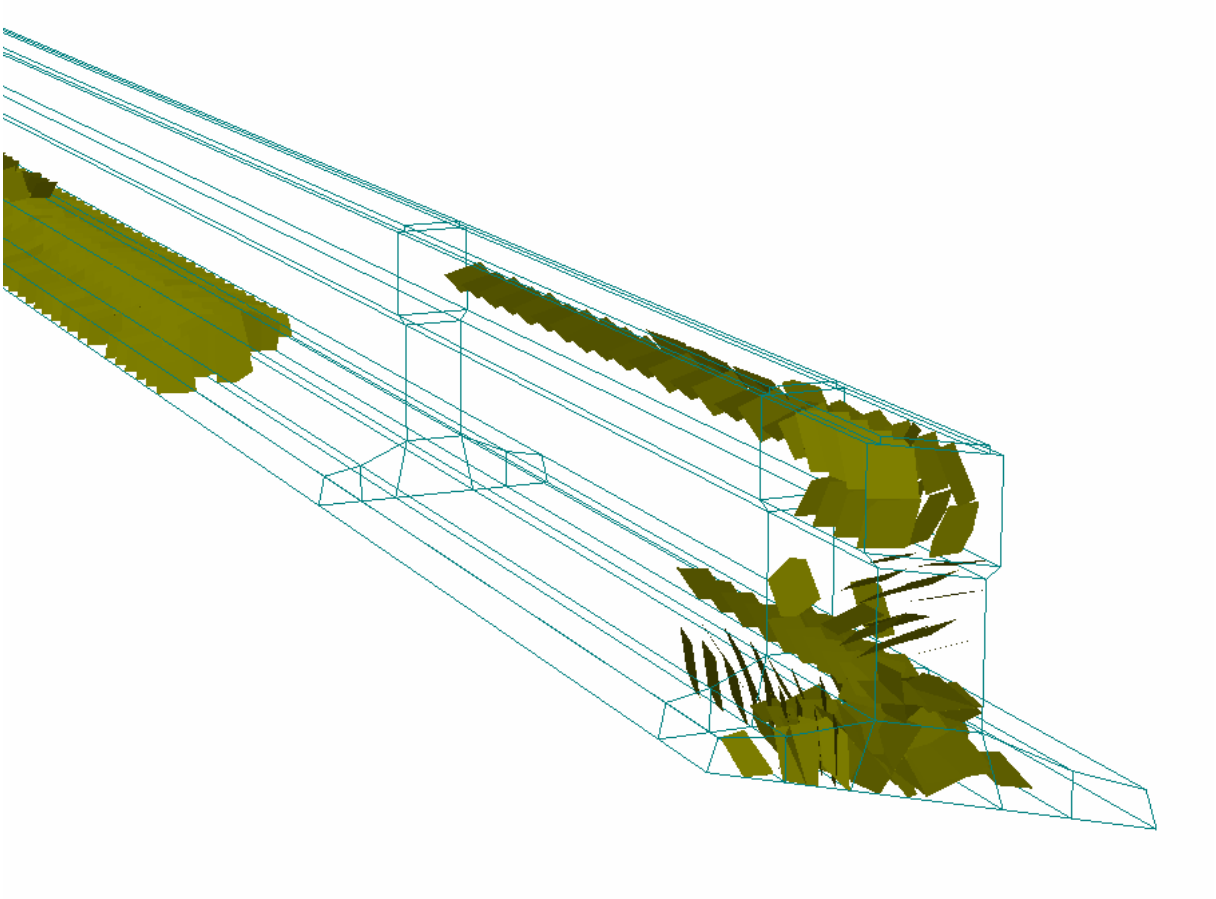

Figure 5-45 Occurring cracks in PNL model I

Remarkable are the cracks occurring in the top of the girder, the maximum crack width is $1.76 \cdot 10^{-4}$ m. In the same zone no flexural cracks are visible. So an uncracked zone appears in which principal stresses can be checked.

5.7.2 PNL model, locally refined with fine quadratic elements

This model is carried out to be sure that a mesh refinement does not influence the results.

5.7.2.1 Check deformations

The deformations can be checked as presented before, yet visualized in Figure 5-46. Only the transverse deformation is presented, it is already noted that this deformation deviates from the reference deformation. The deviation is more severe for 'the refinement with fine quadratic elements' compared with 'the refinement with coarse quadratic elements'.

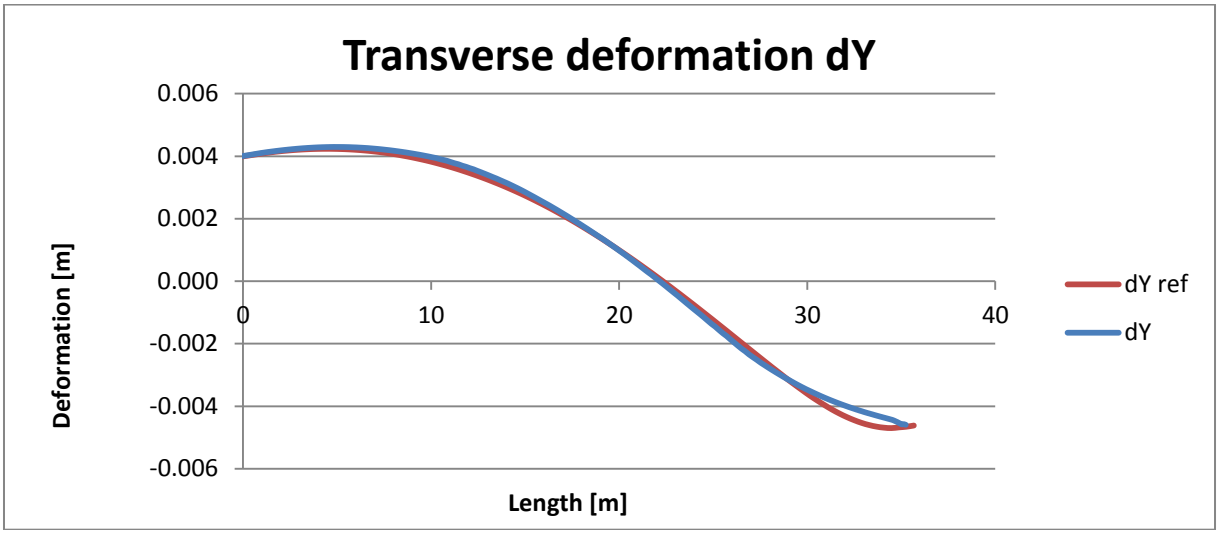

Figure 5-46 Transverse deformation, dY

5.7.2.2 Stresses

The shear stress at x=33.08 meter consists of the following parts:

- Total: 3.00 N/mm^2
- Shear force: 2.28 N/mm^2
- Torsion moment: 0.73 N/mm^2

The shear stresses are presented in Figure 5-47.

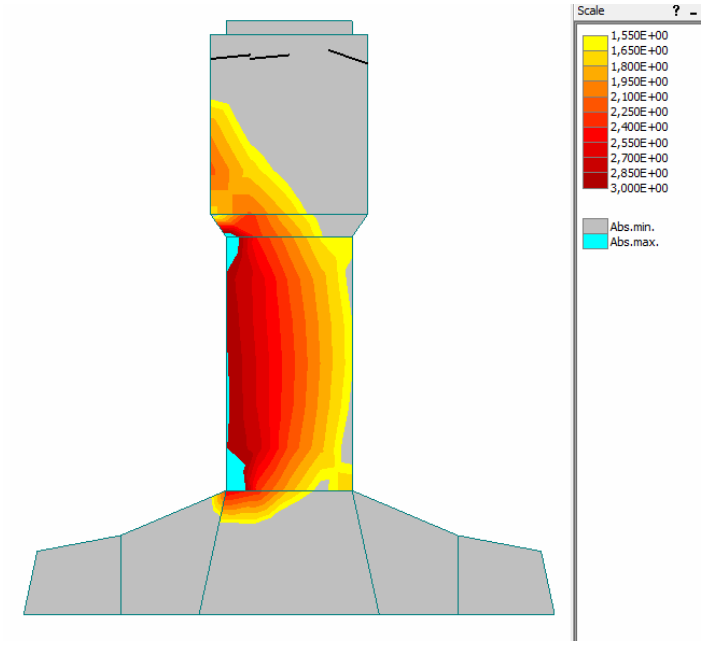

Figure 5-47 Shear stresses in PNL model II

The principal stresses are presented in Figure 5-48.

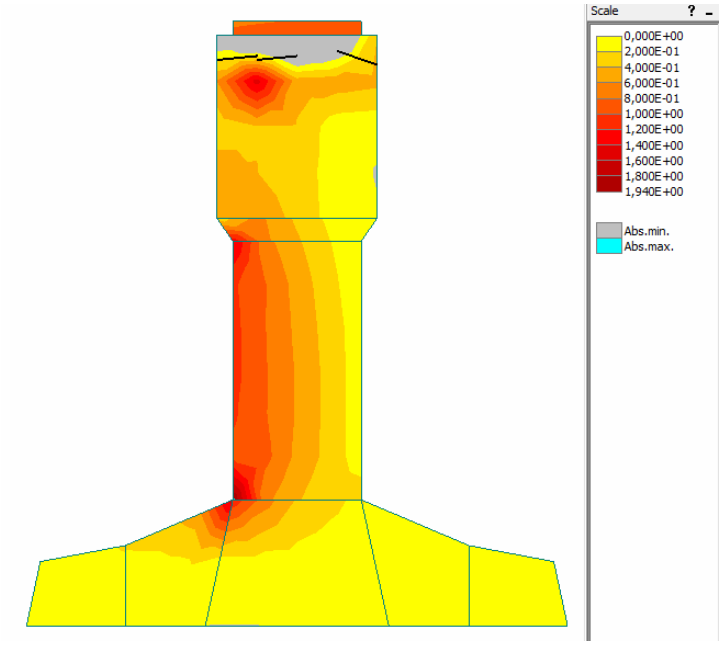

Figure 5-48 Principal stresses in PNL model II

The vertical normal stresses are presented in Figure 5-49.

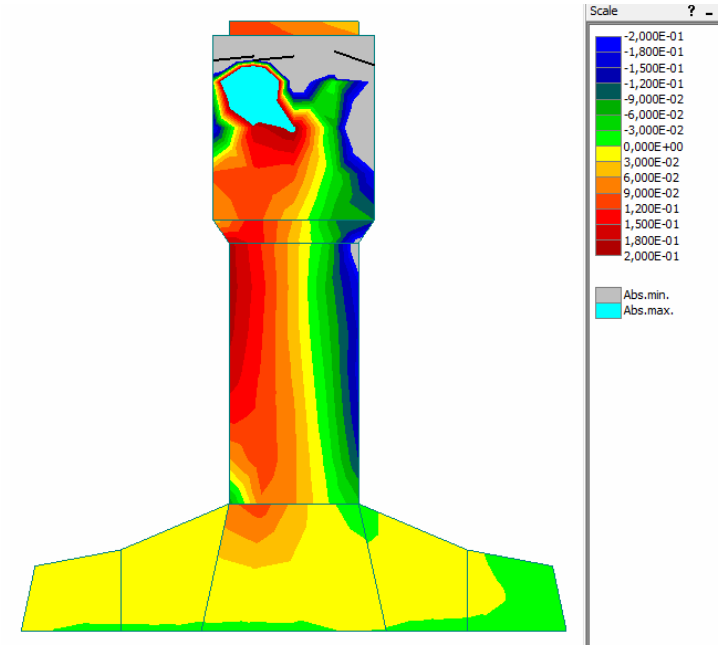

Figure 5-49 Vertical normal stresses in PNL model II

5.7.2.3 Cracking

In the top of the girder cracks with a magnitude of 0.5 mm occur. In relation with the deviating transverse deformations: the applied deformations on top of the girder are not connected with the transverse deformations at the bottom of the girder because the connection is broken. The cracks at the bottom of the web are very small and neglectable (0.002 mm). Also here no flexural cracks are visible.

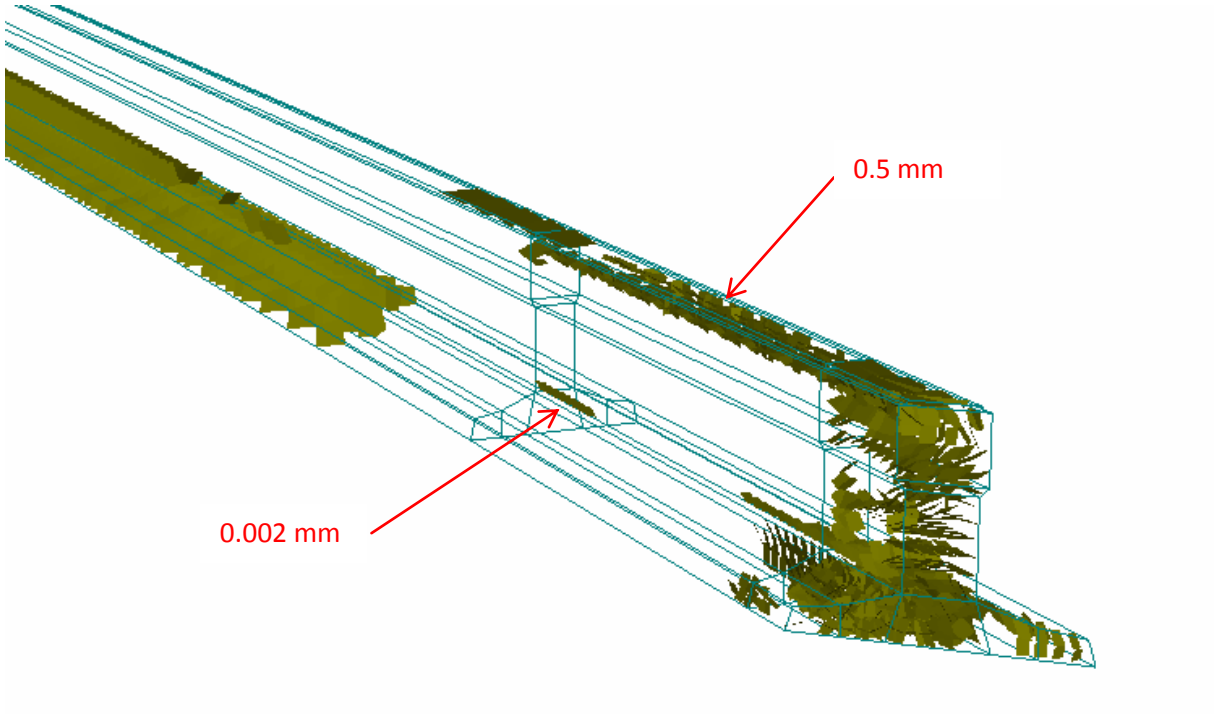

Figure 5-50 Occurring cracks in PNL model II

5.7.3 Comparison observations

The cracking in both models occurs at the same locations. Cracks due to prestressing and flexural cracks are visible. Also cracking in the top is present in both models, this cannot be explained physically. It is visible that beside this cracking in a large zone of the girder no cracking occurs.

The total shear stresses in both models are comparable, the ratio between the part due to shear force and due to torsion changes.

It is visible that this models contains some unexpected phenomena as the mentioned cracking and the changing ratio between shear stresses due to shear force and torsion. Also a vertical tension stress is measured which influences the principal stress. Finally the transverse deformations are not totally correct. This will be investigated further.

5.8 Analysis of unexpected phenomena

The observed phenomena mentioned in paragraph 5.7.3 can be explained. Important is the deviating transverse deformation. This deviation causes vertical tensile stress, but also a deviation in the applied rotations, and consequently a deviation in the applied torsion moments.

5.8.1 Vertical normal stress

5.8.1.1 Introduction

In the models carried out vertical stresses are observed, are these stresses really occurring? The vertical stresses occurring in the model refined with coarse quadratic elements (model I) can be plotted, Figure 5-51.

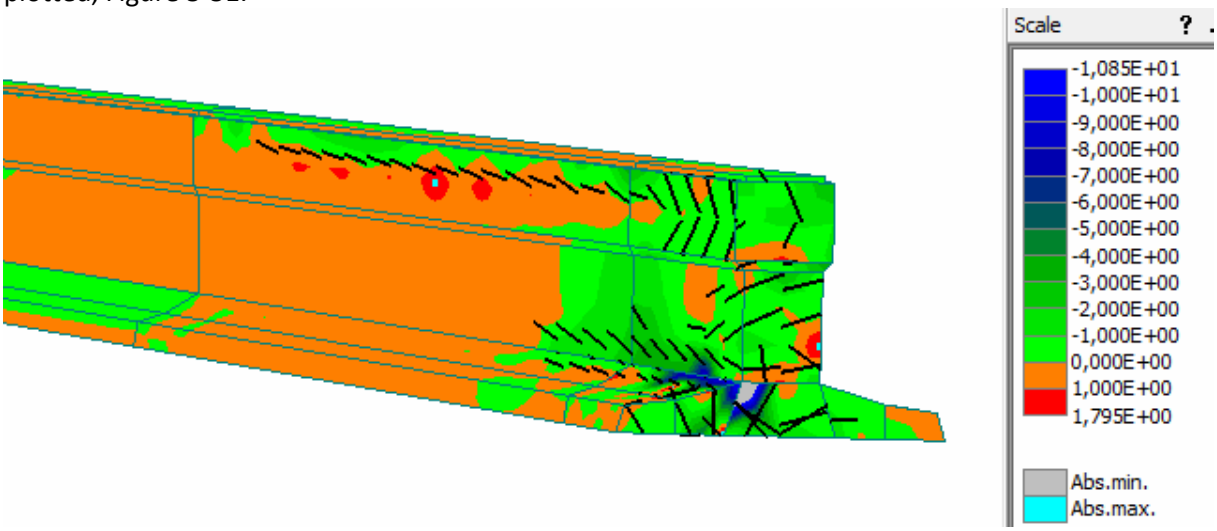

Figure 5-51 Vertical stresses in end of ZIP-girder in PNL model I

When the vertical stresses are analysed in the linear elastic model of the bridge (presented in paragraph 5.2) the following stress distribution is visible, presented in Figure 5-52. This are stresses at the height of the centre of gravity. Only a stress of 0.1 N/mm^2 is found in SLS, this means about 0.14 N/mm^2 in ULS. That is much smaller than the stresses occurring in the physical non-linear model where the stresses are about 1-2 N/mm^2. So it is expected that the observed high vertical stresses are not correct.

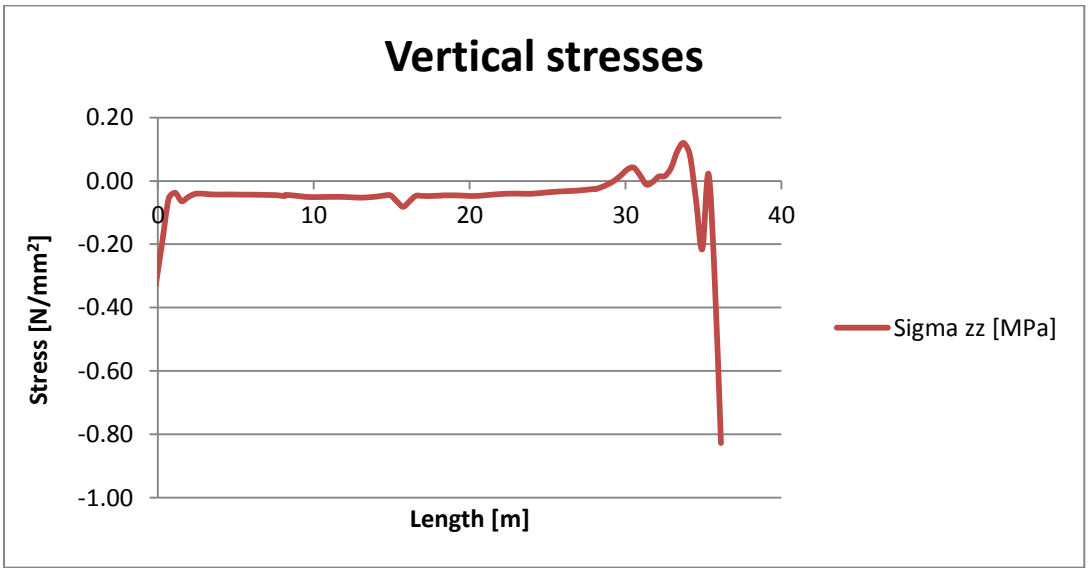

Figure 5-52 Vertical stresses occurring in the linear elastic model of the bridge in SLS at the height of the centre of gravity

5.8.1.2 Compatibility problem

The explanation for the occurring vertical stresses is that the small deviation of the transverse deformation causes a compatibility problem. The difference in transverse deformation in the cracked zone is enlarged from Figure 5-41 and presented in Figure 5-53. It was expected that including the 'clamping effect' of the end diaphragm beam would reduce the difference more.

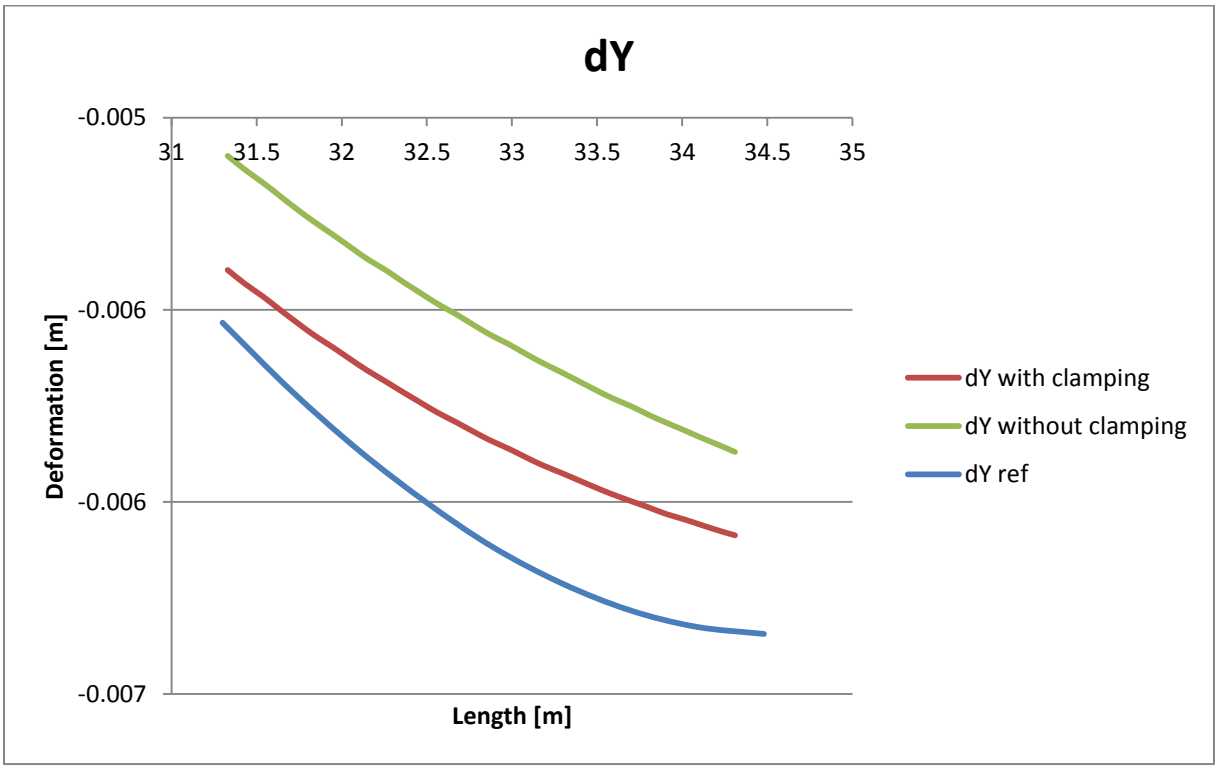

Figure 5-53 Difference in transverse deformation for different models of the end diaphragm beam in ULS

The rotation of the beam was calculated two times in paragraph 5.3.3 when the rotations from the linear elastic model of the bridge were analysed. The two calculations correspond well for that model. The relevant figure is shown again in Figure 5-54.

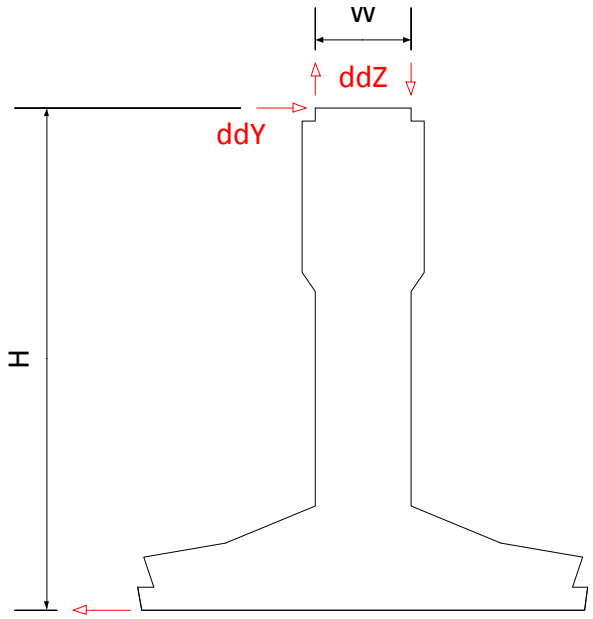

Figure 5-54 Determination of rotations

The deviation in transverse deformation influences the calculation of the rotations. This can be explained with formulae. The used formulae in paragraph 5.3.3 are:

$$\vartheta_{dY} = \frac{ddY}{H}$$
$$\vartheta_{dZ} = \frac{ddZ}{W}$$

When ddY is too small: $\vartheta_{dY} < \vartheta_{dZ}$. This causes vertical stresses.

5.8.1.3 Estimate of stresses

An estimation of the occurring stresses can be made. At 33.3 m a difference of 0.29 mm is found.

The difference in rotation at that location is:

$$\vartheta_{dY} = \frac{0.29 \cdot 10^{-3}}{1.32} = 2.17 \cdot 10^{-4}\ [rad]$$

This leads to an compatibility difference of $2.17 \cdot 10^{-4}$ x 0.28 = $0.61 \cdot 10^{-5}$ m for ddZ. The applied ddZ deformation is $4.35 \cdot 10^{-4}$ m, the deviation is 13%!

The deformations are applied with 400 mm distance on the top of the girder. It is assumed that this is the depth in which the difference in deformation is taken. An estimation of the stress can be made as follows:

$$\varepsilon = \frac{ddZ}{d} = \frac{0.61 \cdot 10^{-5}}{0.4} = 1.525 \cdot 10^{-5}\ [-]$$
$$\sigma = \varepsilon \cdot E = 1.525 \cdot 10^{-5} \cdot 38000 = 0.6\ {}^{N}/_{mm^2}$$

5.8.1.4 Experiment with ATENA

A simple model (length 4 meters) is carried out in ATENA to analyse the occurring vertical tension stresses. The loads and boundary conditions are applied as visualized in Figure 5-55. The found deviation of deformation ($0.61 \cdot 10^{-5}$ m) is applied on all the nodes along the top of the girder.

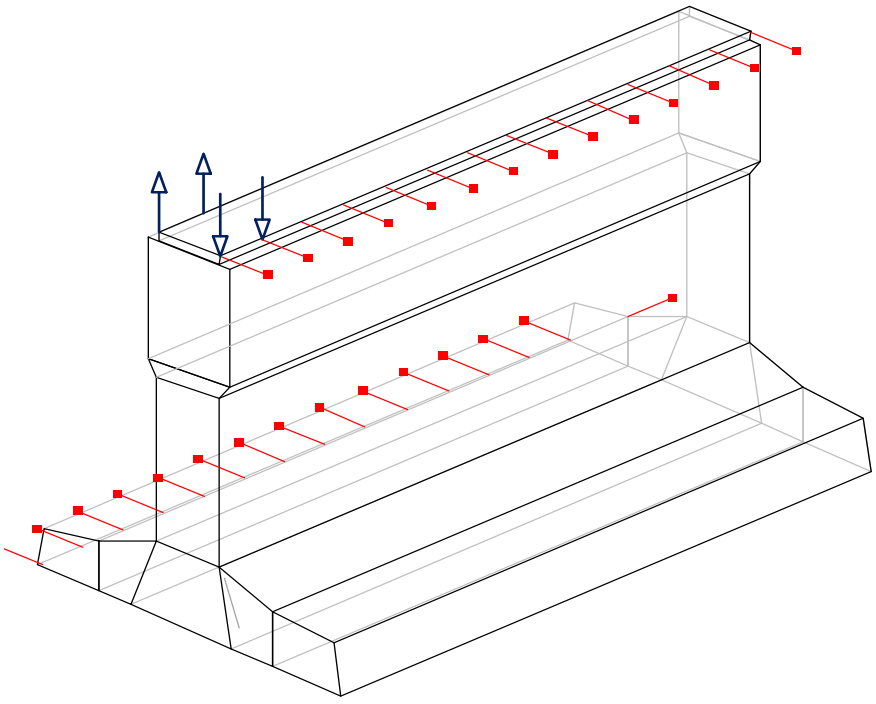

Figure 5-55 Model to simulate imposed deformation

The occurring stresses for the coarse and refined quadratic model are shown in Figure 5-56 and Figure 5-57. Visible is that the local applied deformations causes local peak stresses. Another observation is that in the model with refined quadratic elements the vertical stresses in the web are more localized.

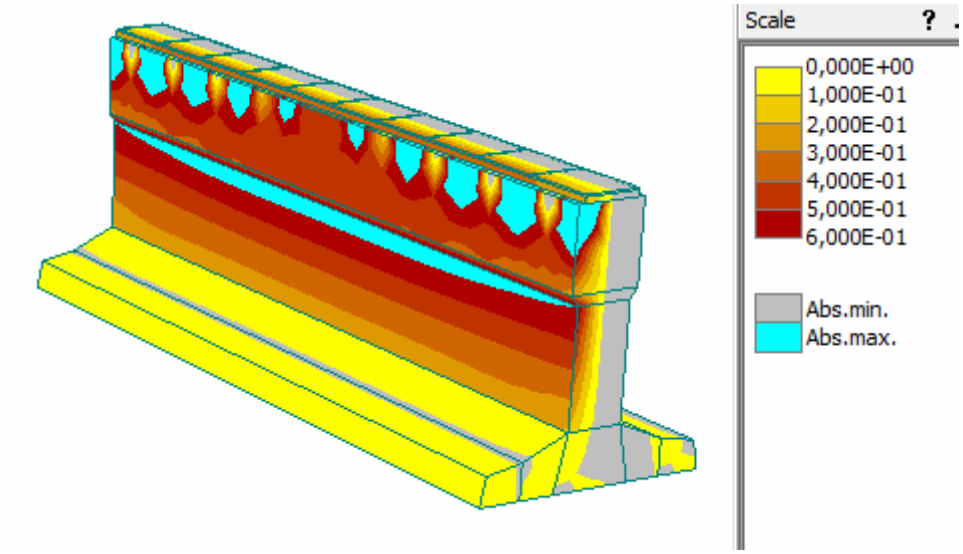

Figure 5-56 Model with coarse quadratic elements, peak stress 1.924, no cracks occur

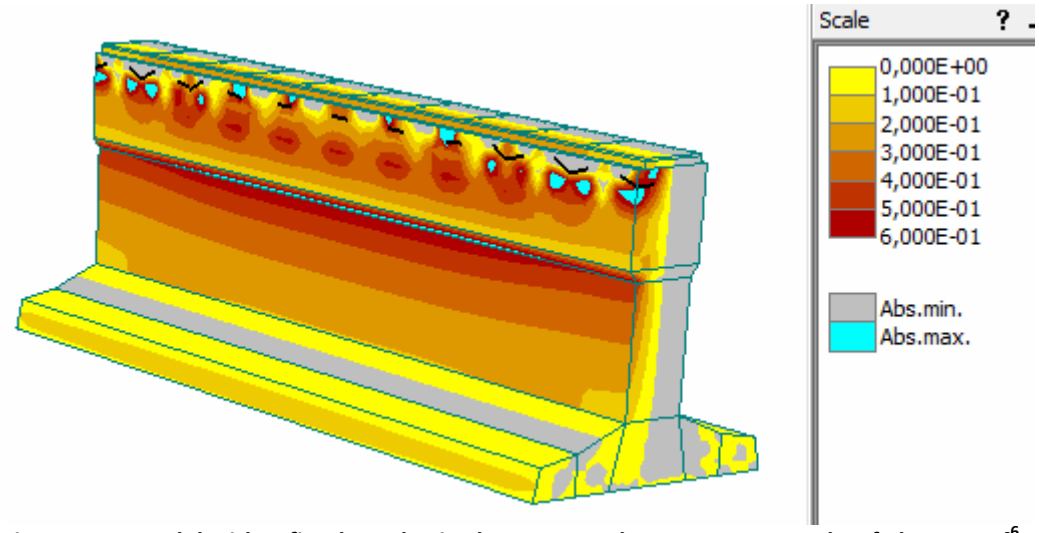

Figure 5-57 Model with refined quadratic elements, peak stress 1.911, cracks of about $5 \cdot 10^{-6}$ m occur

5.8.1.5 Conclusion

From the hand calculation and the experiments with ATENA the relation between the deviating transverse deformations and the vertical stresses is sufficiently proven.

5.8.2 Deviation in applied torsional moments

The torsion moments are applied on the model by prescribed deformations, which represent rotations. When the rotations are deviating this load is also not applied correct anymore. With the knowledge of paragraph 9.3.2 the deviation can be determined.

The calculation of the deviation for model II (refined with fine quadratic elements) is presented. The rotations can be calculated using the function presented in Figure 5-58.

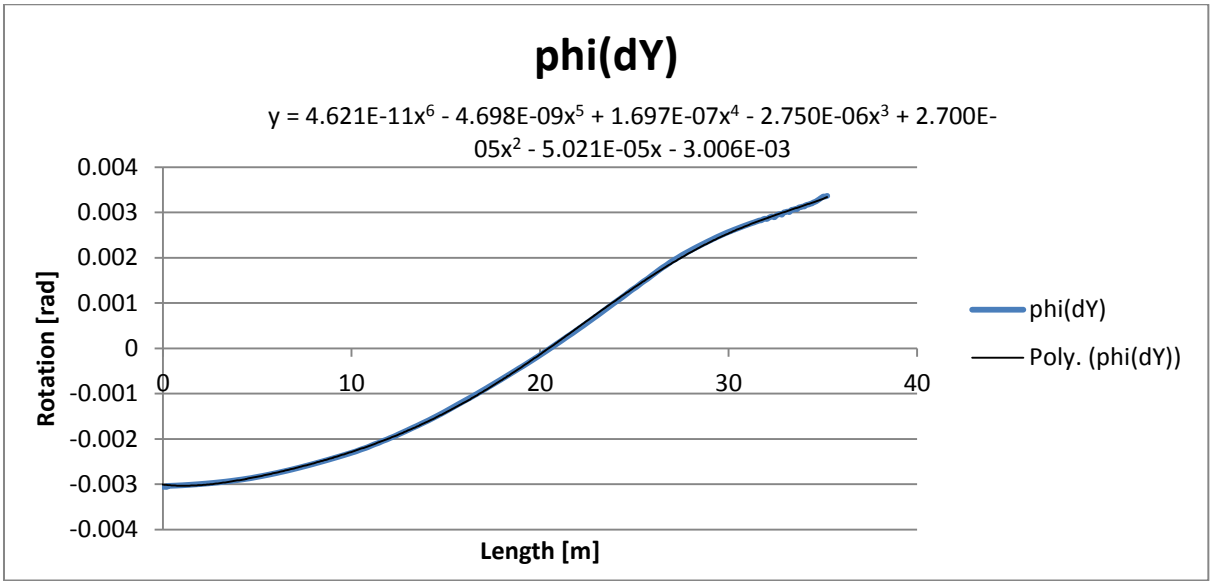

Figure 5-58 Rotation for model I

Using the function of the rotation the torsional moments can be determined, presented in Figure 5-59. The occurring torsional moments can be compared with the torsional moments that should occur, the following curves are plotted:

- Blue: Reference torsional moment (Figure 9-9).
- Green: Torsional moments that occur.
- Red: A substantial difference.

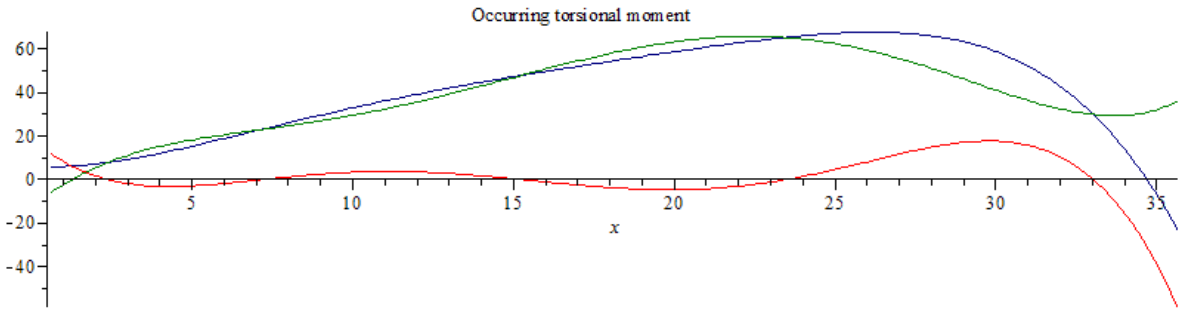

Figure 5-59 Deviations in torsional moments for model I

It is visible that in this model the occurring torsional moments deviates a lot from the intended load due to the deviation in transverse deformation.

5.9 Conclusion

A small deviation in transverse deformation has influence on the stresses and cracking in the model. Firstly the deviation causes vertical stresses. In the analytical calculation of the principal stresses it was assumed that no vertical stresses occur. In the finite element model however these stresses are present and disturb the calculation of the principal stresses. Secondly the deviation influences the applied torsional moments.

Despite the observed deviations in the models an uncracked zone is visible. This zone will be further analysed. This will be done by more detailed analyses of the occurring stresses in that region.

6 Shear stresses due to torsion in cross-section of ZIP girder

It is important to understand the distribution of shear stresses due to torsion in a ZIP girder. In daily practice hand calculations are used to distribute the torsion over the different parts of a cross-section. Calculating correctly the shear stresses needs more attention.

The occurring stresses at the height of the centre of gravity due to a torsional moment of 100 kNm is calculated using different methods.

6.1 Method 1: Calculation of shear stresses with a finite element program

The program ShapeBuilder is used to determine the occurring shear stresses due to a torsional moment of 100 kNm. A shear stress of 2 N/mm^2 occurs at the height of the centre of gravity. This stress is determined by placing the cursor in the interesting point, the program gives than the stress at that location as output.

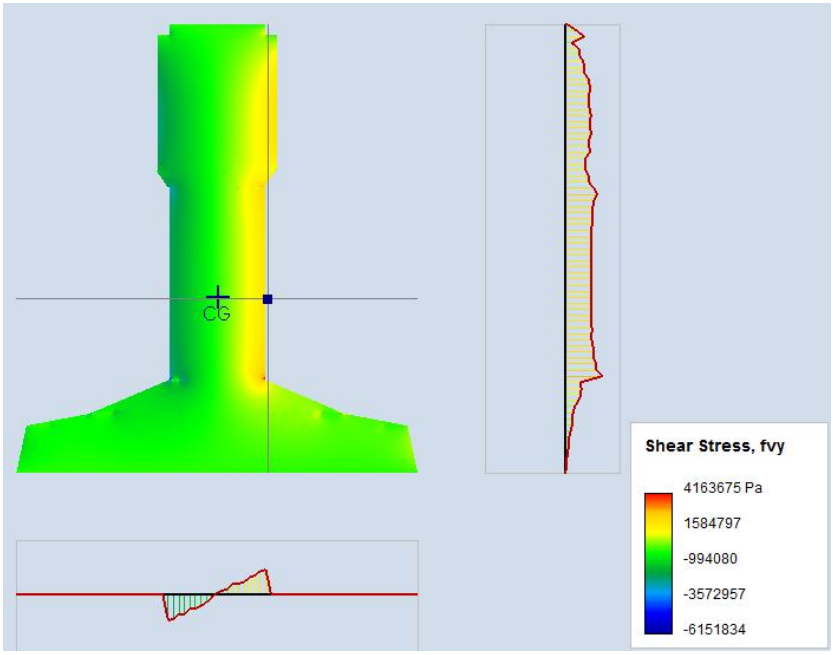

Figure 6-1 Shear stresses due to torsion calculated with ShapeBuilder

Also the program Scia Engineer can be used to analyse the stresses (Figure 6-2), a mesh size of 3 mm is used. In this program the value in a particular point cannot be determined.

The stresses presented in Scia Engineer are too low. The shear stress can be calculated by multiplying the values by a factor 1000·M_T. The value of M_T is 100 kNm. It is visible that at the height of the centre of gravity the stress than is between 1.44 N/mm^2 and 2.01 N/mm^2. This corresponds well with the results found with the program ShapeBuilder.

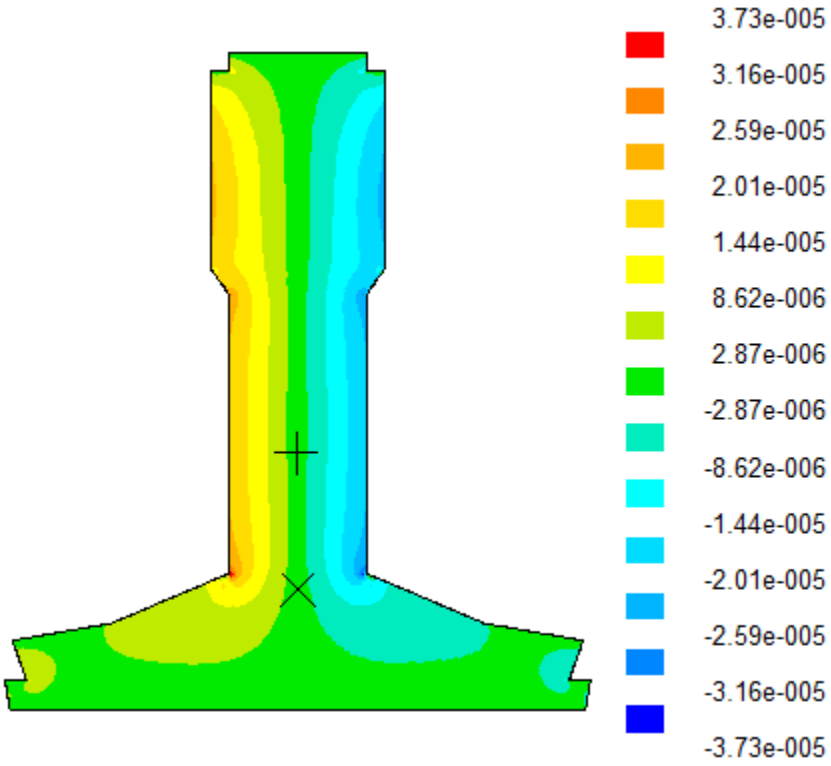

Figure 6-2 Shear stresses due to torsion calculated with Scia Engineer

6.2 Method 2: Estimation of torsion stresses by hand

Some different possible cases are studied to see the influence of the chosen simplification on the results.

Case 1

The girder can be split up in some parts as visualized in Figure 6-3.

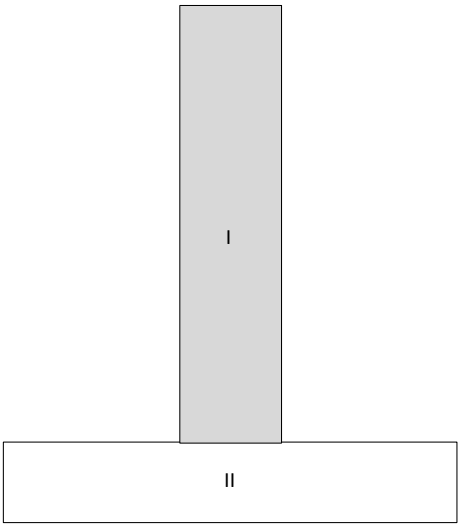

Figure 6-3 Model of first ZIP with deck to distribute torsion moments for case 1

The general formula for torsional stiffness is (can be derived from Table 2-2):

$$I_w = C_{I_w} \cdot b \cdot h^3$$

Applying the formula on the parts of the girder gives:
Part I:

$$\frac{b}{h} = \frac{1127}{280} = 4.03$$
$$I_{w,I} = 0.281 \cdot 1127 \cdot 280^3 = 6.95 \cdot 10^9\ mm^4$$

Part II:

$$\frac{b}{h} = \frac{1180}{193} = 6.11$$
$$I_{w,II} = 0.297 \cdot 1180 \cdot 193^3 = 2.52 \cdot 10^9\ mm^4$$

Part of torsion carried by the web of the ZIP-girder (shaded area in Figure 6-4):

$$\frac{I_{w,I}}{I_{w,total}} = \frac{6.95 \cdot 10^9}{6.95 \cdot 10^9 + 2.52 \cdot 10^9} = 0.73\ [-]$$

A torsional moment of 73 kNm with $C_\tau = 0.288$ will give a shear stress of:

$$\tau = \frac{M_T}{C_\tau \cdot b \cdot h^2} = \frac{0.73 \cdot 100 \cdot 10^6}{0.288 \cdot 1127 \cdot 280^2} = 2.87\ {}^{N}/_{mm^2}$$

Case 2
The girder can be split up in some other parts as visualized in Figure 6-4.

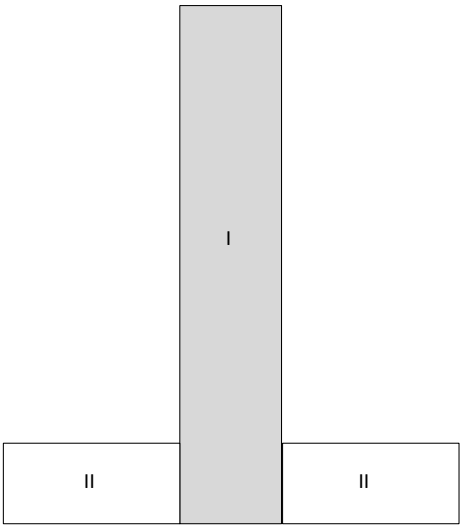

Figure 6-4 Model of first ZIP with deck to distribute torsion moments for case 2

The general formula for torsional stiffness is (can be derived from Table 2-2):

$$I_w = C_{I_w} \cdot b \cdot h^3$$

Applying the formula on the parts of the girder gives:
Part I:

$$\frac{b}{h} = \frac{1320}{280} = 4.71$$
$$I_{w,I} = 0.289 \cdot 1320 \cdot 280^3 = 8.37 \cdot 10^9\ mm^4$$

Part II:

$$\frac{b}{h} = \frac{450}{193} = 2.33$$
$$I_{w,II} = 0.243 \cdot 450 \cdot 193^3 = 7.86 \cdot 10^8\ mm^4$$

Part of torsion carried by the web of the ZIP-girder (shaded area in Figure 6-4):

$$\frac{I_{w,I}}{I_{w,total}} = \frac{8.37 \cdot 10^9}{8.37 \cdot 10^9 + 2 \cdot 7.86 \cdot 10^8} = 0.84\ [-]$$

A torsional moment of 84 kNm with $C_\tau = 0.289$ will give a shear stress of:

$$\tau = \frac{M_T}{C_\tau \cdot b \cdot h^2} = \frac{0.84 \cdot 100 \cdot 10^6}{0.289 \cdot 1320 \cdot 280^2} = 2.81\ {}^{N}/_{mm^2}$$

6.3 Comparison methods

The different methods give deviating results. The hand calculations roughly give 40% higher results than the FEM calculations. A comparison is presented in Table 6-1.

Method	Type	Shear stress τ	Ratio M_T/τ
Method 1	FEM	2.00 N/mm^2	50
Method 2, case 1	Hand calculation	2.87 N/mm^2	34.8
Method 2, case 2	Hand calculation	2.81 N/mm^2	35.6

Table 6-1 Comparison different methods

When the simplified cross-section is analysed with Scia Engineer a shear stress distribution is found as presented in Figure 6-5. The stresses are between 2.41 and 2.85 N/mm^2. That corresponds quite well with the made hand calculations.

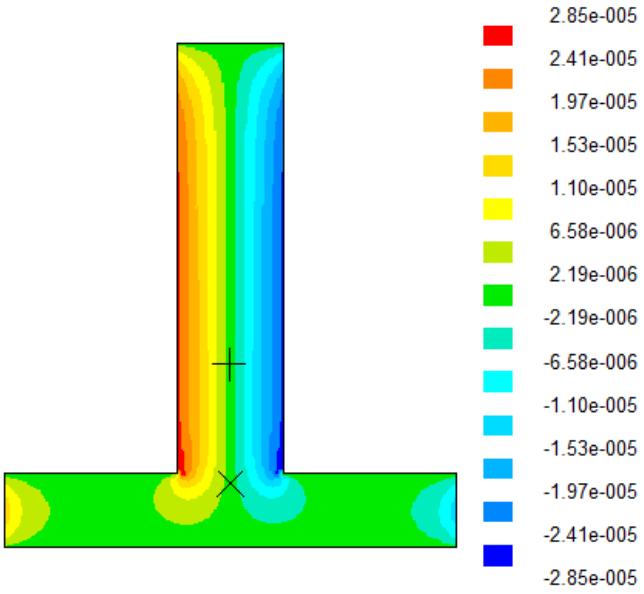

Figure 6-5 Shear stress in simplified cross-section calculated with Scia Engineer

The reason that there is a difference between the results of the two presented methods is that the phi-distributions are not the same. The phi-distribution for the simplified cross-section of the hand calculation is presented in Figure 6-6. In Figure 6-7 the distribution for the real cross-section is presented.

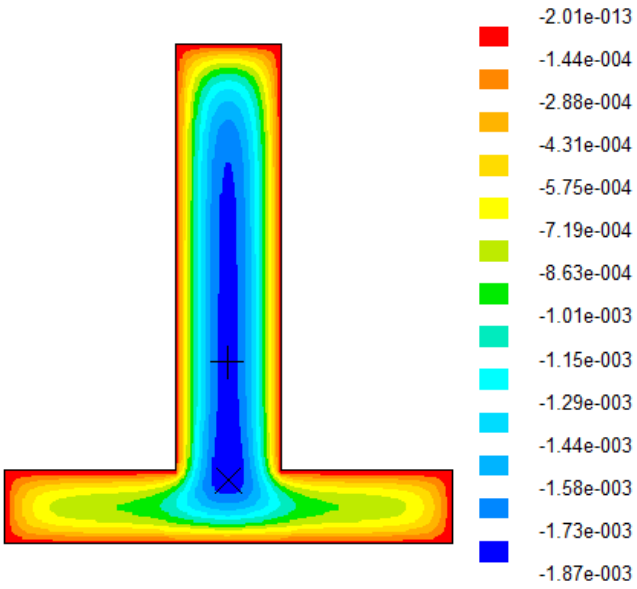

Figure 6-6 Phi distribution in simplified cross-section for hand calculation calculated with Scia Engineer

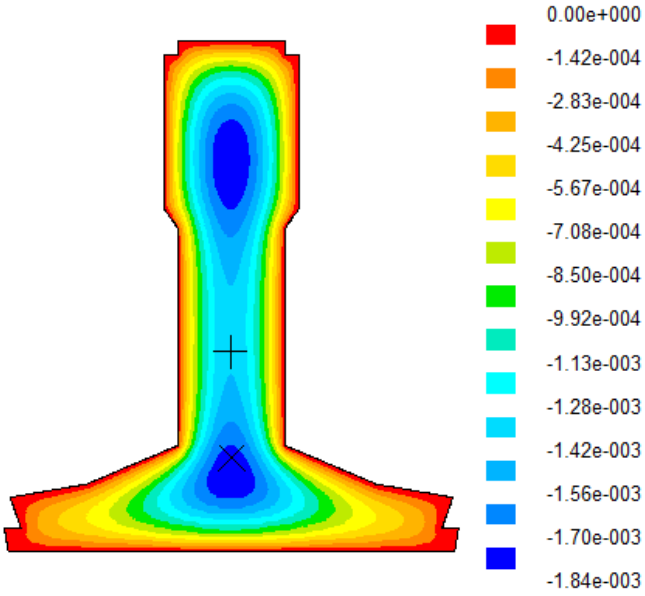

Figure 6-7 Phi-distribution in correct cross-section in FEM calculated with Scia Engineer

When Figure 6-6 and Figure 6-7 are compared follows that the thicker part of the web and the flange attracts shear stress away from the region around the centre of gravity. So using method 2 will be very conservative. The results of method 1 are used for the analytical calculations in this report.

Note: The influence of the deck on the phi-distribution is not presented. A quick check pointed out that this influence is neglectable.

7 Analytical Analysis

7.1 Procedure

To have insight in the behaviour of the girder a hand calculation (as far as possible) is made. When no hand calculation is possible a finite element model is used.

The analytical calculation is only carried out in the ultimate limit state (ULS). This is done because the physical non-linear finite element model of the girder is also carried out in ULS. In that limit state no cracking is expected.

The occurring forces in construction stage A and B are investigated and evaluated in chapter 8 and 9. From this forces the normal and shear stresses can be calculated, presented in chapter 10. Finally the principal stresses will be checked, also presented in chapter 10

7.2 Governing point

For maximal shear stress the severest combination of shear stresses due to shear force and torsional moment is occurring at the centre of gravity. Chosen is the point indicated with a red square in Figure 7-1. This is the centre of gravity of the girder and deck together (h=641 mm). The occurring shear stresses in this point are plotted along the length of the beam in the next chapters. For normal force the top and bottom of the girder are interesting to determine if there is an zone in the girder without flexural cracking. It is assumed that there are no vertical stresses in the girder.

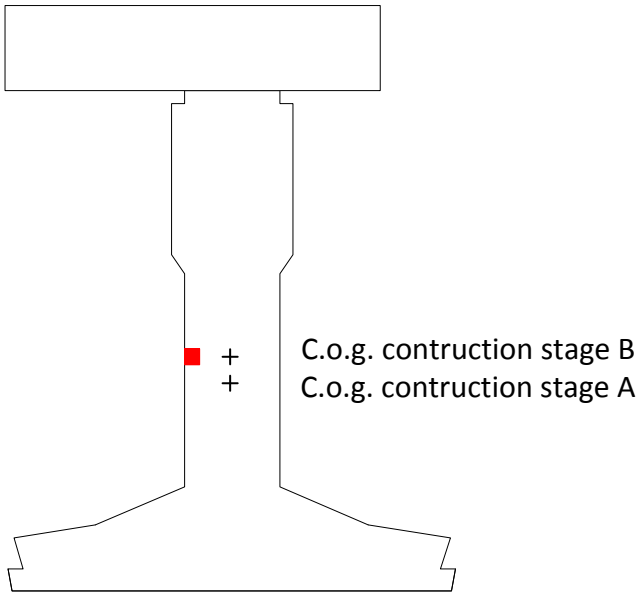

Figure 7-1 Cross-section, indication of governing point for check of principal stress

7.3 Tensile strength of concrete

A boundary tensile strength is necessary to be able to determine if cracks occur. The available design tension strength for concrete C53/65:

- Mean: 4.16 N/mm^2
- Characteristic: 2.91 N/mm^2
- Design: 1.94 N/mm^2

The capacity can be higher when the flexural tensile strength is used, this capacity is not used in this report.

7.4 Determination of stresses

The following formulae are used to calculate the normal and shear stresses:

- For normal stresses the formula: $\sigma_N = \frac{N_x}{A}$
- For shear stresses the formula: $\tau_V = \frac{V_x \cdot S^{(a)}}{I_{xx} \cdot b^{(a)}}$
- For torsion a finite element model is used. This is presented in chapter 6.

This different stresses are combined to principal stresses using the following formulae:

$$\sigma_1 = \frac{\sigma_{xx} + \sigma_{yy}}{2} + \sqrt{\left(\frac{\sigma_{xx} - \sigma_{yy}}{2}\right)^2 + {\sigma_{xy}}^2}$$

$$\sigma_2 = \frac{\sigma_{xx} + \sigma_{yy}}{2} - \sqrt{\left(\frac{\sigma_{xx} - \sigma_{yy}}{2}\right)^2 + {\sigma_{xy}}^2}$$

It is very conservative to check the stress in one outer fibre to the design strength. The shear stresses due to torsion are maximal at that point but decrease quickly to lower values. Pure elastically thinking, the distributions as presented in Figure 7-2 must be used. When plasticity is allowed, the distribution will change to the distribution as presented in Figure 7-3.

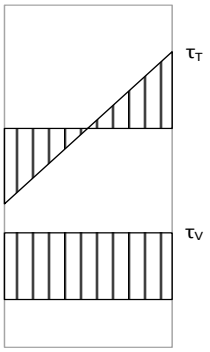

Figure 7-2 Shear stresses due to torsion moment and shear force, elastic distribution

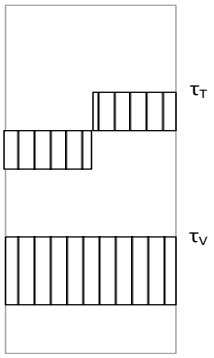

Figure 7-3 Shear stresses due to torsion moment en shear force, plastic distribution

The following to checks are done:

1. Check of principal using the shear stress distribution from Figure 7-2. The stress limit for this check is the mean tensile strength. The name for the check is ‘principal stress elastic’.
2. Check of principal using the shear stress distribution from Figure 7-3Figure 7-2. The stress limit for this check is the design tensile strength. The name for the check is ‘principal stress plastic’.

8 Analysis of 'Construction stage A'

In construction stage A the prestressing force and dead weight are applied. After that the fresh concrete deck is poured and totally supported by the girder. The stresses are calculated at the centre of gravity of the girder.

8.1 Stresses due to prestressing

The prestressing causes normal force, shear force and bending moments in the girder. The bond length of the cables has influence in the first part of the girder. The bond length can be determined following the Eurocode 1992-1-1, a safe assumption is a length of 1.5 meter, appendix C.

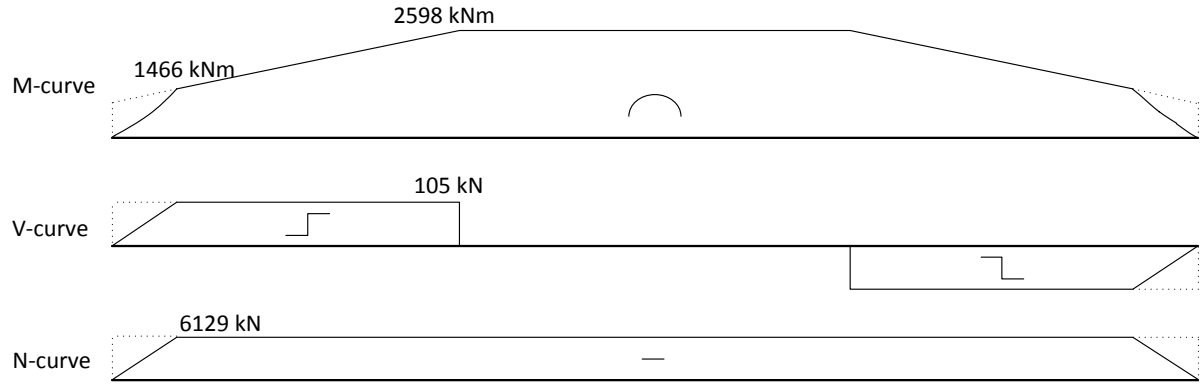

Figure 8-1 Force distributions due to prestressing (for F_p = 161.4 kN in SLS)

The derivation of the force distributions is presented in appendix D.

The stresses due to the occurring shear and normal forces are calculated at the end of the bond length (this stresses develop linear over the bond length, this is the maximum), in ULS:

$$\tau_{V,prestressing} = \frac{V_x \cdot S^{(a)}}{I_{xx} \cdot b^{(a)}} = 0.9 \cdot \frac{-105 \cdot 1000 \cdot 1.072 \cdot 10^8}{1.016 \cdot 10^{11} \cdot 280} = 0.356 \ \frac{N}{mm^2}$$

$$\sigma_N = 0.9 \cdot \frac{-6129 \cdot 1000}{A} = 0.9 \cdot \frac{-6129 \cdot 1000}{5.685 \cdot 10^5} = -9.70 \ \frac{N}{mm^2}$$

8.2 Stresses due to dead weight and fresh poured concrete deck

The weight of the girder and the weight of the fresh poured concrete gives an extra moment. For simplicity the moments are assumed zero above the supports. In reality there is a very small negative moment from the cantilevering part of the beam.

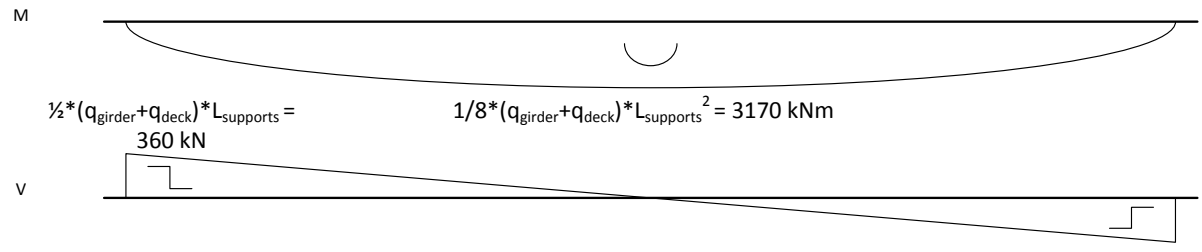

Figure 8-2 Force distributions for dead weight and fresh poured concrete deck in SLS

The stresses due to dead weight and fresh poured concrete are calculated at the supports (that is the maximum shear force), in ULS:

$$\tau_{V,dead\ weight} = -\frac{V_x \cdot S^{(a)}}{I_{xx} \cdot b^{(a)}} = 1.35 \cdot \frac{-360 \cdot 1000 \cdot 1.072 \cdot 10^8}{1.016 \cdot 10^{11} \cdot 280} = -1.832 \ \frac{N}{mm^2}$$

9 Analysis of 'Construction stage B'

9.1 Introduction

The force distribution for construction stage B is calculated using finite element models. The forces are considered in half of the beam (indicated in Figure 9-1).

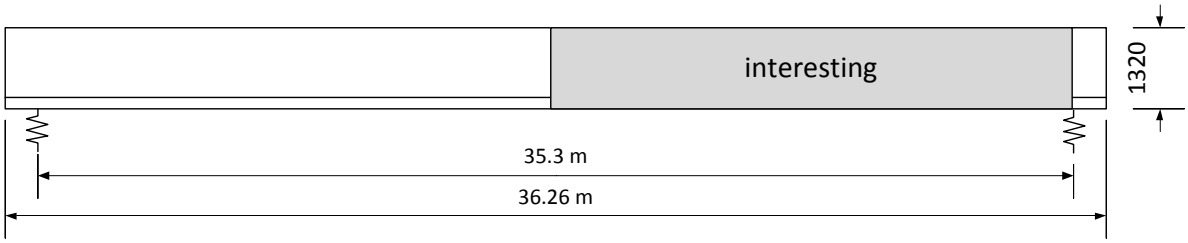

Figure 9-1 Geometry of girder

In the following paragraphs the force distribution is calculated using finite elements models:

1. Orthotropic plate model (2D) without end diaphragm beams, Scia Engineer.
2. Volume element model (3D) without end diaphragm beams, ATENA 3D.
3. Volume element model (3D) with end diaphragm beams, ATENA 3D.

The load case of Spanbeton and Minalu are investigated both.

9.2 Orthotropic plate model of bridge

9.2.1 Parameters model

The bridge is modelled as an orthotropic plate. The function of Scia Engineer to calculate cross-section properties is used, the results are presented in Table 9-1. This properties are used to calculate the stiffness parameters for the orthotropic plate, presented in Table 9-2.

Property	ZIP	First ZIP	TRA	Unity
Width b	1.2	1.023	1.177	m
Effective shear area A_z	0.36989	0.27404	0.36209	m^2
Bending stiffness I_y	0.18260	0.16680	0.14740	m^4
Torsional stiffness I_t	0.015809	0.015669	0.022319	m^4
Centre of gravity (with/without deck)	517/673	517/641	798/888	mm

Table 9-1 Cross-section properties

Formula	ZIP	First ZIP	TRA	Unity
$D_{11} = \frac{E_x \cdot I_x}{b}$	5782	6196	4759	MNm
$D_{22} = \frac{E_y \cdot t^3}{12 \cdot (1 - \nu^2)}$	16.9	16.9	16.9	MNm
$D_{12} = \nu \cdot \frac{E_y \cdot t^3}{12 \cdot (1 - \nu^2)}$	3.4	3.4	3.4	MNm
$D_{33} = \frac{1}{4} \cdot \left(\frac{G_x \cdot I_t}{b} + \frac{G_y \cdot t^3}{6} \right)$	56	64	79	MNm
$D_{44} = \frac{G_x \cdot A_z}{b}$	4880	4241	4871	MN/m
$D_{55} = \frac{G_y \cdot t}{1.2}$	1278	1278	1278	MN/m

Table 9-2 Properties of orthotropic plate in Scia Engineer

9.2.2 Transformation of data

The results found in the made cuts in the orthotropic plate model are transformed to the working forces in the first ZIP girder doing the following steps:

1. Multiply the shear force and bending moments with the width of the strip (representing the first ZIP girder). Width = 1.023 m.
2. Multiply the plate torsion moments with the width of the strip (width = 1.023 m) and the longitudinal distribution factor ($\rho_{longitudinal}$ = 1.9).
3. Reduced the torsion moments, only the part of the torsion carried by the girder is needed. It appears that 97% of the torsion is carried by the ZIP-girder (not demonstrated).

9.2.3 Resulting force distributions

In Figure 9-2, Figure 9-3 and Figure 9-4 the force distributions are presented for the load case of Spanbeton and Minalu. The forces are plotted along the length of the girder.

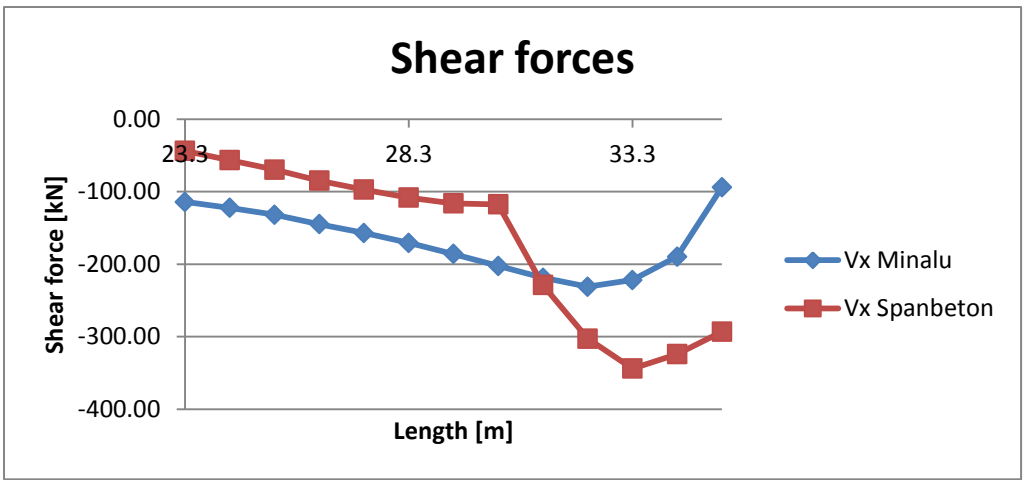

Figure 9-2 Shear force distribution determined with Scia Engineer

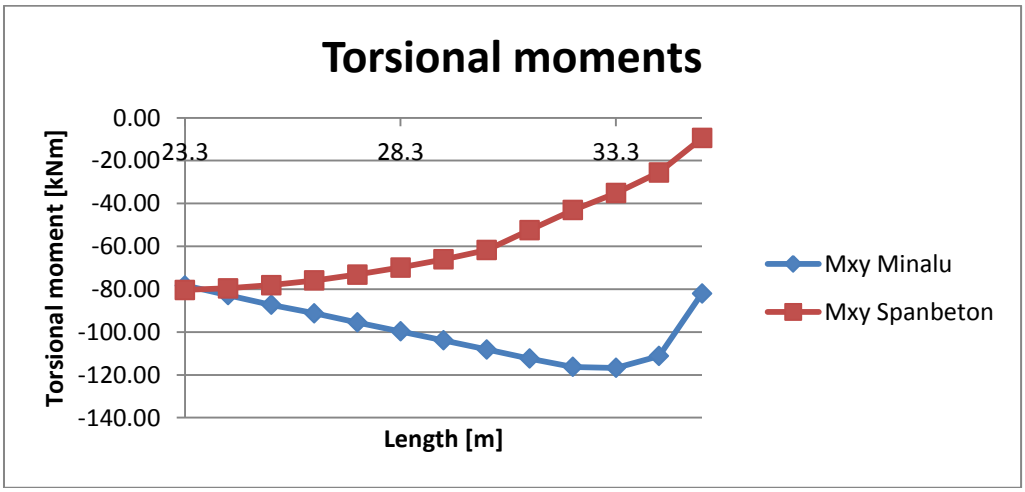

Figure 9-3 Distribution of torsional moments determined with Scia Engineer

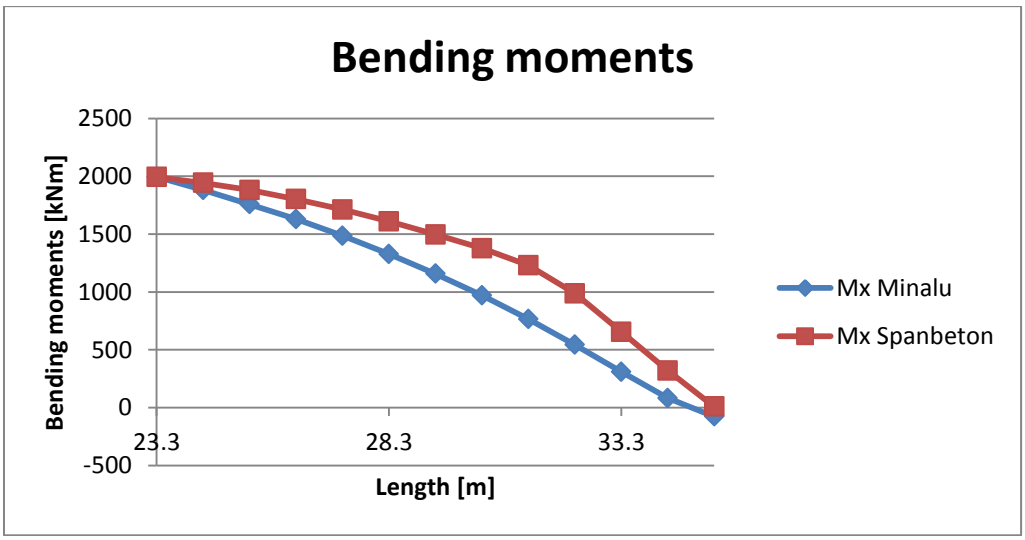

Figure 9-4 Distribution of bending moments determined with Scia Engineer

9.3 Bridge model using volume elements

This model is carried out in ATENA 3D with and without end diaphragm beam for the load case of Spanbeton and Minalu.

The shear stresses due to shear force can be determined in this model. Determine the torsional moments is more difficult because in this model the shear stresses due to torsion are not correct because there is applied only one linear element over the thickness of the web, Figure 9-5. Minalu calculates the torsional moments by integrating the stresses. In this research the known rotations are used to derive the occurring torsional moments.

9.3.1 Shear stresses due to shear force

The shear stresses due to shear force can be calculated taking the average from the indicated nodes in Figure 9-5 (which are approximately at the height of the centre of gravity).

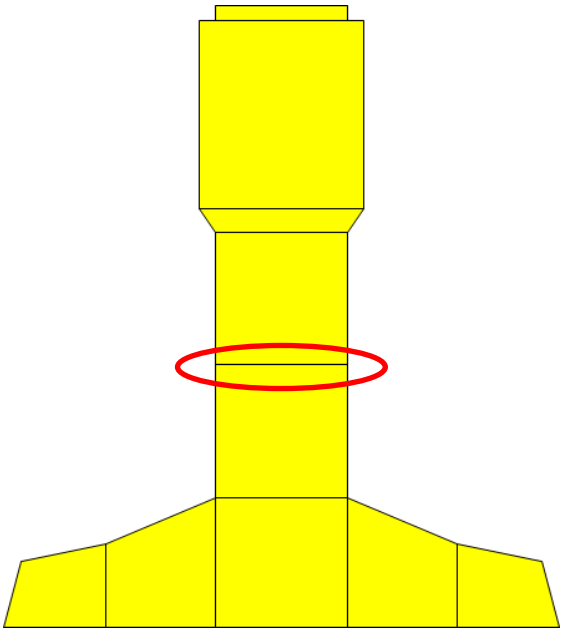

Figure 9-5 Mesh in Linear Elastic model of complete bridge

The determined shear stresses correspond well with the shear stresses calculated with the orthotropic plate model (Scia Engineer, without end diaphragm beam), Figure 9-6 and Figure 9-7.

Note: The visible peaks in the graphs are located on borders of macro-elements and have no physical meaning.

The found shear stresses from ATENA can be compared with the shear stresses from Scia. Little differences are visible between the results, this is presented in Figure 9-6 and Figure 9-7. The small differences are not investigated further.

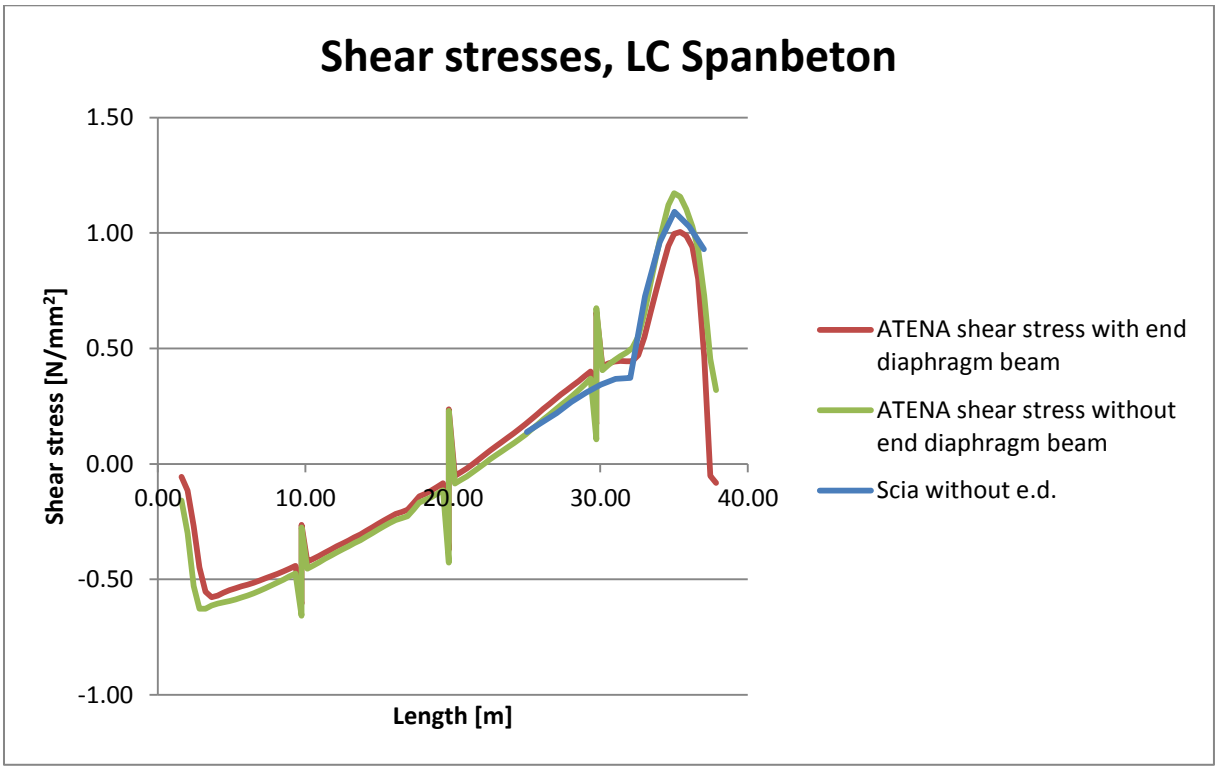

Figure 9-6 Shear stresses compared for the load case of Spanbeton

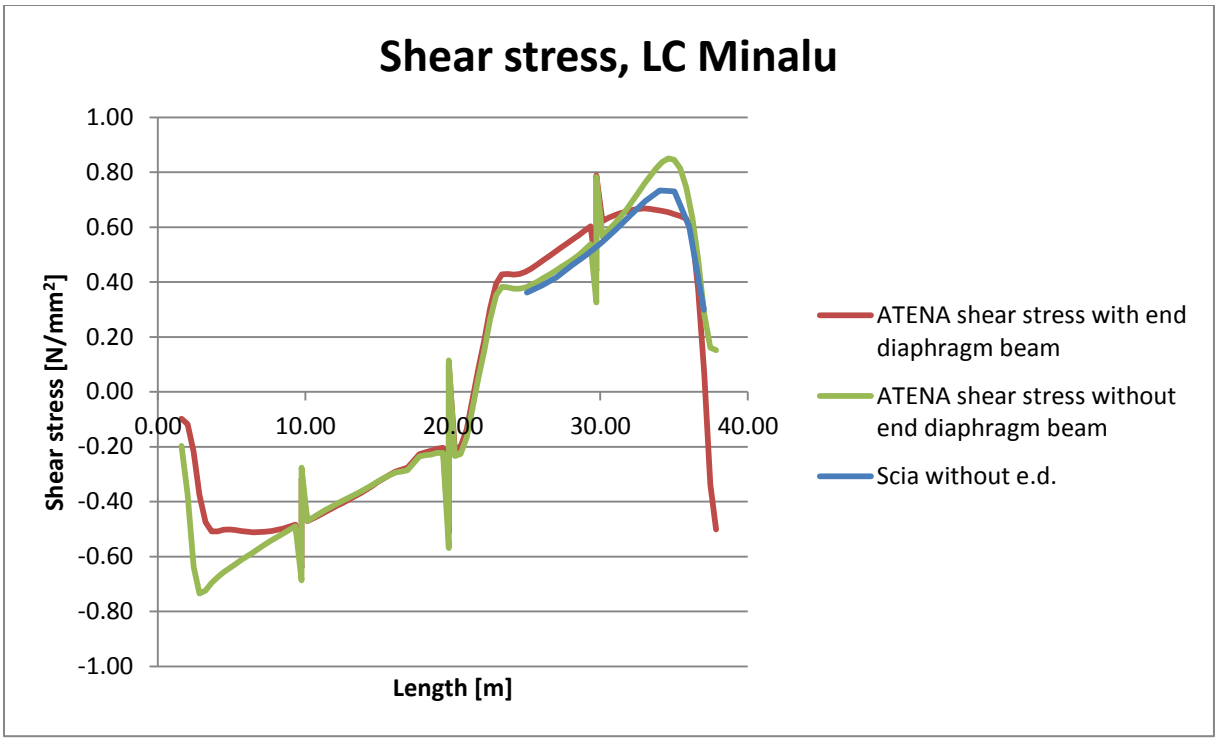

Figure 9-7 Shear stresses compared for the load case of Minalu

9.3.2 Torsional moments

The torsional moment can be calculated using the available data of the rotations. The occurring torsional moment consists of two parts, pure torsion and restrained warping. The following formula is used:

$$M_t = G \cdot I_w \cdot \frac{d\vartheta}{dx} - E \cdot C_w \cdot \frac{d^3\vartheta}{dx^3}$$

Important variables are:

$$E = 38 \cdot 10^6 \ {}^{kN}/_{m^2}$$
$$G = 15.833 \cdot 10^6 \ {}^{kN}/_{m^2}$$
$$I_w = 1.11 \cdot 10^{-2} \ m^4$$
$$C_w = 1.0 \cdot 10^{-3} \ m^6$$

The constants I_w and C_w are determined using respectively the programs Scia Engineer and ShapeBuilder.

9.3.2.1 Analysis of rotations

With Microsoft Excel the rotation curves (determined with ATENA) are estimated with an 6th order polynomial. That formulae are used to take the derivative of the rotation using Maple. The formulae are valid in the interval 0.63 < x < 35.63 meter.

In Figure 9-8, Figure 9-9, Figure 9-10 and Figure 9-11 the following components are plotted:

- Green: restrained warping [kNm]
- Blue: pure torsion [kNm]
- Red: total torsion moment [kNm]

From the figures can be observed that the torsion moment is not carried by restrained warping (normal stresses) but mainly by pure torsion (shear stresses). Only in the support area restrained warping has some influence which is largest for the model with an end diaphragm beam. When no end diaphragm is available no restrained warping is expected, but the warping that occurs is small and neglectable compared with the total occurring torsional moment, so no further investigation is done. The occurring torsional moments are higher when the end diaphragm beams are neglected. Furthermore, it can be observed that the obtuse corner attracts a lot of the torsional moments.

See appendix G for the used Maple code to determine the torsional moments.

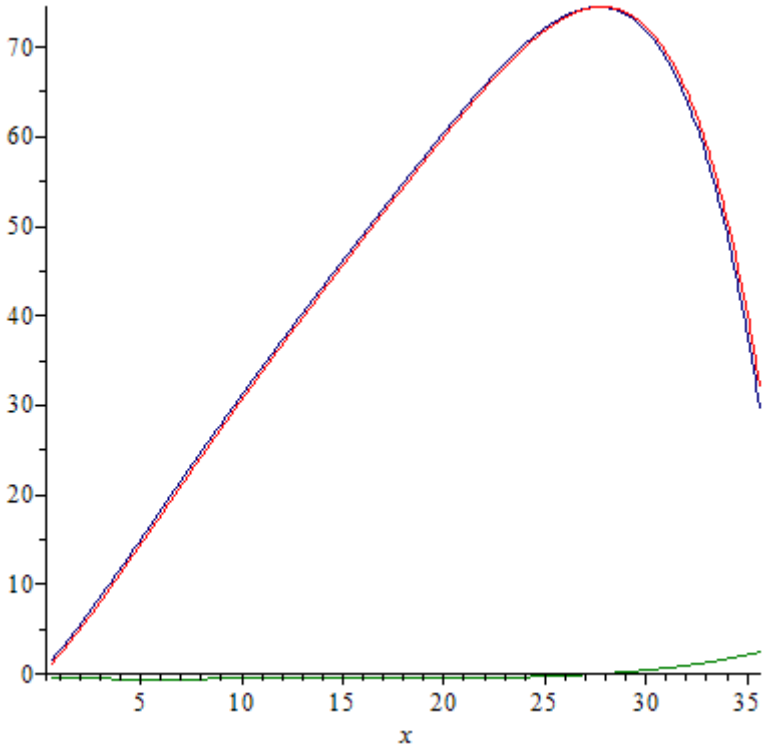

Figure 9-8 Torsional moments [kNm] for the load case of Spanbeton, without end diaphragm beam

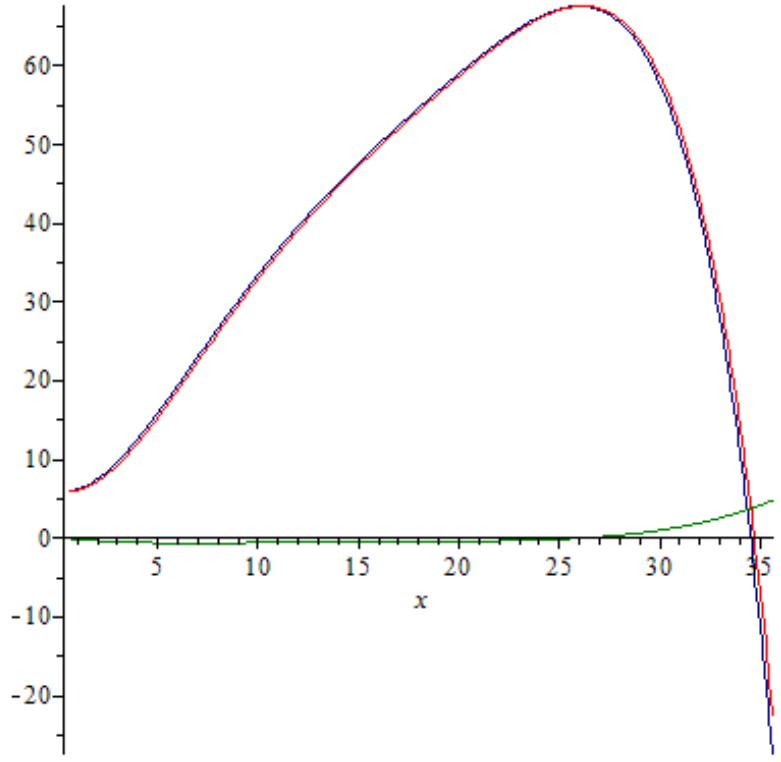

Figure 9-9 Torsional moments [kNm] for the load case of Spanbeton, with end diaphragm beam

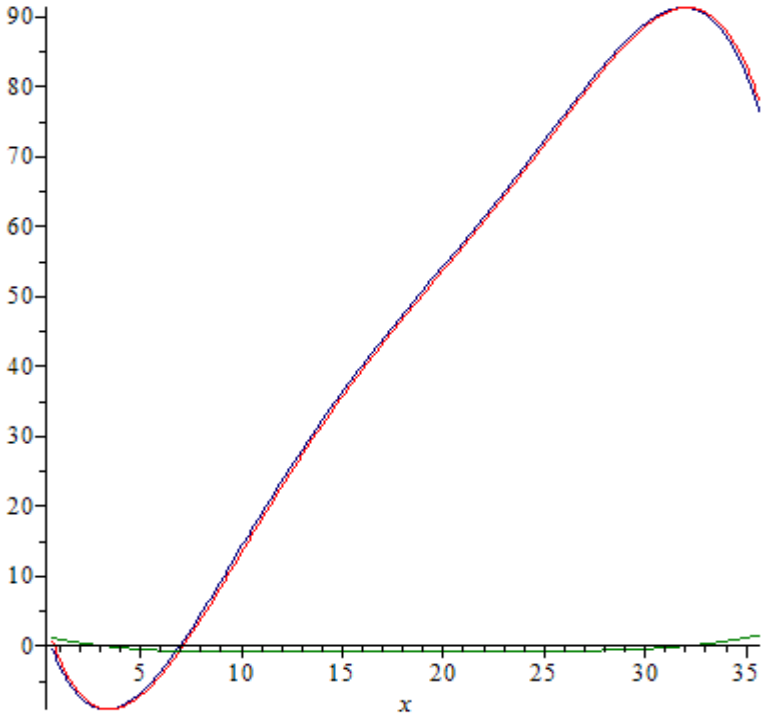

Figure 9-10 Torsional moments [kNm] for the load case of Minalu, without end diaphragm beam

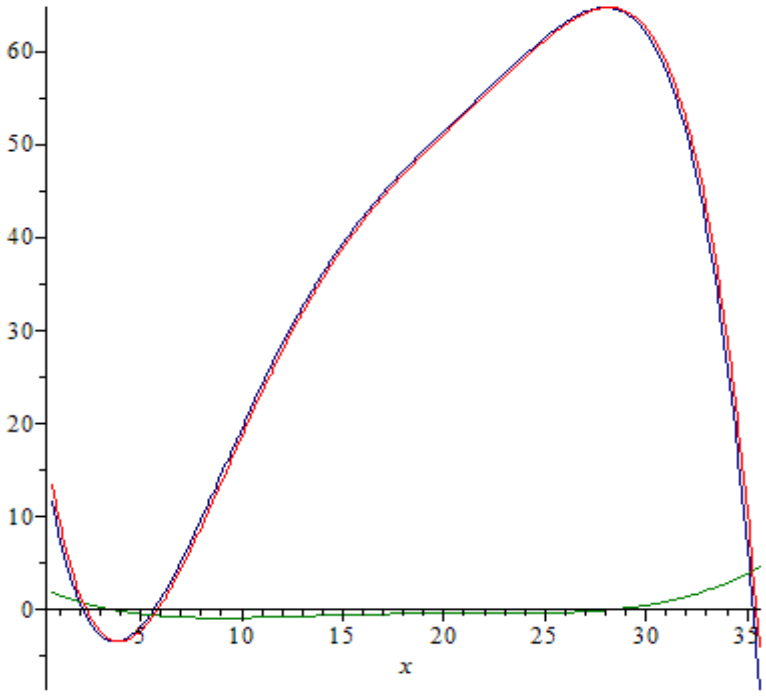

Figure 9-11 Torsional moments [kNm] for the load case of Minalu, with end diaphragm beam

9.3.2.2 Comparison with 2D orthotropic plate model

The determined torsional moments, in paragraph 9.3.2.1, can be compared with the torsional moments determined with the orthotropic plate model, in paragraph 9.2.3.

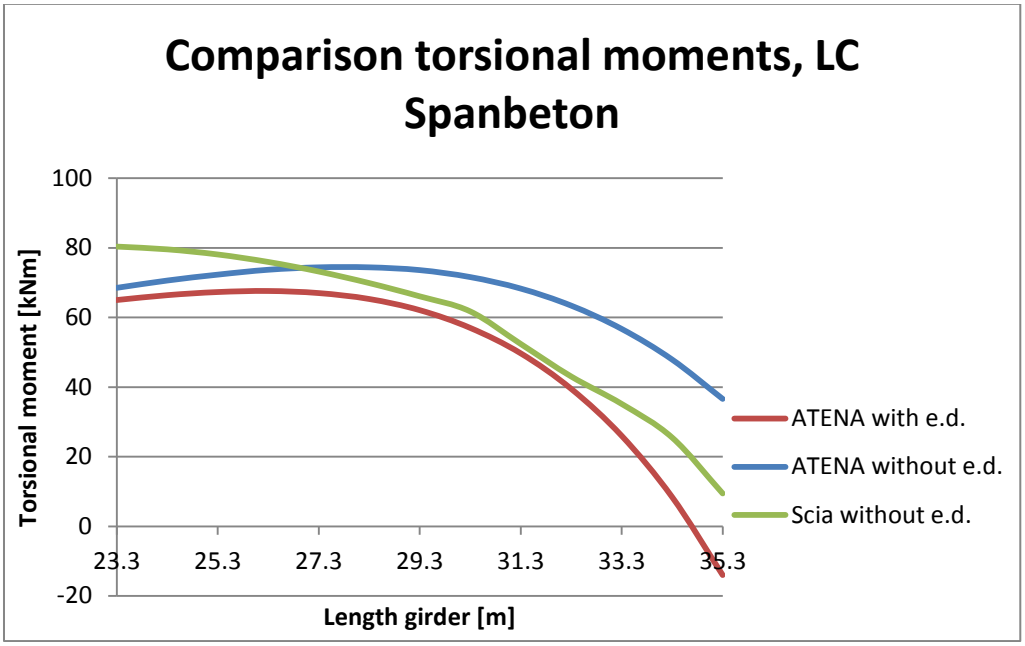

Figure 9-12 Torsional moments compared, LC Spanbeton

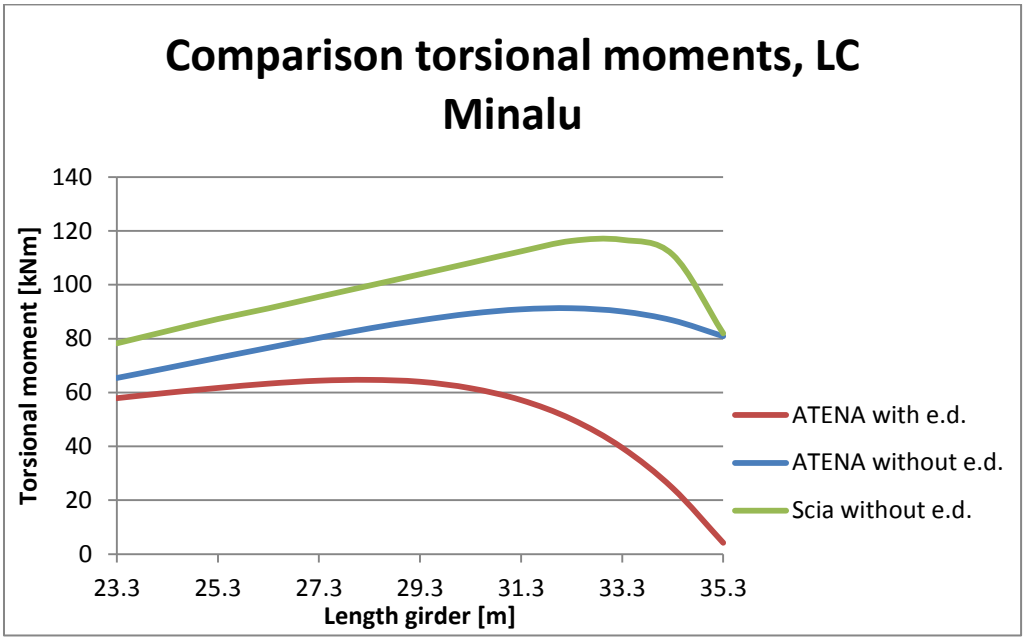

Figure 9-13 Torsional moments compared, LC Minalu

There is one direct comparison possible for the case that no end diaphragm beam is applied. The Scia and ATENA model without end diaphragm beam deviates. So for the linear elastic model a difference is found. Why this difference is found is not further investigated, the presented torsional distributions are all calculated and presented in the next chapters.

10 Evaluation of stresses

The forces from construction stage A and B are determined in chapter 8 and 9. With this knowledge the occurring stresses can be calculated.

In chapter 7 already the governing point in the cross-section is presented and explained. First the stresses in that point will be calculated based on the calculation with the orthotropic plate model. After that a calculation based on the results from the volume model is carried out. Finally at the governing location a complete cross-section is checked.

10.1 Calculation based on the orthotropic plate model of the bridge

10.1.1 Normal stresses

Normal stresses occur in the girder. Normal stresses are caused by:

- Bending moments and normal forces due to prestressing, paragraph 8.1.
- Bending moments due to own weight and the wet concrete of the fresh poured deck, paragraph 8.2.
- Bending moments due to permanent and variable loads on the deck, calculated with the orthotropic plate model, paragraph 9.2.3.

The resultant normal stresses from all these components are calculated and presented in Figure 10-1 and Figure 10-2. It is visible that no flexural cracks will occur for both load cases from 31 meter till the end of the girder. So in that region the principal stresses in an uncracked cross-section can be checked.

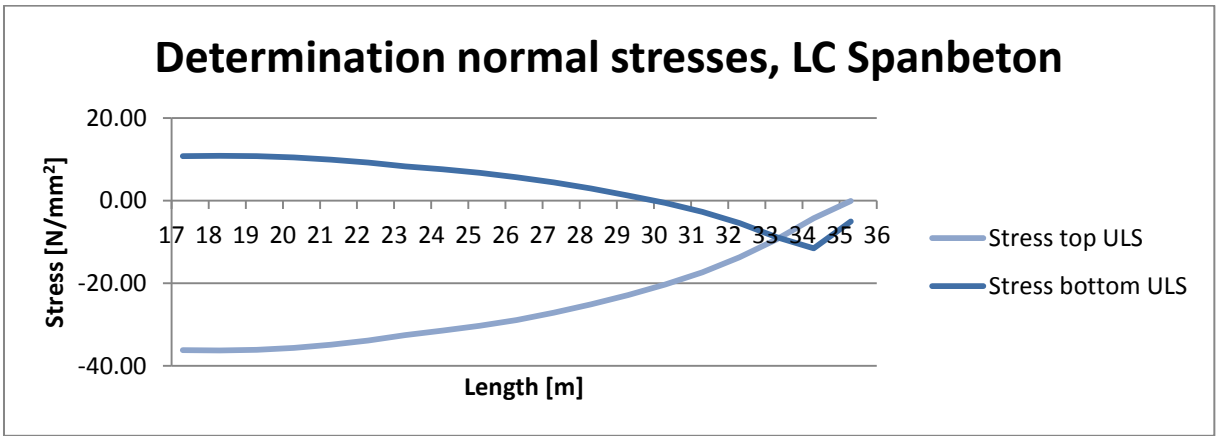

Figure 10-1 Normal stresses in top and bottom of girder, LC Spanbeton

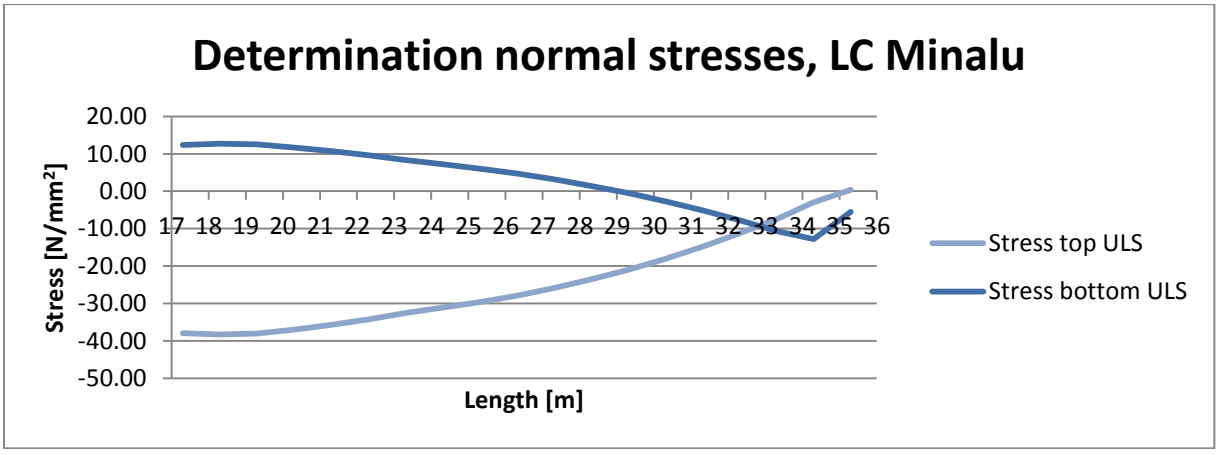

Figure 10-2 Normal stresses in top and bottom of girder, LC Minalu

10.1.2 Stresses due to permanent and variable load on deck

The occurring shear forces and torsional moments in construction stage B are presented in paragraph 9.2.3. The occurring shear stress consists out of shear stresses due to torsion and due to shear force. The calculated stresses for the elastic en plastic shear stress distribution (paragraph 7.4) are presented in Figure 10-3 and Figure 10-4. For the load case of Minalu the maximum occurring shear stress contains more shear stress due to torsion than due to shear force. For the load case of Spanbeton the opposite is the case. It is visible that both load cases have a maximum at about 33.3 meter.

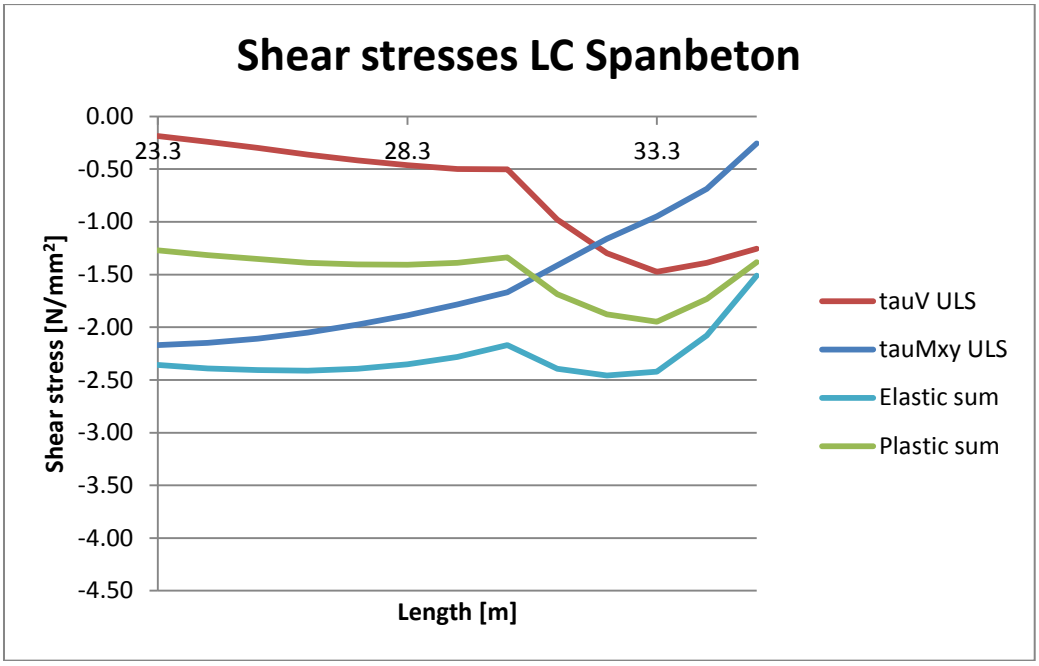

Figure 10-3 Shear stresses from construction stage B, LC Spanbeton

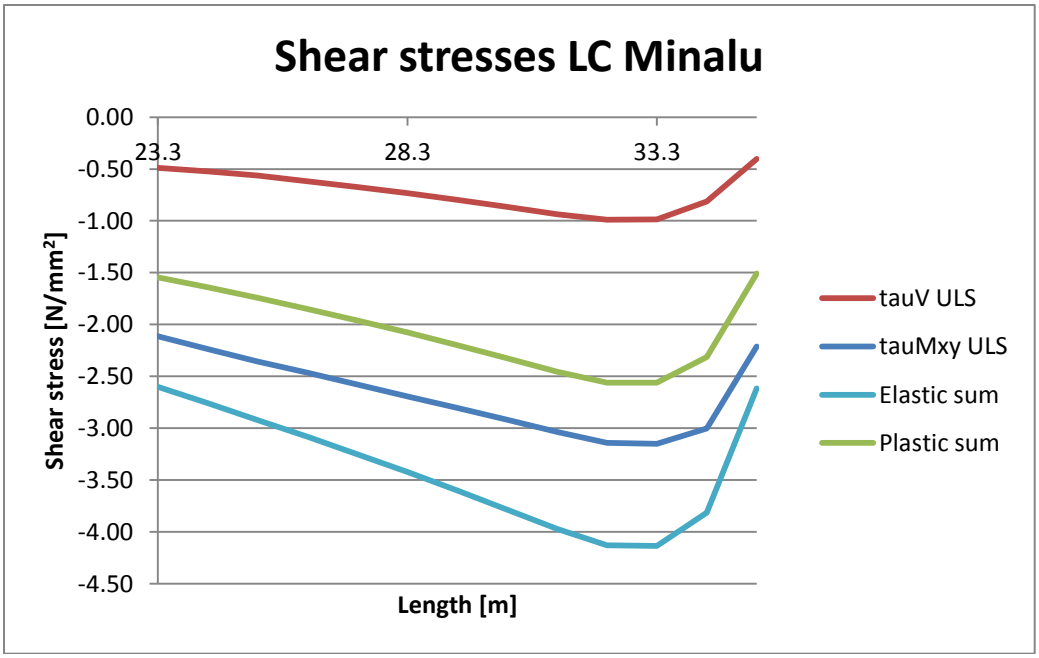

Figure 10-4 Shear stresses from construction stage B, LC Minalu

Note: The presented shear stress 'τ_{Mxy} ULS' is the elastic shear stress (Figure 7-2).

10.1.3 Total shear stresses

The shear stresses of construction stage A and B can be combined using the elastic or plastic sum. The calculated stresses are presented for the load case of Spanbeton and Minalu.

The following formulae are used to determine the stresses:

$$\tau_{ULS,\ elastic} = \tau_{V,prestressing} + \tau_{V,dead\ weight,sls} + \tau_{elastic\ sum\ construction\ stage\ B}$$
$$\tau_{ULS,\ plastic} = \tau_{V,prestressing} + \tau_{V,dead\ weight,sls} + \tau_{plastic\ sum\ construction\ stage\ B}$$

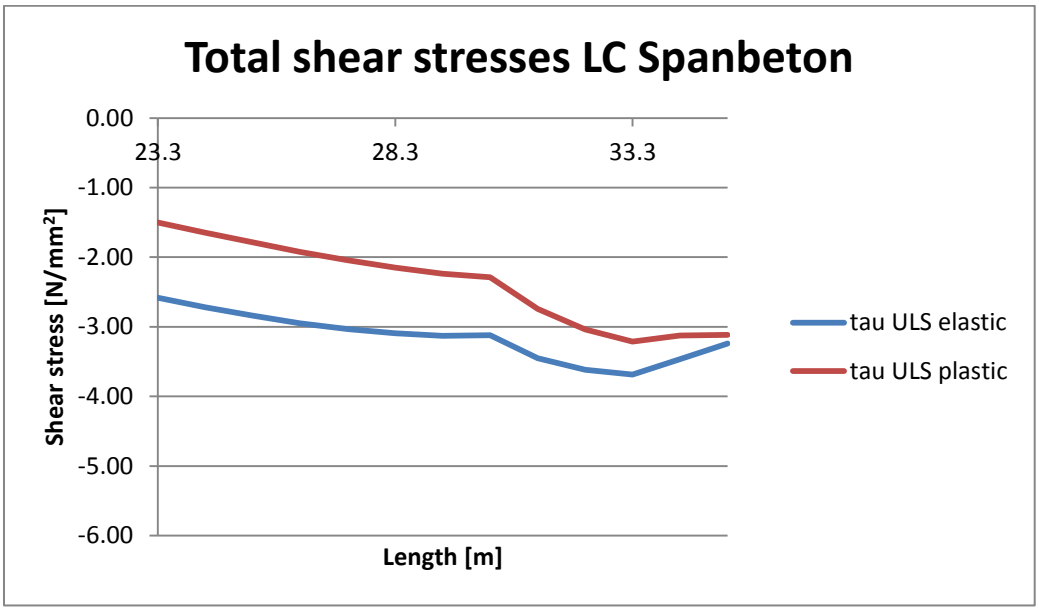

Figure 10-5 Total shear stresses in ULS, LC Spanbeton

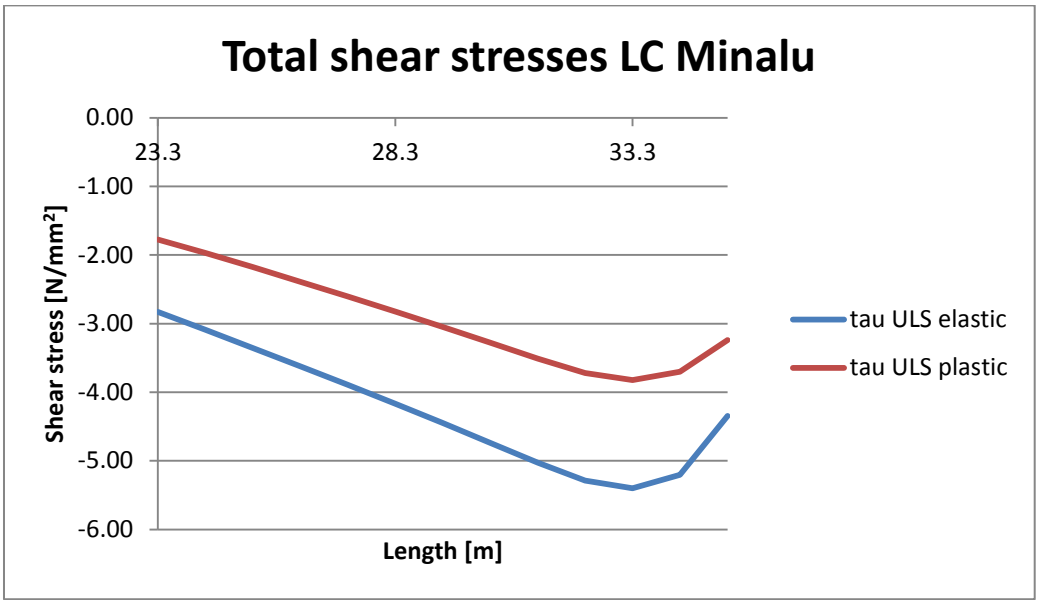

Figure 10-6 Total shear stresses in ULS, LC Minalu

Note: The maximal shear stresses due to the shear force of construction stage A and B are simply added to each other neglecting the different locations of the centres of gravity. This is not totally true but safe based on Figure 10-15.

10.1.4 Principal stresses

The combination of normal and shear stresses can be analysed using principal stresses. The formulae for principal stresses are as follows:

$$\sigma_1 = \frac{\sigma_{xx} + \sigma_{yy}}{2} + \sqrt{\left(\frac{\sigma_{xx} - \sigma_{yy}}{2}\right)^2 + {\sigma_{xy}}^2}$$

$$\sigma_2 = \frac{\sigma_{xx} + \sigma_{yy}}{2} - \sqrt{\left(\frac{\sigma_{xx} - \sigma_{yy}}{2}\right)^2 + {\sigma_{xy}}^2}$$

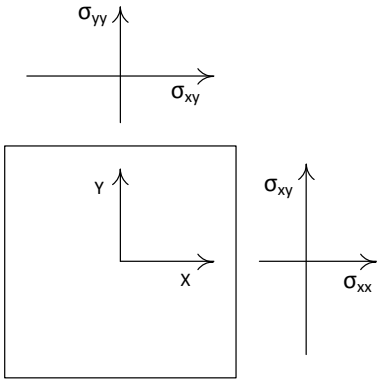

Figure 10-7 Stresses on infinitesimal element

Remember: It is assumed that the stresses in Y-direction (vertical stresses) are zero. The resulting formula for principal tension stress is in that case:

$$\sigma_1 = \frac{\sigma_{xx}}{2} + \sqrt{\frac{{\sigma_{xx}}^2}{4} + {\sigma_{xy}}^2}$$

Interesting is the location where, based on design tension strength, the concrete can bear the load without cracking. In Figure 10-8 and Figure 10-9 the principal tension stresses for the two considered load cases (Spanbeton and Minalu) are visualized. From the figures can be concluded that no cracking is expected.

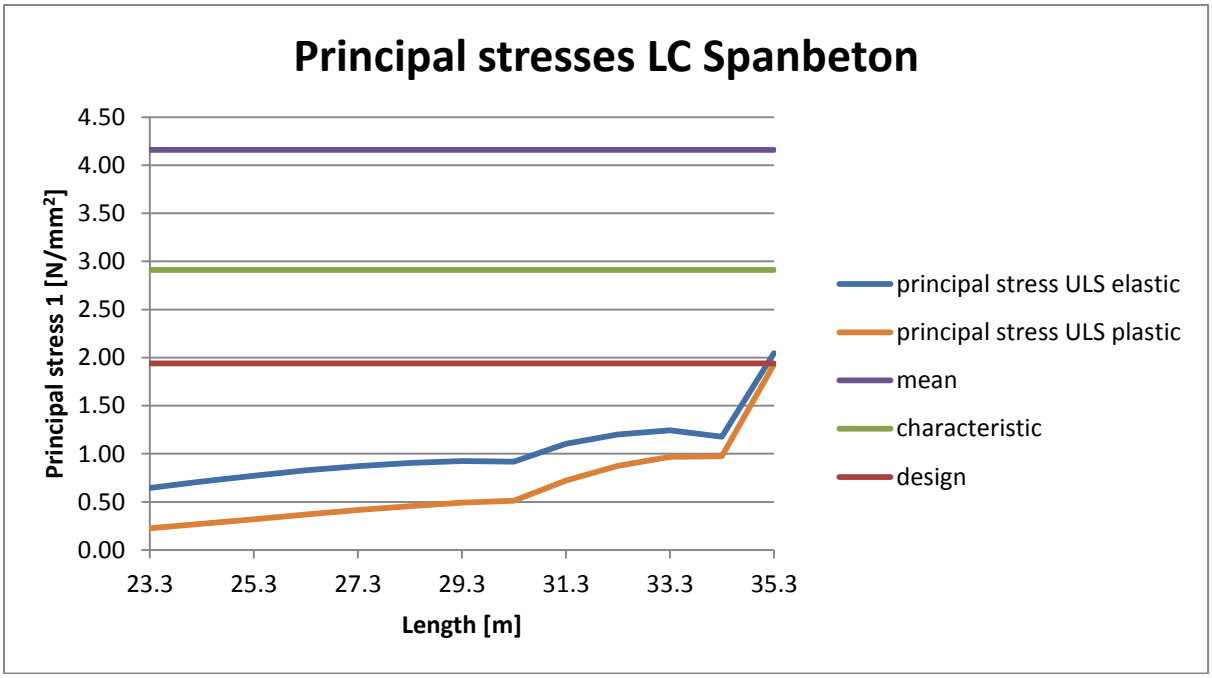

Figure 10-8 Principal stresses LC Spanbeton based on calculation with Scia Engineer without end diaphragm beam

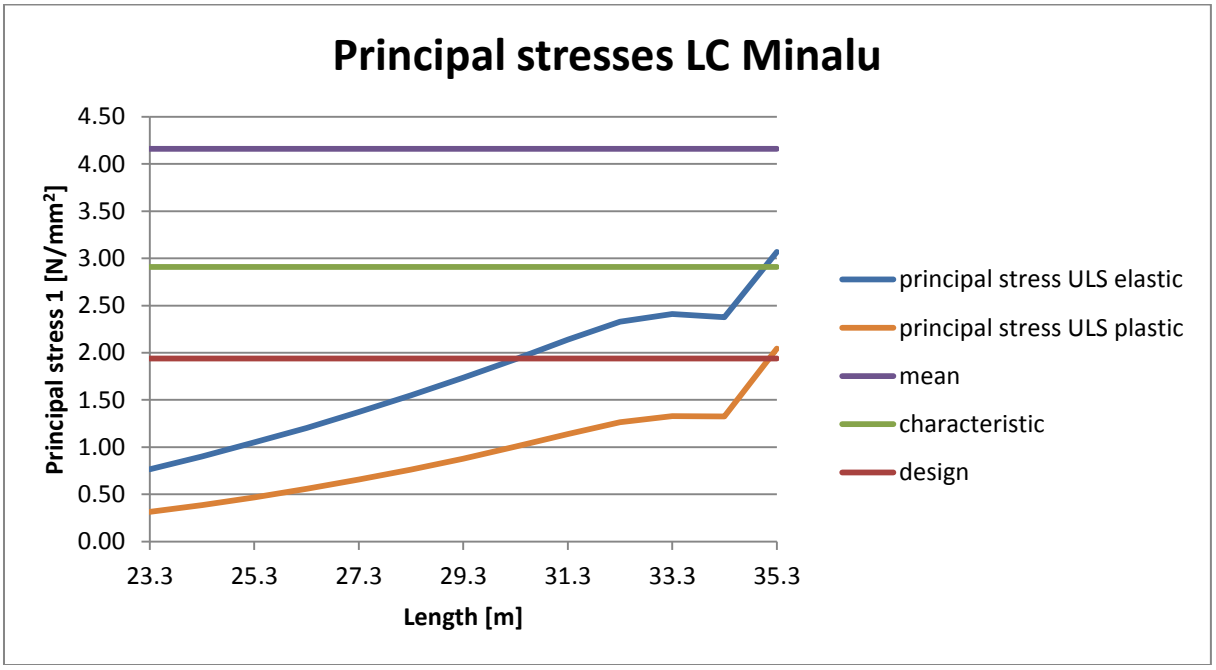

Figure 10-9 Principal stresses LC Minalu based on calculation with Scia Engineer without end diaphragm beam

10.2 Calculation based on the bridge model using volume elements

10.2.1 Principal stresses

Now the principal stresses can be calculated again using the data from the ATENA models. The data from these models can be found in paragraph 9.3. Note that stresses from construction stage A does not differ. Only the forces for construction stage B are adapted. Not the complete calculation is described again, this is already done in paragraph 10.1, only the resulting principal stresses are presented.

10.2.1.1 Model without end diaphragm beams

In the calculation the values for the shear force and torsional moment from construction stage B are changed to the values found with the ATENA model without end diaphragm beam. The principal stresses are presented in Figure 10-10 and Figure 10-11.

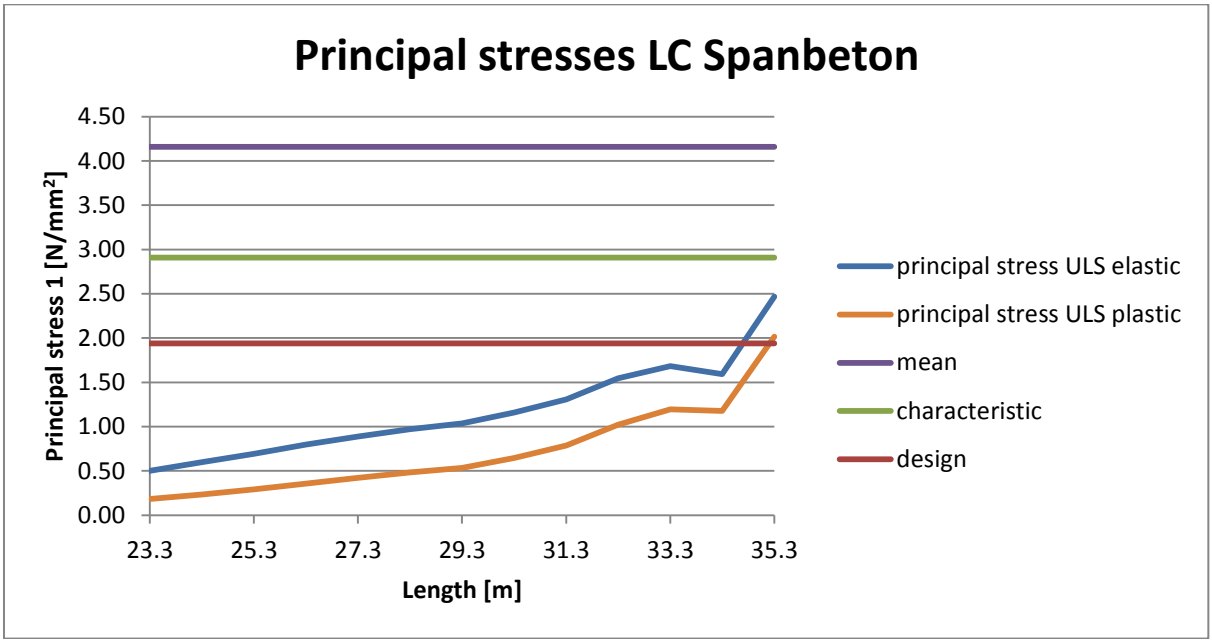

Figure 10-10 Principal stresses LC Spanbeton, based on ATENA calculation without end diaphragm beam

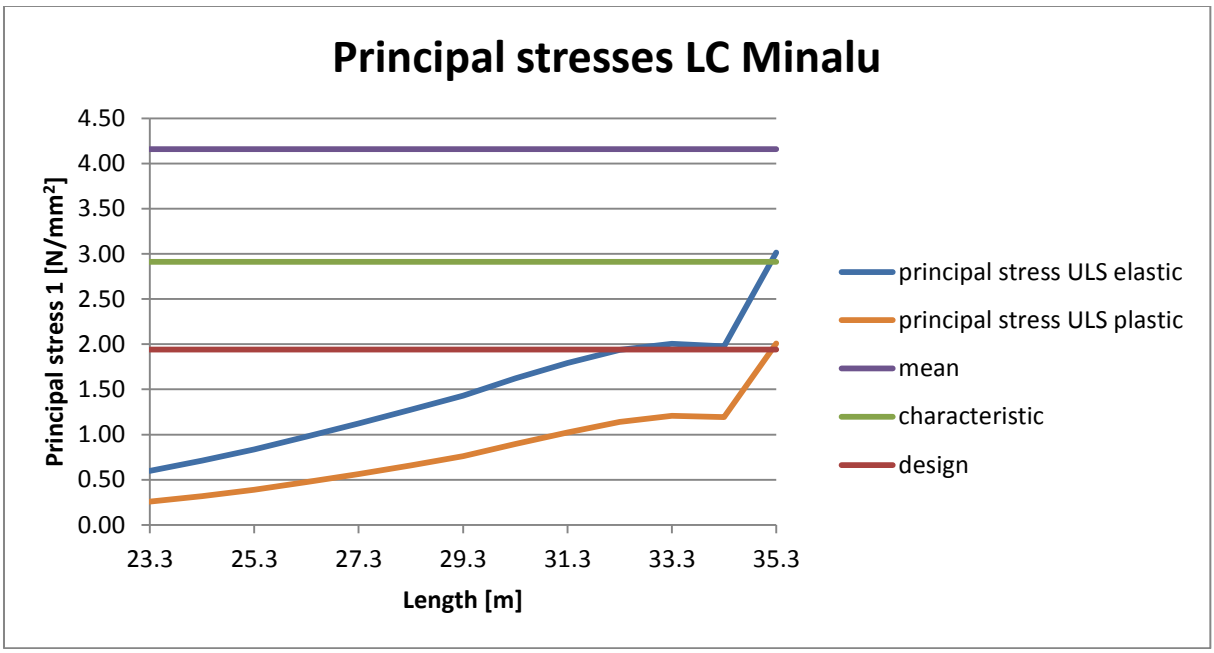

Figure 10-11 Principal stresses LC Minalu, based on ATENA calculation without end diaphragm beam

10.2.1.2 Model with end diaphragm beams

In the calculation the values for the shear force and torsional moment from construction stage B are changed to the values found with the ATENA model with end diaphragm beam. The principal stresses are presented in Figure 10-12 and Figure 10-13.

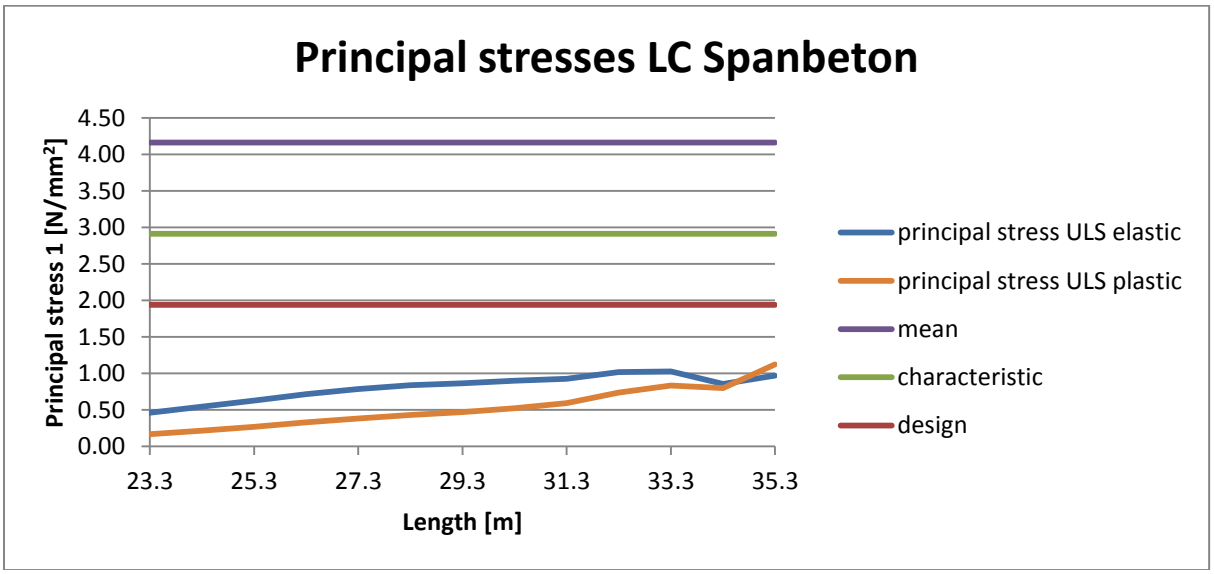

Figure 10-12 Principal stresses LC Spanbeton, based on ATENA calculation with end diaphragm beam

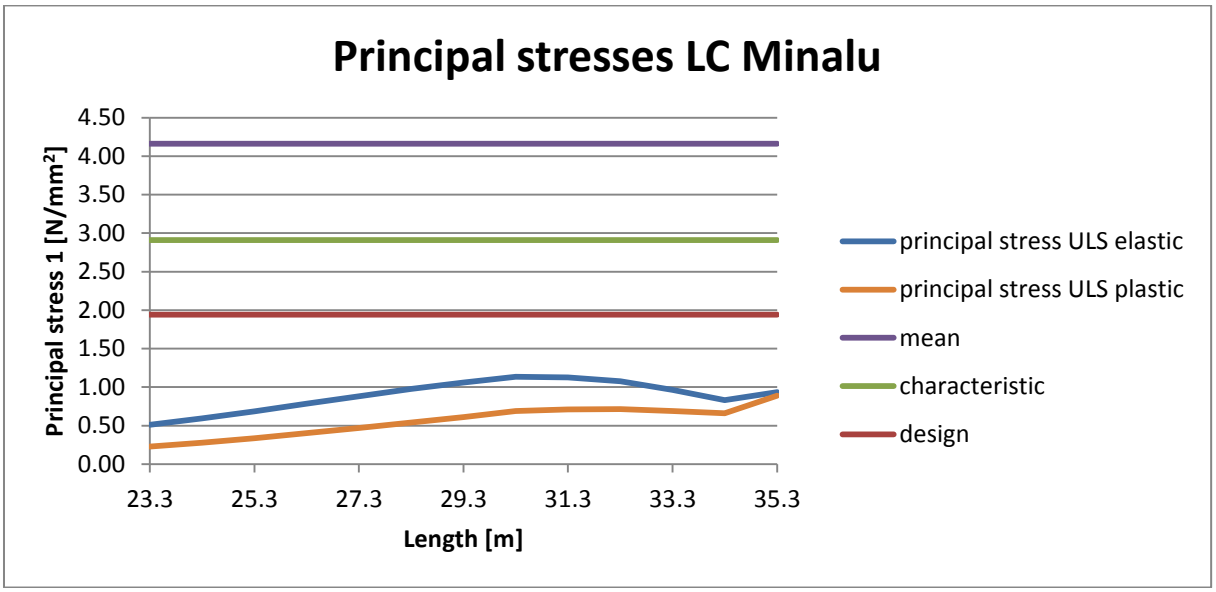

Figure 10-13 Principal stresses LC Minalu, based on ATENA calculation with end diaphragm beam

10.2.1.3 Comparison

It is visible that the principal stresses for all cases (figure Figure 10-8 till Figure 10-13) meets the criteria as formulated in paragraph 7.3, so no cracking is expected.

The presence of end diaphragm beam in the linear elastic model of the bridge decreases the stresses a lot. But Minalu already noted that large torsional moments occur in the end diaphragm beam in that situation which leads to much reinforcement and is likely to be physically impossible[10]. The real principal stresses will be in between the case with and without end diaphragm beam. It is safe make a calculation without end diaphragm beam because that produces governing principal stresses.

[10] Minalu, Kassuhun K. (2010), *Finite element modelling of skew slab-girder bridges.* Page 52.

10.3 Calculation of governing cross-section

Till now the principal stresses are checked in one point of the cross-section based on the location were maximal shear stresses will occur. But the principal stresses depends also on the normal stresses. Lower normal stresses will lead to higher principal stresses. For completeness the governing cross-section will be calculated more detailed to be sure that there is no other governing point in ULS.

When the principal stresses from the presented calculations are compared the largest are observed in Figure 10-9 for the load case of Minalu calculated with Scia Engineer. For that load case a calculation of the cross-section is performed at x=33.3 meter.

10.3.1 Normal stresses

Using the orthotropic plate model has the advantage that the longitudinal moments are calculated already, which are presented again in Figure 10-14.

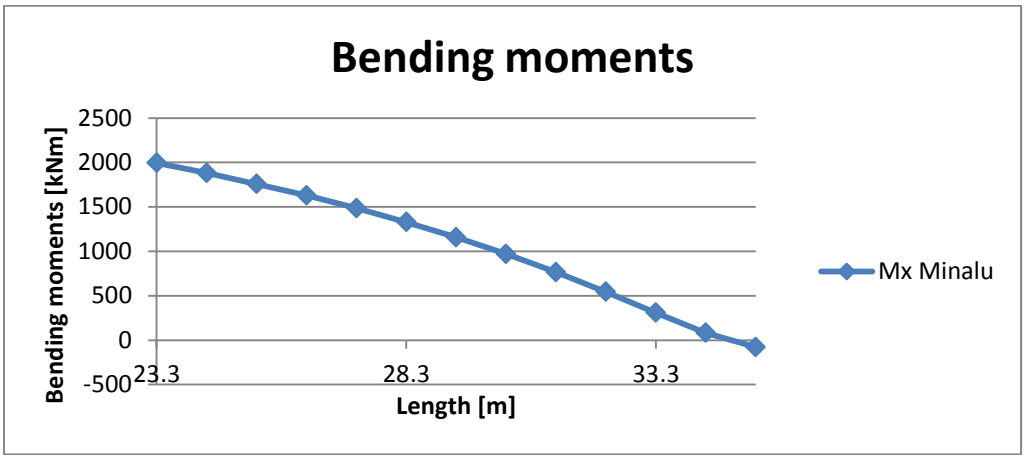

Figure 10-14 Distribution of bending moments for the LC of Minalu

The stresses are checked at x = 33.3 meter. Bending moments:

- Construction stage A (Figure 8-1 and Figure 8-2)
  - Prestressing, M = -1569 kNm
  - Dead weight and weight fresh poured concrete, M = 678 kNm
- Construction stage B, (Figure 10-14)
  - Variable and permanent load on deck, M = 308 kNm.

From this moments follow the stresses in ULS:

- Normal stress top: -7.5 N/mm^2
- Normal stress bottom: -10.6 N/mm^2

10.3.2 Shear stresses

10.3.2.1 Shear force

The shear stress distribution due to shear force can be calculated. Construction stage A and B must be calculated separately for a detailed calculation. The total occurring shear stress can be calculated taking the sum of the shear stresses from construction stage A and B. The results are presented in Figure 10-15.

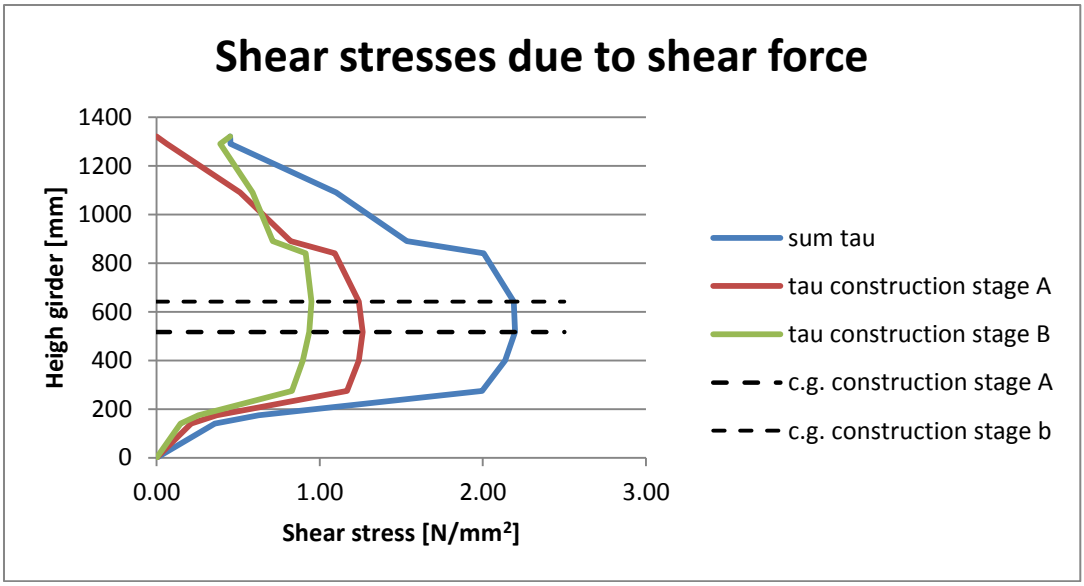

Figure 10-15 Shear stresses in cross-section

10.3.2.2 Torsion

When Figure 6-1 and Figure 6-2 are studied follows that in the thicker top part of the web the shear stresses due to torsion could be a little bit higher than at the height of the centre of gravity. However in the top part of the web the shear stresses due to shear force are relatively low. So it is a safe approximation to take a maximal torsion shear stress of 3.15 N/mm^2 (in the ULS) over the whole cross-section.

10.3.3 Principal stresses

The determined normal and shear stresses can be combined to principal stresses using the formulae, already presented in paragraph 7.4. The resulting stresses over the height of the girder are presented in Figure 10-16.

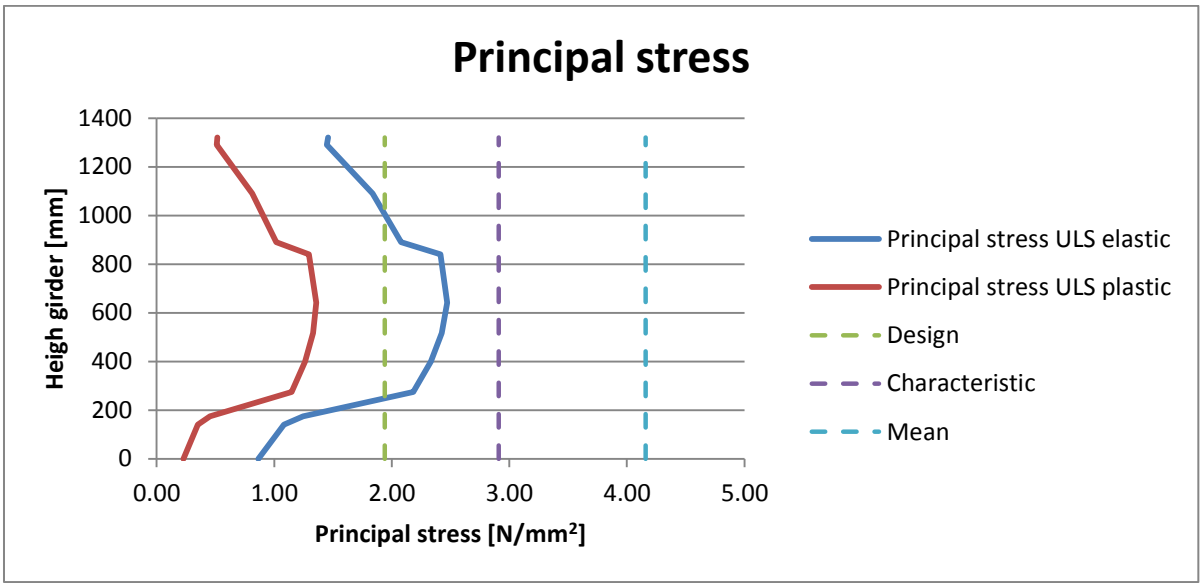

Figure 10-16 Principal stresses in cross-section

This figure can be compared with Figure 10-9. The found maxima from both figures are presented in Table 10-1. The maxima occurred in the centre of gravity of construction stage B (h=641 mm).

Shear stress distribution	Performed calculation of principal stresses		Difference
	Complete cross-section	Only at centre of gravity	
Elastic distribution	2.47 N/mm^2	2.41 N/mm^2	2.4 %
Plastic distribution	1.36 N/mm^2	1.33 N/mm^2	2.2 %

Table 10-1 Comparison calculations

There are two differences between the calculations:

1. In the calculation at the centre of gravity presented in paragraph 10.1 the maximal shear stresses from construction stage A and B are summed up while the maxima are not at the same location. The calculated shear stress is 5.40 N/mm^2 while a detailed calculation of the cross-section gives 5.34 N/mm^2, a difference of 1.2%. This is not significant compared with the next point.
2. From the calculation of the complete cross-section it is visible that taking into account the effects of the bending moments reduces the advantageous normal stresses at the considered centre of gravity. The bending moments of construction stage A reduce the normal stress in the centre of gravity of construction stage B as visualized in Figure 10-17. The normal stress reduces from -9.68 N/mm^2 to -9.08 N/mm^2, a reduction of 6%. This explains the increased principal stresses for the detailed calculation of a complete cross-section.

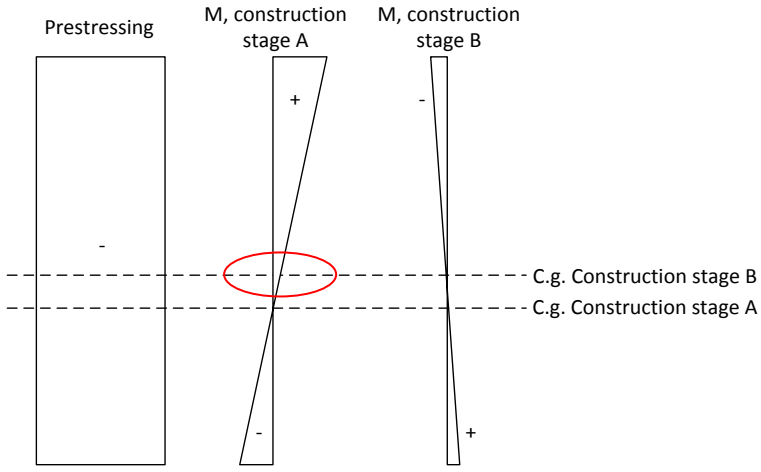

Figure 10-17 Stress diagrams for normal stresses

10.4 Conclusion

Firstly, the load case of Minalu produces the governing principal stresses. Secondly follows from the comparison of the calculations in Table 10-1 that it is valid to check the principal stresses only at the height of the centre of gravity with the presented remark. Important is that the shift of the centre of gravity has influence on the normal stress. The bending moments of construction stage A reduces the normal stress in the centre of gravity of construction B, in the calculated case the normal stresses reduces with 6% which leads to an increased principal stress. For the considered case this do not lead to other conclusions about cracking.

From the calculations can be concluded that there is a zone in the girder from about 31 – 35 meter which is uncracked in ULS. Consequently in the SLS also no cracking will occur. For the straight bridge, presented in paragraph 0, in which lower torsional moments and comparable shear forces occurs also no cracking will occur.

Conclusions

1. It is impossible to model a whole bridge with volume elements including physically non-linear behaviour. From a rough calculation it is expected that this will possibly be daily practice within eighteen years. It is possible to model a whole bridge linear elastically with coarse linear or quadratic volume elements. In this model only one coarse element is available over the thickness of the web. Shear stresses due to torsion are not calculated correctly in this coarse elements. For obtaining accurate torsion stresses at least three quadratic elements in the web thickness are needed (Chapter 4).

2. It is possible to develop an accurate physically non-linear model for one girder. In this model the cracking can be analysed. However, it is difficult to determine a realistic loading to this girder. In theory the linear elastic displacements, determined with the linear elastic model of the bridge, can be imposed to the girder. Firstly this takes a lot of time. Secondly, the local applied deformations and other imperfections lead to wrong stresses in the model. Despite these difficulties the developed model gives a good estimation of the available uncracked zone in the girder (chapter 5).

3. Using a hand calculation to determine the torsion shear stresses at the height of the centre of gravity is conservative. This calculation leads to 40% higher results. This is due to the different phi-distributions in the cross-section used in the hand calculation and the real cross-section. In the real cross-section the phi distribution is maximal in the thickened part of the web and in the flange, the shear stresses are attracted to these zones. This causes a substantial decrease of torsion shear stresses at the height of the centre of gravity. The program Scia Engineer can be used to calculate the shear stresses, a sufficient refined mesh is necessary (Chapter 6).

4. The occurring torsional moments can be determined using the rotations of the first ZIP girder, determined with the linear elastic model of the bridge. From this analysis it follows that the torsion moment is not carried by restrained warping (normal stresses) but mainly by pure torsion (shear stresses). Only in the support area restrained warping has some influence which is largest for the model with an end diaphragm beam (Chapter 7).

5. For the determination of the force distribution in the bridge an orthotropic plate model (Scia Engineer) and a volume model (ATENA 3D) can be used. Comparison of the results from these models show that the shear forces correspond reasonable. However, the torsional moments deviate substantially. This is remarkable because both models are linear elastic which should be comparable (Chapter 7).

6. In the report two load cases are investigated. Using a plastic calculation of the stresses both load cases produce comparable principal stresses. Using the elastic calculation the load case of Minalu produces governing principal stresses.

7. From the calculation of the principal stresses it follows that in the first ZIP girder of the skew bridge in ultimate limit state a large uncracked zone is available. Important is that the stresses within the bond length must be evaluated, depending on the permitted plastic redistribution (Chapter 7). Implicitly this conclusion is also valid for the serviceability limit state. For the straight bridge a comparable uncracked zone will be found because comparable shear forces, but lower torsional moments will occur compared with a skew bridge.

Recommendations

A. The project is started making a time-consuming physical non-linear finite element model. It is important to make first hand calculations and linear elastic finite elements when a similar research project is intended. When necessary a physical non-linear model can be developed.

B. The principal stresses in this research are compared with static tension strengths of concrete. The calculation of fatigue is not incorporated in this research. In the case of a fatigue calculation the tension strength is reduced but also other load configurations must be used. This calculation must be carried out to be sure that the girder also following that calculation contains a large uncracked zone.

C. The presented research can be used to reduce the amount of reinforcement in the uncracked zone to the minimum demands. From research of one bridge with particular geometric properties no general law can be derived. However, a possible procedure can be presented to check if the advantage of the uncracked zone can be used, for a bridge using ZIP girders.

   Possible procedure:

   1) First a distribution calculation must be carried out in which the torsional stiffness is not reduced. The load cases of this report must be considered as a minimum.
   2) The prestressing can be calculated using the standard procedures in serviceability limit state. Important is that no flexural cracks will occur in the top of the beam at the ends.
   3) The length of the uncracked area in ultimate limit state can be determined using the point where the bending moments cause a tension stress. It is safe to avoid any tension stress for this calculation. It is possible that for this calculation the load case for maximal bending in the girder is governing.
   4) The shear stress distribution due to torsion in the cross-section can be determined using Scia Engineer. It is conservative to do this with a simplified hand calculation. The torsion shear stresses can be calculated elastically or plastically. The shear stresses due to shear force can be calculated using the known formula. These two components can be summed up elastically or plastically.
   5) The occurring normal stress varies over the height of the girder. Important is the normal stress at the height of the centre of gravity. The height of the centre of gravity varies for a ZIP-girder and the combined system. The governing height will be somewhere in between these boundaries. When one of the centres of gravity is chosen the reduction due to the bending moments around the other centre of gravity must be incorporated (Figure 10-17). In this research the reduction of the normal stress was at most 6% due to this effect. The advantageous effect of the prestressing in the ultimate limit state must be reduced by multiplying the prestressing force with a factor 0.9.
   6) In the uncracked zone the principal stress can be calculated from the found normal and shear stresses at the governing height. When this stress is below the limits can be concluded that the girder is uncracked. The assumption to take full torsional stiffness in the orthotropic plate model is correct in this case. The minimal reinforcement for shear and torsion must be applied following the Eurocode.

Evaluation

This master project was not a straightforward process. A short description of the occurred problems is given.

Process

The first idea was a research to compressive membrane action (CMA) in ZIP bridge decks with a comparison between the situation with and without end diaphragm beam. At the start meeting a large 3D-model is discussed for a skew and a straight bridge. In this model the effects of CMA and torsion could be investigated. For that model all reinforcement must be calculated by doing a calculation of a whole bridge. Also a short literature study to the effects of CMA and torsion must be done.

When this work was finished, some months later making a large physical non-linear model was started. In the second meeting this idea was discussed further. First some attempts are done combining physically non-linear behaviour and linear elastic elements. This did not work. But it was not decided unanimously to stop making a large physical model. Dobromil Pryl, employer of Cervenka Consulting, believed that it must be possible to model this bridge physical non-linear. That was the reason to continue making the model. After some months of trial-and-error it was decided that it is not possible to make this model. In this stage it was decided to focus on torsion and forget about CMA.

Generating a good alternative was complex. A system is applied using a large linear elastic model to determine the deformations and a small physically non-linear model on which the deformations are applied. In this small physically non-linear model the effects of torsion on cracking should be visible. In the large linear elastic model no reinforcement is applied. In the small physically non-linear model only prestressing and the standard reinforcement at the ends of the girders is applied.

When the deformations were determined (a lot of work) and applied on the small physically non-linear model no torsion cracks were visible, this leads at that moment to the conclusion that in ULS no torsion cracks will occur. At that moment Van der Veen asked for an analytical calculation to be sure that the model is correct and reliable.

This analytical calculation is done using hand calculations and using the found torsional moments with a Scia orthotropic plate model and the analyses from ATENA. From this calculation follows that the load case of Minalu will give shear/torsion cracking based on the elastic distribution of stresses. After making this calculation again the ATENA small physically non-linear model was studied. That model resulted in too low shear stresses. The reason for this is that the large linear elements in the small physical non-linear model do not calculate the torsion stresses correctly. This is of course an important reason that no torsion cracks occur, so refinement of the interesting zones is of importance. So based on the calculations the models must be carried out again with refinement.

A critical reflection of the calculation of torsion stresses using the program ShapeBuilder was carried out. Doing this it was found that it is quite conservative to calculated torsion shear stresses by dividing the cross-section in rectangles. This result gives a better correspondence between the found stresses in the ATENA model and the calculated stresses.

Evaluation

Evaluating the process it is clear that lot of time is spend on preparation (making calculations) and developing a finite element model while at the end a simple calculation appeared to be sufficient to solve the problem. The most important lesson from this is for me that starting a finite element model without making some calculations is not an effective way of doing research.

When this research had to be repeated the following procedure shall be used:

1. Choose one subject from the beginning of the project.
2. Make first analytical calculations.
3. Carry out linear elastic models.
4. When necessary: carry out physical non-linear models.

Appendices

This appendices are presented in an separate document.

Appendices:

A. Literature research about Compressive membrane action.
B. Comparison calculation skew and straight bridge
C. Determination bond length following the Eurocode.
D. Determination force distribution in prestressed ZIP-girder, including effect of bond length.
E. Detailed information about used finite element model.
F. Simple method to take results from ATENA.
G. Maple sheet to determine torsion in a ZIP-girder using rotations as input.

References

1. Minalu, Kassuhun K. (2010), *Finite element modelling of skew slab-girder bridges*
2. Sengupta, dr. Amlan K. et. al. *Prestressed concrete structures*
3. Hoogenboom, P.C.J. (2010), *Aantekeningen over wringing*
4. Zia and McGee (march-april 1974), *Torsion design of prestressed concrete*, PCI Journal, page 46 – 65
5. Rangan, B. V. and Hall, A. S. (March 1975), *Design of Prestressed Concrete Beams Subjected to Combined Bending, Shear and Torsion*, ACI Journal, American Concrete Institute, Vol. 72, No. 3, page 89 – 93
6. Blauwendraad, Prof.dr.ir.J. (2006), *Plate analysis, Theory and Application.*
7. Eurocode 1991-2: *Actions on structures, traffic loads on bridges*.
8. Eurocode 1992-1-1: *Design of concrete structures, General rules and rules for buildings.*
9. Eurocode 1992-2: *Design of concrete structures, Concrete bridges design and detailing rules.*
10. ATENA 3D manuals, available on the website www.cervenka.cz

List of figures

List of tables

SPANBETON
PREFAB BOUWOPLOSSINGEN

TU Delft Delft University of Technology

Master thesis

Torsion in ZIP bridge system - Appendices

Final version

Evert van Vliet
21-1-2012

Contents

A. Literature research

Compressive membrane action (CMA)

Other master students have done detailed literature research about the theory of CMA. In this report their findings will be shortly summarized to give an overview of the theory.

Introduction

CMA is also called " arching action", a very old concept in structural engineering. There are two important conditions that must be met to activate CMA. Firstly, the horizontal translation has to be (partly) restrained. Secondly, the net tensile strain along a longitudinal fibre must be non-zero when there is no horizontal restraint.[1]

To give an idea of the development of the ideas about CMA an short, not complete, historical overview is presented.[2,3] In 'A guide to compressive membrane action in bridge deck slabs' a very nice overview is given when the reader is interested in a more detailed description.

1909 Turner wrote something about arching effects in slabs.
1921 Westergaard and Slater found out some strength enhancement in concrete floor.
1936 Gvodzev published a paper to rationalise CMA in the Soviet Union.
1955 Ockleston did some load test and found out that the strength was higher than expected.
1956 McDowell et. al. proposed a theory to predict relative great strength of constrained masonry walls.
1958 Ockleston found out that CMA was the reason for the strength enhancement.
1960 Kinnunen and Nylander developed a model for punching capacity of unrestrained simply supported slabs.
1961 Wood tries to find a theory for CMA.
1964 Park tries to find a theory for CMA.
1975 Hewitt and Batchelor developed a theoretical approach for the estimation of the punching capacity of laterally restrained slabs by modifying the model of Kinnunen and Nylander.
1979 The Ontario Bridge Design Code utilized CMA as one of the earliest codes.
1980 Park summarized his theory in a book (Park and Gamble). Braestup provided a historical review of the analyses that have been developed. Most models assumed rigid-plastic concrete behaviour and rigid translation restrained. Therefore practical application was limited.
1985 Kirkpartic et. al. has done some experimental and analytical investigation of the punching capacity of the M-beam (commonlu used in UK). They found excessive capacity compared with the British design code. An empirical method was developed. That model wasn't able to handle varying degrees of restrained.
1992 Kuang and Moley investigated influence of the degree of edge restraint, percentage of steel reinforcement and span-depth ratio on the punching shear of columns supported by columns. The strength enhancement was thought to be due to CMA.
1993 Kuang and Moley presented a plasticity model that analyzes the effect of CMA.
1997 Rankin and Long presented a simple method predicting the enhanced ultimate flexural capacity of laterally-restrained slab strips. The loads carried by bending and CMA were considered separately and then added to give the total resistance. They used McDowell et. al.'s derivation.

[1] Bakker, G.J. (2008), *A finite element model for the deck of plate-girder bridges including compressive membrane action, which predicts the ultimate collapse load*, page 6.
[2] Han-Ug Bae (2008), *Design of reinforcement-free bridge decks with wide flange prestressed precast girders,* page 5.
[3] Taylor, dr. S. et.al. (2002), *Guide to compressive Membrane Action*

1998 Mufti and Newhook adapted the model proposed by Hewitt and Batchelor for punching capacity of a fibre reinforced deck.
2001 Taylor et. al. applied the theory of Rankin and Long (1997) to high-strength concrete slabs.
2003 Ruddle et. al. applied the method of Rankin and Long (1997) to Tee beams.
2003 Taylor et. al. proposed a procedure to evaluate the ultimate capacity of bridge deck slabs. The flexural capacity was calculated following the method of Rankin and Long and the punching shear by the method proposed by Kirkpatric et. al. The smallest capacity is the ultimate bearing capacity. This method doesn't include serviceability evaluation.

It's clear that for a long time a lot of research have been done. Also this is not all the research that is been done but a relevant selection for Han-Ug Bae. CMA is nowadays incorporated in the codes of New Zealand, Australia, Canada and the United Kingdom. This gives a good reason to continue research in Europe, especially in the Netherlands, to have also the advantageous effects.

In the next paragraphs a brief description of the basic theories and some interesting conclusions of other master students shall be given. For detailed description of the theory it will be better to read the report of De Rooij, that was the basis for this summary.

The studied reports about CMA are the following:

- Han-Ug Bae (2008), *Design of reinforcement-free bridge decks with wide flange prestressed precast girders*
- Wei, Xuying (2008), *Assesment of real loading capacity of concrete slabs*
- Bakker, G.J. (2008), *A finite element model for the deck of plate-girder bridges including compressive membrane action, which predicts the ultimate collapse load*
- Chamululu, Godfrey (2009), *Compressive membrane in slender bridge decks*
- Rooij, R.F.C. de (2010), *(Preliminary research) Compressive membrane action in transversally prestressed concrete decks*

Theory

Failure mechanism: bending

Theory of Park

The load deformation diagram of a laterally restrained rectangular reinforced concrete slab is shown in Figure A-1. The beneficial effect of CMA is here clearly illustrated. Important for CMA is that cracking is needed, else the compression stresses cannot develop.

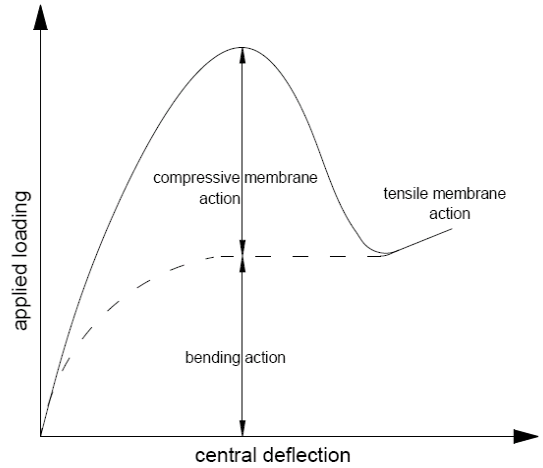

Figure A-1 Load deflection relationship

The transverse direction of the concrete slab is simplified to a one-way strip, that is restrained at both sides. The restraining is caused by the girders and the adjacent concrete. Figure A-2 shows the starting point for Park's CMA theory. The most important assumptions are that the system is symmetric and that rotations and translations are restrained at the supports.

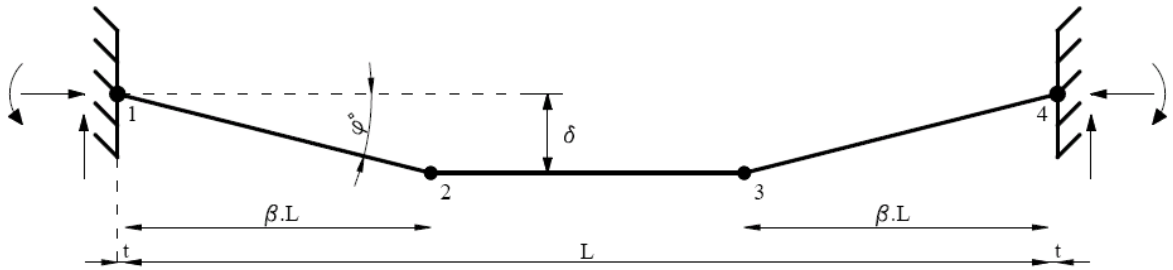

Figure A-2 Mechanism for Park's theory

From geometrical considerations the positions of the neutral axis in the plastic hinges can be solved. The deformed stage is visualised in Figure A-3.

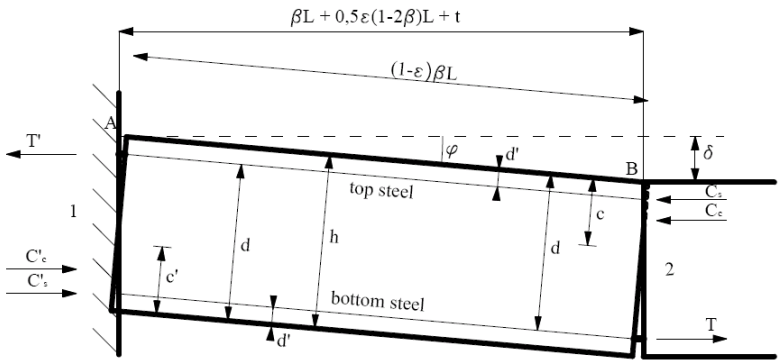

Figure A-3 Section 1-2 in deformed stage

The analytical solutions for the position of the neutral axis are:

$$c' = \frac{h}{2} - \frac{\delta}{4} - \frac{\beta L^2}{4\delta}\left(\varepsilon + \frac{2t}{L}\right) + \frac{T' - T - C_s' + C_s}{1{,}7 f_c' \beta_1}$$

$$c = \frac{h}{2} - \frac{\delta}{4} - \frac{\beta L^2}{4\delta}\left(\varepsilon + \frac{2t}{L}\right) - \frac{T' - T - C_s' + C_s}{1{,}7 f_c' \beta_1}$$

In Figure A-4 is shown how the forces are working in an section of the slab. β_1 is the ratio between the depth of the equivalent stress block (with value 0.85f'$_c$) and the neutral axis depth. This factor depends on the compressive strength of the concrete.

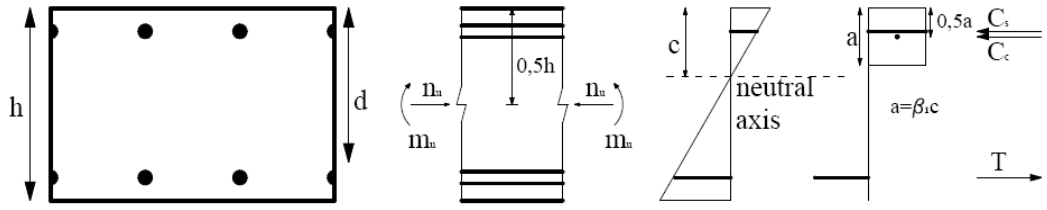

Figure A-4 Forces and moments in section

The forces n'$_u$ and m'$_u$ (left side) and n$_u$ and m$_u$ (right side) can be calculated. A sum of the moments around the mid-depth at one end of the strip is given by:

$$m_u' + m_u - n_u \delta$$

With the principal of virtual work the energy of the internal and external forces can be equated and a relation between the deflection δ of the strip and de load can be evaluated. The first part of the load-deflection curve is not correct because the plastic hinges are not immediate forming. So it's expected that the relationship is accurately only when sufficient deformation has occurred.

The influence of length, thickness, reinforcement ratio, concrete strength and steel strength are investigated by Bakker.[4] His conclusions are:

- The length is only of influence for short spans. The influence on the enhancement factor is rather small.
- The thickness of the slabs have a big influence on both enhancement factor and ultimate load.
- The higher the reinforcement ratio the smaller the enhancement factor.
- The higher the yield strength of the steel the lower the enhancement factor.
- For higher concrete strengths the enhancement factor and the ultimate load will increase both.

Enhancements by Miltenburg

Miltenburg made enhancements on the approach of Park by including the effects of prestressing force, creep, strain-hardening of the steel reinforcement, temperature changes and shrinkage. This advanced model is rewritten without prestressing because this is not the case for the bridge deck.

Elongation

For the derivation the beam is schematized in Figure A-5. This can be further simplified to the model in Figure A-6.

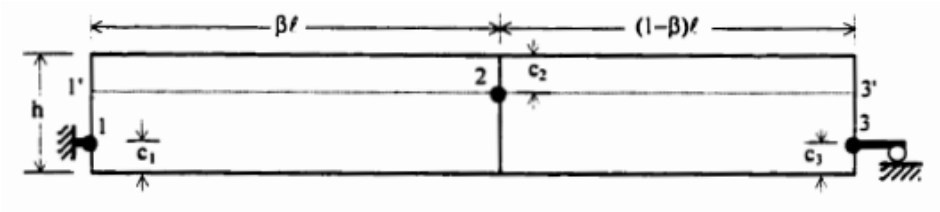

Figure A-5 Model of beam

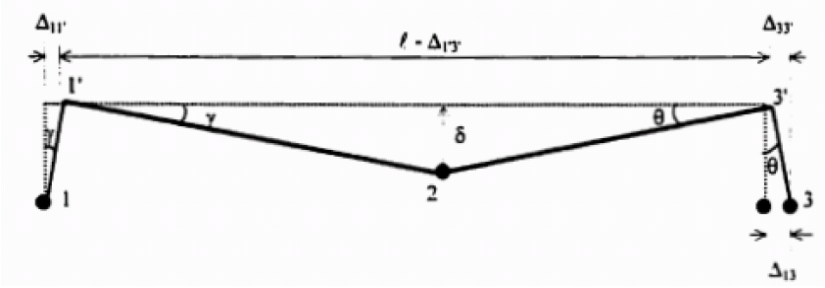

Figure A-6 Model of beam in deformed state

The total geometric elongation of the span length between the supports is given by:

$$\Delta_{13} = (h - c_2 - c_1)\frac{\delta}{\beta l} + (h - c_2 - c_3)\frac{\delta}{(1-\beta)l} - \frac{\delta^2}{2\beta(1-\beta)l}$$

[4] Bakker, G.J. (2008), *A finite element model for the deck of plate-girder bridges including compressive membrane action, which predicts the ultimate collapse load*, page 11-13.

Shortening
Membrane action is of course sensitive to shortening. Therefore al kinds of shortening should be included.

The elastic strain at mid-depth of slab is:

Elastic strain: $\varepsilon_{Nu} = \frac{N_u}{EA}$ with axial stiffness: $EA = E_s A_s + E_c (A_c - A_s)$

The influences of creep, shrinkage and temperature changes also influence the length:

- Creep is included by Meamerian et. al. with a factor k. This factor is the ratio between long term and short term deformations. Because creep is dependent on axial force the strain can be expressed as: $\varepsilon_{cr} = k\varepsilon_{Nu}$
- Shinkage and temperature deformations must be included as separate strain: (ε_{S+T}).

Sum of effects

Total elongation: $\Delta_{13} = (h - c_2 - c_1)\frac{\delta}{\beta l} + (h - c_2 - c_3)\frac{\delta}{(1-\beta)l} - \frac{\delta^2}{2\beta(1-\beta)l} - \left(\frac{(1+k)N_u}{(1+(n-1)\rho)E_c hb} + \varepsilon_{S+T}\right) l$

Lateral restraint
To calculate the membrane action the the lateral restraint is of importance. The model is given in Figure A-7 whereby the to springs are combined to one spring at one side. Here the stiffness of the supports is considered.

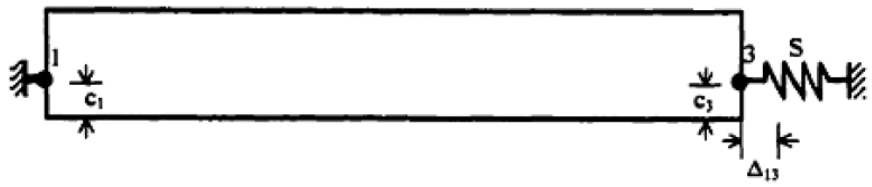

Figure A-7 Equivalent model of restraint

Reaction of the equivalent spring: $N_u = bS \cdot \Delta_{13}$.
(The width b is included because the elongation is given for a width and the spring stiffness S is given per unit width.)

Position of neutral axis
This is done following the CSA standard. The height of the concrete compression zone can be derived from: $C_{ci} = \alpha_1 f_c' (\beta_1 c_i b - A_{si}'), \quad i = 1,2,3$

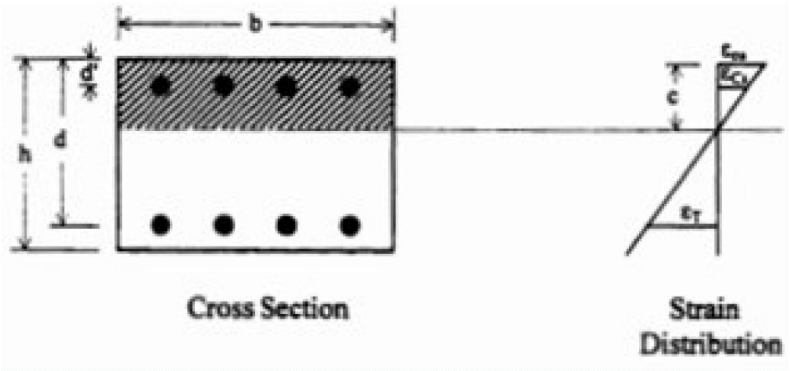

Figure A-8 Position neutral axis and strains in steel

The forces in the reinforcement steel can be derived with:

$\varepsilon_{Ti} = \varepsilon_{cu}\left(\frac{d_i - c_i}{c_i}\right)$ (tension side) and $\varepsilon_{Csi} = \varepsilon_{cu}\left(\frac{c_i - d'_i}{c_i}\right)$ (compression side)

With modified tri-linear idealization (Figure A-9) for mild steel the forces in the reinforcement can be derived using Hookes law.

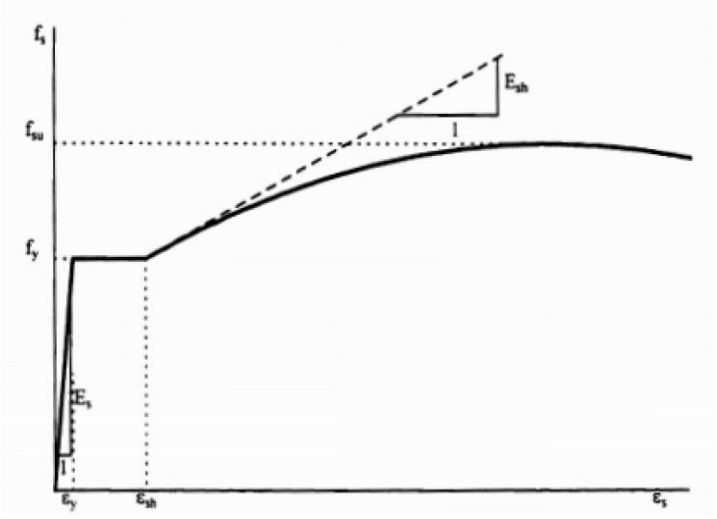

Figure A-9 Stress-strain relationship [Sargin, 1971]

Horizontal equilibrium

Now the sum of horizontal forces can be made to derive the location of the neutral axis. The huge expressions are given in the report of De Rooij. Interesting is the fact that in this expressions the prestressing doesn't play a role.

Finally a big expression is given which relates the displacement at the support with the forces (the force F_{ps} is removed from the equation):

$$\left(\frac{(1+k)N_u}{(1+(n-1)\rho)E_c hb} + \varepsilon_{S+T}\right)l + \Delta_{13} = \left[\frac{1}{1+\alpha_1 f_c' \beta_1 \frac{(1-\beta)\beta l}{2\delta}\frac{(1+k)l}{(1+(n-1)\rho)E_c h} + \frac{1}{S}}\right] \cdot$$
$$\left\{\left(\frac{(1+k)l}{(1+(n-1)\rho)E_c h} + \frac{1}{S}\right)\left[\alpha_1 f_c' \beta\left(\frac{h}{2} - \frac{\delta}{4} + \frac{(\beta-1)(T_1 - C_{s1}) + T_2 - C_{s2} - \beta(T_3 - C_{s3}) + \alpha_1 f_c'\left((\beta-1)A_{s1}' - A_{s2}' - \beta A_{s3}'\right)}{2\alpha_1 f_c' \beta_1 b}\right) + \frac{C_{s2} - T_2}{b}\right] + l\varepsilon_{S+T}\right\}$$

An iterative procedure is required to find the set of forces and locations of neutral axis with this formula.

After this the axial forces and moments can be derived from a sectional analysis. With help of Figure A-10 equilibrium equations can be derived for the left segment. This is also done for the right segment.

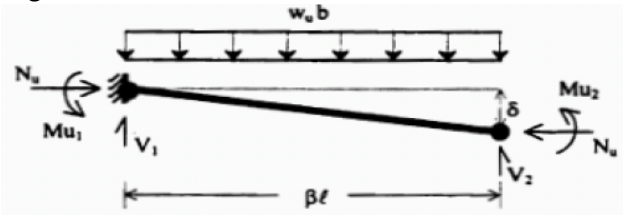

Figure A-10 Left segment of model

From this follows the formula: $$w_u = \frac{2}{bl^2}\left[\frac{M_{u1}}{\beta} + \frac{M_{u2}}{(1-\beta)\beta} + \frac{M_{u3}}{1-\beta} - \frac{N_u \delta}{(1-\beta)\beta}\right]$$ This formula can be solved iteratively.

Important is the position of the central hinge. The location can be found by solving the place where the derivative of w_u is zero.

Note: No idea is given about the stiffness of the supports.

***Model Chamululu*[5]**

Chamululu proposed a theory based on the McDowell's masonry theory. In this model the behaviour of the strip is idealised as shown in Figure A-11. The two capacities are summed up to arrive at the total bearing capacity.

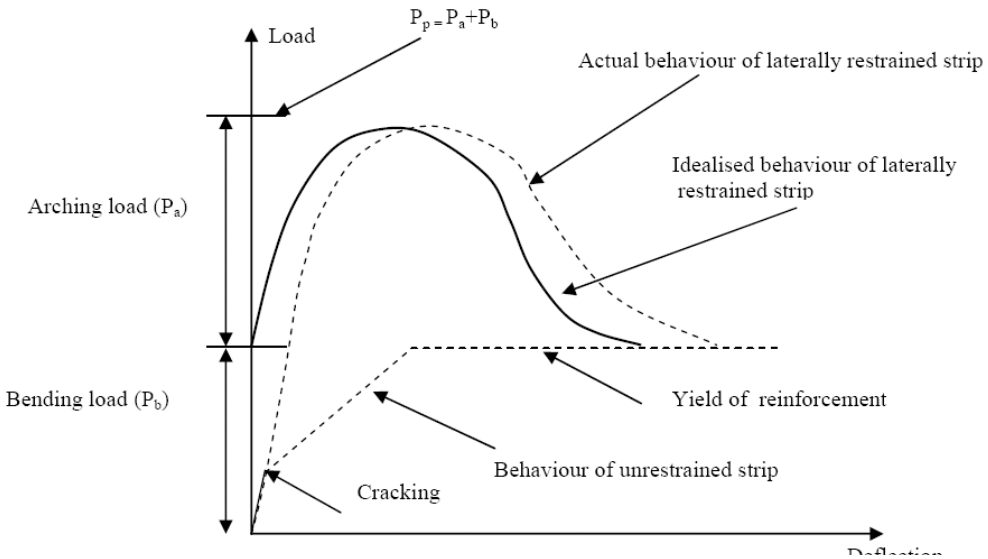

Figure A-11 Idealised behaviour of laterally restrained strip

This practical model isn't found back in other, later published, reports and therefore not further studied.

[5] Chamululu, Godfrey (2009), *Compressive membrane in slender bridge decks.*

Failure mechanism: punch

Plastic theory

The situation is given in Figure A-11

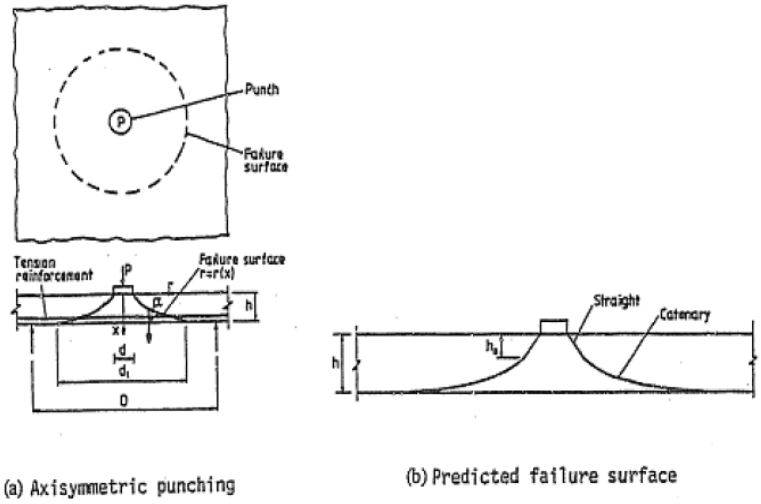

Figure A-12 Punching faillure model using plastic theory (Breastrup and Nielsen)

The basis of this theory is to equal the external and internal energy. Some solutions are given:

- Braestrup and Nielsen (1976): $Pu = \int_0^h \frac{1}{2} f_c u(l - m\sin\alpha) 2\pi r \cdot \frac{dx}{\cos\alpha}$
- Jiang and Shen (1986): $P = \pi f_t \left(\frac{d_1^2}{4} - \frac{d^2}{4} + \frac{2Kh^2}{\ln d_1 - \ln d} \right)$

A simplification of the formulation is also given by Jiang and Shen:
$P = 0{,}21 f_c sh$ with $s = \pi(d + h)$

The tests where done with concrete with a cast-in steel ring. Therefore some CMA was occurring. Due to this way of testing the plastic theory gives the failure load of prestressed deck slabs, for a certain range of prestressing, which is much higher than non-prestressed concrete decks.

Restraint factor concept

Hewitt and Batchelor proposed the usage of a restraint factor η to incorporate unspecified values of the axial forces and moments caused by lateral restraint. They used maximum possible values for these forces found by Brotchie and Holley.

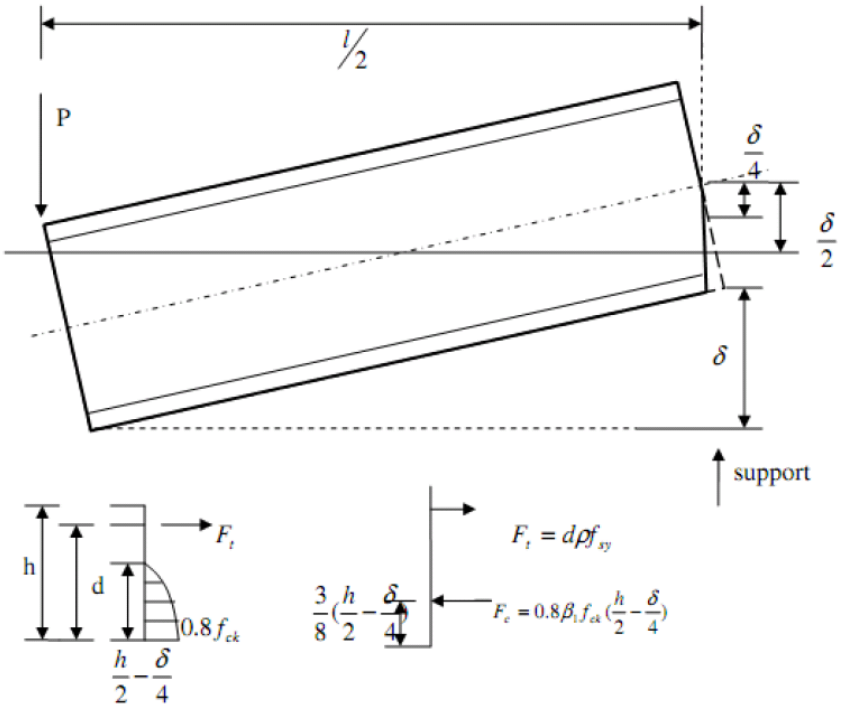

Figure A-13 Idealized displacement and boundary forces in the fully restraint slab

Maximum forces (fully restraint) from Brotchie and Holley:

$$F_{b(\max)} = F_c - F_t$$

$$M_{b(\max)} = F_t(2d-h) - F_c(d - 13h/16 - 3\delta/32)$$

Mean assumption of the model: For non-rigid boundaries it is assumed that the following schematization is possible:

$$F_b = \eta F_{b(\max)}$$

$$M_b = \eta M_{b(\max)}$$

There are some variants:

1. η=0.9, independent of the prestressing force.
2. η follows a linear line and is in relation with the occurring prestress level.
3. Value of F_p is equal to the occurring membrane force.
4. The restraint factor is a ratio of the prestressing force and maximum force: $\eta = \frac{F_p}{F_{b(\max)}}$

Punching failure model and analysis

A portion bounded by shear and radial cracks is considered in this analysis (Figure A-14).

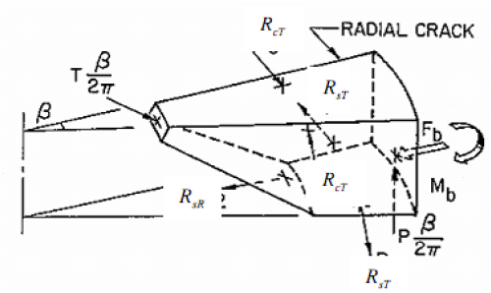

Figure A-14 Forces on sector element

There is a set of implicit equations which can be solved with a computer program. It is not of that importance to present all equations.

Comparison bending and punch

The two different failure modes (bending and punch) both include a kind of stiffness of the supports. The bending model with a physical support stiffness and the punching model with a dimensionless restraint factor. Therefore a direct comparison is not possible, the punching model was adapted by Wei[6] to compare the results.

Wei proposed a value for the lateral stiffness: $S_t = 0.48 c_t \frac{E_c A_c}{c}$ with $c_t = 100\rho\sqrt{\frac{h}{200}}$

From the report of Wei also follows that for a square concrete slab with a concentrated load always the punching capacity is governing.

From the report of Chamululu[7] follows that the enhancement due to CMA for the bending mode is much larger than that of the punching mode.

Bakker[8] gives a comparison from which follows that for low slenderness punch is governing. He didn't define 'low slenderness'.

In the report of Bae[9] one of the conclusions is that the failure mode depends on the lateral restraint. With sufficient lateral restraint punching failure will occur. Without sufficient lateral restraint a flexural failure or snap through instability can occur.

From tests follows that nearly always the punching failure is the governing failure mode.

[6] Wei, Xuying (2008), *Assesment of real loading capacity of concrete slabs,* page 90.
[7] Chamululu, Godfrey (2009), *Compressive membrane in slender bridge decks.*
[8] Bakker, G.J. (2008), *A finite element model for the deck of plate-girder bridges including compressive membrane action, which predicts the ultimate collapse load*, page 20.
[9] Bae, Han-Ug (2008), *Design of reinforcement-free bridge decks with wide flange prestressed precast girders,* Page 206.

Codes

New Zealand[10]

Design loading

Loads:

- (Superimposed) Dead load
  - Weight of structural members.
  - All permanent loads added.
  - A minimum allowance of 0.25 kN/m^2 should be applied for future services.
- HN (normal)
  - A strip of 3 meter width with a load of 3.5 kN/m^2 (10.5 kN/m devided by 3 meter).
  - Pair of axle loads of 120 kN each spaced at 5 meter, on worst location.
  - Area wheel 500 x 200 mm^2.
- HO (overload)
  - Same uniform distributed load as for HN
  - Pair of axle loads of 240 kN each spaced at 5 meter, on worst location. Two alternative wheel contact areas are possible, take most negative one.
- Accident load
  - HN wheel load factored by dynamic factor.
  - Wheel positioned at the outer edge of the slab or kerb.

Load position:

- Loads applied within each load lane.
- Roadway includes carriageway and shoulders. Roadway is bounded by either the face of a kerb or the face of a guardrail or other barrier.

Load combination:

- Normal live load: HN loading shall be placed.
- Overload: HO loading shall be placed.
- Improbability of concurrent loading: factor taking into account number of elements in the load case. This is applicable to HN and HO.

Load groups for ULS, without effects like temperature, settlement etc.:

- Group 1A: $U = 1.35 \cdot (DL + 1.67 \cdot (LL \cdot I))$
- Group 2A: $U = 1.20 \cdot (DL + LL \cdot I)$
- Group 4: $U = 1.35 \cdot (DL + 1.10 \cdot (OL \cdot I))$

(DL: dead load, LL: live load, OL: overload, I: dynamic load factor)

Dynamic load factor:

- Must be applied for HN and HO and is dependent on material and location of the member being designed (graph).

Fatigue:

- Shall represent the expected service loading over the design life of the structure.
- No standard fatigue load spectrum available: use BS5400: Part 10: 1980 clause 7.2.2

[10] *New Zealand Bridge Manual* (september 2004)

Limitations and requirements

When limit's are not met of for cantilevers elastic plate bending analysis shall be used. The requirements are written two times in the code (in clause 4.2.2 and 6.5.2). Clause 4.2.2 gives rules for design, clause 6.5.2 rules for evaluation. The rules for design are relevant for this thesis.

- There are at least three longitudinal girder webs in the system.
- The deck is fully cast-in-place.
- The deck is of uniform depth.
- The deck is made composite with the supporting structural components.
- The core depth is not less than 90 mm (core depth = depth – top and bottom covering)
- Diaphragms at supports (for reinforced and prestressed concrete girders).
- The supporting components are made of steel or concrete.
- The ratio of the span length to slab thickness should not exceed 15. For skew slabs the skew span shall be used (L_s/cos(angle)).
- The maximum slab length does not exceed 4 meter. For skew slabs the skew span shall be used (L_s/cos(angle)).
- The minimum slab thickness is not less than 165 mm.
- The overhang beyond the centreline of the outside beam should be at least 5 times the slab thickness.
- The specified 28 day compressive strength of the deck concrete is not less than 30 MPa.

For skewed slabs with angles greater than 20° in the end region 0.6% reinforcement must be placed, while the minimum is 0.3%. See Figure A-15 for an illustration of the reinforcement.

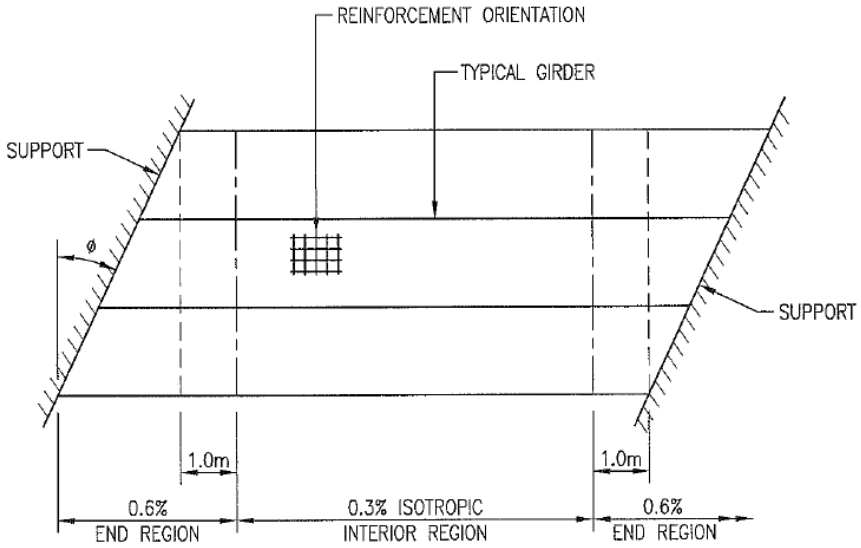

Figure A-15 Reinforcement in skewed slabs by the empirical method

Evaluation

There are two possibilities for evaluation:

1. Rating: define bridge capacity using overload load factors or stress levels (overweigh vehicles)
2. Posting: define bridge capacity using live load factors or stress levels (conforming vehicles)

Because the normal use will be considered the posting procedure will be presented here.

Posting

The formula for live load capacity is:

$$\text{Allowable Axle Load (kg)} = \left[\frac{\textit{Liveload wheel load capacity}}{\textit{Posting load effect}} x\ 8200\right]_{\min}$$

$$= \left[\frac{\phi x(0.6R_i)}{\gamma_L x 40\ x\ I} x\ 8200\right]_{\min}$$

Important:

- $\phi = 0.90 \cdot \phi_D$ (Good or fair, table 6.6) with $\phi_D = 0.5$ (6.5.2.b)
- The values from the charts shall be multiplied by 0.6 (6.5.2.b)
- R_i = section strength (from figure 6.1-6.5)
- $\gamma_L = 1.90$ (table 6.3)
- I = 1.3 (dynamic load factor for slabs, figure 3.2)
- Effects of dead load and other loads are neglected (6.5.2.b)

Canada[11]

Design loading[12,13]

Loads:

- Permanent loads
  - Dead loads (D)
  - Secondary prestress effects (P)

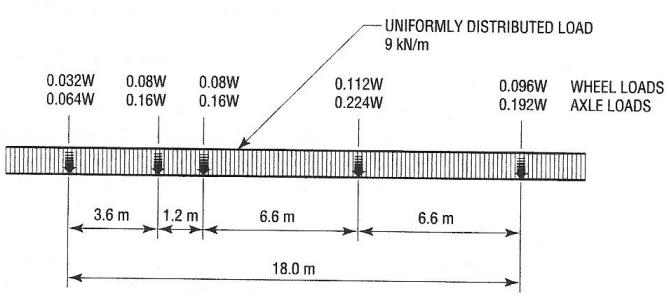

Figure A-16 CL-W Lane Load distribution

- Live load (Figure A-16)
  - 80% of CL-625 Truck
  - A strip of 3 meter width with a load of 3 kN/m^2 (9 kN/m devided by 3 meter). Don't apply when it's beneficial.
  - Area wheel 250 x 250 mm^2 (first axis) other axis 600 x 250 mm^2.

Load position:

- Loads applied within each load lane.
- Roadway includes carriageway and shoulders. Roadway is bounded by either the face of a kerb or the face of a guardrail or other barrier.

Load groups for ULS, without effects like temperature, settlement etc.:

- Load factors from Table A-1.

[11] Fang, I.K. et. al. (1986), *Behaviour of Ontario type bridge decks on steel girders*, page 4-6
[12] Chad, Andrew (2011), *Design of Slab- on-Girder Highway Bridges According to CAN/CSA-S6-00*
[13] Taylor&Francis Group (2000), *Bridge Loads*, chapter 4.4

3.5.1 (a) Load Factors and Load Combinations

	Permanent Loads			Transitory Loads					Exceptional Loads			
Loads	*D*	*E*	*P*	*L*[5]	*K*	*W*	*V*	*S*	*EQ*	*F*	*A*	*H*
Fatigue Limit State												
FLS Combination 1	1.00	1.00	1.00	1.00	0	0	0	0	0	0	0	0
Serviceability Limit States												
SLS Combination 1	1.00	1.00	1.00	0.90	0.80	0	0	1.00	0	0	0	0
SLS Combination 2[2]	0	0	0	0.90	0	0	0	0	0	0	0	0
Ultimate Limit States[1]												
ULS Combination 1	α_D	α_E	α_P	1.70	0	0	0	0	0	0	0	0
ULS Combination 2	α_D	α_E	α_P	1.60	1.15	0	0	0	0	0	0	0
ULS Combination 3	α_D	α_E	α_P	1.40	1.00	0.50[4]	0.50	0	0	0	0	0
ULS Combination 4	α_D	α_E	α_P	0	1.25	1.65[4]	0	0	0	0	0	0
ULS Combination 5	α_D	α_E	α_P	0	0	0	0	0	1.00	0	0	0
ULS Combination 6[3]	α_D	α_E	α_P	0	0	0	0	0	0	1.30	0	0
ULS Combination 7	α_D	α_E	α_P	0	0	0.90[4]	0	0	0	0	1.30	0
ULS Combination 8	α_D	α_E	α_P	0	0	0	0	0	0	0	0	1.00
ULS Combination 9	1.35	α_E	α_P	0	0	0	0	0	0	0	0	0

Table A-1 Load Factors and Load Combinations

Dynamic load factor (Cl. 3.8.4..5.3):

- 0.50 for deck joints
- 0.40 where only one axle of the CL-W truck is used, except for deck joints.
- 0.30 where any two axles of the CL-W truck are used, or axles 1,2 and 3 are used; or
- 0.25 where three axles of the CL-W truck, except for axles 1,2 and 3 or more than 3 axles used.

Reduction factors:

- A reduction factor when there are more lanes Table A-2.

Number of Loaded Design Lanes	Modification Factor
1	1.00
2	0.90
3	0.80
4	0.70
5	0.60
6 or More	0.55

Table A-2 Modification factors for Multilane Loading

Fatigue:

- Special fatigue limit state (Table A-1).

Limitations and requirements

From clause 7.8.5.2 follows:

- A minimum of 0.3%, especially for SLS, not necessary for ULS. Only small haircracks occur.
- The girder space should not exceed 3.7 m.
- The cantilever should at least extend 1 m beyond the centreline of the exterior beam. Also the curb can be used but the cross-sectional area must be at least the same.
- The span length to thickness ratio should not exceed 15. For skew slabs, use skew span.
- For skew angles greater than 20° the end portions of the deck slab shall be provided with 0.6% isotropic reinforcement.

- Slab thickness not less than 225 mm (increased, in previous codes 190 mm, increased for durability) and spacing of isotropic reinforcement bars not exceed 300 mm.
- Diaphragm beams at supports.
- Spacing of shear connectors in composite system should not exceed 0.6 m.
- Edge stiffening for all slabs.

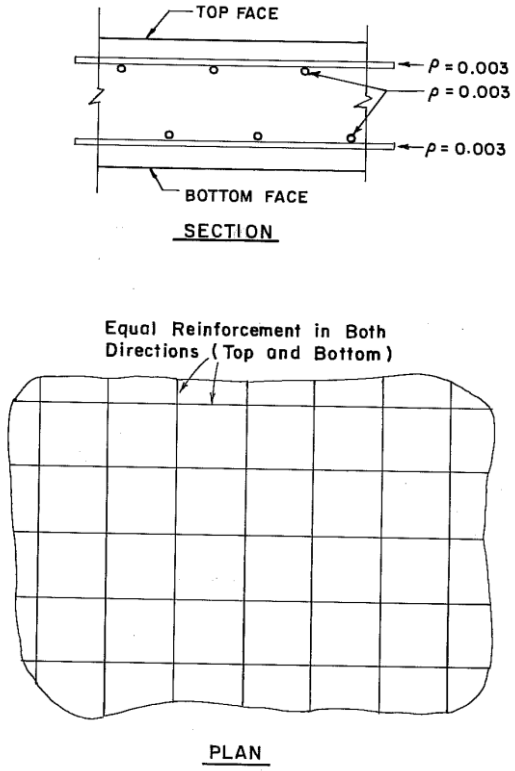

Figure A-17 Reinforcement plan prescribed by empirical method

Evaluation

The basic equation for punching shear is: $0.65 \cdot R \geq 1.20 \cdot D + 1.40 \cdot (1 + i) \cdot L$

Where:
- R: failure load [kN]
- D: dead load effect – about $0.20 \cdot L$ [kN]
- i: impact, 0.45 [kN]
- L: live load effect [kN]

The equation is then: $0.65 \cdot R \geq 1.20 \cdot 0.20 \cdot L + 1.40 \cdot (1 + 0.45) \cdot L = 2.27 \cdot L \rightarrow R \geq 3.49 \cdot L$

In the procedure it is assumed that crack control requirements and shear resistance requirements are met.

United Kingdom[14]

Design loading[15,16]

Loads:

- (Superimposed) Dead load
  - Weight of structural members.
  - All permanent loads added.
- HA (normal), calculated for 'loaded length'
  1. UDL (from figure 5.1 BD 21/01, function for W) and a KEL of 120 kN (Length < 50 m)
  2. A single axle load (Length < 2 m)
  3. A single wheel load of 100 kN (Length < 2 m), circular 340 mm or square 300 mm.
- HB (overload)
  - Special cases.
- Accident load
  - A single appropriate accidental vehicle shall be selected.
  - Wheel positioned at the outer edge of the slab or kerb.

Load position:

- Loads applied within each load lane.
- Roadway includes carriageway and shoulders. Roadway is bounded by either the face of a kerb or the face of a guardrail or other barrier (5.6).
- Width of carriageway between 2.5 m and 3.65 m (See Table A-3).

Carriageway Width (m)	Number of Notional Lanes
below 5.0	1
from 5.0 up to and including 7.5	2
above 7.5 up to and including 10.95	3
above 10.95 up to and including 14.6	4
above 14.6 up to and including 18.25	5
above 18.25 up to and including 21.9	6

Table A-3 Number of Notional Lanes

Load factors and combinations follows from Table A-4 and Table A-5.

Load	Limit State	γ_{fL} to be considered in combination				
		1	2	3	4	5
Dead: Steel	USL	1.05	1.05	1.05	1.05	1.05
	SLS	1.00	1.00	1.00	1.00	1.00
Dead: concrete	USL	1.15	1.15	1.15	1.15	1.15
	SLS	1.00	1.00	1.00	1.00	1.00
Superimposed dead: deck surfacing	USL	1.75	1.75	1.75	1.75	1.75
	SLS	1.20	1.20	1.20	1.20	1.20
Superimposed dead: other loads	USL	1.20	1.20	1.20	1.20	1.20
	SLS	1.00	1.00	1.00	1.00	1.00
Reduced load factor for dead & superimposed dead load where this has a more severe total effect	USL	1.00	1.00	1.00	1.00	1.00

[14] BD 81/02 (may 2002), *Use of compressive membrane action in bridge decks.*
[15] BD 21/01 (may 2001), *The assessment of highway bridges and structures,* Chapter 5.
[16] Olffen, Bram van, *Interactive Course Concrete Bridges,* page 57.

Table A-4 Load combinations and factors for permanent loads

Load		Limit State	γ_{fL} to be considered in combination				
			1	2	3	4	5
Highway: live loading	HA alone	USL	1.50	1.25	1.25		
		SLS	1.20	1.00	1.00		
	HA with HB or HB alone	USL	1.30	1.10	1.10		
		SLS	1.10	1.00	1.00		
	footway and cycle track loading	USL	1.50	1.25	1.25		
		SLS	1.00	1.00	1.00		
	accidental wheel loading	USL	1.50				
		SLS	1.20				

Table A-5 Load combinations and factors for live loads

Dynamic load factor:

- Must be applied for HN and HO and is dependent on material and location of the member being designed (graph).

Reduction factor:

- K = Assesment live loading / Type HA loading. Only for loaded lengths above 2 m.
- Factor AF for different span ranges to account for lateral bunching effect. The HA UDL and KEL are calculated with this effect but at high speed no lateral bunching is the most onerous criterion for bridge loading. Therefore divide by this factor (5.23 BD 21/01).
- Lane factor (5.24 BD 21/01).
    - Lane 1 1.0
    - Lane 2 1.0
    - Lane 3 0.5
    - Lane 4 0.4

Fatigue:

- Shall represent the expected service loading over the design life of the structure.
- Use BS5400: Part 10: 1980 clause 7.2.2

Limitations and requirements

- (3.6) Slab at least 160 mm thick.
- (3.6) At least grade 40 (characteristic compressive strength after 28 days) concrete.
- (3.6) The local strength may be assumed adequate for up to 45 units of HB.
- (3.11) Deck slab reinforcement shall be derived in accordance with BD 24 on basis of global effects only.
- (3.11) The resistance to local affects shall be derived from 5.2-5.9 (punching included).
- (3.12) Without adequate boundary restraint the effects of the global and local effects shall be derived from the direct strain due to global effects combined with the flexural strain due to local effects in accordance with BD 24.
- (3.13) Minimal reinforcement 0.3%. Spacing not greater than 250 mm. Not less than 750 mm^2/m
- (5.10) Span of slab panel should not exceed 3.7 m.
- (5.10) The slab shall extend at least 1.0 m beyond the centre line of the external longitudinal supports. Or use kerb.
- (5.10) The span length to thickness ratio should not exceed 15. Skew slabs: skew spans.
- (5.10) For skew angles greater than 20° end portions of deck in accordance with BD 24 and 44.
- (5.10) Transverse edges at ends of bridge or at supports should be supported by diaphragms or other suitable means.
- (5.10) Diaphragms at support lines of all bridges. For prestressed beams only at the ends.
- (5.10) All slabs having main reinforcement parallel to traffic should have edge beams.

Evaluation

The method assumes that the slab reinforcement makes no contribution to the local load carrying capacity.

Notation:

d	average effective depth to the tensile reinforcement (mm)
f_{cu}	characteristic concrete cube strength (N/mm^2)
h	overall slab depth (mm) (for precast concrete participating formwork panels, to allow for the reduced depth at panel joints, h shall be taken as the overall depth minus 10 mm)
L_r	half span of slab strip with boundary restraint (as defined in 1.8) (mm)
γ_M	= partial safety factor for strength
φ	= diameter of loaded area (mm)

Concrete compressive strength:

$$f_c = \frac{0.8 f_{cu}}{\gamma_m} \qquad \text{Equation 1}$$

The plastic strain of an idealised elastic-plastic concrete is given by:

$$\varepsilon_c = (-400 + 60 f_c - 0.33 f_c^2) \times 10^{-6} \qquad \text{Equation 2}$$

Non-dimensional *parameter* for arching moment of resistance (R), must be less then 0.26 to apply CMA:

$$R = \frac{\varepsilon_c L_r^{\,2}}{h^2} \qquad \text{Equation 3}$$

Non-dimensional arching moment *coefficientI:*

$$k = 0.0525\,(4.3 - 16.1\sqrt{3.3x10^{-4} + 0.1243R}) \qquad \text{Equation 4}$$

Effective reinforcement ratio:

$$\rho_e = k\left[\frac{f_C}{240}\right]\left[\frac{h}{d}\right]^2$$

Ultimate predicted load for a single wheel:

$$P_{ps} = 1.52(\varphi + d)d\sqrt{f_c}(100\rho_e)^{0.25} \qquad \text{Equation 6}$$

For axle loading (two wheels on one slab or two wheels on adjacent axles):

$$P_{pd} = 0.65 P_{ps} \qquad \text{Equation 7}$$

Modelling concrete

Introduction

It's important to make an argued choice for a model. For that reason the reports of other master students were studied to tackle the most important problems.

Information from other reports

Report Han-Ug Bae

Han-Ug Bae did also a FE analysis. He used, beside other models, the model showed in Figure A-18.

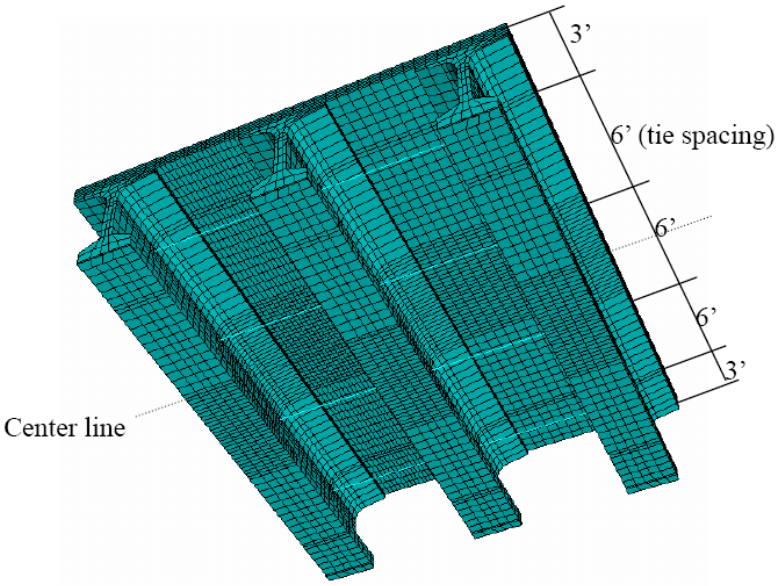

Figure A-18 Modelling of the bridge for parameter study

Report Bakker

For membrane action cracking is important. For bending a 2D-model will be sufficient, for punching a 3D-model is necessary. Load steps can be applied in two different ways, by displacements or by forces.

Way of modelling

Bakker compared five different FE-models. It was shown in his study that the 2D beam model and 3D shell model give almost the same results. The same conclusion holds for the results obtained with the 2D plane stress and the 3D solid model. An overview of the found results is given in Table A-6.

	input	graphical output	realistic model	punch behaviour	calculation time
2D beam model	++	--	+	irrelevant	++
2D plane stress model	+	+	+	irrelevant	+
3D curved shell model	o	-	+	--	o
3D solids model	-	++	++	o	--
axi-symmetric model	+	+	-*	++	+

* : rectangular slabs cannot be modelled with this model

Table A-6 Overview of different FE models and their results

Cracking

There are two cracking models possible, smeared cracking or total strain cracking. Smeared cracking depends on principal stresses.

The total strain crack model describes the tensile and compressive behaviour of a material with one stress-strain relationship. Within both rotating or fixed cracking this model can be chosen. The difference is that for fixed cracking the cracks lies in the same direction for all the load steps, while by rotating cracking, the direction of the crack is calculated separately for each load step.

Bakker applied the total strain rotating crack model and the direction of the cracks varied for each load step.

Concrete in tension - Post-cracking behaviour
The Dutch code is based on models with brittle cracking, but including tension softening may give result, that lie closer to the real collapse load. Bakker used both the brittle and Hordijk model.

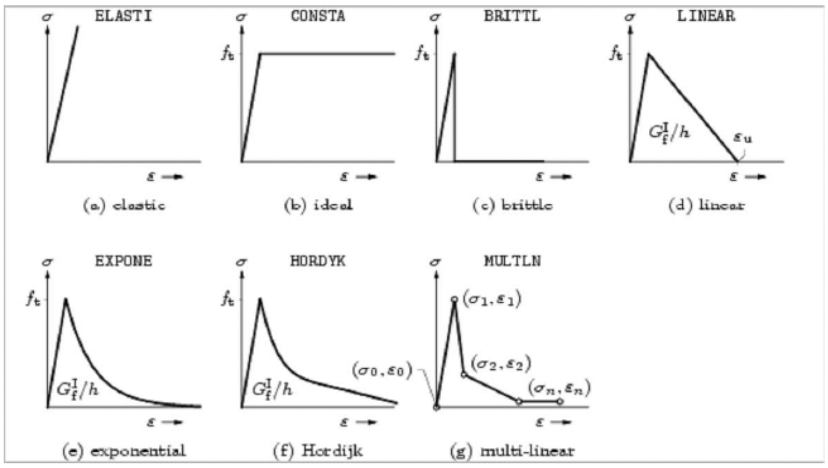

Figure A-19 Different models for concrete behaviour after cracking

Concrete in compression
Bakker used the ideal elasto-plastic model in his calculations.

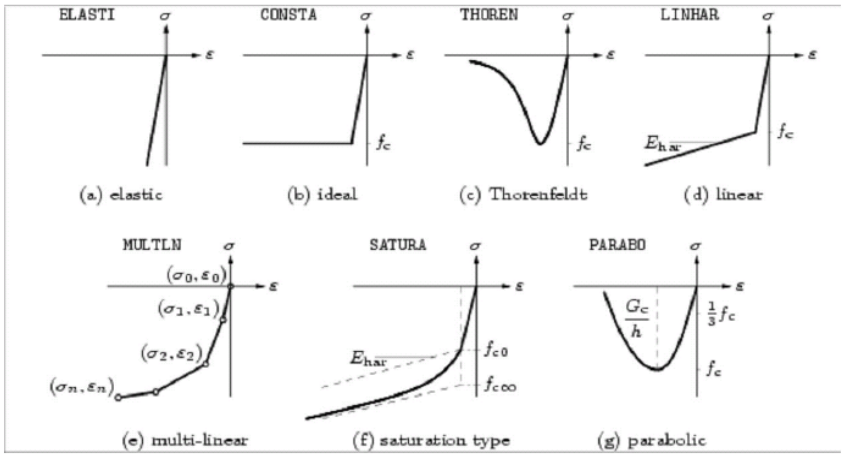

Figure A-20 Concrete behaviour under compression

Reinforcement
For the reinforcement there are three options, ideal plastic, a work-hardening diagram or a strain-hardening diagram. The ideal plastic model is used.

Model
The models that Bakker used:

- Total strain rotating crack model.

- Both brittle and Hordijk tension softening in tension
- Ideal plastic model in compression
- Ideal plastic model for the reinforcement

FEM for bending action
Bakker used the 2D plane stress model to analyse the stresses.

The brittle material model gives slightly less enhancement factor than the model with tension softening.

From comparison with test results Bakker concluded that the brittle model seems to give a better approximation of the collapse load than the tension softening model.

The tension softening model is much more ductile than the brittle model.

The brittle model needs more iterations to reach its convergence criterion in each step. For a fully 3D solids model this will be something to keep in mind.

FEM for punching failure
Bakker used the 3D plane stress model or the axi-symmetric model.

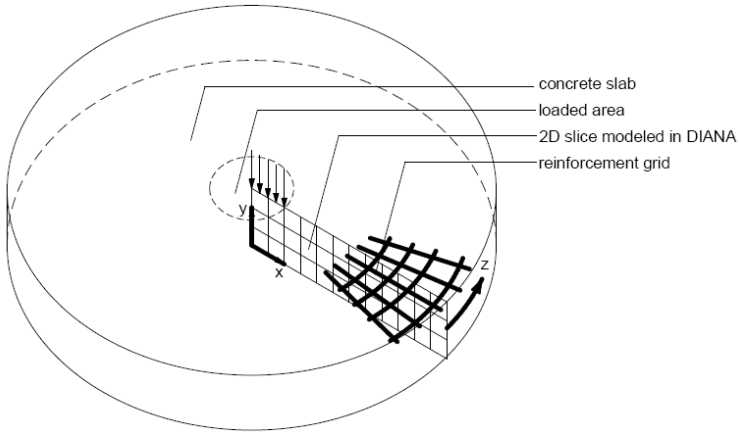

Figure A-21 Axi-symmetric model

Four models where compared:

- Brittle material model, all sides simply supported
- Brittle material model, all sides clamped
- Tension softening material model, all sides simply supported
- Tension softening material model, all sides clamped

For the brittle model the collapse load was already reached before punching occurred.

After this Bakker applied the axi-symmetric model. With this model big differences in ultimate load capacity were found when the brittle or tension softening material model was applied. The conclusion was that the axi-symmetric model with brittle material behaviour is the fastest and best.

Report Minalu

Minalu compared different modelling techniques:

Orthotropic plate model

An equivalent slab is calculated with different stiffness in both directions. The transverse stiffness of the beams is neglected. Minalu calculates this model with SCIA Engineer with a Mindlin plate element.

Limitations:

- The modelling technique fails to deal with the following aspects of bridge deck behaviour: transverse and longitudinal in plane forces, distortion of beam members, local bending effects.
- The different position of the neutral axis in the transverse direction of the bridge is not taken into account.
- Location of support system is normally under the beams, but in the model the supports are located at the neutral axis.

Centric beam elements for the girders and plate bending elements for the deck

The deck slab has been modelled by using quadrilateral plate bending elements. The precast prestressed girders and end diaphragms have been idealized using beam elements. The centroid of each of the girders and diaphragm coincided with the centroid of the concrete slab. SCIA Engineer commercial finite element software package is adopted for this model.

Limitations:

- The following things cannot be taken into account: transverse variation in the level of the neutral axis, transverse and longitudinal in-plane forces.
- Model fails to consider distance between the centre of the deck and girders: underestimation of flexural strength.
- Location of support system is normally under beams, but in the model at the neutral axis.

Eccentric beam elements for the girder and shell elements for the deck.

The eccentricity of the beams is realised with a rigid vertical member. This is also possible with SCIA Engineer. With this model tension in the deck was found.

Shell elements for both the deck and the girders

Some approximations had been done to couple the beam to the slab. The approximation increases the bending and torsion inertias of the girders. Hence, this model predicted higher torsion moments.

Limitations:

- SCIA Engineer failed to connect the shell elements of the deck with the shell elements of the beams by a rigid link.

3D model with volume elements

Minalu used ATENA 3D. ATENA 3D is especially designed to simulate real behaviour of concrete and reinforced concrete structures including concrete cracking, crushing and reinforcement yielding. Geometrical and physical non-linear analysis is also possible in ATENA 3D. In this case study, 3D linear elastic analysis has been carried out using standard brick elements. To decrease computational time first order linear interpolation elements were employed. The cracking of the structure was incorporated by reducing the stiffness of the elements.

For the reduction of the torsion stiffness two solutions are possible:

- Reduction of torsion moment of inertia: not possible for shell and volume finite elements.
- Reduction of the shear modulus: in ATENA 3D is was not possible to change the shear modulus keeping the modulus of elasticity and poison's ratio unchanged. Consequently Minalu only investigated SLS with full torsion stiffness.

Limitations:

- In ATENA 3D it is impossible to create an orthotropic deck having different stiffnesses in the transverse and longitudinal direction. To consider the effect of cracking for the deck slab half of young's modulus was used in both directions for all finite element models.

B. Comparison calculation skew and straight bridges

Objective

Two calculations are made to have a starting point for the 3D models.

Comparison

The most important parameters of the bridges are compared. One of the first figures in the report of Minalu was about the load distribution in a skew bridge and is shown in Figure B-1. Minalu also made an analysis of the effect of skewness on the load distribution.[17] The differences found between the straight and skew bridge are compared with his conclusions.

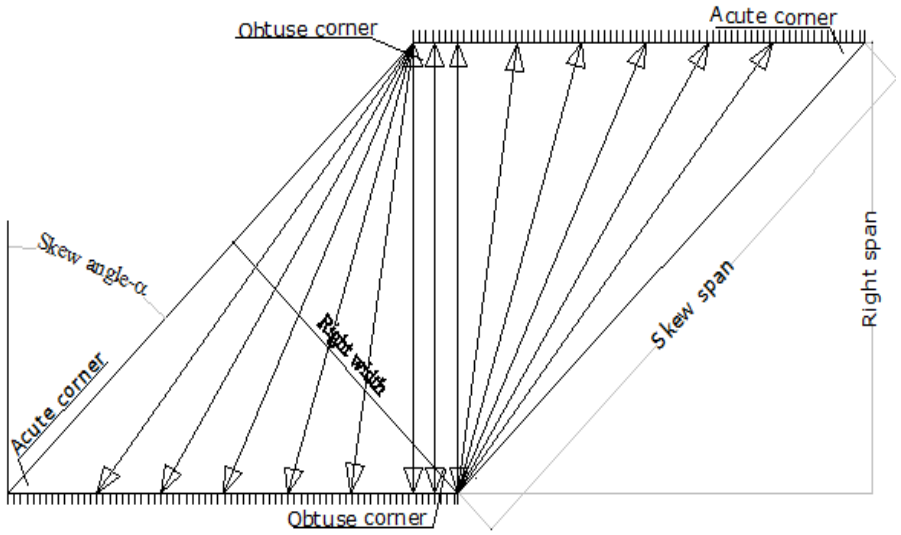

Figure B-1 Load paths in torsion stiff skew bridges[18]

Note: Minalu also calculates an orthotropic plate model, so the absolute values should be the same. This is not the case due to a small mistake in the calculation. Minalu applied the supports correctly at some distance from the ends of the girder, but didn't specify the distance in his report. In the model used for the calculations presented in this report the supports where placed at the ends of the girders, which is physically impossible. So the span between the supports was 36 m instead of 35.3 m, assuming that Minalu used a 0.35 m distance. This will give higher longitudinal moments. However, in the calculation of the cross-section in the program Span the correct span was used. So finally the mistake will not have big impact for the prestressing. In the model however there will be little deviation in the values.

Note: the stiffness matrix of Minalu differs with the stiffness matrix used for the calculations of this report. Parameter D11 is much bigger in this report. That will give some differences in load distribution, the longitudinal direction will attain a bigger part of the load. Also the used matrices in the models of Minalu do not correspond with the matrices presented in his report.

Longitudinal moment in girders

The applied loads are given in Figure B-2.

[17] Minalu, Kassuhun K. (2010), *Finite element modelling of skew slab-girder bridges.* Page 100-106.
[18] Minalu, Kassuhun K. (2010), *Finite element modelling of skew slab-girder bridges.* Page 2.

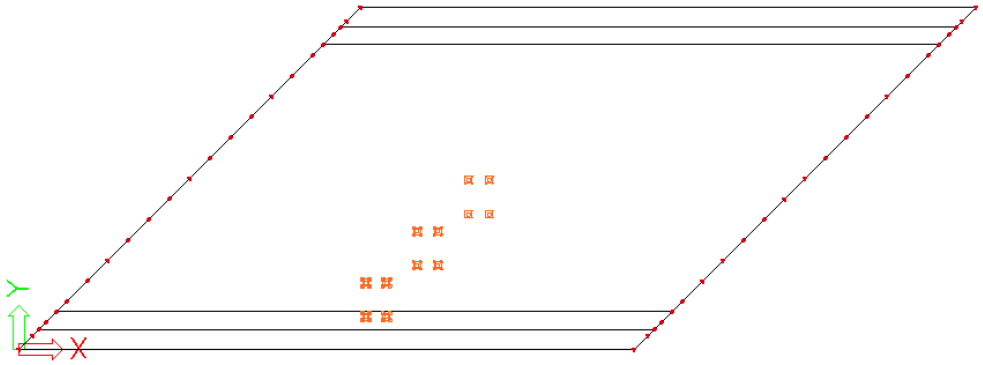

Figure B-2 Loads for maximum longitudinal moment (with corresponding negative working lane loads)

From this load case follows governing moments, presented in Table B-1.

Girder	Straight bridge [kNm]	Skew bridge [kNm]	Deviation [%]
ZIP	3524.3	3430.6	-2.65
1st ZIP	3387.4	3339.5	-1.41
TRA	2467.9	2435.2	-1.33

Table B-1 Comparison longitudinal moment

The differences are negligible. Minalu also found a reduction in longitudinal bending moment in the first ZIP, but in his case this reduction was larger: -3.83 %.

Transversal moment in deck

The applied loads for the negative and positive moments in the deck are given in Figure B-3 and Figure B-4.

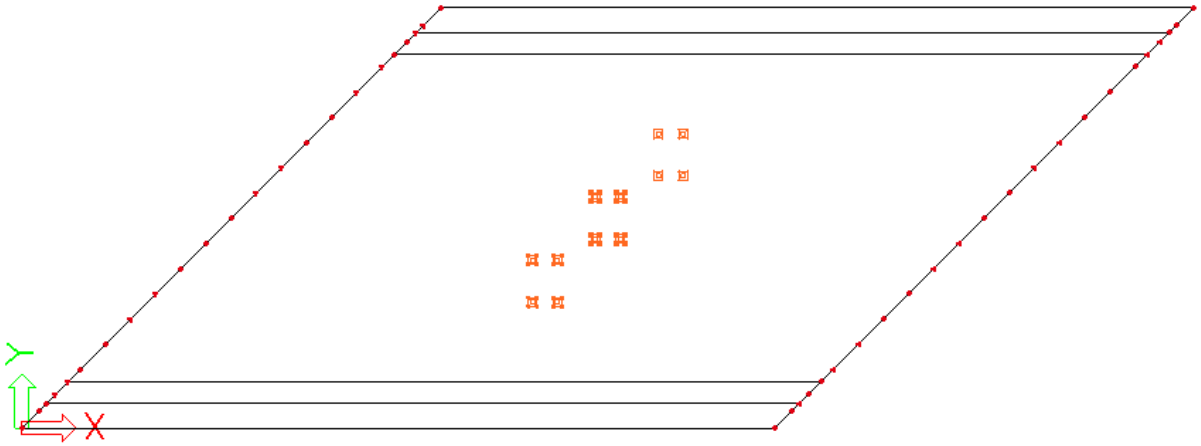

Figure B-3 Applied axle loads for maximum positive moments (with corresponding lane loads)

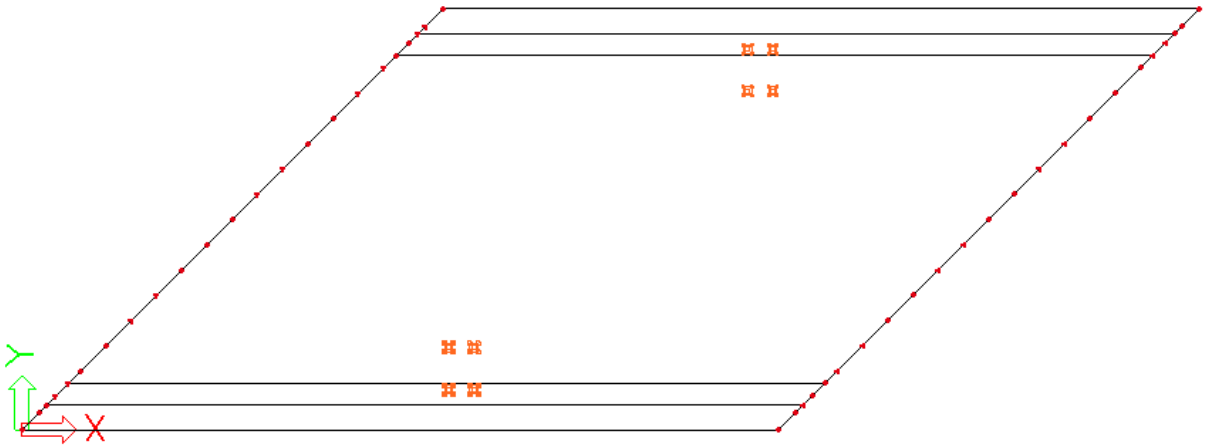

Figure B-4 Applied axle loads for maximum negative moments (with corresponding negative working lane loads)

From this load case follows governing moments, presented in Table B-2.

Position	Straight bridge [kNm]	Skew bridge [kNm]	Deviation [%]
Deck positive	+28.0	+31.7	+13.21
Deck negative	-16.5	-12.5	-24.24
Deck corner negative	-35.6	-46.8	+31.46

Table B-2 Comparison transversal moment

To get insight, the distribution of the transverse bending moment is visualized in Figure B-5, Figure B-6 and Figure B-7 and Figure B-8 for both the straight and skew bridge. The color range was set the same to be able to compare the colours.

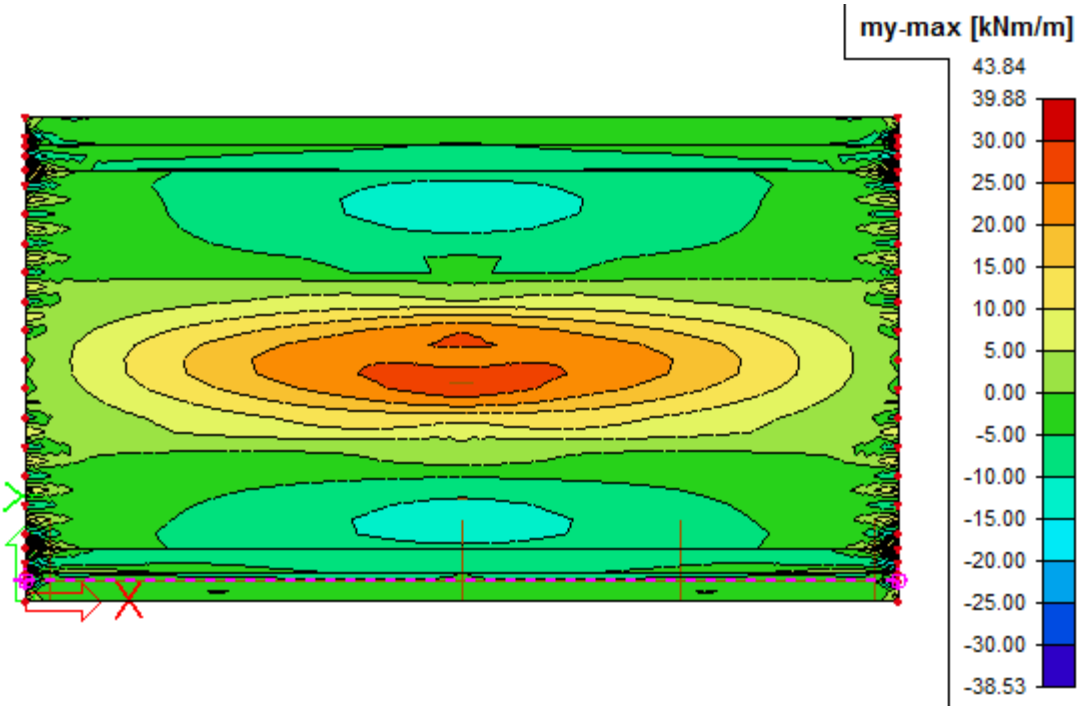

Figure B-5 Positive moments in deck straight bridge

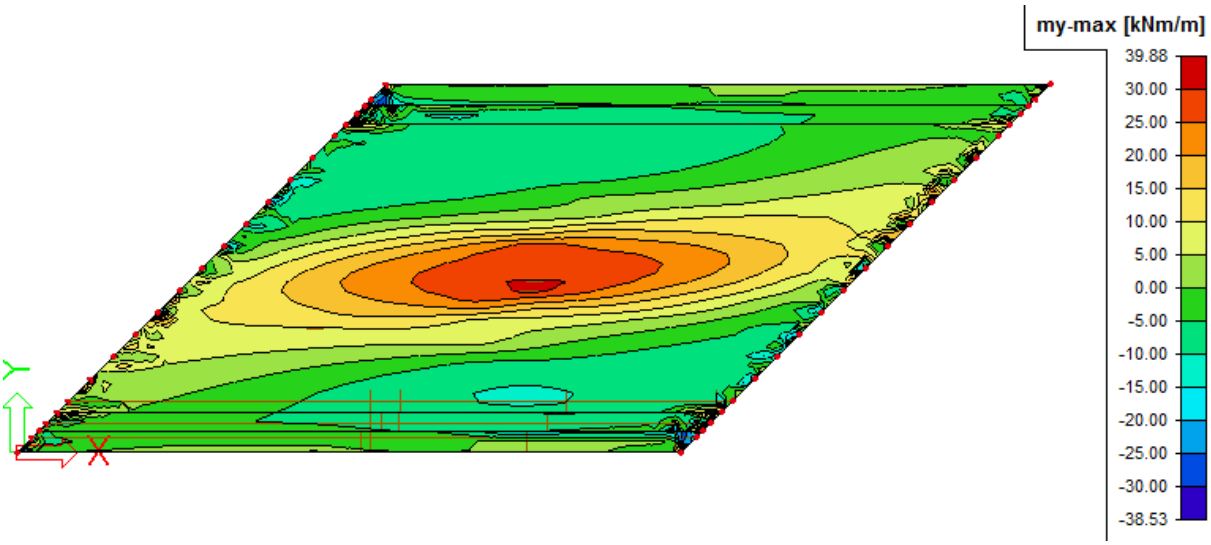

Figure B-6 Positive moments in deck skew bridge

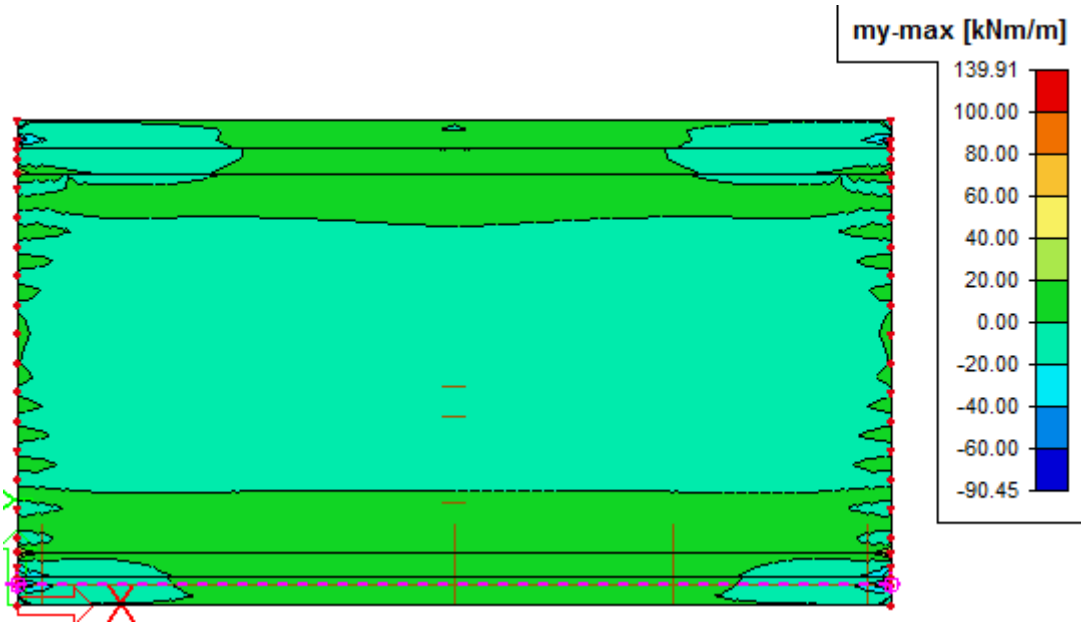

Figure B-7 Negative moments in deck straight bridge

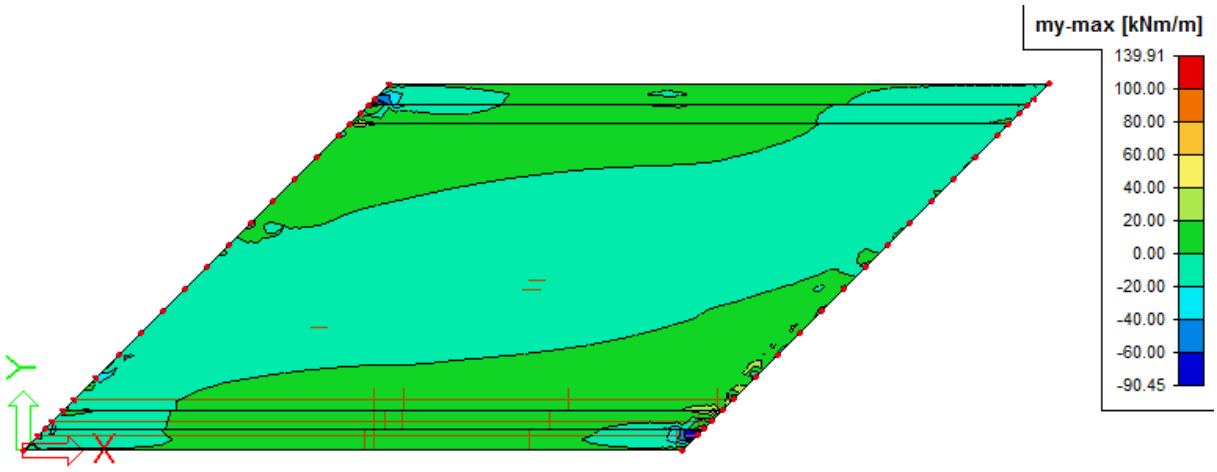

Figure B-8 Negative moments in deck skew bridge

Positive moments in deck
The positive moment in the deck is higher for the skew bridge (Table B-2).

Minalu gets the same result, also an increase of transversal moments, but only of 7.4 %. Minalu compared some angles of skewness and founds that with angles larger than 45 degree the moments increase much more compared to a straight bridge. It is clear that the load transfer will be more direct to the obtuse corners dependent on the skewness, logically the transverse moments increase in that case.

Negative moments in deck and corners
The negative moment in the deck is lower for the skew bridge in the middle but higher in the corner of the bridge, Table B-2. That the negative moments decrease for the skew one is remarkable. A calculation of a skew bridge based on a straight bridge model consequently will give an underestimation of the negative moments. The negative moments at the obtuse corners enhance a lot. A reason for this could be: When the obtuse corner attracts more load it attracts more negative moments.

Minalu did not analyse the occurring negative moments in the deck, so no comparison can be made with his results.

Relation between torsion and moments in deck
Interesting is the question: why is are there differences in the moments in the deck between the skw and straight bridge? For that reason the distribution of the torsion moments is visualised in Figure B-9 and Figure B-10.

Some remarkable points:

- In the straight bridge the positive and negative torsion moments are bounded in the quadrants. In the skew one the negative quadrants are joining together.
- For the straight bridge the maxima of the torsion moments are +26.09/ -26.10 kNm. For the skew one they are +69.1/ -82.7 kNm.
- The green color between -10 and -20 kNm is occurring more in the skew bridge: more torsion.

From this it can be concluded that the transversal bending moment in the middle of the deck is decreasing because the torsion moments are bearing a larger part of the load.

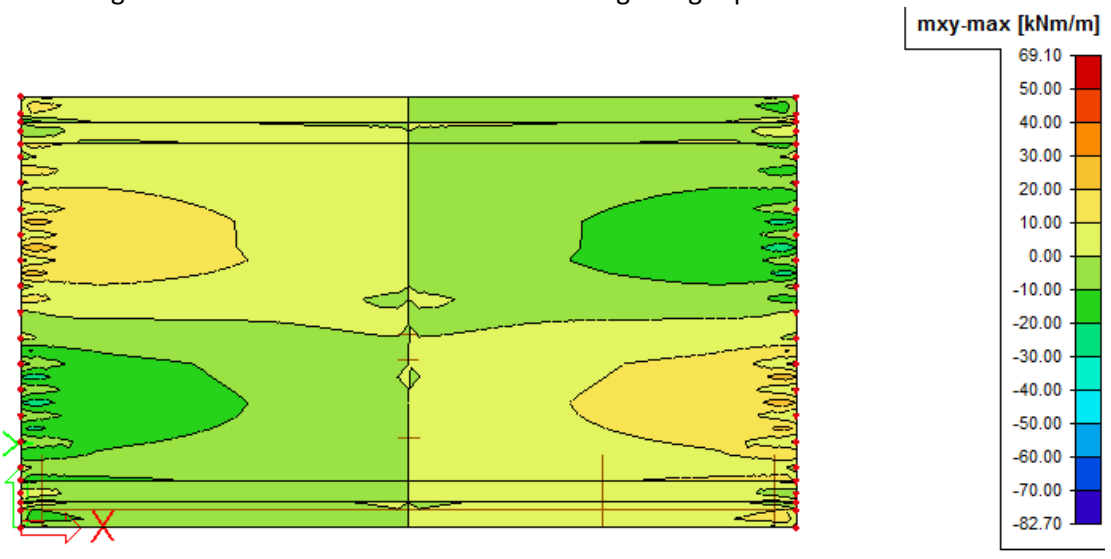

Figure B-9 Torsion moments occurring together with positive bending moments in deck for straight bridge

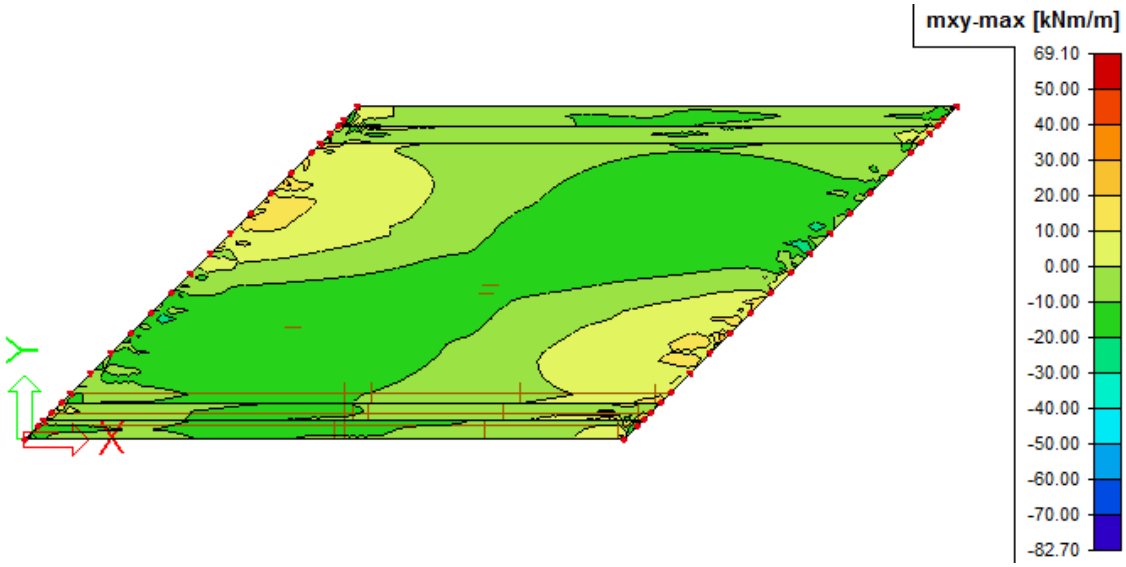

Figure B-10 Torsion moments occurring together with positive bending moments in deck for skew bridge

Torsion and Shear force in girders

Intended comparison

- First it will be investigated if it was a save assumption to use the practical models and neglect the models found by Minalu.
- After that differences between the skew and straight bridge will be analysed.

Load models

The load models used for the determination of the shear and torsion reinforcement are presented in Figure B-11 and Figure B-12. In practice train loads are used to model this load cases in one run.

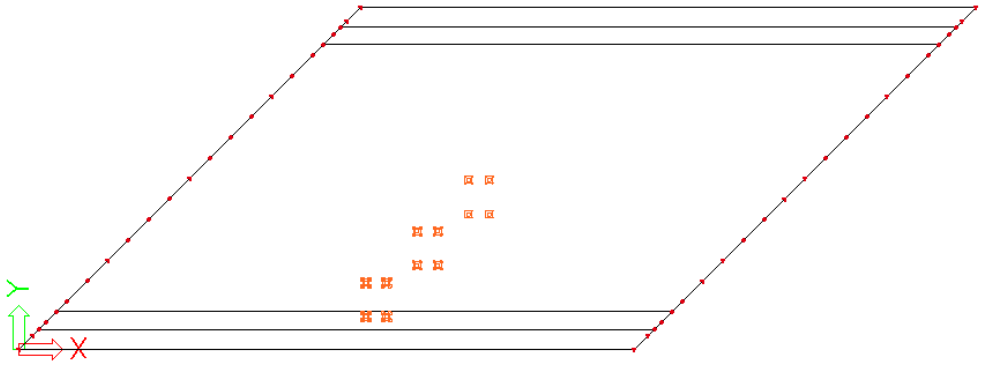

Figure B-11 Case 1: Loads for maximum longitudinal moment and shear (with corresponding negative working lane loads)

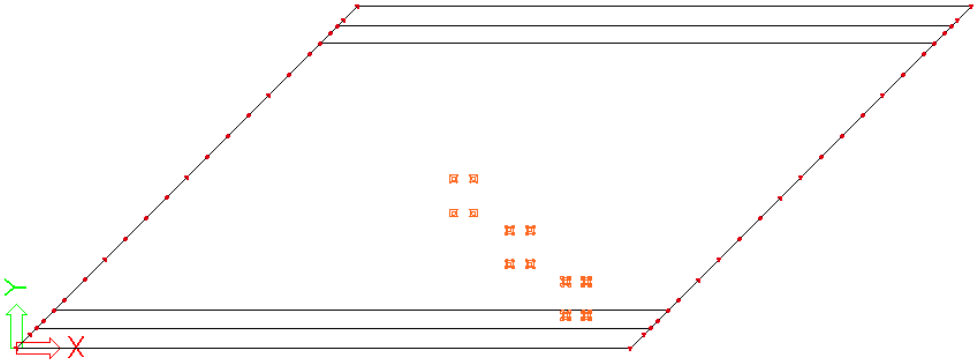

Figure B-12 Case 2: Loads for maximum shear and torsion (with corresponding negative working lane loads)

Minalu developed load configurations for maximum torsional moment in the first ZIP girder presented in Figure B-13 and Figure B-14. That configuration is not used to calculate the reinforcement in this report because in practice it is not used too.

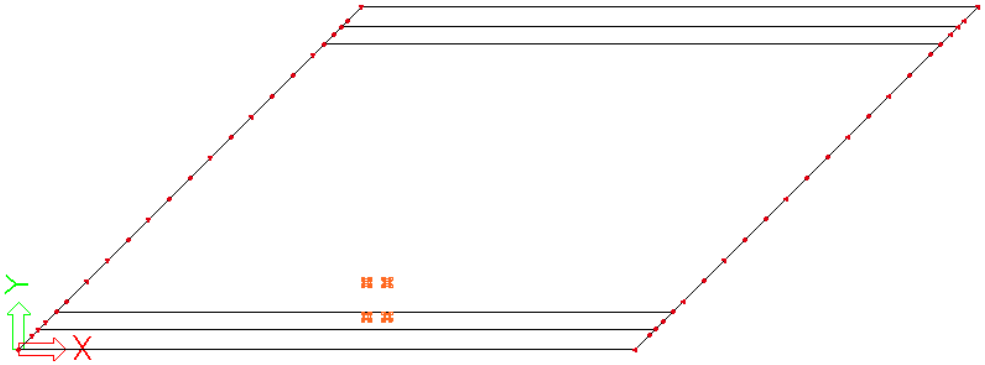

Figure B-13 Case 3: Load case for maximum negative torsional moment (with corresponding negative working lane loads)

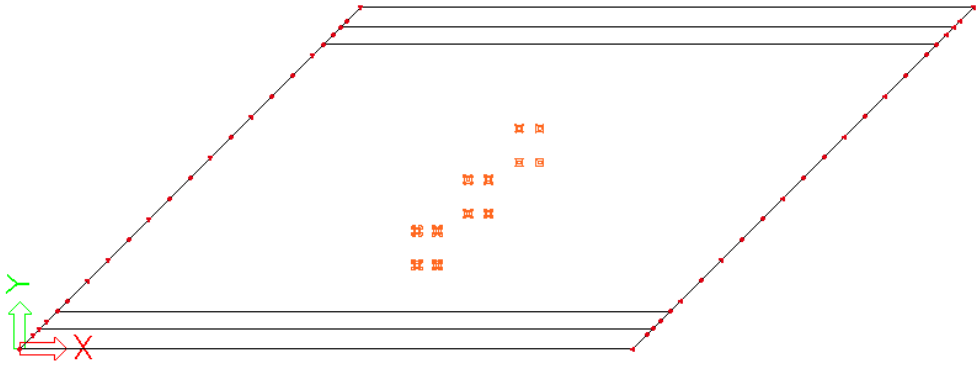

Figure B-14 Case 4: Load case for maximum negative torsional moment (with corresponding positive working lane loads)

Output for straight bridge

The four presented models give output which is presented in Table B-3 (shear force) and Table B-4 (torsion).

Remarks:

- The used values in the calculation, following from load case 1 and 2 are marked grey. The calculation is based on three points at end, quarter and half of span. So the point 0.88 L is not used but only added for comparison.
- Highest values, following from all loud cases, are marked bold and underlined.
- The values of the ZIP and first ZIP are all compared, the maximum is taken and applied to one design ZIP girder.

Girder		Straight bridge [kN]			
		Case 1	Case 2	Case 3	Case 4
ZIP	0	313,3	252,7	265,1	179,4
	0.5L	0,0	**18,2**	0,0	0,0
	0.75L	**204,1**	103,1	170,8	118,2
	0.88L	**255,5**	185,4	214,3	156,2
	L	313,3	**418,0**	265,1	179,4
1st ZIP	0	268,8	215,3	237,7	143,8
	0.5L	0,0	12,1	0,0	0,0
	0.75L	182,1	104,9	162,7	89,7
	0.88L	250,2	146,4	228,0	128,5
	L	268,8	342,3	237,7	143,8
TRA	0	284,6	233,5	302,4	116,1
	0.5L	0,0	**5,6**	0,0	0,0
	0.75L	**148,2**	100,3	151,7	47,8
	0.88L	198,7	162,2	**200,7**	77,4
	L	284,6	265,1	**302,4**	116,1

Table B-3 Shear forces from Scia in straight bridge

Girder		Straight bridge [kNm]			
		Case 1	Case 2	Case 3	Case 4
ZIP	0	10,4	9,3	36,7	-35,9
	0.5L	0,0	-2,6	0,0	0,0
	0.75L	-10,6	-9,5	**-30,5**	25,7
	0.88L	-15,3	-8,2	**-40,6**	32,2
	L	-10,4	0,6	-36,7	35,9
1st ZIP	0	23,0	21,2	47,0	-21,7
	0.5L	0,0	**-2,8**	0,0	0,0
	0.75L	-6,0	-9,4	-23,4	18,7
	0.88L	-12,7	-10,5	-35,8	21,5
	L	-23,0	-16,1	**-47,0**	21,7
TRA	0	-9,9	-6,6	10,9	-28,5
	0.5L	0,0	**-3,6**	0,0	0,0
	0.75L	-4,3	-12,2	**-25,5**	22,1
	0.88L	-3,4	-4,5	**-29,1**	27,6
	L	9,9	18,0	-10,9	**28,5**

Table B-4 Torsion moments in straight bridge

Applied forces on straight bridge

From Table B-3 and Table B-4 the maximum forces can be extracted and used in the calculation. This is done with the standard method of Spanbeton presented in Table B-5 and Table B-6.

Remarks:

- The maximum forces are split up in to parts. That is done in relation to the fatigue calculation. One example how to find the relation between the 'output' and 'applied forces' is: Maximum shear in ZIP at location L, output gives 418 kN, that is presented as 82,3 + 335,7 kNm.
- The moments due to own weight of the girders and deck is simply calculated with $1/8*q*L^2$
- The dead loads already give torsion in the girders ($T_{rep;rust}$), only when the live loads give higher torsion the differences are added ($T_{rep;nut}$).

Cut at:	$V_{rep;eg;pref}$ [kN]	$V_{rep;eg;dl}$ [kN]	$V_{rep;rust}$ [kN]	$V_{rep;nut}$ [kN]	$T_{rep;rust}$ [kNm]	$T_{rep;nut}$ [kNm]	V_d [kN]	T_d [kNm]
γ =	1,35	1,35	1,35	1,35	1,35	1,35	-	-
Support	251,5	127,1	82,3	335,7	28,8	0	1075	39
1/4 L_T	125,8	63,5	52,9	151,2	13,7	0	531	18
1/2 L_T	0	0	0	18,2	0	2,8	25	4

Table B-5 Applied loads for ZIP girders

Cut at:	$V_{rep;eg;pref}$ [kN]	$V_{rep;eg;dl}$ [kN]	$V_{rep;rust}$ [kN]	$V_{rep;nut}$ [kN]	$T_{rep;rust}$ [kNm]	$T_{rep;nut}$ [kNm]	V_d [kN]	T_d [kNm]
γ =	1,35	1,35	1,35	1,35	1,35	1,35	-	-
Support	247,1	134,1	146,4	138,2	10,7	7,3	899	24
1/4 L_T	123,6	37,1	51,7	96,5	17,8	0	417	24
1/2 L_T	0	0	0	5,6	0	3,6	8	5

Table B-6 Applied loads for TRA girders

Evaluation used load models for straight bridge

The reinforcement from the four load cases will be compared with the calculated reinforcement from the calculation (based on load case 1 and 2).

Two cases will be compared:

1. Maximum shear force with occurring torsion at same time, Table B-7.
2. Maximum torsion with occurring shear force at same time, Table B-8.

Girder		Straight bridge [kN]		Check	Needed area reinforcement [mm]	
		Shear force	Torsion		Case 1 and 2	Max shear
ZIP	0.5L	18,2	-2,8	OK		
	0.75L	204,1	-10,6	OK		
	0.88L	255,5	-15,3	OK		
	L	418,0	-16,6	OK		
TRA	0.5L	5,6	-3,6	OK		
	0.75L	148,2	-4,3	OK		
	0.88L	200,7	-29,1	?	0	0
	L	302,4	-10,9	?	1222	**1261**

Table B-7 Maximum shear force with occurring torsion, maximum from all cases

Girder		Straight bridge [kNm]		Check	Needed area reinforcement [mm]	
		Shear force	Torsion		Case 1 and 2	Max torsion
ZIP	0.5L	18,2	-2,8	OK		
	0.75L	170,8	-30,5	?	0	0
	0.88L	214,3	-40,6	?	0	0
	L	265.1	-47,0	?	1457	1160
TRA	0.5L	5,6	-3,6	OK		
	0.75L	151,7	-25,5	?	0	0
	0.88L	200,7	-29,1	?	0	0
	L	116,1	28,5	?	1222	828

Table B-8 Maximum torsion with occurring shear force, maximum from all cases

From Table B-7 it appears that one time load case 3 needs more reinforcement, but this is only 3 % more. The applied reinforcement will be always a bit more, so this will not give differences in practice. So for the straight bridge it is sufficient to use only load case 1 and 2.

Output for skew bridge

The four presented models give output which is presented in Table B-9 (shear force) and Table B-10 (torsion).

Remarks:

- The used values in the calculation, following from load case 1 and 2 are marked grey. The calculation is based on three points at end, quarter and half of span. So the point 0.88 L is not used but only added for comparison.
- Highest values, following from all loud cases, are marked bold and underlined.
- The values of the ZIP and first ZIP are all compared, the maximum is taken and applied to one design ZIP girder.

Girder		Straight bridge [kN]			
		Case 1	Case 2	Case 3	Case 4
ZIP	0	295,1	253,4	271,8	144,0
	0.5L	2,5	31,6	12,6	14,3
	0.75L	**205,4**	91,4	176,0	112,1
	0.88L	241,2	**291,2**	191,6	160,9
	L	281,6	**371,8**	212,2	203,9
1st ZIP	0	256,0	221,3	241,3	132,0
	0.5L	**98,9**	26,7	96,3	5,3
	0.75L	184,2	93,8	168,5	86,4
	0.88L	265,0	281,3	243,4	133,3
	L	249,6	330,2	203,4	158,5
TRA	0	292,5	254,5	289,2	162,7
	0.5L	10,7	5,9	**18,6**	15,2
	0.75L	**162,0**	114,8	158,9	63,0
	0.88L	222,3	194,6	**224,1**	85,3
	L	308,5	296,4	**328,1**	109,6

Table B-9 Shear forces from Scia in skew bridge

Girder		Straight bridge [kNm]			
		Case 1	Case 2	Case 3	Case 4
ZIP	0	12,3	10,8	29,6	-24,6
	0.5L	-33,9	-32,0	-25,1	-26,6
	0.75L	-39,5	-34,8	**-52,7**	3,9
	0.88L	-33,9	-25,7	-54,9	18,8
	L	-19,2	-7,8	-43,0	32,2
1st ZIP	0	16,3	13,5	33,7	-8,0
	0.5L	**-34,3**	-31,6	-26,8	-23,6
	0.75L	-35,6	-35,2	-47,4	-0,7
	0.88L	-37,8	-28,3	**-59,3**	10,9
	L	-44,2	-27,7	**-71,5**	12,5
TRA	0	-21,2	-17,6	-8,1	-29,1
	0.5L	**-47,1**	-41,6	-36,0	-32,1
	0.75L	-43,7	-49,1	**-56,3**	-6,2
	0.88L	-36,6	-30,4	**-59,8**	8,6
	L	-16,9	-0,9	**-41,3**	27,0

Table B-10 Torsion moments in skew bridge

Applied forces on skew bridge

From Table B-9 and Table B-10 the maximum forces can be extracted and used in the calculation. This is done with the standard method of Spanbeton presented in Table B-11 and Table B-12.

Remarks:

- The maximum forces are split up in to parts. That is done in relation to the fatigue calculation. One example how to find the relation between the 'output' and 'applied forces' is: Maximum shear in ZIP at location L, output gives 371,8 kN, that is presented as 101,8 + 270 kNm.
- The moments due to own weight of the girders and deck is simply calculated with $1/8*q*L^2$
- The dead loads already give torsion in the girders ($T_{rep;rust}$), only when the live loads give higher torsion the differences are added ($T_{rep;nut}$).

Cut at:	$V_{rep;eg;pref}$ [kN]	$V_{rep;eg;dl}$ [kN]	$V_{rep;rust}$ [kN]	$V_{rep;nut}$ [kN]	$T_{rep;rust}$ [kNm]	$T_{rep;nut}$ [kNm]	V_d [kN]	T_d [kNm]
γ =	1,35	1,35	1,35	1,35	1,35	1,35	-	-
Support	251,5	127,1	101,8	270	37,1	7,1	251,5	127,1
1/4 L_T	125,8	63,5	88,3	117,1	22,3	17,2	125,8	63,5
1/2 L_T	0	0	4,9	94	9,2	25,1	0	0

Table B-11 Applied loads for ZIP girders

Cut at:	$V_{rep;eg;pref}$ [kN]	$V_{rep;eg;dl}$ [kN]	$V_{rep;rust}$ [kN]	$V_{rep;nut}$ [kN]	$T_{rep;rust}$ [kNm]	$T_{rep;nut}$ [kNm]	V_d [kN]	T_d [kNm]
γ =	1,35	1,35	1,35	1,35	1,35	1,35	-	-
Support	247,1	134,1	154	154,5	28,1	0	931	38
1/4 L_T	123,6	37,1	55	107	28,9	20,2	436	66
1/2 L_T	0	0	0,9	9,8	10,3	36,8	14	64

Table B-12 Applied loads for TRA girders

Evaluation used load models for skew bridge

The reinforcement from the four load cases will be compared with the calculated reinforcement from the calculation (based on load case 1 and 2).

Two cases will be compared:

1. Maximum shear force with occurring torsion at same time, Table B-13.
2. Maximum torsion with occurring shear force at same time, Table B-14.

Girder		Skew bridge [kN]		Check	Needed area reinforcement [mm]	
		Shear force	Torsion		Case 1 and 2	Max shear
ZIP	0.5L	98,9	-34,3	OK		
	0.75L	205,4	-39,5	OK		
	0.88L	291,2	-28,3	OK		
	L	371,8	-27,7	OK		
TRA	0.5L	18,6	-36,0	?	0	0
	0.75L	162,0	-43,7	OK		
	0.88L	224,1	-59,8	?	0	0
	L	328,1	-41,3	?	1382	**1560**

Table B-13 Maximum shear force with occurring torsion, maximum from all cases

Girder		Skew bridge [kNm]		Check	Needed area reinforcement [mm]	
		Shear force	Torsion		Case 1 and 2	Max torsion
ZIP	0.5L	89,9	-34,3	OK		
	0.75L	176,0	-52,7	?	0	0
	0.88L	243,4	-59,3	?	0	0
	L	241,3	-71,5	?	1445	1290
TRA	0.5L	10,7	-47,1	OK		
	0.75L	158,9	-56,3	?	0	0
	0.88L	224,1	-59,8	?	0	0
	L	328,1	-41,3	?	1382	**1560**

Table B-14 Maximum torsion with occurring shear force, maximum from all cases

From Table B-13 it appears that one time the TRA needs more reinforcement for load case 3, this is 13 % more. This is available due to the fatigue calculation that is governing, so it will not give other reinforcement. However, it is a serious difference.

Comparison with results of Minalu

Minalu searches the largest torsional moments in the first ZIP girder. He didn't look to the shear forces at all, so the interaction between torsion and shear wasn't investigated. Furthermore he takes an cut along the length of the beam, but didn't apply averaging over the width of the girder. Another difference is that he models the end diaphragm beam, that was not done in this calculation. Comparison with his values is therefore not possible.

Comparison straight and skew bridge

The results for the straight and skew bridge are analysed in detail. Now a comparison between the two bridges is made.

Two effects are visible:

1. In the skew bridge the shear force is normally higher.
2. In the skew bridge also the torsion moments are higher.

The effects are visualized in Table B-15, Table B-16, Figure B-15 and Figure B-16. It follows clearly that there is much more torsion in a the skew bridge compared with the straight one.

Girder		Straight	Skew	Deviation [%]
ZIP	0.5L	18,2	98,9	442,9
	0.75L	204,1	205,4	0,6
	L	418,0	371,8	-11,1
TRA	0.5L	5,6	10,7	91,1
	0.75L	148,2	162,0	9,3
	L	284,6	308,5	8,4

Table B-15 Comparison shear force in straight and skew bridge

Girder		Straight	Skew	Deviation [%]
ZIP	0.5L	-2,8	-34,3	1125,0
	0.75L	-10,6	-39.5	178,3
	L	-23,0	-44,2	92,2
TRA	0.5L	-3,6	-47,1	1208,3
	0.75L	-12,2	-49,1	302,5
	L	18,0	-16,9	-6,1

Table B-16 Comparison torsion moment in straight and skew bridge

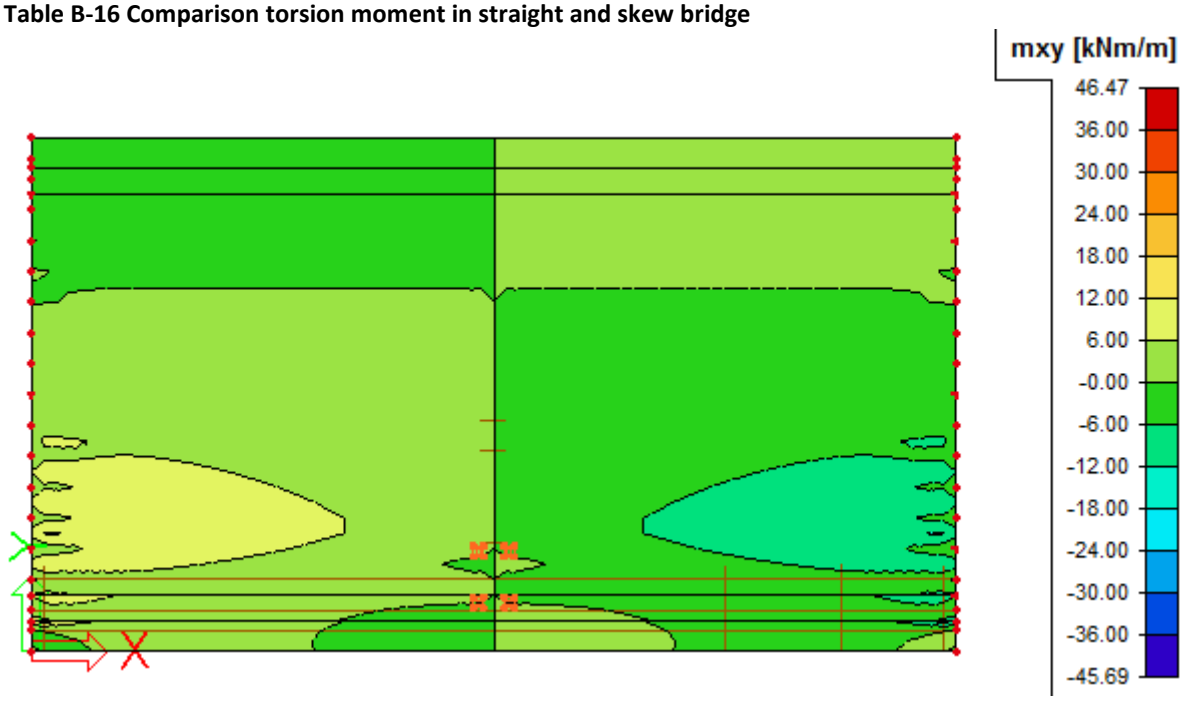

Figure B-15 Torsion in straight bridge due to load case 2

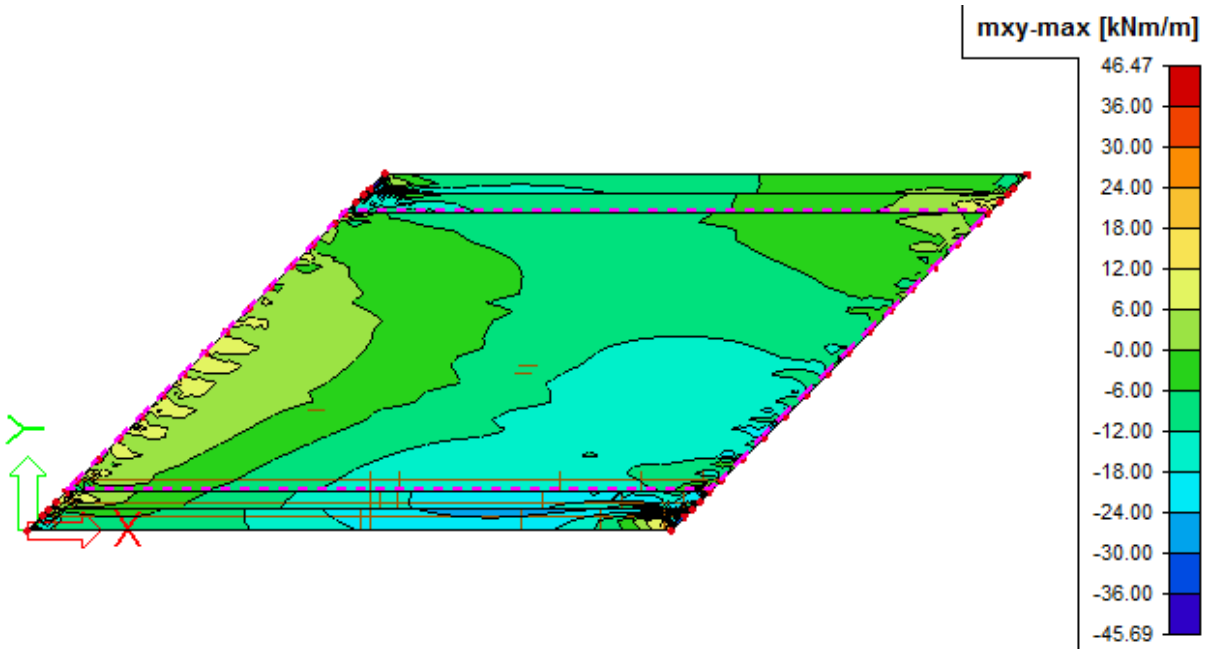

Figure B-16 Torsion in skew bridge due to load case 2

Answer to intended comparison

- The developed load cases by Minalu have no effect on the reinforcement of the ZIP girders. For the TRA sometimes load case 3 (Figure B-13) will give the most severe combination. A practical rule would be to check the TRA for load case 3. On the other hand, due to the fatigue rules no problems will occur because that is the governing phenomena.
- In a skew bridge occurs higher torsion moments and shear forces.

Issues from analysis

- When the positive moments in the deck of a skew bridge are based on a straight bridge model an underestimation of that moment can occur.
- The torsional moments reduces the negative moments in the middle of the deck. When these torsional moments are neglected higher negative moments in the deck are found. Consequently there will be an underestimation of the positive moments.
- Is it true that heavy negative moments occur at the corner of the deck in the orthotropic plate model?[19]

[19] Minalu, Kassuhun K. (2010), *Finite element modelling of skew slab-girder bridges.* Page 68.

C. Determination bond length following the Eurocode

Inleidingslengte voorspanning l_{pt2} = 1139 mm NEN-EN1992-1-1:2005 (8.18)

$l_{pt2} = 1{,}2 \cdot l_{pt}$

Bepalen inleidingslengte:

$f_{bpt} = \eta_{p1} \cdot \eta_1 \cdot f_{ctd}(t)$

η_{p1} = 3,2

η_1 = 1,0

$f_{ctd}(t)$ = 1,50 N/mm²

$\Rightarrow f_{bpt}$ = 4,8 N/mm²

$l_{pt} = \alpha_1 \alpha_2 \phi \sigma_{pm0} / f_{bpt}$

σ_{pm0} = 1222 N/mm²

α_1 = 1,25

α_2 = 0,19

ϕ = 15,7 mm

$\Rightarrow l_{pt}$ = 949 mm

NEN-EN 1992-1-1:2005

(2) Voorspankanalen voor nagespannen elementen behoren in het algemeen niet te zijn gebundeld met uitzondering van het geval van twee voorspankanalen die verticaal boven elkaar geplaatst zijn.

(3) De minimale vrije afstand tussen voorspankanalen behoort in overeenstemming te zijn met hetgeen is getoond in figuur 8.15.

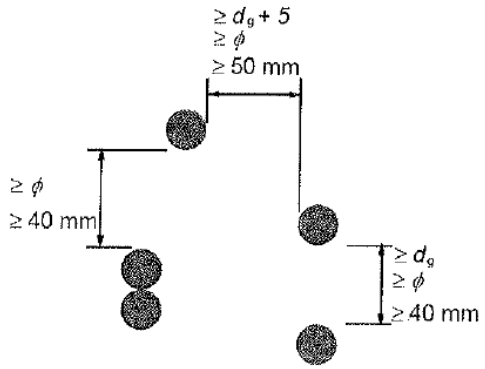

OPMERKING ϕ is de diameter van voorspankanalen voor nagerekt staal en d_g is de maximale korrelafmeting.

Figuur 8.15 — Minimale vrije afstand tussen voorspankanalen

8.10.2 Verankering van voorspanelementen met voorgerekt staal

8.10.2.1 Algemeen

(1) In verankeringsgebieden van voorspanelementen met voorgerekt staal behoren de volgende lengteparameterss te zijn beschouwd, zie figuur 8.16:

a) De overdrachtslengte l_{pt}, waarover de voorspankracht (P_0) volledig is overgedragen op het beton; zie 8.10.2.2 (2);

b) De spreidingslengte l_{disp} waarover de betonspanning geleidelijk is gespreid tot een lineaire verdeling over de betondoorsnede, zie 8.10.2.2 (4);

c) De verankeringslengte l_{bpd}, waarover de spankracht F_{pd} in de uiterste grenstoestand volledig is verankerd in het beton; zie 8.10.2.3 (4) en (5).

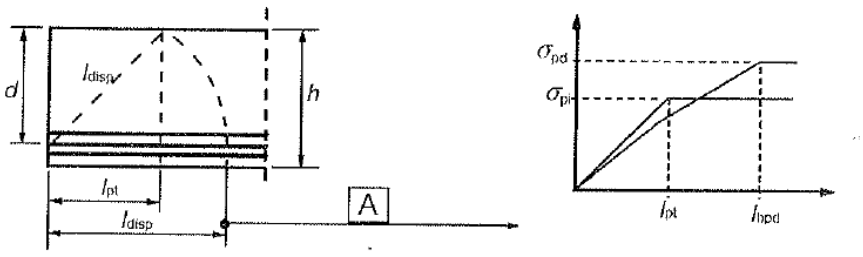

Verklaring

A lineaire spanningsverdeling in de dwarsdoorsnede van een element

Figuur 8.16 — Overdracht van voorspanning in elementen met voorgerekt staal; lengteparameters

156

8.10.2.2 Overdracht van de voorspanning

(1) Bij het aflaten van de spanelementen mag zijn aangenomen dat de voorspanning op het beton is overgedragen door een constante aanhechtspanning f_{bpt}, waarin:

$$f_{bpt} = \eta_{p1}\,\eta_1\,f_{ctd}(t) \tag{8.15}$$

waarin:

η_{p1} is een coëfficiënt die rekening houdt met het type spanelement en de aanhechtingssituatie bij het aflaten;
η_{p1} = 2,7 voor gedeukte draden;
η_{p1} = 3,2 voor 3- en 7-draads strengen;

η_1 = 1,0 voor goede aanhechtingsomstandigheden (zie 8.4.2);
= 0,7 in andere gevallen, tenzij een hogere waarde kan zijn gerechtvaardigd met betrekking tot speciale omstandigheden bij de uitvoering;

$f_{ctd}(t)$ is de rekenwaarde van de treksterkte op het tijdstip van aflaten;

$f_{ctd}(t)$ = $\alpha_{ct}\cdot 0{,}7\,f_{ctm}(t) / \gamma_c$ (zie ook 3.1.2 (8) en 3.1.6 (2)P).

OPMERKING Waarden van η_{p1} voor andere dan hierboven gegeven typen spanelementen kunnen zijn gebruikt op grond van een Europese Technische Goedkeuring.

(2) De basiswaarde van de overdrachtslengte l_{pt}, is gegeven door:

$$l_{pt} = \alpha_1\,\alpha_2\,\phi\,\sigma_{pm0}/f_{bpt} \tag{8.16}$$

waarin:

α_1 = 1,0 voor geleidelijk aflaten;
= 1,25 voor plotseling aflaten;

α_2 = 0,25 voor spanelementen met cirkelvormige doorsnede;
= 0,19 voor 3- en 7-draads strengen;

ϕ is de nominale diameter van het spanelement;

σ_{pm0} is de spanning in het spanelement juist na het aflaten.

(3) Voor de rekenwaarde van de overdrachtslengte behoort de meest ongunstige van twee waarden te zijn genomen, afhankelijk van de ontwerpsituatie:

$$l_{pt1} = 0{,}8\,l_{pt} \tag{8.17}$$

of

$$l_{pt2} = 1{,}2\,l_{pt} \tag{8.18}$$

OPMERKING In het algemeen wordt de lagere waarde gebruikt voor toetsing van lokale spanningen bij het aflaten en de hogere waarde voor de uiterste grenstoestanden (dwarskracht, verankering enz.).

(4) Aangenomen mag zijn dat de betonspanning buiten de spreidingslengte een lineaire verdeling heeft, zie figuur 8.17:

$$l_{disp} = \sqrt{l_{pt}^2 + d^2} \tag{8.19}$$

(5) Een alternatieve opbouw van de voorspanning mag zijn aangenomen als dit afdoende kan zijn gerechtvaardigd en als de overdrachtslengte overeenkomstig is aangepast.

8.10.2.3 Verankering van de trekkracht in de uiterste grenstoestand

(1) De verankering van voorspanelementen behoort te zijn gecontroleerd in doorsneden waarin de betontrekspanning $f_{ctk,0,05}$ overschrijdt. De kracht in het voorspanelement behoort te zijn berekend voor een gescheurde doorsnede inclusief het effect van dwarskracht volgens 6.2.3 (6); zie ook 9.2.1.3.
Indien de betontrekspanning kleiner is dan $f_{ctk,0,05}$, is controle van de verankering niet nodig.

(2) De aanhechtsterkte voor verankering in de uiterste grenstoestand is:

$$f_{bpd} = \eta_{p2}\, \eta_1\, f_{ctd} \qquad (8.20)$$

waarin:

η_{p2} is een coëfficiënt die rekening houdt met het type spanelement en de aanhechtingssituatie bij de verankering;
η_{p2} = 1,4 voor gedeukte draden of
η_{p2} = 1,2 voor 7-draads strengen;

η_1 is zoals gedefinieerd in 8.10.2.2 (1).

OPMERKING Waarden van η_{p2} voor andere dan de hierboven gegeven types voorspanelementen kunnen zijn gebruikt op grond van een Europese Technische Goedkeuring.

(3) Ten gevolge van toenemende brosheid bij beton met hogere sterkte behoort $f_{ctk,0,05}$ hierbij te zijn beperkt tot de waarde voor C60/75, tenzij kan zijn getoetst dat de gemiddelde aanhechtsterkte uitstijgt boven deze grens.

(4) De totale verankeringslengte voor het verankeren van een voorspanelement met spanning σ_{pd} is:

$$l_{bpd} = l_{pt2} + \alpha_2 \phi\, (\sigma_{pd} - \sigma_{pm\infty})/f_{bpd} \qquad (8.21)$$

waarin:

l_{pt2} is de grootste rekenwaarde van de overdrachtslengte, zie 8.10.2.2 (3);
α_2 als gedefinieerd in 8.10.2.2 (2);
σ_{pd} is de spanning in het spanelement overeenkomend met de in (1) beschreven kracht;
$\sigma_{pm\infty}$ is de voorspanning na alle verliezen.

(5) Spanningen in het voorspanstaal in het verankeringsgebied zijn geïllustreerd in figuur 8.17.

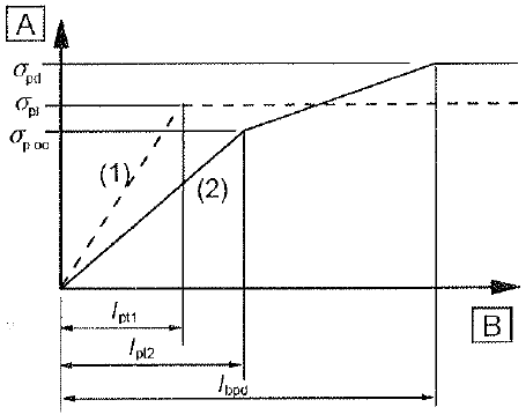

Verklaring

A spanning in het voorspanstaal
B afstand vanaf het uiteinde

Figuur 8.17 — Spanningen in het verankerinsgebied van elementen met voorgerekt staal: (1) bij het aflaten van de spanelementen, (2) in de uiterste grenstoestand

(6) Bij combinaties van gewone wapening en voorspanwapening mogen de verankeringscapaciteiten van beide bij elkaar zijn opgeteld.

8.10.3 Verankeringszones van elementen voorgespannen met nagerekt staal

(1) Het berekenen van verankeringszones behoort in overeenstemming te zijn met de toepassingsregels in deze paragraaf en die in 6.5.3

(2) Bij het beschouwen van de effecten van de voorspanning als een geconcentreerde kracht op de verankeringszone behoort de rekenwaarde van de voorspanelementen in overeenstemming te zijn met 2.4.2.2 (3) en behoort de lagere karakteristieke treksterkte van het beton te zijn gebruikt.

(3) De oplegdruk achter verankeringsplaten behoort te zijn gecontroleerd in overeenstemming met de van toepassing zijnde Europese Technische Goedkeuring.

(4) Trekkrachten ten gevolge van geconcentreerde krachten behoren te zijn bepaald met een staafwerkmodel of een andere geschikte methode (zie 6.5). Bij het detailleren van de wapening behoort te zijn aangenomen dat de staalspanning gelijk is aan de rekenwaarde van de sterkte. Als de spanning in deze wapening is beperkt tot 300 MPa, is controle van de scheurwijdte niet nodig.

D. Derivation of force distribution in ZIP girder

The force distribution from the prestressing is derived, including the effects in the bond zone.

Geometry

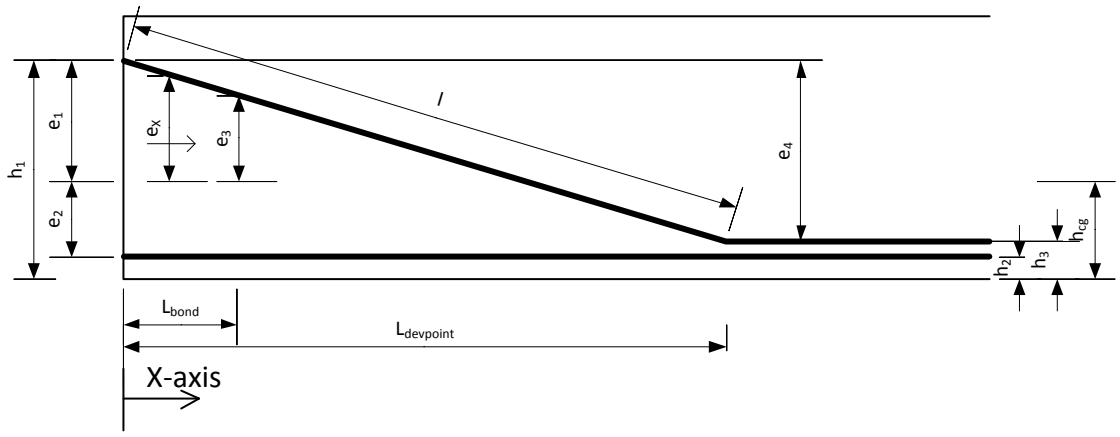

$$l = \sqrt{L_{devpoint}^2 + e_4^2}$$

$$e_1 = h_1 - h_{cg}$$

$$e_2 = h_{cg} - h_2$$

$$e_3 = \frac{(L_{devpoint} - L_{bond})}{L_{devpoint}} \cdot e_4 + h_3 - h_{cg}$$

$$e_4 = h_1 - h_3$$

$$e(x) = e_1 - \frac{e_1 - e_3}{L_{bond}} \cdot x \; voor \; 0 < x < L_{bond}$$

Forces

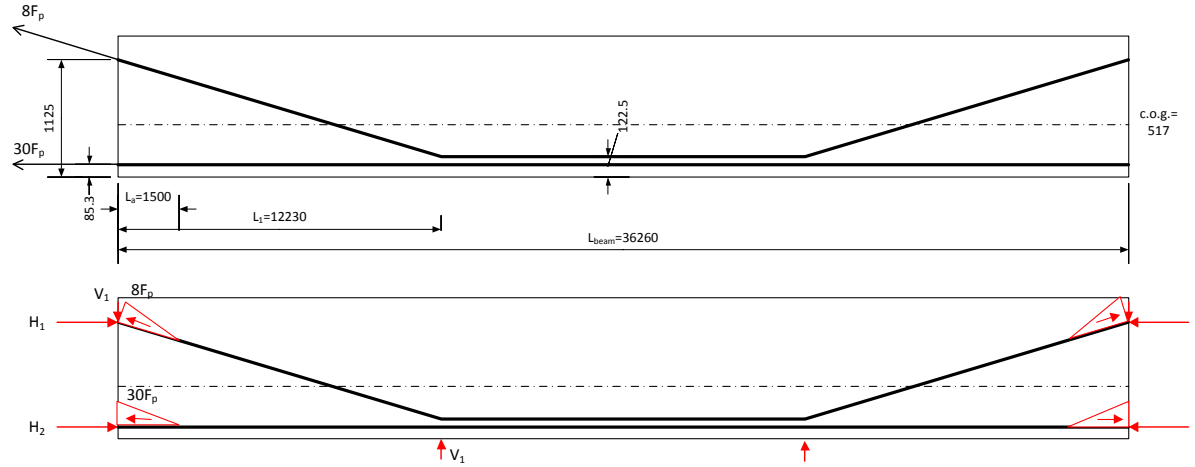

$$H_1 = \frac{L_{devpoint}}{l} \cdot 8 \cdot F_p$$

$$V_1 = \frac{e_4}{l} \cdot 8 \cdot F_p$$

$$H_2 = 30 \cdot F_p$$

Moment, shear and normal force

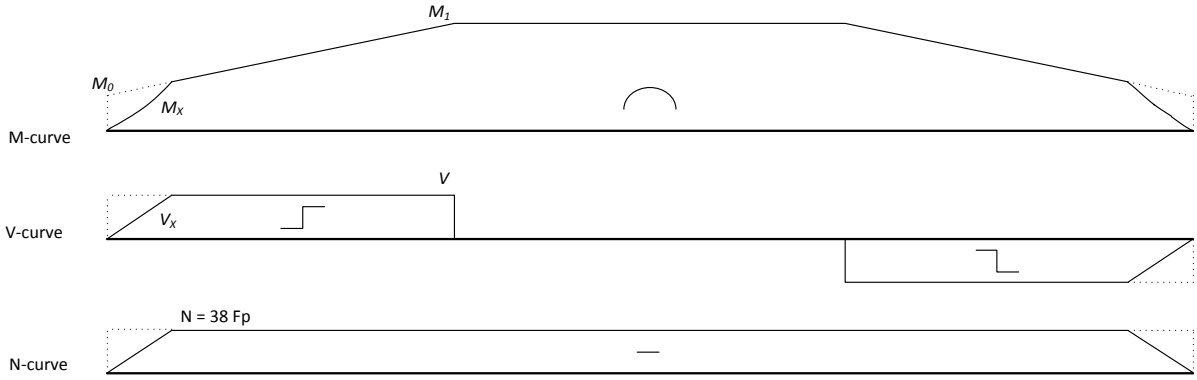

Following a simple method neglecting the bond influence gives enveloping curves:

$$V = V_1$$
$$N = -(H_1 + H_2)$$

$$M_0 = H_1 \cdot e_1 - H_2 \cdot e_2$$
$$M_1 = H_1 \cdot e_1 - H_2 \cdot e_2 - V_1 \cdot L_{devpoint}$$

$$\begin{cases} M(x) = M_0 + \dfrac{x}{L_{devpoint}} \cdot (M_1 - M_0) \text{ for } 0 < \mathrm{x} < \mathrm{L_{devpoint}} \\ M(x) = M_1 \text{ for } \mathrm{L_{devpoint}} < \mathrm{x} < \dfrac{\mathrm{L}}{2} \end{cases}$$

Influence of bond length on distributions

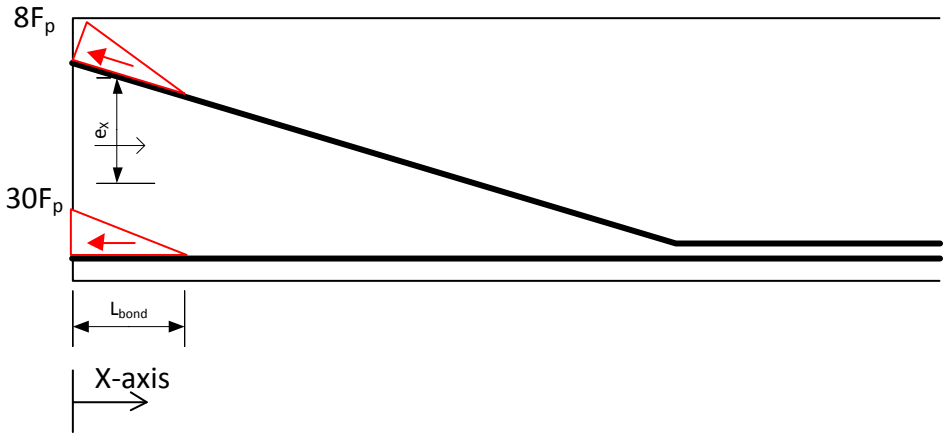

The bond length influences the moment en shear force distribution. Forces and eccentricities are written as functions of X to get the distribution. There is made an distinction between the deviated and straight strands.

$$F_{deviated}(x) = 8 \cdot F_p - \frac{8 \cdot F_p}{L_{bond}} \cdot x$$
$$F_{straight}(x) = 30 \cdot F_p - \frac{30 \cdot F_p}{L_{bond}} \cdot x$$

$$N_{deviated}(x) = \frac{L_{devpoint}}{l} \cdot F_{deviated}(x) = \frac{L_{devpoint}}{l} \cdot \left(8 \cdot F_p - \frac{8 \cdot F_p}{L_{bond}} \cdot x\right)$$
$$N_{straight} = F_{straight} = 30 \cdot F_p - \frac{30 \cdot F_p}{L_{bond}} \cdot x$$

$$V(x) = \frac{e_4}{l} \cdot F_{deviated}(x) = \frac{e_4}{l} \cdot \left(8 \cdot F_p - \frac{8 \cdot F_p}{L_{bond}} \cdot x\right)$$

Difference in the distribution of forces for the bond length.:

$$\Delta N(x) = N_{deviated}(x) + N_{straight} = \frac{L_{devpoint}}{l} \cdot \left(8 \cdot F_p - \frac{8 \cdot F_p}{L_{bond}} \cdot x\right) + 30 \cdot F_p - \frac{30 \cdot F_p}{L_{bond}} \cdot x$$

$$\begin{aligned}\Delta M(x) &= -N_{deviated}(x) \cdot e(x) + N_{straight} \cdot e_2 \\ &= -\frac{L_{devpoint}}{l} \cdot \left(8 \cdot F_p - \frac{8 \cdot F_p}{L_{bond}} \cdot x\right) \cdot \left(e_1 - \frac{e_1 - e_3}{L_{bond}} \cdot x\right) + \left(30 \cdot F_p - \frac{30 \cdot F_p}{L_{bond}} \cdot x\right) \cdot e_2\end{aligned}$$

$$\Delta V(x) = -V(x) = -\frac{e_4}{l} \cdot \left(8 \cdot F_p - \frac{8 \cdot F_p}{L_{bond}} \cdot x\right)$$

Resulting force distribution:

$$\begin{cases} \Sigma M(x) = M(x) + \Delta M(x) \text{ for } 0 < \mathrm{x} < \mathrm{L_{bond}} \\ \Sigma M(x) = M(x) \text{ for } \mathrm{L_{bond}} < \mathrm{x} < \dfrac{\mathrm{L}}{2} \end{cases}$$

$$\begin{cases} \Sigma N(x) = N + \Delta N(x) \text{ for } 0 < \mathrm{x} < \mathrm{L_{bond}} \\ \Sigma N(x) = N \text{ for } \mathrm{L_{bond}} < \mathrm{x} < \dfrac{\mathrm{L}}{2} \end{cases}$$

$$\begin{cases} \Sigma V(x) = V + \Delta V(x) \text{ for } 0 < \mathrm{x} < \mathrm{L_{bond}} \\ \Sigma V(x) = V \text{ for } \mathrm{L_{bond}} < \mathrm{x} < \dfrac{\mathrm{L}}{2} \end{cases}$$

E. Detailed information about used FEM

Before modelling some important things are prepared and presented in Part I of the report:

- Calculation of straight bridge (Appendix I-A – Calculation straight bridge)
- Calculation of skew bridge (Appendix I-B – Calculation skew bridge)
- Drawing with all dimensions and details (Appendix I-C – Drawings reinforcement and cables)

Assumptions and simplifications:

- Influences of temperature, creep and shrinkage are neglected. Shrinkage will have some effect, but that shall be very small. Creep is not relevant for the short term traffic loads.
- For the calculation of the reinforcement the method of the VBC, still valid and used by Spanbeton, was used. With this method a design was made as starting point for the model.
- For the model Eurocode is used. Used codes:
    - NEN-EN 1992-1-1 2005 nl, Design and calculation of concrete construction, general rules and rules for buildings.
    - NEN-EN 1992-1-1 NB 2007 nl. National Annex
    - prEN 10138-3,

The program ATENA 3D is chosen to use for this model. This models shall be refined dependent on the considered phenomenon.

Optimization cross-sections

ZIP-girder

Minalu already built a 3D model, linear-elastic, for the skew bridge to compare the results with results of other linear elastic models. In this model the shape shown in Figure E-1 was used.

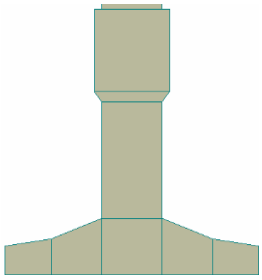

Figure E-1 Equivalent cross-section ZIP used by Minalu

Comparison of the properties of this simplified cross-section with the real ZIP cross-section shows that the simplification is unsafe. Especially the stiffness I_z shows a big deviation.

	ZIP	Simplification	Deviation
A	**5,68E-01**	**5,73E-01**	0,9%
Iy	**1,02E-01**	**1,02E-01**	0,0%
Iz	**2,41E-02**	**2,59E-02**	6,9%
It	**1,39E-02**	**1,40E-02**	0,7%
c ZLCS	**519**	**512**	-1,4%

Table E-1 Comparison cross-section (Figure E-1) with ZIP cross-section

It's important to have an equivalent cross-section that is as accurate as possible. The cross section of Minalu takes a massive bottom part of the cross-section. That part is adapted (Figure E-2), and from the comparison (Table E-2) follows that the new simplification of the cross-section is indeed more accurate. The complexity does not increase because only two nodes are shifted and no elements are added.

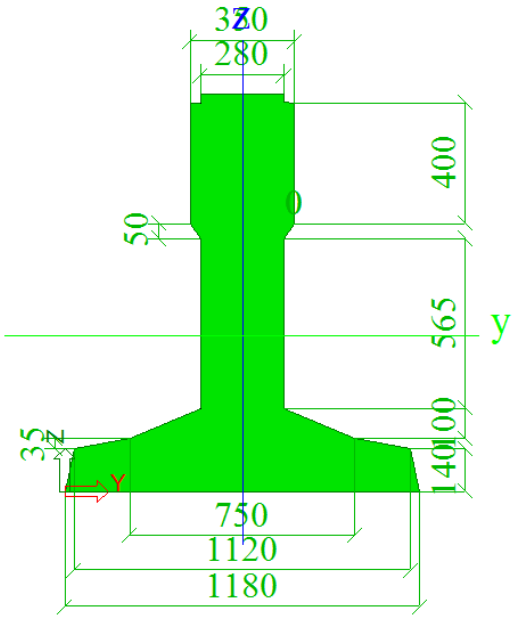

Figure E-2 Equivalent cross-section ZIP non-linear part, simplification 1

	Real ZIP	**Simplification**	Deviation
A	5,68E-01	**5,67E-01**	-0,2%
Iy	1,02E-01	**1,01E-01**	-1,0%
Iz	2,41E-02	**2,40E-02**	-0,4%
It	1,39E-02	**1,40E-02**	0,7%
c ZLCS	519	**517**	-0,4%

Table E-2 Comparison cross-section (Figure E-2) with ZIP cross-section

Check of deformations ZIP-girder

For the ZIP-girder some models are investigated to find a good balance between calculation time and accuracy. Especially the deformations are important because that's the output which is needed.

Applied test load: 10 kN/m -> $3{,}571 \cdot 10^{-2}$ kN/m^2 on top of girder (width 280 mm)
Length between supports: 35,3 m

Moment of inertia: $1{,}0175 \cdot 10^{-1}$ m^4
Distance to top fibre: 0,802 m
Distance to bottom fibre: 0,518 m

Moment: $1/8 \cdot 10 \cdot 35{,}3^2$ = 1557.61 kNm
Stress top: 7,93 N/mm^2
Stress bottom: 12,28 N/mm^2
Deformation: 52,30 mm

Three models are considered;

1. Linear elements, coarse (identical to model of Minalu), 939 elements
2. Quadratic elements, coarse, 939 elements
3. Linear elements, fine, >3000 elements

A comparison is presented in Table E-3.

Model	Stress top [N/mm^2]	Stress bottom [N/mm^2]	Deformation [mm]
Hand calculation	7,93	12,28	52,30
Lin. El. Coarse	6,74	11,31	49,44
Quadr. El. Coarse	9,86	13,99	52,99
Lin. El. Fine	7,16	12,05	52,02

Table E-3 Comparison different models

Obviously model 3 is the best option because it don't underestimate the deformations, but the calculation time will be much longer than for model 1. Model 2 overestimates the deformation a bit, but also in that case much more calculation time is needed. Model 1 is chosen to be used. The margin of the solution will be investigated, so in later stage it will be visible if this assumption gives troubles.

Material model Large linear-elastic model

In first instance the average values will be used following from the Eurocode. For the values about energy etc. the values given by ATENA will be hold. In practice this are the buttons to fit the model to the test results, in this case there are no tests.

Model girders

The material '3D Elastic Isotropic' is chosen. The title of the material is 'concrete girders linear elastic'. The properties presented in Table E-4 are used to model the structure. Concrete quality C53/65 is used.

Tab	Constant	Value	Unit
Basic	E	38000	MPa
	ν	0.2	-
Miscellaneous	ρ	$2.5 \cdot 10^{-2}$	MN/m^3
	α	n.v.t.	1/K

Table E-4 Parameters for linear elastic concrete girders

Model deck

The material '3D Elastic Isotropic' is chosen. The title of the material is 'concrete deck linear elastic'. The properties presented in Table E-5 are used to model the structure. Concrete quality C28/35 is used.

Tab	Constant	Value	Unit
Basic	E	16000 (0.5*32000)	MPa
	ν	0.2	-
Miscellaneous	ρ	$2.5 \cdot 10^{-2}$	MN/m^3
	α	n.v.t.	1/K

Table E-5 Parameters for linear elastic concrete deck

Material model Physical non-linear detail model
For non-linear behaviour the following points are included:

- Reinforcement
- Properties of prestressing cables, including bond model
- Properties of concrete (both girders and deck)

The presented mean strengths are measured from data of Spanbeton. That values are not used in the report.

Properties of reinforcement steel
For the reinforcement the material 'reinforcement' is chosen, with properties given in Table E-6 and Figure E-3. The title of the material is 'reinforcement'. The material B500B of the Eurocode is used.

Tab	Constant	Value			Unit
		Mean	Characteristic	Design	
Basic	Type	Bilinear (with hardening)			
	E	$2.74 \cdot 10^5$	$2{,}00 \cdot 10^5$		MPa
	σ_y	548.2	500	500/1.15=435	MPa
	σ_t	628.6	500	500/1.15=435	
	ε_{lim}	7.86	n.v.t.		%
	Active in compr.	No			-
Miscellaneous	P	n.v.t.			MN/m^3
	A	n.v.t.			1/K

Table E-6 Parameters for non-linear reinforcement model

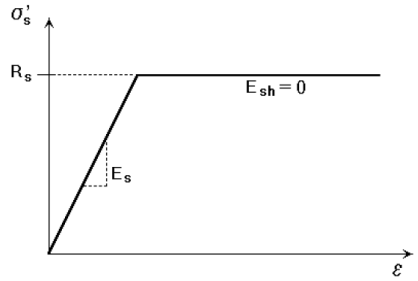

Figure E-3 Bi-linear reinforcement model of ATENA 3D

Properties of prestressing steel
For the prestressing steel also material 'reinforcement' is added. The title given to the material is 'prestressing'. The material Y1860S7 of the EN 10138-3 is used.

The properties as given in Figure E-4 are modelled with the strain hardening. The used values are given in Table E-7.

Tab	Constant	Value			Unit
		Mean	Characteristic	Design	
Basic	Type	Bilinear with hardening			
	E	$2{,}0 \cdot 10^5$	$1{,}95 \cdot 10^5$		MPa
	σ_y	1737	0.9·1860 =1674	1674/1.1=1521	MPa
	σ_t	1937	1860	1860/1.1=1690	
	ε_{lim}	6.0	1.0·3.5		%
	Active in compr.	No			-

Miscellaneous	P	n.v.t.	MN/m^3
	A	n.v.t.	1/K

Table E-7 Parameters for prestressing steel model

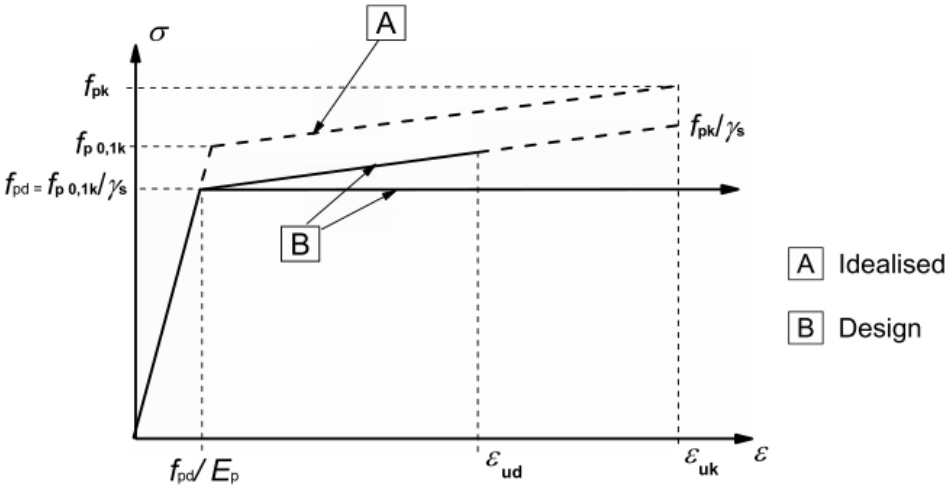

Figure E-4 Properties of prestressing steel according to the Eurocode

A bond model is used to avoid cracking of the girder in the zone where the prestressing force is transferred to the concrete. In ATENA the bond-slip law of Bigaj is available, presented in Figure E-5. The curve depends on two variables, the concrete cubic compressive strength and the bar radius of the reinforcement.

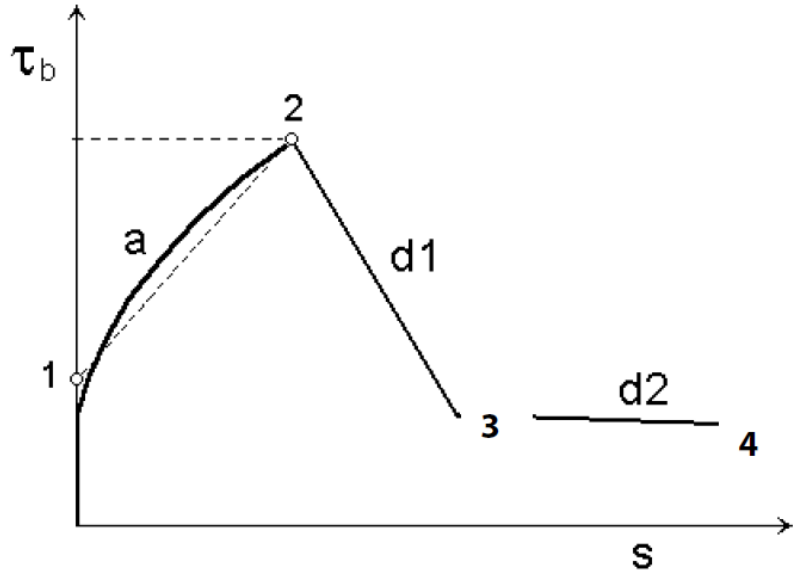

Figure E-5 Bond law by Bigaj 1999

Point	Slip [m]	Bond stress [MPa]
1	0	2.646
2	$5.520 \cdot 10^{-4}$	5.292
3	$6.486 \cdot 10^{-4}$	3.704
4	$6.624 \cdot 10^{-3}$	0

Table E-8 Applied parameters for Bigaj model

Properties of concrete

The philosophy of ATENA is to use a uniaxial stress-strain law to model the 3D effects properly, Figure E-6. The numbers in that figure indicates the state of damage in the structure which can be get from the output of ATENA. The peak values of stress in compression and in tension comes from the biaxial stress state as shown in Figure E-7.

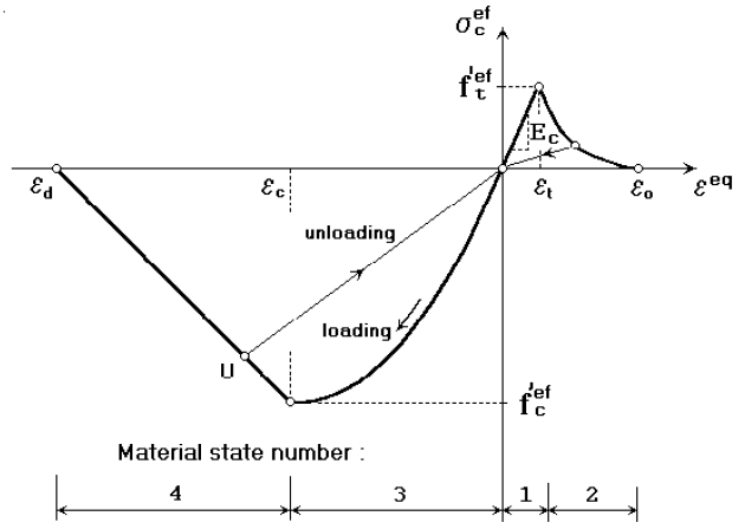

Figure E-6 Uniaxial stress-strain law for concrete of ATENA 3D

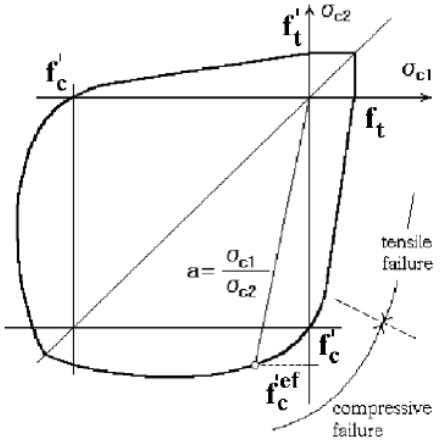

Figure E-7 Biaxial failure function for concrete

The four material states are briefly commented:

1. Tension before cracking: assumed linear elastic.

2. Tension after cracking: fictitious crack model based on crack-opening law and fracture energy. The exponential crack opening law of Hordijk is used, Figure E-8.

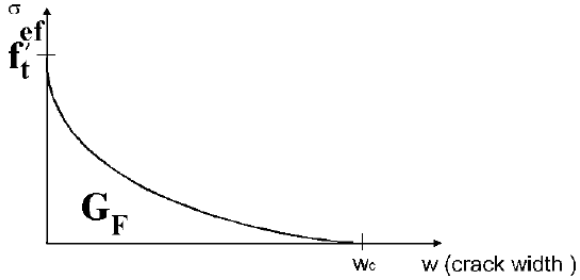

Figure E-8 Exponential crack opening law of Hordijk

3. Compression before peak stress: Formula recommended by CEB-FIP Model Code. Distributed damage is considered before the peak stress is reached, Figure E-9.

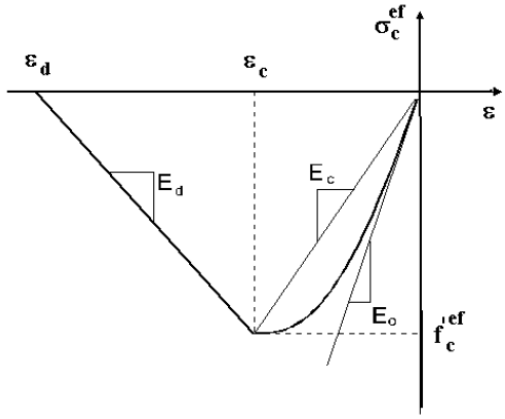

Figure E-9 Stress-strain relation of ATENA for concrete in compression

4. Compression after peak stress: It is assumed that compression failure is localized in a plane normal to the direction of the compressive principal stress. It is assumed that the plastic deformation (w_d) is independent of the size of the structure, Figure E-10. This must be transformed to the stress-strain relation for the corresponding volume of continuous material, as shown in Figure E-9 Stress-strain relation of ATENA for concrete in compressionFigure E-9.

1.

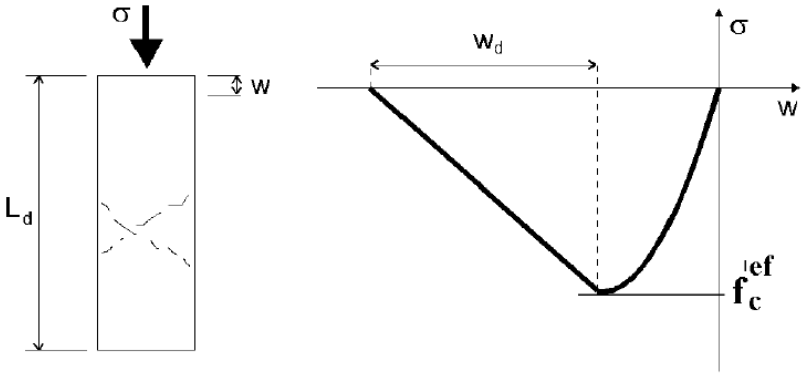

Figure E-10 Compression strength after peak stress

In ATENA 3D the tension cracking behaviour and plastic compression behaviour are combined in a material model called '3D Nonlinear Cementitious 2'.

Note: When the crack spacing calculated by the standard algorithm of ATENA is smaller than the element size the calculated widths may be overestimated. In that case the crack width must be reduced manually, ATENA takes the lowest value.

Model girders

The material '3D Nonlinear Cementitious 2' is chosen. The properties presented in Table E-9 are used to model the structure. Concrete quality 53/65 is used.

Tab	Constant	Value			Unit
		Mean	Characteristic	Design	
	f_{cu}		65	65/1.5=43.3	MPa
Basic	E	22*(82.6/10)^0.3 = 41450	38000		MPa
	N	0.2			-
	f_t	2,12*ln(1+82,6/10) = 4,72	2.91	2.91/1.5=1.94	MPa
	f_c	82,6	53	53/1.5=35.3	MPa
Tensile	G_F (0.000025·f_t)	Automatic by ATENA			-
Compres.	W_d	Automatic by ATENA			m
	ε_{cp}	Automatic by ATENA			-
	$r_{c,lim}$	Automatic by ATENA			-
Shear	S_F	Automatic by ATENA			-
	Aggr. Interlock	Automatic by ATENA			
Miscel.us	Fail. surf. excentr.	Automatic by ATENA			-
	B	Automatic by ATENA			-
	P	$2.5 \cdot 10^{-2}$			MN/m^3
	A	n.v.t.			1/K
	Fixed cr. m. coëff.	0			-

Table E-9 Parameters for non-linear concrete girders

F. Simple method to take results from ATENA

Introduction

For one element the process of finding the results is illustrated. For other element types it is assumed that the same procedure is valid.

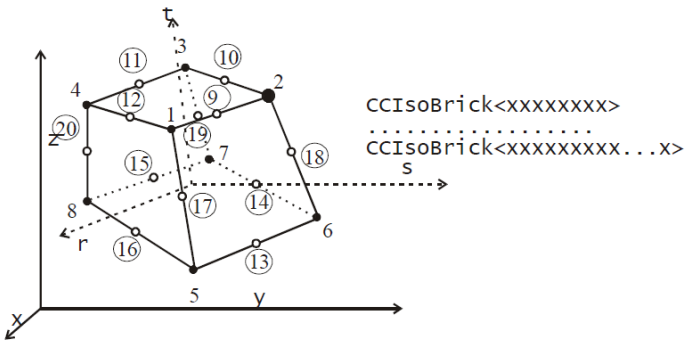

Fig. 3-8 Geometry of CCIsoBrick<...> elements.

(from ATENA 3D theory manual)

Step 1: Macroelements, Geometry of structure

The geometry of the structure is defined with macro-elements. The dimensions are input of the user and thus known. In the output the name for the macroelement is: group

Step 2: Definition of elements, Finite Element Mesh

The mesh is chosen as explained in the manuals of ATENA. The elements are defined by nodes and element numbers. The name for the finite element is: element

The results can be found by clicking  in the Post-processor. You can get the values as follows:

- Nodal coordinates: Step 1 (or other step) -> Nodes -> Reference Nodal Coordinates
- Element indices: Step 1 (or other step) -> Elements -> Element Indices

Nodes

For the nodal coordinates results are given in the following form. There is given an table for every macro-element.

Node	x(1) [m]	x(2) [m]	x(3) [m]
1	value	value	value
2	value	value	value
3	value	value	value
:	:	:	:
N	value	value	value

Example: When there is a macroelement with 4 quadratic finite elements inside that will give 56 nodes in the table.

Elements

The elements are defined by the nodes, the place of the nodes in the element are important. In this way information is connected and the place of the elements is fixed. Following the quadratic brick element as presented above the elements has 20 nodes. This numbers are connected with the node numbers in the following way (example):

Group	Element	No 1	No 2	No 3	No 4	No 5	..	No 6
1	1	3	8	5	n-1	n-10		2

Step 3: Position of Integration Points

When the position of the elements is known the position of the Integration points can be found simply.

Again: The results can be found by clicking  in the Post-processor. You can get the values as follows:

- Integration points: Step 1 (or other step) -> Integration points -> Reference Ip Coordinates

The results are presented as follows (example):

Group	Element	Ipt	x(1) [m]	x(2) [m]	x(3) [m]
1	2	1	value	value	value
1	2	2	value	value	value
1	2	3	value	value	value
:	:	:	:	:	:
1	n	N	value	value	value

Practical

The following steps are practical to obtain solutions from the nodal coordinates:

- Copy-paste the list of reference nodal coordinates in an excel sheet (see remark how to do this).
- Past the results you like to analyse beside this coordinates.
- Use ‘sorting and filtering’ (see illustrations) and use the filter to select a point from the (enormous!!) long list.

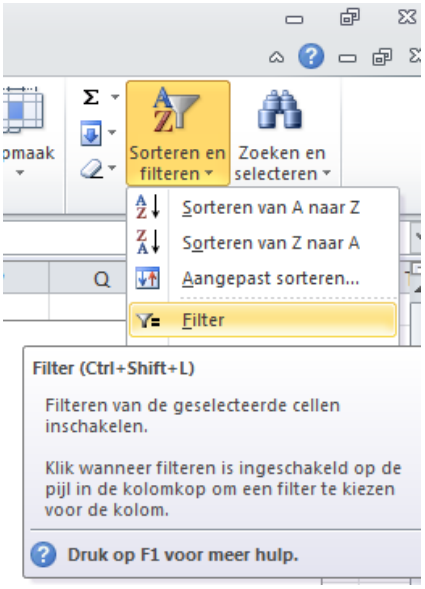

	A	B	C	D	E	F	G	H	I	J	K	L
1	COÖRDINATEN					SPANNINGEN						
2		X	Y	Z								
3							SIGMA XX	SIGMA YY	SIGMA ZZ	TAU XY	TAU YZ	TAU XZ
4												
5	ANALYSIS STEP 5					ANALYSIS STEP 5						
6	POSITION: NODES					POSITION: NODES						
7	MACROELEMENT 1 - REFERENCE NODAL COORDINATES					MACROELEMENT 1 - STRESS						
8	Reference nodal coordinates					Stress						
9	Node	x(1) [m]	x(2) [m]	x(3) [m]		Node	Sigma xx [MPa]	Sigma yy [MPa]	Sigma zz [MPa]	Tau xy [MPa]	Tau yz [MPa]	Tau xz [MPa]
10	1	-2,00E-01	0,00E+00	2,00E-01		1	-9,15E-01	-1,93E-01	-6,90E+00	1,21E+00	7,22E+00	-2,24E+00
11	2	2,00E-01	0,00E+00	2,00E-01		2	-2,46E+01	-4,80E+01	-3,40E+01	-1,53E+00	3,96E+00	4,49E+00
12	3	2,00E-01	0,00E+00	5,00E-01		3	9,14E-01	-3,34E+00	-3,51E+00	-1,81E+00	-8,01E+00	1,58E+00
13	4	-2,00E-01	0,00E+00	5,00E-01		4	3,18E+01	7,97E+01	2,85E+01	-6,55E-02	-7,00E+00	-1,74E-01
14	5	0,00E+00	-4,00E-02	3,50E-01		5	-2,28E+01	-5,03E+01	-2,75E+01	1,41E+00	2,25E+00	1,24E+00
15	6	1,00E-01	-2,00E-02	2,75E-01		6	-1,16E+01	-2,11E+01	-1,93E+01	-1,52E+00	2,21E+00	2,86E+00
16	7	-1,00E-01	-2,00E-02	2,75E-01		7	-1,19E+01	-2,52E+01	-1,72E+01	1,31E+00	4,73E+00	-5,02E-01
17	8	0,00E+00	0,00E+00	2,00E-01		8	-1,07E+01	-2,09E+01	-1,78E+01	-3,62E-01	4,77E+00	7,00E-01
18	9	2,00E-01	0,00E+00	3,50E-01		9	3,15E+00	1,11E+01	-4,16E+00	-3,81E+00	-3,24E+00	3,47E+00
19	10	1,00E-01	-2,00E-02	4,25E-01		10	-4,65E+00	-1,15E+01	-9,47E+00	-3,62E-01	-3,06E+00	1,30E+00
20	11	-1,00E-01	-2,00E-02	4,25E-01		11	1,53E-01	2,52E+00	-3,20E+00	9,94E-01	-3,31E+00	-4,58E-03
21	12	0,00E+00	0,00E+00	5,00E-01		12	1,36E+00	1,38E+00	-2,07E+00	1,20E+00	-6,29E+00	2,69E-01
22	13	-2,00E-01	0,00E+00	3,50E-01		13	1,34E+01	3,66E+01	8,14E+00	7,71E-01	9,34E-01	-7,83E-01
23	14	0,00E+00	0,00E+00	3,50E-01		14	-5,19E-04	-1,77E+00	-5,20E+00	-3,04E-01	-3,97E-01	-3,30E-01

For the integration points the same procedure can be used. Only the values aren't nice values, you can use another filter to search for coordinates between two boundaries.

Remarks:

1. The results can be exported to excel by control + A, then control + C and paste it than in an excel-sheet.
2. In my case X(1), X(2) and X(3) corresponds with X, Y and Z. But you have to verify that!

G. Maple sheet to determine torsional moments from rotations

```
> restart; It := 1.39e-2 : G := 15.833e6 : E := 38e6 : Cw := 100e-5 :
      G·It; E·Cw;

phi := -2.627e-11·x^6 + 2.299e-9·x^5 - 7.863e-8·x^4 + 1.237e-6
    ·x^3 - 1.567e-6·x^2 + 2.788e-5·x - 3.080e-3;

dY := diff(phi, x) : ddY := diff(dY, x) : dddY := diff(ddY, x) :
Mtwringing := G·It·dY :
Mtwelving := -E·Cw·ddY :
Mt := Mtwringing + Mtwelving;
with(plots) :
a := plot(Mtwringing, x = 0.63 ..35.63, color = "NavyBlue"); b
     := plot(Mtwelving, x = 0.63 ..35.63, color = "Green"); c
     := plot(Mt, x = 0.63 ..35.63, color = "Red")
> display(a, b, c, title = "wringing");
```